Pneumatic artificial muscles for human-friendly mobile service robots

_____

A thesis submitted to the University of Dublin in partial fulfilment of the requirements for the degree of Ph.D.

Michael Cullinan

Department of Mechanical and Manufacturing Engineering

Parsons Building

Trinity College

Dublin 2

Ireland

June 2019

DECLARATION

I declare that this thesis has not been submitted as an exercise for a degree at this or any other university and it is entirely my own work.

I agree to deposit this thesis in the University's open access institutional repository or allow the library to do so on my behalf, subject to Irish Copyright Legislation and Trinity College Library conditions of use and acknowledgement.

_____

Michael Cullinan, June 2019

RESEARCH QUESTION

Through a scientific understanding of the working principle of pneumatic artificial muscles, how can these actuators be made a compelling proposition for human-friendly mobile service robots.

SUMMARY

Developing robotic systems which can operate in complex, human centred environments is a major challenge, but one which holds the promise of dramatically improving human living standards in several areas including manufacturing/assembly, the service industry, elder care and domestic assistance. In such applications it will be necessary for machines not only to work in the same space as people, but also to interact with them, often involving physical contact. This raises many concerns regarding the safe operation of such robots and how it can be guaranteed. Of crucial importance is the actuation method used to control such a robot. The actuation paradigms which have been established for industrial robots (high stiffness, accuracy etc.) are altered for this application, with inherent compliance, light weight, small size and energy efficiency becoming more significant.

Pneumatic artificial muscles (PAMs) are a powerful class of actuator with highly advantageous properties for physical human-robot interaction. They can exert large forces, while being lightweight. They are also inherently compliant and can be manufactured relatively cheaply in a range of sizes. However, due to their inherent inefficiencies, the requirement for a compressed air supply, limited contraction and difficulties in modelling and control, they have not frequently been used for mobile service robots. The sleeve PAM addresses some of these shortcomings by incorporating a solid internal structure which reduces the volume which must be filled with compressed air while increasing the force output and contraction ratio.

This thesis proposes design improvements to the sleeve PAM which is applied to the case of the McKibben type muscle. The modular nature of the design simplifies manufacture and makes it more adaptable for various implementations. The design also allows force output along the central axis of the PAM which simplifies system integration. Efficiency was also improved over that of the previous implementation due to a greater proportion of the volume being occupied by the internal element. In order to alter the force/contraction characteristics of the PAM an optional internal pulley mechanism was installed in the PAM which may be useful in applications where space is at a premium.

A dynamic testing apparatus was constructed in order to further characterise and model the sleeve PAM under a variety of operating conditions. The bandwidth of sleeve and traditional PAMs were compared. Under isometric conditions the pressure bandwidth with no contraction was increased by approximately 100%. When the muscle contracts this improvement gradually reduces as the proportion of the volume of the PAM which is occupied by the internal element decreases. When the force bandwidth of the actuator is tested under similar conditions there is a further 20% increase in bandwidth across the range of contraction due to the lower pressure required to achieve the same force output. Testing with a constant force profile as the PAM contracts showed a more modest increase in bandwidth.

A phenomenological dynamic model of the traditional and sleeve PAM was constructed based upon a popular existing model in order to further understand the differences between both muscles and facilitate control. This model was fitted to the PAMs using both static and dynamic tests. An empirical model of the PAMs' volume was also constructed based on the measurement of pressure change in the PAMs as they contract or elongate under closed system conditions. Combining these models with an established model of gas flow through control valves it was possible to accurately predict the behaviour of both the PAMs.

The use of sleeve PAMs in an antagonistic configuration to operate a revolute joint is also investigated. Comparing a traditionally actuated joint with two configurations of a sleeve PAM it is shown that the torque can be increased by between 25% and 100% (depending on joint angle/direction) or the joint range can be increased by 14%. While isobaric stiffness is comparable, closed system stiffness is increased by up to 300% using sleeve PAMs. A theoretical energy analysis of the operation of PAM actuated joints is presented which show substantial energy savings when sleeve PAMs are used.

PUBLICATIONS

The following publications have been produced over the course of this PhD:

"Towards an embodied system-Level architecture for mobile robots", Conor McGinn, Michael Francis Cullinan, George Walsh, Cian Donavan, Kevin Kelly; International Conference on Advanced Robotics (ICAR), 2015. pp. 536-542. doi: 10.1109/ICAR.2015.7251508

"A McKibben Type Sleeve Pneumatic Muscle and Integrated Mechanism for Improved Stroke Length", Michael F. Cullinan, Eamonn Bourke, Kevin Kelly, Conor McGinn; Journal of Mechanisms and Robotics, 2017. Volume 9, Issue 1: pp. 011013-011013-9. doi:10.1115/1.4035496

"A human-oriented framework for developing assistive service robots", Conor McGinn, Michael F. Cullinan, Mark Culleton, Kevin Kelly; Disability and Rehabilitation: Assistive Technology, 2017. Volume 13, Issue 3: pp. 293-304. doi: 10.1080/17483107.2017.

"Design of a terrain adaptive wheeled robot for human-orientated environments", Conor McGinn, Michael F. Cullinan, Moyin Otubela, Kevin Kelly; Autonomous Robots, 2018. Volume 43, Issue 1: pp. 63-78. Doi: 10.1007/s10514-018-9701-1

"Dynamic characterization and phenomenological modelling of sleeve pneumatic artificial muscles", Michael F. Cullinan, Eamonn Bourke, Kevin Kelly, Conor McGinn; Journal of Dynamic Systems, Measurement and Control, 2019 [under review].

"Sleeve Pneumatic Artificial Muscles for Antagonistically Actuated Joints", Michael F. Cullinan, Conor McGinn, Kevin Kelly; International Conference of Robotics and Automation (ICRA), 2019

ACKNOWLEDGEMENTS

The work presented in this thesis would not have been possible without the guidance, encouragement and trust granted to me by a large number of people.

Firstly, to my family who have always believed in me and supported me through my education and upbringing more generally. I could not hope to have had a better start in life and there is no doubt that I could not have done any of this without you. From the beginning you encouraged me to follow my own path and reach my potential. Thank you for everything you have done for me. To my mother, Marie, you have given me some of the best advice in guiding my efforts in life. I can only imagine what more I could have done if I had followed your words more closely. To my father, Denis, thank you for introducing me to engineering and giving me that questioning attitude to the world around me. I am still in awe of your knowledge in so many fields. To my sister, Mary-Ellen, for the kind words and the laughs, thank you. As a companion through childhood no one else could come close. Keep on doing amazing things

A constant source of insight, amusement and distraction, my colleagues in the Robotics and Innovation Lab have been a defining feature of the past four years. Thank you all for putting up with my terrible jokes and messy desk. Eamonn Bourke, you are one of the finest designers anyone could find. With your carefully calibrated eye and ability to reduce the complex to merely a series of chances to be taken, you have seen many improbable projects through to completion. Patrick Lynch, while coping with the greatest magnitude of minor misfortunes, you contribute massively to those around you with innovative ideas and a manner which is both welcoming and insightful. Thank you for being there all those weekends and late nights. The tightest bond in the history of social entrepreneurship is surely that between Robbie Fryers and Talita Saad. Robbie Fryers, you are one of the strangest people I have ever met. What goes on in your head is complex beyond my understanding but what you have achieved speaks for itself. Thank you for all the laughs we shared. Talita, if everyone was as conscientious, driven and brave as you the world would have already figured out how to integrate people with intellectual disabilities and a great many other things. Thank you for being there to talk with, to debate and to educate us all. Vanessa

Nappi, thank you for tolerating everything that happens in our office. You are the voice of reason in what would otherwise be a dysfunctional mess. Your good nature, helpfulness and forthright opinions made working with you very special. It was an honour to teach alongside you. Cian Donovan, for someone who makes a habit of turning up at 4pm, you have been a (sometimes shaky) pillar of what we do. Your passion, desire to know all you can and commitment to build the very best systems you can is a shining example of what all young engineers should aspire to. Andrew Murtagh, while we may never agree on the optimum level of tidiness there is no doubt that however you arrange your environment it certainly works. You are inspirational in what you achieve. Thank you for helping all of us with your skills. Moyin Otubela, if I do graduate there will probably be free food after the ceremony so you should come along. As the one who will hopefully continue this research in one form or another I can only wish you well. Aran Sena, you may have moved onto bigger and better things but your time here will always be remembered fondly. For your expertise and willingness to help all those around you, thank you. Mark Culleton, though our time working together was short, in gave me some warning as to difficulties faced as a PhD draws to a close. I only wish I could have learned more.

I have had the great honour to work alongside several talented masters and undergraduate students over the course of this work. Working on projects with them helped me to view problems differently and find new solutions. While they may have been students through our shared experience I learned just as much. In particular, Eamonn Bourke, for all of the work we did together around the design of the sleeve PAM, thank you. Collaborating with you has been rewarding and insightful. Satish Reddy, thank you for your assistance in the design of the testing apparatus. Your design instincts served us well. Tyron Pretorious, your help in constructing the testing apparatus and initial testing was invaluable. Your dedication to your project as well as enhancing the environment for everyone around you was immense and certainly aided in the work presented here.

The environment in which I completed this work had a major effect on the ultimate outcome. The department of Mechanical and Manufacturing Engineering has been

like a second home to me and I would like to thank everyone who works there. In particular, all of the workshop technicians who assisted in the manufacture of the various aspects of this work. Also, to the wider college community and specifically the rifle club where I have happily been a member for many years. This club brings out the best in people and allows them to develop into confident, responsible adults. Though many people make this club great it would not be what it has become without the tireless work of Siobhan Scarlett. Thank you for your incredible effort which benefits so many.

My supervisor, Prof. Kevin Kelly, has been my greatest advocate over the course of this study and indeed before. Thank you for giving me the opportunity to conduct this research and the support you have provided me throughout. You have given me the guidance I required, while trusting me to make key decisions about the project. Thank you also for creating the environment in which I have had the honour to work. Your belief in students and commitment to providing them with what they need to reach their potential has greatly enhanced generations of engineers. Also, Prof. Conor McGinn, for his technical guidance and advice I am most grateful. Thank you for giving me the motivation to make decisions when I may have otherwise wavered on the fence between different options. Your energy and dedication to robotics, as well as the encouragement you give others in their pursuit of research in this field will no doubt yield bountiful reward.

CONTENTS

LIST OF FIGURES

LIST OF TABLES

NOMENCLATURE

ACRONYMS

AC	Alternating Current
ADC	Analogue to Digital Converter
CAD	Computer Aided Design
DC	Direct Current
DOF	Degrees of Freedom
HRI	Human Robot Interaction
I^2C	Inter-Integrated Circuit
LDPE	Low Density Polyethylene
MOSFET	Metal-Oxide-Semiconductor Field-Effect Transistor
PAM	Pneumatic Artificial Muscle
PET	Polyethylene terephthalate
pHRI	physical Human Robot Interaction
PID	Proportional Integral Derivative
PPAM	Pleated Pneumatic Artificial Muscle
PSU	Power Supply Unit
PVC	Polyvinyl Chloride
PWM	Pulse Width Modulation
ROS	Robot Operating System
SEA	Series Elastic Actuator
SPI	Serial Peripheral Interface
USB	Universal Serial Bus
VIA	Variable Impedance Actuator
VSA	Variable Stiffness Actuator

OPERATORS

a_i	Model constant found experimentally
b	Length of individual PAM braid fibres
B	Phenomenological PAM model damping coefficient
b_p	Critical back-pressure ratio of a valve
b_i	Model constant found experimentally
c	Viscous damping coefficient
C	Sonic conductance of a valve
c_i	Model constant found experimentally
d	Diameter of mass on link
D_p	Pulley diameter
D	PAM diameter
dr	Inner surface displacement of PAM
ds	Area vector of PAM
D_1	Diameter of internal element in sleeve PAM
$D_{45°}$	PAM diameter when the braid is at a braid angle of 45°
D_{90}	PAM diameter when the braid is at a braid angle of 90°
E	Energy
E_y	Modulus of elasticity
F	Force
F_A	Phenomenological PAM model applied force
F_{ce}	Phenomenological PAM model contractile force
I	Second moment of area
J_0	Second moment of inertia
k	Linear spring stiffness
K	Phenomenological PAM model spring constant
L	Active PAM length
L_t	Supply tube length
m	Mass of air in a PAM
m_a	Mass of actuator

M	Bending moment
n	The number of times each fibre in a PAM braid wraps around the PAM
P	Absolute pressure
p_n	Magnitude of nth peak/trough during oscillation
P'	Gauge pressure
Q	Volumetric flow rate
R	Individual gas constant for air
r_p	Pulley radius
r_t	Supply tube radius
s	Actuator stroke
S	Surface area of the PAM
t	Thickness of mass on link
T_0	Temperature of air under standard reference atmosphere
V	PAM volume
w	Link mass
W	Work
x_{0A}	x position of actuator A of antagonistically actuated joint
x_{0B}	x position of actuator B of antagonistically actuated joint
y	PAM contraction
α	The ratio of specific heats for a gas undergoing some process
β	Joint angle
β_{range}	Range of joint rotation
δ	Logarithmic decrement of the decay
ε	PAM strain
η	Viscosity
θ	Braid angle
κ	Joint stiffness
λ	Angle of deflection of bending beam
ζ	Damping ratio
ρ_0	Density of air under standard reference atmosphere
τ	Torque

Subscripts

$down$	Down stream
i	Integer value to differentiate related constants
in	Into system
out	Out of system
SM	Traditional PAM
TM	Traditional PAM
up	Up stream

Actuator

A device which converts energy to mechanical form.

Agonist Actuator

In an antagonistically actuated joint, this is the actuator which provides the main force/torque output.

Antagonist actuator

In an antagonistically actuated joint, this is the actuator which acts against the agonist PAM.

Antagonistic actuation

An antagonistically actuated joint has an actuator for each direction of movement. For a typical resolute joint this means one two actuators are used, with one moving the joint clockwise and the other anticlockwise.

Compliance

The inverse of stiffness. The amount of deformation or deflection of a body due to the applied load. In particular compliant actuation allows deflection of the actuated joint in response to loading.

Cutoff frequency

The cutoff frequency, corner frequency, or break frequency is a boundary in a system's frequency response at which energy flowing through the system begins to be reduced (attenuated or reflected) rather than passing through. Most frequently the 3dB point is used, that is when the signal amplitude reduces by 3dB or half the power in the passband.

Dead space

The internal volume of a pneumatic muscle which is contained between the two end fittings. The pressure here does not contribute to the force output of the PAM.

Degrees of freedom (DOF)

The degrees of freedom (DOF) of a system are the number of independent parameters that describe its configuration. The degrees of freedom of a robot typically corresponds with the number of actuated joints or controllable degrees of freedom (CDOF) it possesses.

End fitting

The part of a PAM which seals each end of the cylindrical bladder and holds the braid. Typically the end fittings are attached to the system being actuated and compressed air enters and leaves through one of them.

Human–Friendly robot

A robot which can operate safely in close proximity to people.

Human-robot interaction (HRI)

The field of HRI studies the interactions between humans and robots. HRI is a multidisciplinary field with contributions from areas including human computer interaction, artificial intelligence, robotics, natural language understanding, design, and social sciences.

Inherent compliance

Refers to those actuation technologies which are compliant by their nature/working principle.

McKibben PAM

Also known as braided PAM. A type of PAM consisting of an inflatable bladder surrounded by a braid with fibres arranged helically. When inflated, the bladder

pushes out on the fibres causing the PAM to expand radially. As the fibres are stiff (but flexible), this results in contraction.

Muscle-like actuator/Artificial muscle

An actuator which behaves in a similar way to skeletal muscle. It generates a force in response to a stimulus which results in a contraction. The position/contraction is stable in the open loop, i.e. with a constant stimulus and applied load contraction is stable. This differs from actuators such as electric motors whose velocity is stable in the open loop.

Phenomenological Model

A scientific model that describes the empirical relationship of phenomena to each other, in a way which is consistent with fundamental theory, but is not directly derived from theory.

Physical human-robot interaction (pHRI)

HRI involving physical contact between the robot and people

Pneumatic Artificial Muscle (PAM)

An artificial muscle which operates using compressed air.

Sleeve PAM

A PAM with a rigid internal element which reduces the dead space in the PAM. This internal element is attached to one end fitting and protrudes through the other end fitting (called the sliding end fitting). When the PAM contracts, the sliding end fitting moves along the internal element.

Service Robot

According to the International Federation of Robotics (IFR), robots that perform useful tasks for people (excluding industrial applications) are broadly known as

‘service robots’. Service robots can be subcategorised into personal or professional service robots.

1 INTRODUCTION

1.1 MOTIVATION AND CHALLENGES

Robots have long been a feature of the industrial environment, where their precision, speed and resilience has the capacity to drastically increase productivity. However, increasingly it is becoming desirable to remove the barriers between man and machine, facilitating collaborative operation, in a shared physical space, both in professional and domestic environments [1]. A host of technical challenges exist on the path to this goal, not least the actuation technology used to control the movement of the limbs of such robots in order to facilitate physical human-robot interaction (pHRI). Additional performance criteria must be considered, such as safety when working with people and power efficiency for mobile platforms which must move about their environment [2], [3]. Simple roles such as floor cleaning [4] and lawn cutting [5] can now be performed autonomously, however creating general purpose robots that can interact in a more holistic way with their environment and the people in it is still far from a reality [6]. While robots of this sort have been developed as research platforms, few have been commercialised, perhaps due to the costs and risks involved [7].

In order to meet these challenges, novel means of actuation must be considered. Electric motors have been the norm for industrial applications [8]. These can be accurately controlled and are capable of high frequency movement. However the stiff nature of the actuation technique together with the large mass of the actuators results in significant inertial forces, making them disadvantageous for use on robotic applications which operate in close proximity to humans [2], [9]. A different actuation technique is required which delivers compliant properties with a large force to mass ratio.

Pneumatic Artificial Muscles (PAMs) are a promising actuation technique for robotic systems, in particular those which work collaboratively with humans[10]–[12]. They are capable of delivering large driving forces while being lightweight, facilitating the development of actuated assemblies with low inertia[13]–[16]. PAMs are inherently compliant due to the compressible nature of their driving fluid (usually air) making them safer and more adaptive to unstructured environments. The similarities in performance

between human muscles and PAMs is highly advantageous in applications such as exoskeletons and rehabilitation devices that are closely physically coupled to humans[17]–[21]. Additionally the actuator may be manufactured relatively cheaply and is easily adapted to a range of applications by adjusting the length, diameter and other actuator properties [22], [23].

Despite their favourable characteristics, PAMs have yet to see widespread use in mobile service robots (robots which can move around their environment while performing tasks which assist humans). There are several reasons for this. Firstly, PAMs are more difficult to control than other actuation techniques due to their compliance and nonlinear force/contraction relationship. They also require a compressed air supply which are typically heavy, bulky and noisy. Efficiency is also an issue, with PAMs consuming a lot more energy than electromechanical systems due to inefficiencies in producing compressed air and in converting that energy to mechanical work at the PAM. Additionally, due to the limited contraction of PAMs they can be difficult to accommodate on robotic systems. In order for PAMs to be viewed as a compelling actuator for service robots these issues must be addressed.

1.2 RESEARCH OBJECTIVES

The aim of this project was to develop a PAM which is more suitable for use on mobile service robots for human-centred environments by addressing some of their fundamental shortcomings. This requires an evaluation of the characteristics of such an actuator and what is needed for them to be of practical use in this context. To advance the state of the art in PAM technology, a scientific understanding of their operation must be developed. By analysing their working principle, it is possible to identify inefficiencies and ways in which these may be overcome. Through this process it is hypothesised that structural changes to the actuator can be instrumental in improving performance characteristics. In order to test this hypothesis, a theoretical model of the effect of the proposed modification must be developed, before this can be confirmed experimentally. This experimental validation necessitates a comparison with the traditional (unmodified) actuator under both static and dynamic conditions. Parameters such as the force output which is possible at every stage of contraction, the compressed air

consumption, the upper limit on bandwidth and the range of possible stiffness must be evaluated. Further, for the modified PAM to be of practical use, robust modelling techniques must be developed and applied to the actuator.

Concretely, the objectives of this thesis are to:

- Understand the requirements of an actuator for use on human-friendly, mobile robots.
- Develop a scientific understanding of the operation of PAMs and their fundamental characteristics.
- Using this knowledge, develop a PAM which better meets the requirements of human-friendly mobile robots.
- Analyse the behaviour of such a PAM under static and dynamic conditions and compare this to the traditional actuator.
- Develop modelling techniques for such an actuator which can enable further theoretical characterisation and control of the PAM.

1.3 OVERVIEW

A review of pHRI in service robots is presented in Chapter 2, which outlines the importance of this growing field of robotics. Emphasis is placed on the actuation requirements of such systems with regards to safety and adaptability for their environment. Pneumatic artificial muscles are examined as a possible solution including previous implementations of such actuators, their operating principle and problems which must be resolved in order to motivate their use in a greater range of applications.

In chapter 3, the sleeve PAM is introduced as a basis for development in this area. The design of a new sleeve PAM is proposed. Making use of the McKibben type PAM affords significant design freedoms in the selection of materials and actuator dimensions. This allows a number of key design objectives to be met, and the implementation of the solution is described. Chapter 4 presents static characterisation of the new PAM, and a comparison is made with the traditional PAM. The force output at each contraction is examined as well as the range of contraction, efficiency and hysteresis. Structural changes designed to alter the torque contraction profile are also tested.

In order to conduct further testing of the PAM, particularly dynamic testing and antagonistic actuation of a joint, a testing apparatus is developed. This has the capability to regulate and measure the pressure to up to two PAMs, while simultaneously measuring their individual force output and contraction or joint rotation. This is subsequently used in chapter 6 to establish the improvements in dynamic response which are possible with the new PAM design. The maximum bandwidth of the actuator is evaluated under number of operating conditions. Chapter 7 advances a dynamic model of both the sleeve and traditional PAMs, using an adapted version of a phenomenological model widely used in the literature. This is combined with an experimental procedure to generate a model of PAM volume and an established model of gas flow through a valve to accurately predict the contraction of the new PAM.

Chapter 8 applies this model to the case of a joint actuated antagonistically with two sleeve PAMs. This, together with experimental results allow a comparison to be made with the same joint actuated with traditional PAMs. Torque capacity, stiffness under isobaric and closed system conditions, damping and energy efficiency are compared. Chapter 9 discusses the conclusions which may be drawn from this work as well as identifying areas for future work.

1.4 CONTRIBUTIONS OF THIS THESIS

This thesis proposes an updated design of the sleeve pneumatic artificial muscle which offers a number of advantages over previous designs; as well as comprehensive testing on this actuator under dynamic conditions and experimental modelling. Further, the advantages of the sleeve PAM are applied to an antagonistically actuated joint. More concretely:

1. A new design of a sleeve PAM which:
    - Applies the concept to the McKibben type PAM for the first time.
    - Increases the proportion of the ‘dead space’ occupied by the sleeve and consequently:
        - Increases efficiency

- Increases force output
- Increases maximum contraction
- Includes a mechanism to alter the force contraction profile.
- Improves modularity
- Simplifies system integration by allowing force output through the axial central axis
- Improves resistance to dust ingress and damage at the sliding seal
- Facilitates pressure sensor integration

2. Bandwidth testing of individual traditional and sleeve muscles shows:
   - Under isometric conditions, the maximum frequency of operation is increased by
     - up to 100% if pressure is considered as the output
     - up to 120% if force is considered as the output
   - Under constant force profile operation, the sleeve PAM showed a modest improvement in contraction bandwidth.
3. A phenomenological model is adapted and applied to traditional and sleeve PAMs. The model consists of a contractile force, spring and damping element.
   - The model is modified to include a dependence of the spring constant on contraction.
4. The model is applied to both PAM types using an alternative testing procedure than previously employed.
   - The contractile and spring element are characterised from static tests whereby the PAM contracts freely and is then extended by an applied force before being allowed to contract isobarically.
   - The damping coefficient is determined with the PAM acting against a constant force profile with step changes in muscle pressure.
   - Muscle volume is modelled experimentally, by forcing muscle elongation with the PAM operating as a closed system (no air in or out). Pressure changes can then be related to volume change.
5. Antagonistic PAM operation with traditional and sleeve PAMs is also evaluated and shows:

- Sleeve actuated joints can have 13% greater range or up to 50% greater torque than comparable traditional muscle actuated joints depending on their configuration.
- The stiffness of the sleeve PAM actuated joints when acting as a closed system is greater than that of a comparable standard PAM actuated joint.
- Damping of the sleeve muscle actuated joint is 50% greater than the traditional PAM actuated joint. There is no apparent dependence on PAM pressure or contraction.
- Energy use is analysed theoretically for the antagonistic case using the model previously developed and a methodology adopted from the literature for arbitrary joint movements. This showed the sleeve PAM offers considerable energy savings which are dependent on the joint configuration.

2 LITERATURE REVIEW

In order to establish the requirements of actuation systems for mobile service robots to operate in a human-friendly way, the state of the art in this area is examined, including the current research in service robotics, safety considerations and the actuation techniques commonly in use. Once the rationale for pursuing pneumatic artificial muscles (PAM) is evident, this actuator is reviewed in some detail regarding the different type of actuator commonly employed, its current applications, characteristics, and modelling.

2.1 SERVICE ROBOTS

The International standards organisation defines a service robots as one “that performs useful tasks for humans or equipment excluding industrial automation applications” [24]. This categorisation can be further subdivided into personal service robots (“used for a non-commercial task, usually by lay persons”) and professional service robots (“used for a commercial task, usually operated by a properly trained operator”). The market for service robots continues to expand. In 2016 the total number of professional service robots sold worldwide increased by 24% from the previous year (up to 59706 units) [25]. The main applications are logistics systems, defence robots, field robots (milking robots), public relations robots, powered human exoskeletons and medical robots. Similarly there was a 25% increase in the sale of personal service robots between 2015 and 2016 (up to 4.6 million units). Typical applications include vacuum and floor cleaning, lawn-mowing robots, and entertainment and leisure robots, including toy robots, hobby systems, education and research.

A large number of robots have been developed which attempt to address the requirements of a general-purpose mobile service robot. A subset of these are examined here in more detail to better understand the state of the art in this field.

2.1.1 EXAMPLES OF MOBILE SERVICE ROBOTS

Care-o-bot 4

Developed by the Fraunhofer Institute for Manufacturing Engineering and Automation IPA, Care-o-bot 4 is the fourth generation of a family of personal robots [26]. These robots

are designed to be used in a range of environments including households, hotels, care homes and hospitals. While previous generations of the robot were aimed mainly at technical advancement, Care-o-bot 4 was built with a view to commercialisation, with a modular product family. The vision for the Care-o-bot project is to create an "electronic butler"; friendly and helpful, but in the background and discrete. The robot retains a close alignment with the human form, possessing an identifiable head and arms (see Figure 2-1). It was important to the designers however, that the robot would not become too human as this would "encourage false expectations with regard to its capabilities".

Due to its modularity, Care-o-bot 4 can be configured for a variety of tasks[27]. It can operate solely as a moveable platform, and function as a serving trolley or porter. A body and head may be added to enable social interaction with a user and applications such as museum guide or offering assistance in DIY stores and airports. A Care-o-bot with the alias "Paul" has been operating as a "charming helper" in Saturn-Markt Ingolstadt since the end of October 2016 (see Figure 2-1) [28]. The robot accompanies customers through the store and directs them to the relevant shelves. Additionally, up to two arms may be added to allow the robot to perform pick and place operations.

Actuation of the robot is achieved using ball joints in the torso and Schunk PowerBalls in the arms [29]. These electric motor actuators are compact and provide a large amount of controllability. The arms offer a payload capacity of 5Kg while weighing 13.9Kg themselves. These motors are however not compliant in nature and though sensing can provide some protections should a collision occur, in general the Care-o-bot must rely on its sensors to avoid these.

(a) (b)

Figure 2-1: Care-o-bot 4 configured with torso, head and arms [27]***(a) and operating in Saturn-Markt*** [28] ***(b).***

Robear

The nursing-care assistant robot “Robear” was developed by RIKEN-SRK Collaboration Centre for Human-Interactive Robot Research (see Figure 2-2) [30]. It is the third generation of robot developed in response to the growing elderly population in Japan and the shrinking numbers of people available to care for them. It is especially aimed at providing assistance when lifting patients, for example in and out of a wheel chair or bed. Robear stands at a height of 1.5 m and weighs 140Kg, which is considerably lighter than its predecessor, RIBA II [31]. A lighter robot is safer for operation with humans as the risk from the robot falling is not as great. It also improves battery life allowing Robear to operate for about 4 hours on a single battery charge.

Using both arms Robear can lift 80Kg using AC stepper motors [31]. The choice of stepper motors means the robot’s movement is rigid, although a low gearing ratio allows the joints to be back drivable [32]. The designers have mitigated against the potential risk to

users by using padding on the robot's arms, using torque sensing on the joints and smart rubber capacitive type tactile sensors.

Robots such as Robear can greatly reduce the workload and stress on those who care for the elderly or disabled by reducing the effort required to manoeuvre the person. As this task would typically place large physical strain on the carer, Robear can make their working environment safer. Robear is as yet a research platform and will not be used in real applications. Robots which can exert such large forces and operate in close proximity to humans are few, owing perhaps to cost and safety concerns should the robot lose control.

Figure 2-2: Robear lifting a human [30].

PR2

The PR2 (see Figure 2-3) was developed as a mobile manipulation platform, designed to make robotic software development easy [33]. More specifically its developers, Willow Garage, wanted a platform which could be used by multiple research institutions to develop the Robot Operating System (ROS). This open source software aims to provide functionality for robotics, without individual researchers needing to re-implement

functionality already developed elsewhere. This greatly increases the productivity and rate of development of the robotics community.

The PR2 was designed to be suitable for a variety of applications and work in environments built for humans [34]. These include:

- In an industrial setting where repetitive tasks must be completed. Applications such as taking inventory, manufacture and assembly are suggested.
- In the home, to complete operations such as setting the table, emptying a dishwasher doing laundry or making meals.

This required a platform which can move through spaces typically occupied by humans. The PR2 achieves this by having a footprint similar to that of a wheelchair and omnidirectional wheels, which allow it to move in any direction in its environment. Additionally a suite of sensors including a Microsoft Kinect, multiple stereo cameras, accelerometers and laser scanners allow the robot to perceive its environment so that accurate models can be built from it [35]. The modular nature of the PR2 design allows the platform to be configured for a particular application. The number of arms, the component parts of the arm and the head and sensors, can all be changed with relative ease.

PR2 is actuated with back drivable electric motors [35]. These allow the robot to operate in unstructured environments, as the arms can react with obstacles they come in contact with. A spring counterbalance is used so that the arms “float” even when power is off. This feature allows the motors used in the arms to be quite small, as they do not need to lift the mass of the arm, only the payload. Using smaller motors means they do not have the power to do as much damage as they might if a different actuation system was used. While this approach improves safety, it does limit the payload of the robot substantially (4 lbs). The mass of the overall system is also a potential cause for concern. At 220Kg [36], should the robot fall it has the possibility to cause significant injury.

The PR2 provides a sensor rich platform with which researchers can collaboratively develop the algorithms and software necessary for mobile service robots. It is however lacking when actual user interaction is required. Its large mass and low payload limit its

working environment and capabilities. A price tag of $400,000 [37] underlies the fact that the PR2 is aimed at research institutions and not private individuals.

Figure 2-3: The PR2 robot [34]***.***

Honda ASIMO

Differing from the other robots examined here, ASIMO is a bipedal humanoid robot. It was developed by Honda to work in environments made for humans, from office spaces to the home, its humanoid morphology giving it a clear advantage in these spaces [38]. Currently in its fifth generation of development (and coming from a long line of humanoid research in Honda going back to the mid-1980s), ASIMO has been used as a research platform [39] and to introduce the public to the concept of robots in daily life [40], [41].

ASIMO features high physical capabilities which allow it to perform actions such as running (up to 9 km/hour) , going up and down stairs, walking over uneven ground (see Figure 2-4) pouring from a bottle and kicking a ball [41]. This is made possible due to the 57 degrees of freedom on the robot which allow natural movement. For a robot with a mass of 48Kg and height of 130cm this is very impressive [42].

ASIMO uses electric motors with harmonic gearing for actuation [43]. Harmonic gearing provides a small lightweight method to greatly increase the torque output from the

motors. However harmonic gears are not back drivable, meaning compliance is more difficult to achieve. There have been attempts to introduce compliance on ASIMO using torque control with favourable results [43]. This relies on sensor feedback to adjust the current supplied to the motors and so is not as robust as an inherently compliant technology.

ASIMO has been successful in sparking an interest in robotics across the world. Its capabilities, especially in terms of dynamic movement, are highly impressive. However, the lack of inherent compliance limits the trust which can be placed in the system and its ability to react to unstructured environments. ASIMO also has a relatively low payload capacity of just 300g per arm[42], severely limiting the range of tasks it can complete.

Figure 2-4: ASIMO walks on uneven ground [42]***.***

2.1.2 SAFETY IN HUMAN ROBOT INTERACTION

The major requirement for robots that operate in close proximity to humans is safety [44]. Traditionally robots in the industrial setting have been isolated from humans, separated by cages, laser fencing and visual acoustic signals to warn of their operation [45]. These robots have been optimised for speed of execution, high accuracy and high repeatability, however their weight, high speeds and stiff characteristics make them hazardous to humans with the potential to cause serious injury or death [9], [46].

A number of authors have identified risks associated with robots in human centred environments. Achieving safety for pHRI under these conditions is a complex problem with many approaches which must work in parallel[47]. A compressive list of hazards is

available in the international standard for Safety Requirements for Personal Care Robots[48], however by far the greatest safety risk to users is that of unintended collisions with the robot. Figure 2-5 illustrates range of areas of interest for pHRI. Naturally, it is most desirable that sensing and planning in combination with robust control be used in order to prevent any unwanted collisions between the robot and its environment or people within it. Non-contact proximity and depth sensors[49], [50] as well as vision systems [51] may be employed for this purpose. In addition, should a collision occur it is necessary for the robot to detect this to be able to respond to it. While force and torque sensors are commonly used for this purpose they can usually only detect collisions which occur on certain parts of the robot such as the end effector. Instead, tactile sensing may be used which can be mounted on various parts of the robot [52].

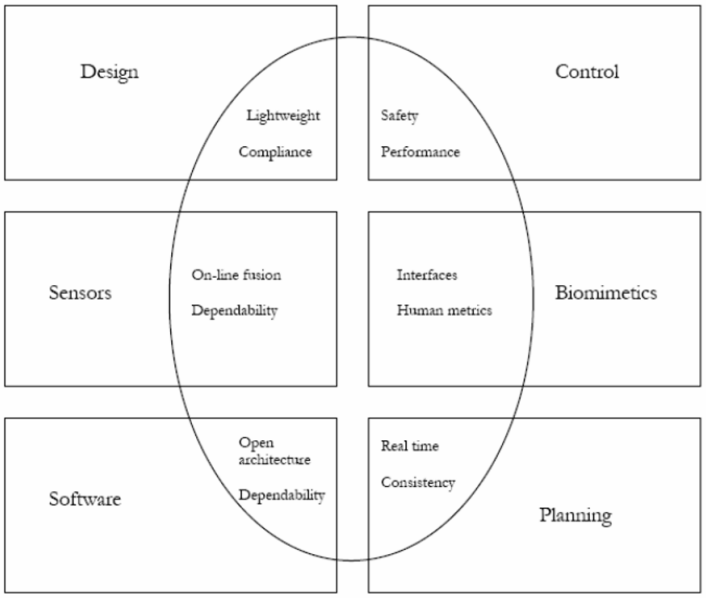

Figure 2-5: Map of areas relating to physical human robot interaction [47].

While sensing and active control certainly have a large role to play, it is the physical characteristics of the robot system which ultimately limits the safety of the robot due to the inherent safety it assures should a collision occur [47], [53]. Perception is very difficult in human centred environments specifically because the presence of humans and items they bring to the environment make it unpredictable[45], [47]. Even the most advanced perception and control systems may malfunction leading to the robot acting erroneously [44], [45], [54]. Not only this, but even if the robot does sense its environment correctly,

it must also draw the correct inferences from this data. Consider Figure 2-6 which contrasts the idealised kitchen environment to the complexity of a real world environment, where variable lighting, clutter and unknown objects are a challenge [55]. Robots built to operate in these environments must be able to safely recover from errors in interpreting their surroundings. As noted in [53], this has lead robotics in this area to move from the classic industrial paradigm "rigidity by design, safety by sensors and control", to "safety by design, performance by control" philosophy.

Figure 2-6: An idealised kitchen environment (left) where traditional model-based approaches to robot manipulation and safety are appropriate and the alternative real-world environment (right) where perception and model building is more difficult [55]***.***

Unexpected collisions between a robot and a user fall into a number of categories including blunt unconstrained impacts, blunt constrained impacts and sharp impacts (these are examined in more detail in Appendix A). A summary of the robot characteristics which are relevant to these collisions are shown in Figure 2-7 [56]. Naturally the means of actuation has a large bearing on the safety characteristics of any such system. Compliance is especially important if the robot is operating close to its singularity (limit of robot reach where the joints are almost straight), where clamping is a possibility and where a tool is in use under dynamic conditions. Robot mass is important for all dynamic conditions as is the robot velocity.

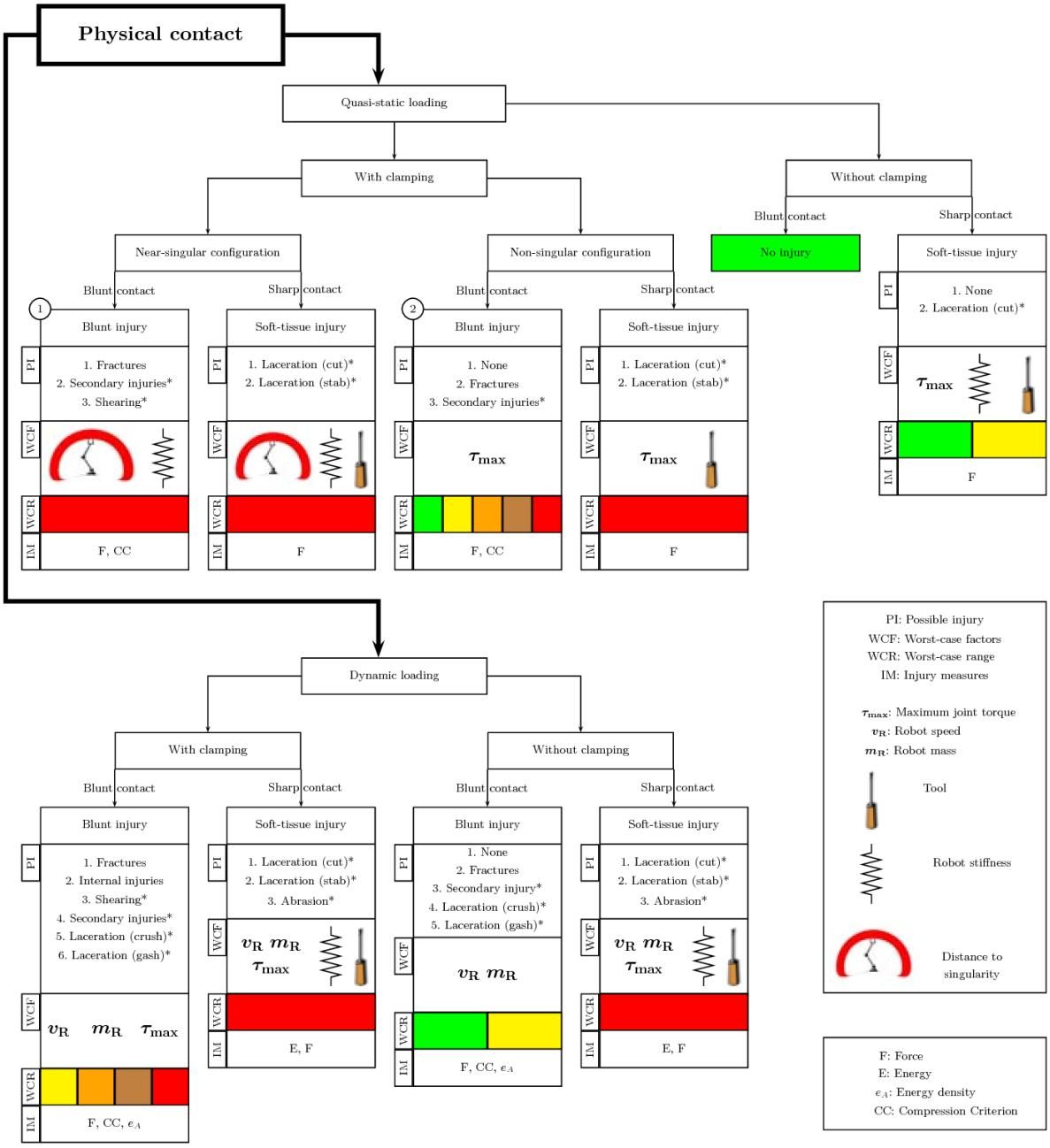

Figure 2-7: Summary of the relevant manipulator properties for various types of human-robot collisions. (PI) is possible injury, (WCF)are major worst-case factors and (WCR) is the possible worst-case range. From [56]***.***

The main aspects of robot physical design which affect robot safety during impacts are mass, system compliance, cover compliance, shape and surface friction [57], [58]. Manipulators with more mass are slower to stop should an imminent collision be detected, and for dynamic impacts, impart greater forces to the human (although there is a saturation effect for unconstrained impacts). System compliance is usually achieved through compliance in the joints though small amounts are also present in robot limbs

themselves [1]. Compliance can reduce the effective mass of the manipulators, as it reduces the coupling between the link where the collision occurs and its parent links. In the case of static situations it can also limit the force and allow the robot to be manually manoeuvred. Compliant coverings on robots help to absorb the severity of impacts and spread the impact force over a greater area. This is similar to the robot shape which may be designed to contact the person over a larger area to distribute contact loads. The shape (or that of the tool being manipulated) can also lead to stabbing or cutting of a person in certain situations. Surface friction is rarely covered in the literature, but it is postulated that robots with low coefficient of friction coverings will remain in contact with the obstacle they collide with for a shorter period of time (the robot slipping by the obstacle), therefore reducing the force transferred [57], [58].

2.2 COMPARISON OF ACTUATORS FOR MOBILE SERVICE ROBOTS

The nature of the requirements of actuators for robots are dependent on the tasks they are intended for. For example, a number of tasks have been identified by researchers that would be desirable to be completed by a robot in the domestic setting. Christensen divides these into three main areas, entertainment, everyday tasks and assistance to elderly and handicapped [59]. These each require different “performance metrics”. The performance metrics of “entertainment applications” are least demanding. So long as the robot performs some interesting actions which keeps the user engaged, the need is satisfied. This presents little challenge for actuation technology as power requirements and forces are small and non-critical. Typical activities included in “everyday tasks” include vacuum cleaning, fetch-and-carry task, ironing clothes, window cleaning etc. These are demanding tasks as a result of the complex setting where they must be carried out. Finally, “robotic assistance to the elderly or disabled” has the performance metric of flexibility and ease of use. When the above requirements are analysed a number of key areas are identified which are major challenges to the future of domestic robotics. One of these is mobile manipulation which is required, to pick up objects from a range of areas. Flexible grippers are required to achieve this but those developed thus far are expensive or inadequate for the tasks required. Also considered is mobility. The robot

must be able to move around its environment under its own power without the needed to be tethered to a permanent power supply.

As section 2.1.1 illustrates, there is large variation in the methods used to actuate robots, even if only electric drives are considered. Other popular technologies to actuate mechanical systems include hydraulics and pneumatics. Removing the barriers between humans and machine requires a re-examination of the performance metrics we apply to actuation systems. For human-friendly robots, speed of operation is typically not required to be at the same level as industrial robots [60]. Likewise the requirements for spatial accuracy are typically less critical for service robots [44], [54]. As previously noted, safety is the most important criteria, and actuation has a role to play in meeting the safety requirements. Power consumption is also a key consideration for mobile robots which cannot easily be connected to a dependable power supply.

The following actuation parameters are considered important for mobile service robots. While a wide range of actuators have been proposed in the literature the focus here is on electric motors and pneumatic systems as these are the most widely researched and relatively mature technologies. Other muscle like actuators have been developed which, although experimental, may be useful for this application in the future. These actuators include electrostatic [61], [62], elastomer composite [63], [64], twisted fibre [65], [66], shape memory alloys [67], [68] and shape memory polymers[69] actuators .

2.2.1 LIGHTWEIGHT

Actuator mass, and the mass of the actuated system in general, is important for the payload capabilities of the robot, its efficiency and the inherent safety of the system. A large portion of the mass of a robotic system is composed of its actuators, increasing the torque requirements of the joints, reducing payload capacity and necessitating larger actuators[70]. Heavier actuators also tend to decrease energy efficiency as a larger mass must be displaced in order to achieve the same result. Furthermore, larger inertial forces limit the dynamic characteristics of manipulators in terms of speed and accuracy[71]. More importantly however are the safety implications of robots with a large mass. In the case of unconstrained impacts this is shown to be of less concern than might initially been thought as there is a saturation effect owing to the fact that the inertia of the object

impacted must resist that of the robotic system[72]. However, the likelihood of constrained impacts in unstructured environments is significant, making this an important consideration.

In order to compare the mass of actuation techniques the capability of each actuator must be taken into account such as the force they produce and speed of operation. Thus the power to mass ratio (often referred to as power to weight) may be used to compare alternatives. This is a product of the actuator force and velocity divided by the mass. Table 2-1 compares the power to mass ratios of a range of actuators. It should be noted however that these values do not account for the auxiliary equipment required for the actuators to operate such as pumps, valves, control systems etc. Hydraulic actuators are clearly extremely advantageous in this regard. Pneumatic artificial muscles also feature highly. There is a large variance in the values quoted reflecting the highly variable nature of the muscle characteristics based on its design. For example the materials used in the end fittings will greatly change the mass of the actuator. Caldwell et al. notes that the air flow rate is the most important factor when considering power to mass ratio in these actuators and so should be quoted as well, even though it is a property of the pneumatic system rather than the actuator itself [73].

Actuation type	Power to mass ratio kW/kg
Hydraulic	28[74]
Electromechanical	0.2[74]
Pneumatic cylinder DSN-25	0.1[75]
Pneumatic artificial muscle	0.8-2 with a 3 l/s flow rate[73], 5[76], 1[77]

Table 2-1: Power to mass comparison of popular actuation techniques.

Some researchers have suggested that power to mass ratio may not be the most appropriate metric for actuator comparison. For example the velocity of the actuator is not as significant a parameter in many applications. As an alternative, energy to mass ratio is proposed by Plettenburg [78] and defined as

$$Etm = \frac{\int F(s)ds}{m} \tag{2.1}$$

where $F(s)$ is the force output as a function stroke (s), and m is the actuator mass. Plettenburg points out that although very promising values of power to mass ratio are

presented in the literature for PAMs there is scant detail as to how they are calculated. It is unclear if the maximum or average force output and velocity are used. Using the energy to mass ratio it is shown that a 10mm diameter Festo muscle is superior by approximately 30% to other standard pneumatic actuators, though ultra-lightweight pneumatic cylinders can outperform all these by a factor of 10. Tavakoli et al. used the same criteria though adapted for joint rotation to allow comparison with electromechanical actuators with harmonic drive reductions [79]. Here $\tau.\alpha$, the product of torque and the angle through which the joint is required to rotate, is compared with mass. In contrast to joints actuated with electric motors, which can deliver the same torque at any point of rotation, those actuated with PAMs have reduced torques as the PAM approaches the end of its stroke. It was found that except for joints requiring quite small rotations (< 1 radian), the electric motor option provided a lower mass solution. Much of the reason for the poor performance of PAMs in this regard was the doubling in actuator mass required to operate the joint antagonistically. However this analysis does not consider the intrinsically compliant nature of PAMs. For applications where variable compliance is a requirement and an electric motor is used, it is necessary to have a second actuator to regulate joint stiffness (this is discussed further in the compliance section below). This greatly increases the mass of electromechanically actuated systems making PAMs a more appealing prospect in applications where variable compliance is a necessity.

Solutions have been offered to allow the use of relatively heavy actuators while keeping robot manipulators lightweight. These usually involves the use of cable driven systems; whereby the actuators are housed separately and move the system by means of cables [80]. However this approach creates control complexities due to the cable compliance and transmission elasticity [81]. The artificial Intelligence Laboratory in Stanford University aimed to overcome some of these challenges with the distributed macro–mini (DM^2) actuation system [82] whereby small, high frequency actuators (motors) are added at the cable actuated joint. Low frequency actuation for force or position control is achieved with the cable driven system, while the small actuators operate in parallel for disturbance rejection. However, heavy actuators must still be stored close by and occupy space here, a major disadvantage in a mobile robot. This and other considerations led

the research group to pursue pneumatic artificial muscles instead of the cable drive system [83].

2.2.2 ACTUATOR SIZE

Partially linked to actuator mass is the volume occupied by actuators. As robot systems are frequently complex with many degrees of freedom, in order to fit all the necessary actuators into a reasonable spatial footprint, the actuators must be relatively small. For example, the DLR hand arm system has a total of 26 degrees of freedom and 52 motors, all contained in in an anthropomorphic arm and part of an upper torso [84].

Volumetric power may be used to quantify the power output of an actuator per unit volume, with the same criticisms as power to mass ratio. Table 2-2 gives a comparison with a range of sample actuators. While hydraulic power will always exceed the power output of most relevant actuation techniques in this regard, pneumatic artificial muscles perform well when compared to electric and other pneumatic actuation techniques. However as discussed extensively in the literature, PAMs do have a relatively short stroke length, meaning that even though their volume may be small, their overall length may exceed that of robot limbs, making it impossible to mount them on the robot directly [79], [85]–[87]. This can be overcome with cable drive systems, although this does introduce additional frictional losses and may lead to backlash [18], [80]. It should also be remembered that the values shown in Table 2-2

Actuation type	Volumetric Power (kW/m^3)
Hydraulic cylinder	500,000 [74]
Pneumatic cylinder DSN-25	286 [75]
Sanyo Denki Bipolar Stepper Motor	176 [88]
89810 DCmind Brushed DC motor	152 [89]
Pneumatic artificial muscle	488 [73]

Table 2-2: Volumetric power per unit volume for a range of sample actuators.

2.2.3 COMPLIANCE

Compliance plays a major role in the safety of robot systems. As seen in section 2.1.2 the severity of a number of collision types may be reduced by introducing compliance. Reduced stiffness of a robot joint partially decouples each link from the parent, so that in the case of an impact the apparent inertia is reduced as the effect of the mass of the parent links is minimised [2], [90]. Removing rigidity from such systems also acts to

distribute the impact through more time, thus reducing its overall severity [91]. However, introducing compliance does not necessarily equate to making a robot safe. Compliance entails that potential energy be stored at the joints and this must be carefully controlled. For example in [46] it was shown that the type of controller used played a major role in the safety characteristics of a lightweight robotic system actuated with PAMs, with proxy-based sliding mode control outperforming proportional integral derivative control.

Compliance is also a means by which to limit damage to the robot itself, by absorbing the severity of impacts which would otherwise be transmitted to the rest of the robot structure including potentially sensitive drivetrains [92], [93] . Thus the robustness of the system can be improved. The inclusion of compliance in robotic systems also has advantages in unstructured environments such as the home, where a complete model of the environment is not available. Positioning errors leading to unintended contact with the environment will not result in large forces on the robot or obstacles, and constant forces can be maintained as a manipulator moves along an uneven surface [94]. By using this approach there can be a large reduction in the requirement for traditional sensor-based control [95]. This is due to the ability of the manipulator to deform around objects and passively react to physical contact with the environment such as in the case of a grasper, which needs to conform to a wide range of objects while providing a secure grip [96]. Similarly, errors in alignment, for tasks which require one object to be placed into another (e.g. plug into a socket), do not have to be executed as precisely as the manipulator can be guided by direct contact with its environment. A number of tasks have been identified and classified which can benefit from compliance [97]. A tree hierarchy of these tasks is shown in Figure 2-8. These include a range of tasks relevant to the domestic environment. In particular, wiping tasks, where the robot must move a tool across a surface while maintaining a normal force and overcoming friction, are considered. In these tasks the contact conditions may change for example when wiping a window with more or less water. Compliance plays a role here as it allows the manipulator to react to these uncertainties without the requirement for a precise model of the operation.

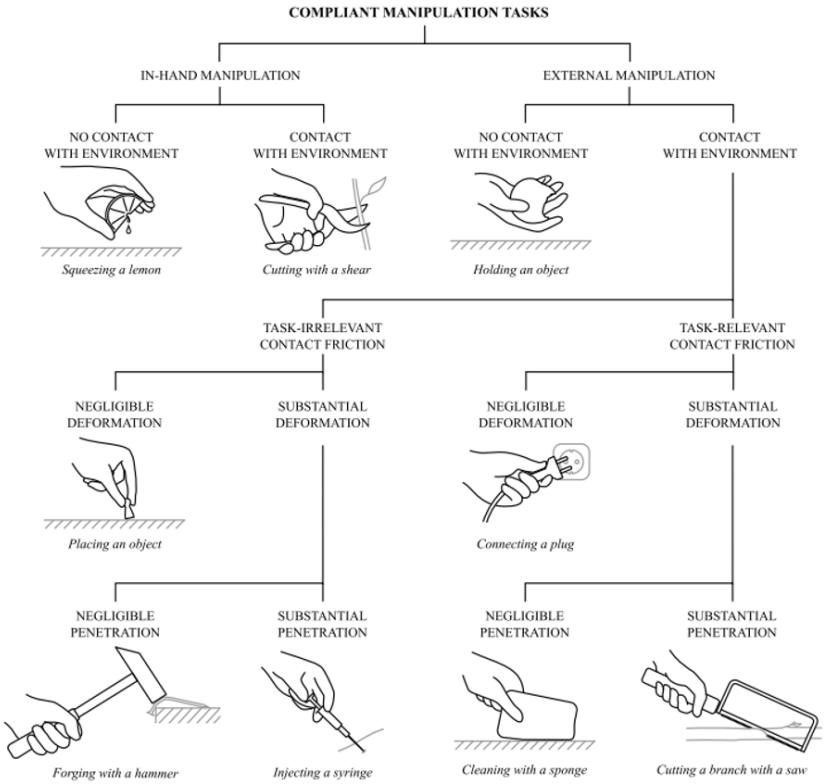

Figure 2-8: Hierarchy of types of compliant manipulation tasks with an example of each [97]**.**

Compliance can also improve the energy efficiency of robotic systems by utilising the energy storage potential of the elastic elements. This is especially true for cyclical tasks such as walking where it offers the potential for fast, energy efficient locomotion if tuned correctly for the locomotion speed [85], [98], [99]. Further, in this application, the impacts as the robot makes contact with the ground are also reduced [100]. Energy storage can also be used to enable explosive movements where a high velocity is required for a short period of time (e.g. kicking or throwing a football or flicking a finger) [94], [101]. Building up elastic energy before the movement and then releasing it greatly reduces the performance requirements of the actuator [102], [103].

Despite these benefits, compliance presents major challenges, particularly in the areas of performance and control. In contrast to traditional stiff actuators, which can move to a specific position or track a trajectory accurately irrespective of the forces applied (ideally), compliant actuators deviate from their position in response to external forces and accelerations making force output fundamental to control [94]. This increases the complexity of the control problem as more inputs must be considered. Compliant

transmission can also negatively affect performance in terms of increased oscillations and settling time [44], [54]. The manipulator will respond slowly as the elastic element must reach the required force output to overcome the forces on the system (inertia, friction etc.) before it begins to move or stop moving. This must be compensated for in control, generally requiring a reduction in speed/bandwidth when compared to a stiff system.

In an effort to improve the performance and adaptability, methods which allow compliance to be dynamically altered have been suggested[60], [94], [104]–[108]. This allows the stiffness to be increased when greater acceleration is required or during fine manipulation tasks. For illustration, Figure 2-9 shows an optimal approach to moving a link and bringing it to rest again. Greater stiffness is used to start and stop the link moving while low stiffness is preferable while the link is moving at speed to reduce the risk of injury. Dynamically variable compliance can also improve efficiency as the fundamental frequency of the system can be altered to suit a cyclical task [94].

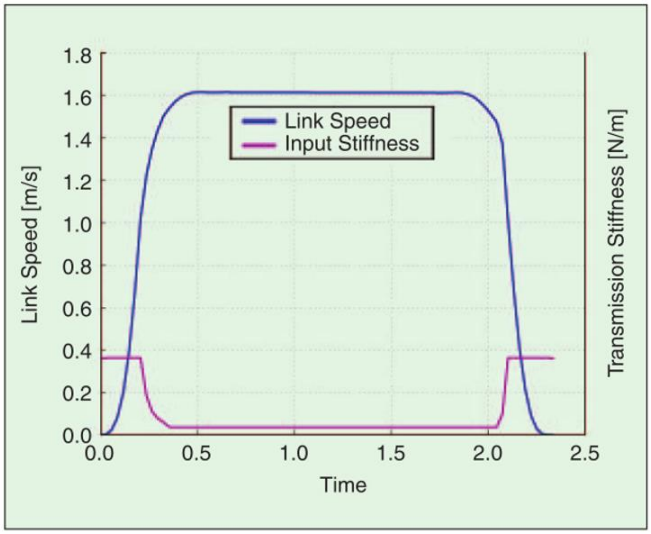

Figure 2-9: Optimal joint stiffness during a rest to rest movement [44]***.***

This is most keenly appreciated in the case of legged robots. While passive-dynamic walkers such as those described in [109] have been shown to be very efficient, they cannot perform any tasks other than walk at the speed they were designed to walk at [108]. As discussed, compliant systems allow energy storage which can increase efficiency and speed across a range of frequencies. However, by tuning the joint stiffness

for the speed of travel, the energy input can be minimised for different speeds and gaits [110]–[112].

A number of methods of achieving compliance have been proposed in the literature. Active compliance makes use of a stiff actuator but uses sensing and control to deliver compliant properties. Force control and impedance control are the two main approaches [45]. While these are useful to carry out actions such as automatic deburring [113], these methods are not designed to control collision forces. As the bandwidth and response time of the actuators used are limited, the stiffness experienced during such a collision is that of the system with stiff actuation [114]. It also means that a failure in the control system could result in instability or dangerous behaviour[91].

Passive compliance introduces a mechanical component in the drivetrain which is compliant in nature. Many implementations take the form of a stiff actuator, coupled via an elastic element to the joint it actuates, and are known as series elastic actuators (SEAs) [100], [115]. The stiffness of such configurations is fixed when the joint is initially configured. More advanced versions can vary the effective stiffness of the joint irrespective of its position (Variable Stiffness Actuator (VSA)), or vary both stiffness and damping (Variable Impedance Actuator (VIA)). There are four main means by which to achieve variable passive compliance [106], [108]:

Equilibrium Controlled Stiffness

In this arrangement, a spring with linear stiffness is placed in series between the actuator and joint, in the same way as an SEA. The equilibrium position of the spring is controlled to exert the desired force or stiffness [116], [117]. While the stiffness of the spring cannot be changed, the effective stiffness of the joint can be altered by controlling the motor position relative to the joint. While this can be achieved simply mechanically, the control of joint stiffness is limited by the bandwidth of the actuator and so during an impact the hardware stiffness will be felt rather than the controlled stiffness[106].

Antagonistic Controlled Stiffness

This approach most closely mirrors that of biological systems, where two muscles actuate a joint, both with adjustable force and stiffness characteristics. Two actuators control the joint, each providing a tensile force through a spring element. By adjusting

the elongation of the springs, the force output and position of the joint can be controlled. In order to achieve variable compliance, it is necessary to use nonlinear springs. The reason for this is apparent when Figure 2-10 is considered, whereby a linear joint is actuated antagonistically through two linear springs. The force on the central block is:

$$F = -k(x - x_{0A}) + k(x_{0B} - x) \tag{2.2}$$

$$F = -2kx + k(x_{0A} - x_{0B}) \tag{2.3}$$

Therefore, the force output can be adjusted by the controllable parameters x_{0A} and x_{0B}. However, this is not the case if stiffness is considered:

$$\kappa = \frac{dF}{dx} = -2k \tag{2.4}$$

If alternatively, quadratic springs are used, the equations for force and stiffness become:

$$F = -2kx(x_{0A} - x_{0B}) + k({x^2}_{0A} - {x^2}_{0B}) \tag{2.5}$$

$$\kappa = \frac{dF}{dx} = -2k(x_{0A} - x_{0B}) \tag{2.6}$$

This allows both the position and force to be controlled.

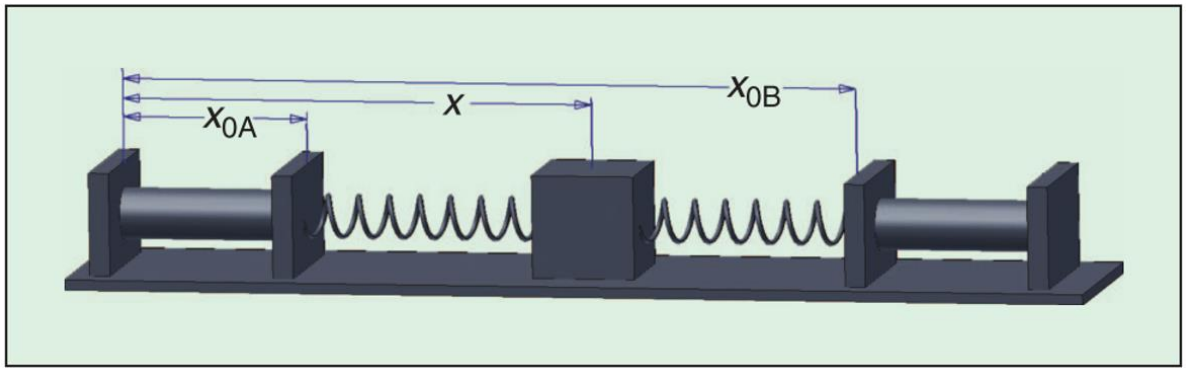

Figure 2-10: Illustration of a antagonistically actuated joint using linear springs[106].

A number of methods which make use of electric motors have been investigated to realise springs that behave non linearly in this context [108], [116], [118], [119].

Antagonistically actuated joints making use of PAMs also fall in this category, as they are effectively springs with dynamic spring constant control.

Structure Controlled Stiffness:

This involves varying the effective stiffness of joint by modifying the structure of a spring between the actuator and joint. There are a number of ways in which this can be done as can be seen from the well-known bending moment equation

$$M = \frac{E_y I}{L} \times \theta \tag{2.7}$$

Where $E_y$is the Young's modulus, I is the second moment of area, L is the effective beam length and θ is the angle of bending. E is a material property which can be changed with heat, but this is usually too slow for most applications[106]. The moment of inertia can be effectively changed by rotating the beam (or a leaf spring in the case of [120]). Other approaches involve controlling the clamping force applied to a number of layers of material which make up a leaf spring [121]. This method provides a large stiffness range, but control is difficult due to the reliance on friction. Examples also exist of the effective length of the spring element being changed to adjust compliance. In [122] a slider is used to reduce the length of a leaf spring which is available for bending. Similarly the length of a "Jack Spring" which is available for compression/elongation can be controlled [123].

Mechanically Controlled Stiffness

This is similar to structure controlled stiffness but, the mounting point of the spring element is modified rather than the structure. Examples of this include the MACCEPA actuator [124]. An embodiment of this actuator is depicted in Figure 2-11. The extension of the spring element is controlled by the stiffness motor. This sets the stiffness of the joint at 0°. The position motor rotates the joint about the gear acted upon by the spring element. This sets the equilibrium position of the joint which is a weighted sum of the positions of both motors depending on joint stiffness. The actual position of the joint will then be dependent on both motors and the forces applied.

Other examples of the use of mechanically controlled stiffness include the use of preloaded springs holding rollers against cams[104]. As the joint is moved from the

equilibrium position, the roller must move up the cam, depressing the spring. By controlling the length of the spring the stiffness of the joint can thus be regulated.

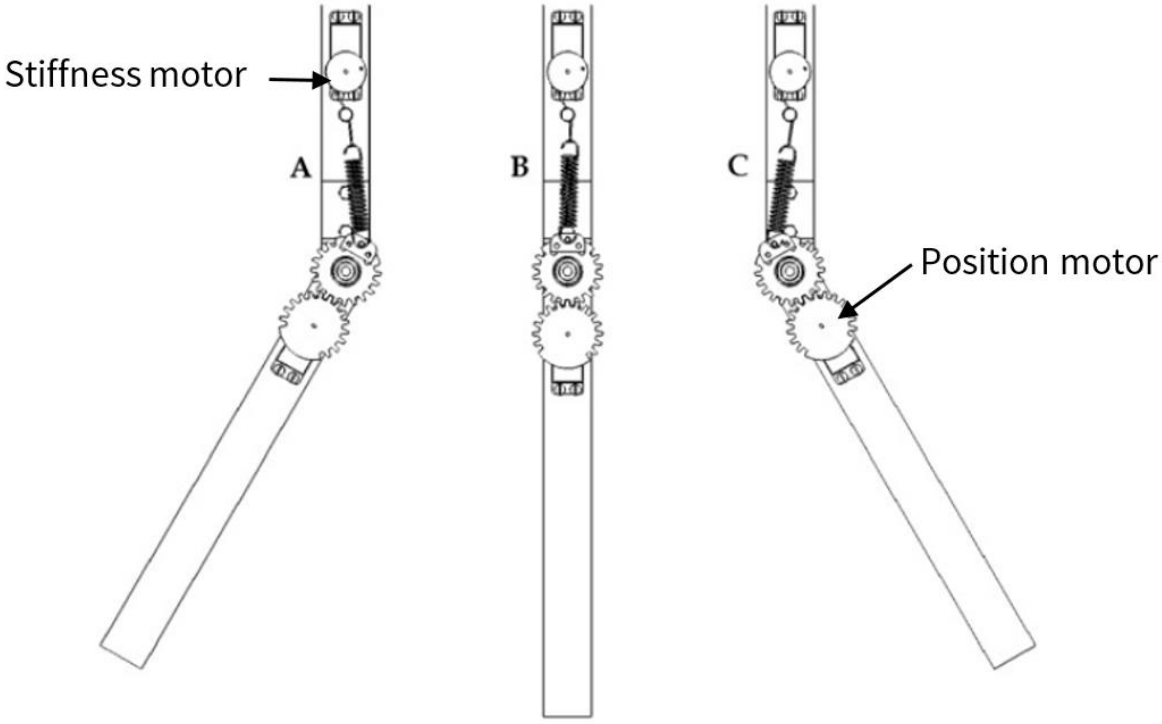

Figure 2-11: The MACCEPA actuator, as depicted in [124]***. Three positions are shown (A: -30°,B:0°, C:+30°).***

With the exception of equilibrium controlled stiffness (which has serious bandwidth limitations), all of the variable stiffness actuation methods require two actuators, either to apply the control force applied to the joint in each direction separately, or to adjust the joint position and stiffness independently. This has the effect of increasing cost, system complexity and mass of the system versus a joint using stiff actuation where a single actuator can control a joint [94]. While the ability to store energy in the elastic element can improve performance, there are efficiency considerations in the use of VSAs. If the stiffness is changed without adjusting position, there is in effect no work output for the work put in. These limitations are necessary to consider when comparing actuators for use in applications requiring variable compliance.

2.2.4 ACCURACY

The achievable accuracy available with a robotic manipulator is dependent not just on the actuator used but also the quality and type of sensing available, the control system

implemented and the dynamics of the system. Industrial robots employing stiff actuation, even those with payloads in excess of 1000Kg and with a 7m range are capable of repeatability well below 0.5mm [125] and some to the micron level[126]. Such systems have been extensively researched and accurate models are available to facilitate their control. Relatively simple control strategies, such as PID control, have been shown to provide impressive performance.

Systems actuated with PAMs struggle to achieve the positional accuracy offered by more established actuation technologies. Individual joints may have errors of over 1 degree[127], [128]. This is due to the highly nonlinear behaviour of the PAM as force output decreases with contraction. There is also a hysteresis effect due to friction at the muscle fibres [129]–[131] which makes dynamic control more challenging. The development of accurate dynamic models, while extensively researched, is still far from a resolved issue[131], [132]. Pneumatic actuators in general are more difficult to control than electrical systems, as the performance of the valves and the entire pneumatic system will play a role in the dynamic response [133]. However, as discussed previously, the ability of the joint to react to external forces reduces the requirement for accurate control. Indeed the ability to control a robotic manipulator in a compliant way makes force control a more compelling prospect than pure position control [97].

2.2.5 ENERGY EFFICIENCY

The efficiency of the overall robotic system is of critical importance for mobile personal service robots. In order to be useful, such robots must be able to operate for a reasonable length of time, usually without the ability to be tethered to a power source. This means all the required energy to operate the robot must be carried on-board which results in additional robot mass and occupies a significant volume. By employing more energy efficient actuators, the total energy requirements of the robot are reduced thus reducing the energy storage requirements or increasing the maximum operating time. Table 2-3 shows representative efficiencies for some forms of actuation technology.

Actuation type	Efficiency
Hydraulic system	40% [134]
Electric Motor (excluding reduction gearing)	60-95% [135]
Pneumatic artificial muscle	32-49% [136] 10-84% [13]19% [137], 24%[138]

Table 2-3: Approximate comparison of several actuation technologies in terms of efficiency.

There are a number of factors which complicate the comparison of energy efficiency in robotic actuators. For instance, a common requirement of an actuator is to hold a joint in a stationary position often against the force of gravity. While energy may be expended to do this, there is no work output as the joint does not move therefore the efficiency is 0%. Alternately a non-back-driveable mechanism (such as a lead screw or worm and worm-wheel) can be used which prevents the joint moving unless powered from the actuator, in which case no energy is expended, and efficiency is meaningless. The form in which energy is available is also particularly important to this study. Should the energy used to compress the air be included in the efficiency calculation for pneumatic systems or only how efficiently the energy in the air is used be considered? If for instance, the compressed air supply can be replenished from an external source (such as a large off board air compressor), then only the compressed air to mechanical work conversion may be relevant. If, however the air is compressed on-board the robot, using another form of stored energy (such as batteries), then the efficiency of the compressed air production process must be considered. In addition, the system in which the actuator functions has a large effect on efficiency. Reduction gearing for electric motors is used to reduce the speed and increase the torque output, giving more desirable characteristics for joint control. However, due to friction in the gearing, the overall efficiency of the motor/gearbox system is reduced. Likewise, efficiency improvements due to the addition of compliance has already been discussed. Ultimately, the efficiency of an actuator must be considered in the context in which it is to be applied, and it is difficult to attribute an efficiency to an actuator in an absolute sense. With this caveat the following attempts to give some indication of the efficiency of electromechanical and pneumatic systems.

The efficiency of electric motors is dependent not only on the electric motor design but also the load applied relative to the rated load of the motor and operating speed [126].

Typical operating conditions see efficiencies of 70-95% (see Figure 2-12) although higher efficiencies can be achieved [139].

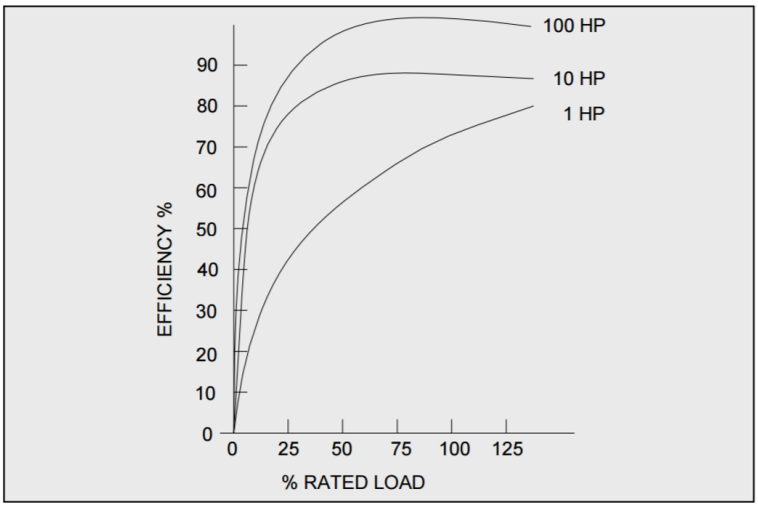

Figure 2-12: Typical motor efficiency with varying load[126].

While a full comparison of the efficiency of the types of electric motors is out of the scope of this work, larger AC motors tend to have better efficiency, though are generally not suitable for robotic applications[126]. Brushless DC motors are typically more efficient than their brushed counterparts as the current flow in the windings can be more accurately controlled in the control circuitry and there is no voltage drop across the brushes [140].

Reduction gearing will further reduce the efficiency of an actuated joint. The degree to which this occurs varies depending on the choice of gearbox, but it may have an efficiency as low as 50% for a lead screw or worm gear [141] whereas epicyclic/planetary gearboxes can be 80-90% efficient [142], albeit with lower gear reductions, Efficiencies in excess of 70% are possible for harmonic/strain wave gearboxes and up to 84% for cycloid drives [143] both of which are capable of large reductions in a compact single stage.

Pneumatic actuators have the advantage on not generally requiring a reduction transmission due to their large output forces, however they have other major inefficiencies. Generating compressed air is a highly inefficient process. Although it depends on the technology used, estimates suggest that the process is only 20% efficient [144], [145], although this is dependent on the output pressure. Further energy can also be lost through air preparation and leakages.

Few studies have evaluated the efficiency of pneumatic muscles in absolute terms, rather focusing on efficiency improvements etc. Chou and Hannaford [136] considered the energy consumption of PAMs under a number of conditions. These were evaluated theoretically, making idealised assumptions and using a hypothetical compressor. Valves are not considered, and the tubing is taken to have zero volume. The compressor is assumed to be reciprocating and sized so that a single stroke provides the necessary air input. For the case of a PAM which starts at atmospheric pressure, is held at constant length while being inflated and then allowed to contract as much as possible at constant pressure before being deflated, the maximum efficiency was found to be approximately 30% at 500kPa. In the second scenario considered, when shortening occurs, isotonic (constant force output) conditions are maintained. For any operating pressure this means that the force output and/or the maximum contraction must be limited to ensure the force can be maintained throughout the contraction. Once contracted the tension is relaxed and the PAM returns to its initial condition. The efficiency of the process at 500kPa was found to be approximately 22%. The final condition attempts to move the previous closer to a real-world scenario by modifying the case so that before the contraction occurs, the gas must be pressurised sufficiently to maintain the force output to full contraction. This is more similar to a PAM operating with a supply and valve where the air must be pressurised before being applied to the muscle. The efficiency at 500kPa was found to be 20%.

Meller et al. experimentally verified one of the above tests [137], [138]. In these tests the muscle is held at its maximum length before being pressurised to its test pressure. This pressure is maintained as the muscle then contracts. As the authors were interested in comparing the efficiencies for different operating fluids, the tests were conducted hydraulically, using water. From this analysis the case of a pneumatically actuated muscle could be established by accounting for the compressibility of this medium using Boyle's law. Under these tests the pneumatic muscle had an efficiency of approximately 24%. The hydraulically actuated muscle had a much higher efficiency, between (between 38% and 60% depending on pressure). However, as noted by the authors, using a

hydraulic fluid increases stiffness dramatically (by 800%) and increases the mass of the actuator.

Of course, the cases presented here are highly idealised and do not account for real world conditions where air is usually pressurised to above the pressure used in the PAM to ensure responsive behaviour, isothermal conditions are less likely, there are losses in pressure reducers and valves and energy is required to operate the valves. Such losses will reduce the efficiency further.

2.2.6 LIFETIME

Like any appliance, the user expects a service robot to operate for a reasonable amount of time before needing to be serviced, repaired or replaced. Thus, actuators must be chosen which are capable of robustly coping with the expected physical challenges. This is important not just for the value proposition of the robot, but also safety, as the behaviour of a robot in a failure scenario can be unpredictable [146].

Industrial robots have expected lifetimes between five and twenty years [147], and although it is unlikely that the same would be expected from domestic service robots (which would likely have to be constructed at a lower price point), this gives an indication of what is possible with today's established technologies and electromechanical systems.

By contrast, the lifetime of PAMs is a poorly studied subject and tends to be much shorter. The main mode of failure is rupture of the elastic bladder due to fatigue [148]–[150]. Two common materials used for this are natural latex rubber and silicone rubber. It was found experimentally that the fatigue life with silicone, when undergoing relatively large deformations at 30kPa was only 180 cycles. Latex performed better with 4320 cycles [148]. Smaller contractions dramatically improve the fatigue life with 12,400 cycles possible with a latex bladder when only 10% contraction is allowed. Still, this represents a considerable reduction in performance versus an electromechanical system.

Kingsley and Quinn tested muscles with Latex bladders at higher pressures (655 kPa) and found failures occurred at as low as 90 cycles [150]. A number of failure modes were observed including rupture of the bladder, braid pull out and pin-hole failure in the

bladder. Several means were investigated to improve this, including the addition of a spandex sleeve between the bladder and braided mesh, pre-stressing the muscle to ensure the fibres return to their original position after each cycle, and the use of a braided mesh with more tightly arranged fibres. This allowed the actuators to perform up to 16000 cycles.

Woods et al. proposed a new muscle end-fitting design which greatly increased the lifetime of muscles (in excess of 120,000,000 cycles) [149]. This design consisted of a swaging method to ensure the muscle fibres and latex tube were held in a progressive way, and that there was a region where the braid alone was held. This coupled with the use of an epoxy resin ensured that the muscle fibres in the end-fitting could not move during operation. This is a highly promising result for these actuators though has yet to be repeated by other researchers. It should also be noted that the actuators were cycled at 30 Hz which did not allow the muscles to be completely depressurised between cycles, a factor which could extend their lifetime according to [148]. The contraction was also relatively small, at 6% of the initial length. Commercially available Festo pneumatic muscles are specified to have a lifetime of between 1 and 10 million cycles depending on the load applied [14].

Operational conditions will play a large role in the lifetime of an actuator. The sealed nature of PAMs make them ideal for work in dusty environments [14]. This is a distinct advantage over electromechanical systems which can suffer from overheating due to dust covering, wear on moving parts and short circuits [151]. In certain environments where explosive dust is present, the motor may trigger an explosion.

2.2.7 COST

Actuator cost is critical to overall affordability of a robotic system and therefore influences the market which can be reached with any solution. Electromechanical systems generally require reduction gearing which tends to dramatically increase the associated cost of the actuator. While it is difficult to generalise the cost of these actuators, as an example, a brushed DC motor with planetary gear assembly which can supply 20W of power and 15NM of torque costs approximately €375[152]. More specialised motors and those with more sophisticated gear reductions can cost much

more, as will adding mechanisms to introduce variable compliance, which normally require an additional motor. Pneumatic muscles are often produced in house and can be manufactured for as little as $5 [76]. Commercial versions, such as a 20mm diameter 250cm long (although length has little effect on cost) Festo pneumatic muscle can be purchased for approximately €150 [153]. This muscle is capable of supplying up to 1500N of force, or if two are arranged antagonistically for a joint requiring 90 degrees of rotation, at least 12Nm of torque. Assuming 1 Hz operating frequency, this delivers 40W of power [14]. Given the relatively immature nature of this technology and the low number of units being produced it is expected that the cost of the actuator could reduce further overtime, especially given the simplicity of the PAM in comparison with a geared motor system.

It is important to also consider the auxiliary components necessary to operate actuators when comparing their cost. In the case of an electromechanical system this consists mainly of motor controller hardware responsible for regulating the voltage and current supplying the motor, and the accompanying power source. In the case of compliant systems, additional sensing is required to measure the stiffness and force applied (for example load cells or spring tension/compression). For pneumatic systems the requirement is more complex. A compressed air supply is needed (consisting of a compressor and/or storage tanks) along with control valves and pressure sensing [111], [154], [155]. This adds considerable expense to the overall system. For example a high quality proportional regulator can cost in excess of €400 [156]. Due to this high cost many researchers have elected to use on/off solenoid valves [111], [157]. High quality versions are available below €50 [158].

A useful comparison can be made by considering the Shadow Robotics dexterous hand system [159]. This robot hand has 20 degrees of freedom and is available in both a motor powered, and PAM powered configuration. The motor powered version costs £115,000 while the PAM version costs £75,000[160].

2.2.8 SPEED/BANDWIDTH

The speed of operation is an important factor for most robotic systems. For cyclical operations, this can be measured using bandwidth or the maximum number of cycles which may be achieved per unit time.

While actuator bandwidth (or operating speed) does not have to reach the same performance levels for service robots as might be required for industrial applications [60], it is nonetheless important that the robot can operate at speeds which make the robot useful [161]. Especially pertinent to human-friendly robots is how the actuator can react during collisions as well as the speed at which it may be able to react to changes the robot perceives in its environment (for example a human entering its work envelope).

Traditional stiff actuation technologies facilitate high bandwidth operation. They are therefore ideal for industrial applications The introduction of compliance to human-friendly systems results in a reduction in the maximum possible bandwidth, restricting the control bandwidth to 1/3 of the fundamental frequency of the system [82], [162]. This is an intrinsic limitation of PAMs in this respect. This has led to the operating speed of PAMs often being considered one of their major limiting factors with some suggesting they are too slow for practical application [133].

Table 2-4 compares a number of different actuator type in terms of bandwidth. The entire system will however play a role in the ultimate achievable bandwidth both in terms of the mechanical stiffness, mass etc. and also the control system for the actuator (valves, motor drivers etc.).

Actuation type	Maximum frequency (Hz)
Hydraulic cylinder	50-300[74]
Moving coil transducer	50,000 [74]
Pneumatic cylinder	100 [74]
Pneumatic artificial muscle	4-8[150], 35Hz [163]
Muscle	50-500Hz [74]

Table 2-4: Maximum bandwidth of a variety of actuator technologies.

2.2.9 REMARKS

From this analysis, pneumatic muscles have some favourable characteristics for use on mobile service robots. In applications where large forces and variable compliance are required, they can meet these needs in a lightweight actuator. In comparison to electromechanical systems they deliver more force per unit mass and area. They also deliver inherent compliance in the actuator itself, rather than relying on additional components or control. PAMs also have the advantage of being able to passively maintain joint position and stiffness without consuming energy simply by maintaining

the mass of air in the PAM. They also offer a relatively low-cost solution which does not require reduction gearing for effective operation. While the robustness of PAMs is an ongoing area of research, there is promising work in this area which suggests they are capable of long term operation. However, electromechanical systems can be a better solution where variable compliance is not a necessity. Therefore, it is necessary to analyse the requirements of any system before deciding which actuator is most appropriate, and indeed some applications a combination of approaches may be most advantageous.

For these reasons, PAMs are worthy of consideration for use in service robots, although concerns over their efficiency for mobile systems remain to be addressed.

2.3 CONCEPT OF PNEUMATIC ARTIFICIAL MUSCLES

2.3.1 ORIGINS OF PNEUMATIC ARTIFICIAL MUSCLES

According to Marcincin and Palko [164], a pneumatic powered muscle was first proposed by a Russian inventor, S. Garasiev, in 1930. Charles R. Johnson and Robert C. Pierce patented a device similar in construction to a pneumatic muscle in 1941 as an alternative to dynamite in the mining industry, using the radial expansion of an "Expansible Cover" to crack rock [165]. In 1949 De Haven patented a "tensioning device for producing a linear pull" [166]. This device used gunpowder to release a charge of compressed air and produce a sudden pull. The proposed application was pilots' safety belts. In 1953 a patent was awarded to Morin[167] which describes "an elastic diaphragm adapted to be subjected to the pressure of any fluid and adapted to transmit any change in the pressure of said fluid to a controlling device such as measuring instruments, regulators, valves and similar devices". The device described is very similar in structure to both the straight fibre and McKibben muscle but the application is different.

In 1955 Gaylord patented the "fluid actuated motor system and stroking device", which offered advantages over pistons and cylinders in terms of size weight and cost [168]. He also provided the first equations which attempted to describe its behaviour.

$$F = \frac{P\pi {D^2}_{45^\circ}}{2}(3\,cos^2\theta - 1) \tag{2.8}$$

where F is the tension force, P' is the gauge pressure in the PAM, $D_{45°}$ is the diameter of the muscle at θ =45° and θ is the braid angle as in Figure 2-13.

Physicist Joseph L. McKibben popularised the actuator in 1957 when he used it to actuate a wrist-driven hand orthosis for his daughter who suffered from Polio [22]. McKibben had previously worked on the Manhattan project and was the person who "pushed the button" on the first atomic bomb, code named Trinity [169]. The term McKibben muscle is still used to refer to this type of PAM, consisting of an outer expandable mesh with an internal elastic bladder. While it received significant attention as an actuator for prosthesis, it had limited success due to difficulty in controlling the actuator.

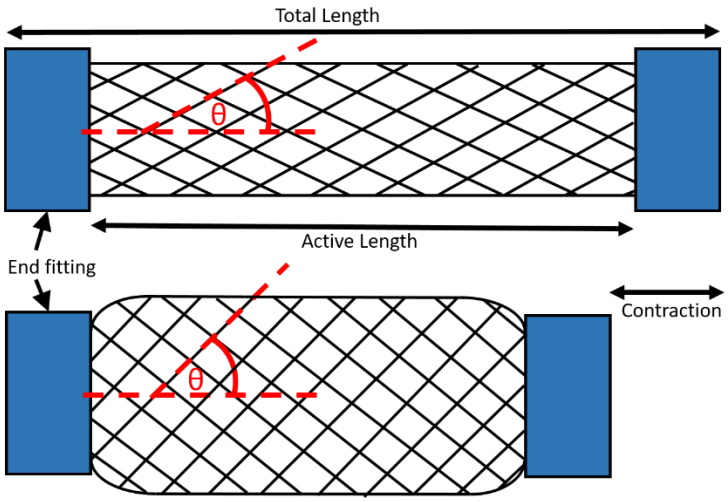

Figure 2-13: Conceptual McKibben muscle in a relaxed/extended state (above) and contracted state (below). θ represents the braid angle in the mesh.

In the 1980s there was renewed interest in the actuator, with the first commercial pneumatic muscle, the Bridgestone Rubbertuator [170]. Despite the demonstration of a number of robotic applications including arms [170], [171] and a climbing robot [172], production ultimately ceased in the 1990s. Since then a number of companies have produced PAMs, most notably the Shadow Robotics Company[173] and Festo [14]. There has also been considerable interest in the use of this actuator among the research community with approximately seventy-seven research groups having published work relating to PAM technology as of 2011 [174].

2.3.2 OPERATING PRINCIPLE OF PNEUMATIC ARTIFICIAL MUSCLE

A wide range of pneumatic artificial muscles have been developed with various operating principles. Most contractile pneumatic muscles have a similar basic structure[10]. They are cylindrical in shape with a flexible membrane which can be inflated to produce a contractile force. At the ends of the cylinder, end fittings seal the tubular construction and allow the muscle to be attached to the structure it actuates. The end-fittings also allow compressed air in and out of the muscle and attach it to the actuated system.

In order to characterise a muscle and its performance, a number of parameters are used including the diameter, length etc. Generally, when length is referred to it is the active length; that is the length of the membrane between the end fittings, as this is what correlates with muscle performance. The overall length, including the end fittings, is important to a robot designer however, as this is what must be accommodated on a robot. Another performance metric is the contraction which is possible with the muscle, often specified with the applied load when it is non-zero. This is usually given as a percentage of the active length. For muscles which make use of elastic membranes, some initial pressure may be required in order to overcome the initial higher stiffness of the material. This 'threshold pressure', is the internal muscle pressure at which the muscle starts to expand.

Here, the McKibben or braided PAM is discussed as is a commercial adaptation of this design developed by Festo. Other pneumatic muscle designs are described in Appendix B.

McKibben Muscles

Also referred to as braided pneumatic muscles[175], these are the most frequently used and attract the most attention in the research community [10]. It consists of an inner elastic bladder, which may be inflated by a compressed air supply. This is surrounded by a separate expandable braided mesh tube. The fibres in the braided tube are arranged helically in opposing directions. These fibres may be considered inelastic. As the inner bladder is inflated, it pushes outwards on the braided mesh causing it to expand. Given that the fibres are inextensible, some other dimension must change to account for the increase in diameter of the helix. An even number of fibres are arranged in a clockwise

and counter clockwise direction. As a result, the expansion of the mesh does not cause the end fittings to rotate relative to each other, the forces opposing each other. Instead the radial expansion of the helically arranged fibres causes the muscle to contract (Figure 2-13).

It should be noted that this behaviour is dependent on the design of the braided mesh, in particular the braid angle (the angle between the braid fibre and the longitudinal axis of the muscle). This angle will change as the muscle expands radially. It can be shown analytically that at an angle of 54.74°, the addition of more fluid to the muscle will not produce any further dimensional change [22]. This is due to the energetics of the muscle and defines the theoretical contractile limit. Similarly a minimum braid angle (maximum muscle length) can be calculated as in [176]. At angles less than 54.74°, addition of fluid pressure in the muscle causes the muscle to expand radially and contract longitudinally. If the braid is configured such that the braid angle is greater than 54.74, the addition of fluid will tend to elongate the muscle. This is generally impractical for use as an actuator as buckling is likely. Krishnan et al. explored a general class of pneumatic artificial muscle, whereby the braided mesh was adapted to give different behaviours [177]. Here it shown that not only is it possible to produce contraction and elongation, but also a rotational behaviour by varying braid angle of the helix in the clockwise direction versus the anti-clockwise.

Several groups have proposed designs for this type of muscle, usually adapting the materials used for the bladder and braid as well as the end fitting design [178]. Some of these are summarised in Table 2-5 with accompanying images in Figure 2-14. The level of detail provided of the implemented designs varies widely as many authors are concerned with applications or modelling rather than muscle design, using very simplistic end fittings such as hose connectors or bolts [137], [179]–[182]. Murillo [183] and Woods [184] both give a detailed account of the design considerations, especially the difficulties in securely attaching the bladder and braided mesh to the end fittings. This is often a reason for failure in these actuators as the high forces generated cause the braid to be pulled out [150].

Table 2-5 includes key muscle dimensions and performance indicators. Understanding the relationship between the design parameters and muscle performance is key to designing systems capable of taking advantage of these actuators. This is explored in detail in section 2.6 . However, it is not always possible to physically realise materials with the properties which muscle models suggest are preferable, resulting in the use of commercially available alternatives. For example, the butyl rubber used in [182], [183] is bicycle tyre inner tubing. Similarly the braided mesh is usually that intended for holding cables or protecting pipes [138], [182]–[184]. These design compromises may limit the potential of the actuator, but the use of commercial products makes it practical for researchers to construct the muscle in a repeatable way. Indeed one of the advantages often given of this type of pneumatic muscle is the ease of manufacture [185].

Primary Author	Year	Braid material	Bladder material	End fitting	Rest diameter (mm)	Unstrained braid angle (degrees)	Length (active) (mm)	Length (overall) (mm)	Mass (g)	Max contraction (%)	Max Force (N)	Max pressure (kPa)
Schulte [22] (w-4	1961	nylon	Latex	Aluminium and brass	12.1	40	127	155	-	30	436 (limited)	551
Caldwell	1995	nylon	rubber	Acrylic bung	12.7	30.7	79	-	10.5	34	-	750
Chou [136]	1996	Nylon Fiberglass	-	Plug fitting	11 9	-	140 200	-	-	25 15	110 56	500 500
Reynolds	2003	nylon	Butyl	steel (bolt)	31.8	30	140	-	59	26 (483 kPa)	1000	621
Murillo [183]	2013	PET: Flexopet Flexopet	Butyl Silicone	Stainless steel conical surfaces	14 14	19 19	300 300	406 406	120 120	34 32	2400 2700	1420 1420
Woods [184]	2014	Kevlar PET	Latex Latex	Swaged stainless steel	15.9 22.2	29.2 27.7	150 150	270 270	150 150	28 26	814 1486	620 620
Meller [138]	2014	Kevlar	Latex LDPE Viton	Hydraulic hose fitting	12.7 12.7 12.7	28.7 28.7 28.7	146-173	-	-	25 33 22	400 500 360	700 700 700

Table 2-5: Summary of selected McKibben type pneumatic muscles.

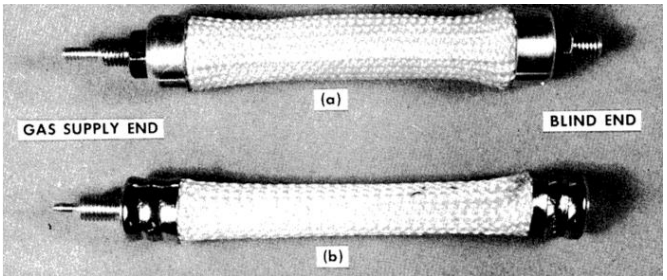

(a) Schulte [22]

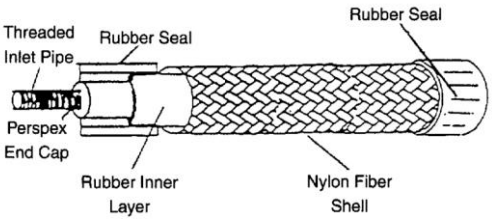

(b) Caldwell [186]

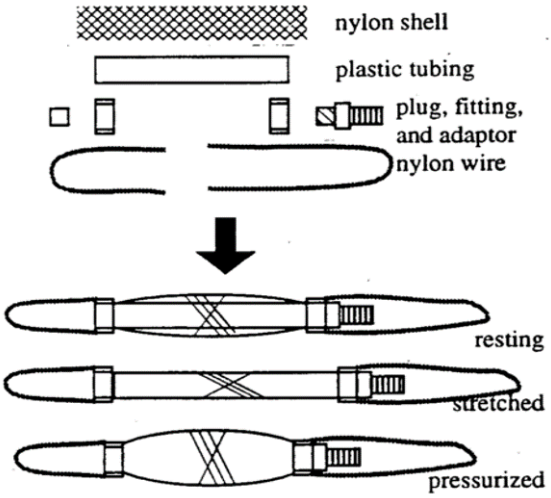

(c) Chou [136]

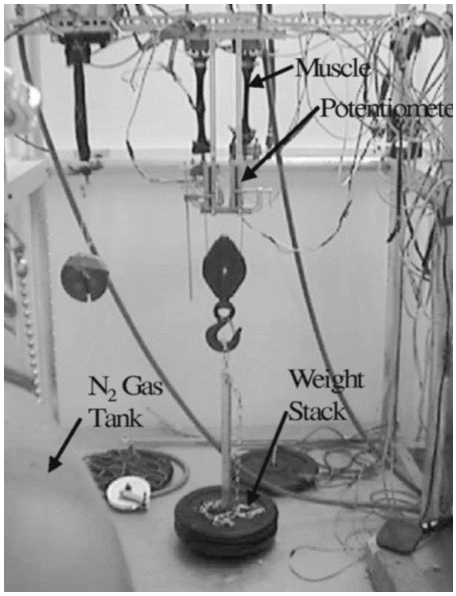

(d) Reynolds [182]

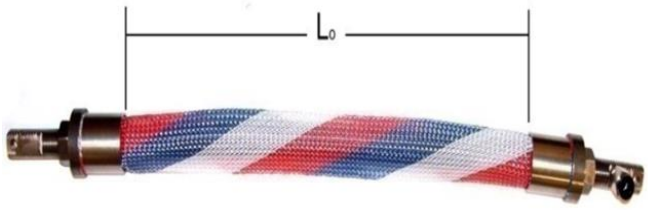

(e) Murillo [183]

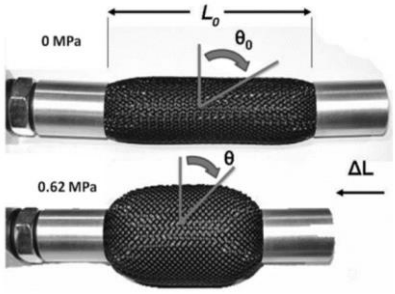

(f) Woods [184]

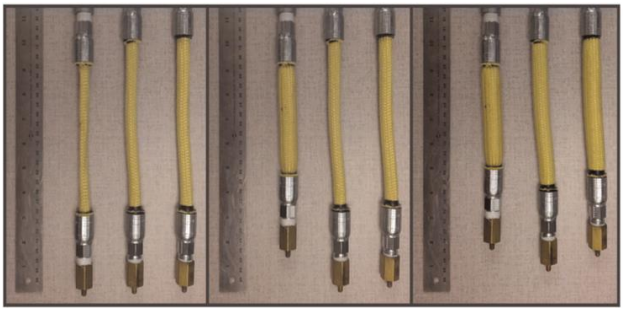

(g) Meller [138]

Figure 2-14: A selection of McKibben type muscles.

Festo Fluidic Muscles

The “fluidic muscle” developed by Festo is a commercially available derivative of the McKibben type muscle. It has been used extensively in the literature [99], [187]–[190] in part due to the consistency in manufacture which cannot be guaranteed with McKibben muscles manufactured in house. It is also more resistant to fatigue than most McKibben muscles, being rated for 1-10 million cycles depending on the load applied [14].

The structure of the Fluidic muscle differs from the traditional McKibben muscle in that the helical fibres are embedded in the elastic membrane [191]. The fibres are arranged in two layers, one with a clockwise helix, the other anti-clockwise (Figure 2-15). This separation eliminates the need for the fibres to be interwoven with the helix in the opposite direction. Friction in the braid is therefore eliminated, and the fibres can be held in a simple helix rather than the wave pattern required to go under or over the opposing helical fibres. The latter effect reduces the load being carried by the fibres.

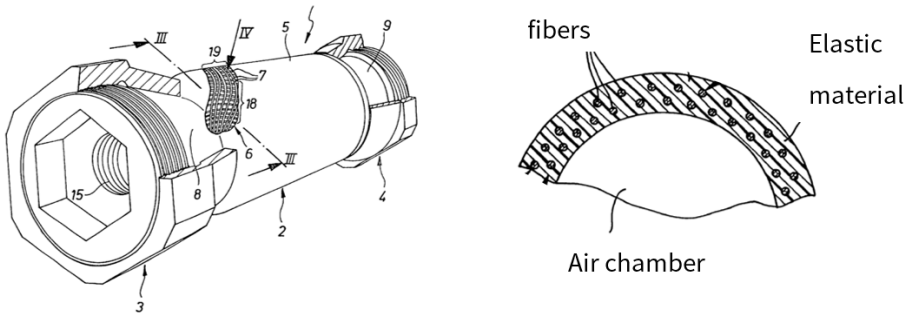

Figure 2-15: The Festo Fluidic muscle concept (left) with a cross-section of the elastic membrane and fibres (right) [191].

The Fluidic muscle is produced with two different end fitting types, a threaded conical design (Figure 2-15) and a crimped end-fitting (Figure 2-16). They are available in 4 diameters (5mm, 10mm, 20mm and 40mm) and are custom made to the required length. A range of connectors, both pneumatic and mechanical are also supplied. Some researchers have created their own end fittings for this type of muscle to reduce the overall length and mass [192].

Figure 2-16: Festo fluidic muscle MAS type crimped end fittings[14]***.***

2.4 APPLICATIONS OF PNEUMATIC MUSCLES

Due to the highly favourable characteristics of pneumatic muscles, they have been considered for a wide range of applications, in both research and industry. Unsurprisingly given their close resemblance to natural muscle performance, they have been used in many bio-inspired designs some of which are described below. A number of other application areas are also discussed, but this is far from a complete list and is only intended to give an indication of the diversity of possible uses. More examples can be found in a review by Andrikopoulos et al [11].

2.4.1 LEGGED ROBOTS

As previously described, affording legged robots adjustable joint stiffness allows them to be tuned to a particular gait, offering potential energy savings and fluidity of movement. Combined with the high power to weight ratio available with PAMs, they make an attractive option, although the requirement for a compressed air supply is a limiting factor. The ability to perform explosive movements has also been investigated, for example to perform jumping movements. A number of these robots are illustrated in Figure 2-17.

The Shadow biped, developed between 1987 and 1997 was the first bipedal robot that could stand that was built outside of Japan [193]. It made use of 14 pneumatic muscles developed by the Shadow Robotics Company in each leg. It was designed with the aim allowing a robot to move freely around a house, overcoming obstacles such as stairs. The robot stood 160cm tall and weighed approximately 31 Kg. The robot was built in a low cost manner, with a wooden frame and simple solenoid valves. It was capable of standing but only ever took a few steps. An interesting personal description of the project by David Buckley is available in [194] which details issues that were encountered with sensors and valves that illustrates some of the practical difficulties in building a robot that are rarely

discussed in the literature. The Shadow Biped is now housed in the Science Museum, London.

The bipedal robot Lucy is actuated by pleated PAMs (PPAMs). It has 6 degrees of freedom, 12 pneumatic actuators, weighs 30 Kg and is 150cm tall [85], [111], [195]. Each leg is composed of 3 modules which simplified their manufacture. The linkages between the muscle and the joint they actuate are designed so as to linearise the inherently non-linear force output of the muscle. The valves used were solenoid valve 821 2/2NC made by Matrix as these weigh only 25g and so maintain the good power to weight ratio offered by the PPAM. They also offer fast response times with a 1ms opening time. They were further modified to improve upon this response time [196]. A bang-bang controller was used for pressure control in the muscles. By using multiple valves in parallel the flow rate could be controlled more precisely and flow rate increased[197]. The position control was achieved with an adaptive PID controller. A trajectory generator and a joint trajectory tracking controller were also implemented to allow the robot to perform a walking manoeuvre. Speeds of up to 0.15 m/s were achieved. Faster speeds were not possible due to the design of the feet and limited flow in the valves. While not implemented due to the insufficient speed of the robot, control of joint compliance to exploit natural dynamics to reduce energy consumption was investigated [110].

The “Athlete Robot” was developed in the University of Tokyo to investigate bipedal running [198], [199]. PAMs were used as their performance is analogous to natural muscle. This robot makes use of bi-articulate muscles; that is a muscle which actuates two joints simultaneously. The rectus femoris is an example of such a muscle in the human leg, as it actuates both the hip and knee. The human lower leg behaves like a non-linear spring during dynamic locomotion. This fact is used by human athletes who require lower leg prostheses in the form of blade prostheses. A similar device is used on the athlete robot which has control advantages on rough terrain and at high frequency. In order to control the robot, the muscle activation pattern of a human was studied and repeated on the robot after being tested and tuned in simulation. This allowed the robot to run three steps at 1.2m/s before falling.

Mowgli is designed as a jumping robot[155]. It weighs 3Kg, has a body height of 0.9m and can jump as high as 0.5m with its 6 DOF actuated by McKibben type muscles. It makes use of biological principles such as bi articulate muscles. The torque in one joint affects the movement of others, assisting the jumping movement. The robot is controlled using solenoid valves mounted on the robot, although compressed air is supplied from an external source. The number of actuators required is reduced by using passive springs to provide the antagonist on each joint. The natural dynamics of the robot are such that the only control input to execute a vertical jump is to open and close the solenoid valves.

Being the fastest land animal, the Cheetah has been much studied by those wishing to investigate fast dynamic movement. One approach taken by Li et al. involved the use of PAMs (40mm diameter Festo fluidic muscles) to reproduce the effects of the animal's muscles [99], [200]. The robot is of course a simplification of the Cheetah; thus simulation was used to determine how best to arrange the PAMs. In all 38 muscles are used, the pressure in which is controlled with proportional regulators positioned off the robot. The maximum muscle pressure was 600kPa. Although full speed tests are yet to be reported on, leg swinging and vertical hopping tests have shown good agreement with the biological system.

Robot design based on insects has also been explored in the form of Robot V (Ajax) which is inspired by the death head cockroach *Blaberus discoidalis* [192], [201]. As the fifth iteration of this robot, it has evolved substantially. The first two versions were powered by DC motors, the third by pneumatic cylinders, the fourth by McKibben type actuators and the fifth with Festo fluidic muscles, modified to have smaller, lighter end fittings. The three pairs of legs are configured for their particular task, as in the insect. The front pair are the most dexterous, with five degrees of freedom, but are relatively weak in order to manipulate objects or navigate difficult terrain. The middle legs are largely responsible for turning and so require more power. Dexterity is sacrificed to achieve this and the legs only have four DOF. The rear legs are the most powerful and propel the robot forward with their three DOF. Torsion springs are used in some of the joints to help account for the asymmetric load (more force being required to move the joint in one direction than

the other). The robot has been demonstrated standing and performed some basic walking like movements.

Shadow Biped [194]

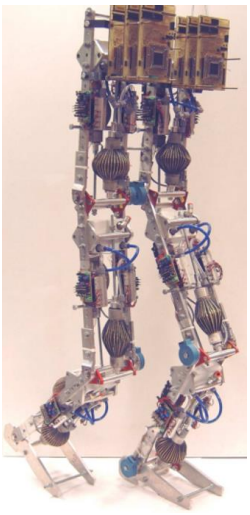

Lucy

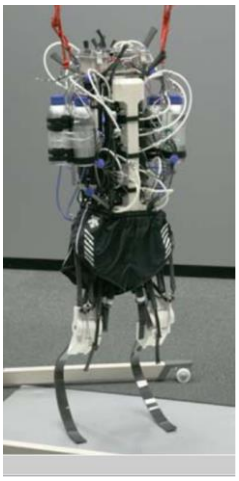

Athlete Robot [199]

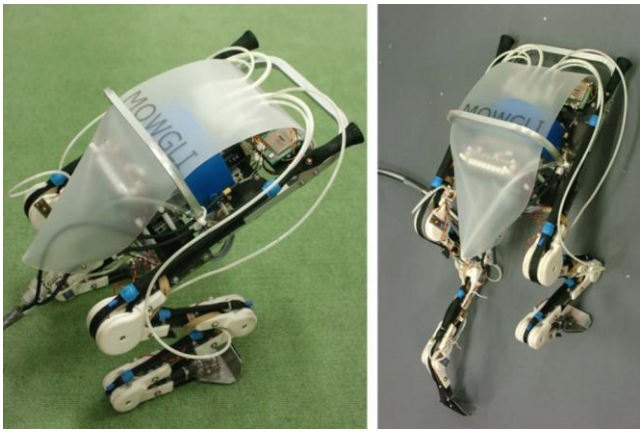

Mowgli [155]

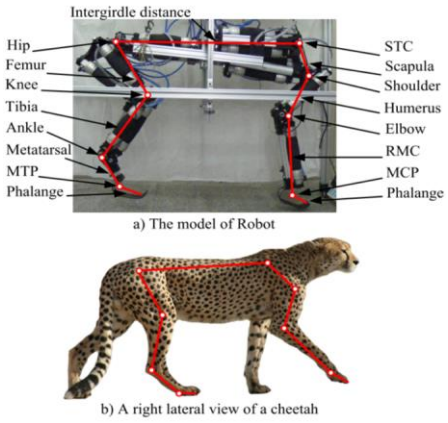

Cheetah [99]

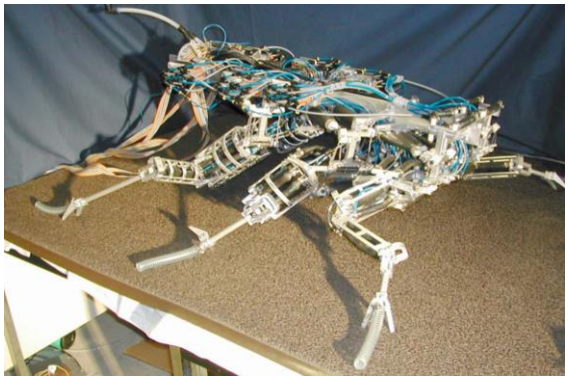

Ajax V [192]

Figure 2-17: Some of the legged robots which use PAMs.

2.4.2 ROBOT UPPER BODIES AND ARMS

Although there have been several embodiments in this area, many of the most impressive have been developed by, or in collaboration with Festo. These take inspiration from the natural world. A number of robots actuated entirely or in part by PAMs are shown in Figure 2-18.

The "Zwei-Arm-Roboter" (ZAR5) is a humanoid robot torso developed by the Technische Universität Berlin and Festo [202], [203]. It is the fifth stage of development in the project. The robot is capable of following the actions of a human operator. The body and arms of the robot contain 20 muscles and there are a further 16 to actuate each of the hands. 4 different muscle diameters are used as required. 5 port 3 way solenoid valves are used to control the air flow to the muscles. The robot is constructed using high grade aluminium and weighs 90 Kg. The robot can be supplied with air either by an in-house air compressor or a 200 bar tank commonly used for scuba diving.

Airic's arm, developed by Festo, is a much closer analogy to the human torso though still a significant simplification [204]. While the human arm, including shoulder and hand is composed of 64 muscles, the Airic's arm contains 30 muscles. The robot's structure is made from polyamide and manufactured using a laser sintering process. The robot makes use of piezo proportional valves which allow silent, precise, energy efficient control of the muscle pressure in a small, lightweight package. The total weight of the robot is only 6.3 Kg. The arm has demonstrated the ability to write on a touch screen display, testament to its accuracy and compliant behaviour. It can also lift 1Kg weights with little effect on performance.

The AirArm is a four degree of freedom arm which is biologically inspired by analysis of lobsters' and grasshoppers' legs and of human pointing gestures [205]–[207]. The design goal of the arm is to be able to reach as many points as possible in a hemisphere around a point in space. The arm has an external "skeleton" similar to that of insects, with muscles actuating the joints internally. The upper arm joint and elbow joint are each actuated by 4 muscles, a pair of muscles working in series to minimise the contraction required of any muscle. AirArm is controlled using nested feedback loops. When a movement is to be executed, this is first converted into a pressure profile for each muscle

based on a muscle and system model. If deviations are detected during execution adjustments are made, so the system “learns” and adapts. Only pressure deviations rather than positional errors are corrected for, thus reducing vibration in the dynamic movement. A pressure regulator for each muscle ensures a stable pressures in each.

RoboThespian is a life sized human robot designed for human interaction in public places and developed by Engineered Arts Ltd. [208], [209]. It is actuated with a combination of electromechanical and pneumatic systems. Joints requiring large actuating forces such as those in the elbow and shoulder are controlled with Festo fluidic muscles as they do not require energy input in order to maintain their positions. Over 60 of the robots are in operation worldwide as both a social interface in museums, exhibitions etc., but also in research. While the robot is humanoid in form, its legs are held rigidly in place and so it is not a true humanoid.

The Stanford Safety Robot, S2P uses a combination of PAMs and small electric drives, operating in parallel [83], [161], [210]. The PAMs provide the main actuation power, but small disturbances, especially those at high frequencies are compensated for using the electric drives. This allows a high level of performance to be maintained on a lightweight system. Hybrid actuation in this manner was shown to increase the maximum frequency of operation from 6Hz with muscles alone to 26Hz. Lightweight distributed pressure regulators are imbedded in the robot limbs which improve control. Multiple muscles operate in parallel to improve the range of motion without the arm becoming bulky. Safety characteristics of the robot were shown to be superior to that even of a human arm in terms of effective mass, though this does not account for the load capacity. Compliant skin with embedded proximity sensors also improve the suitability of the robot for use with humans. From the literature it appears that only one arm of the robot has been built to date.

ZAR5 [202]

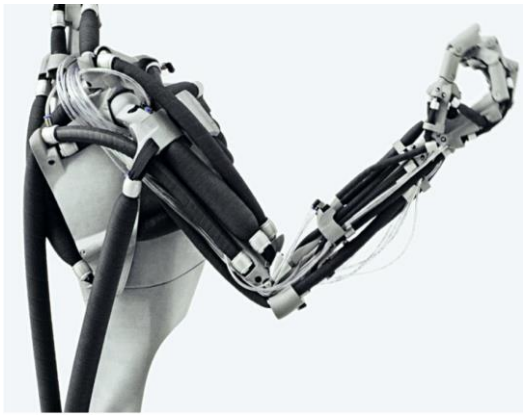

Airic's_arm [204]

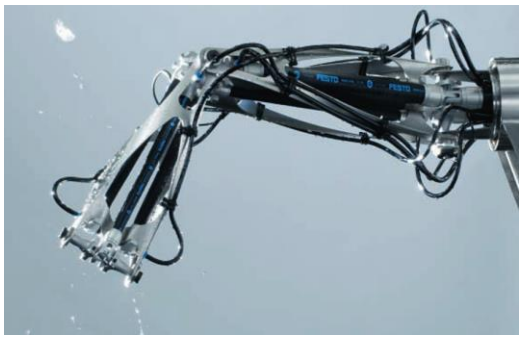

AirArm [205]

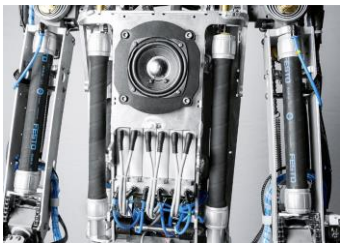

Robothespian [209]

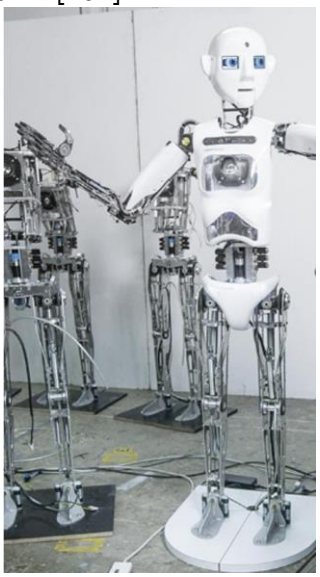

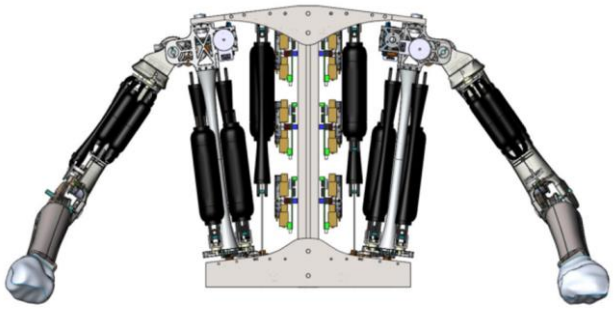

S2P [210]

Sasaki [270]

Figure 2-18: A selection of arm and torso robots.

Sasaki et al, developed a pair of PAM actuated robotic arms for the remote control of construction equipment, specifically operating a backhoe[211], [212]. This is useful, for example, for disaster response, where having the operator on board the equipment could

be dangerous. The arms developed are each composed of three modules with two DOFs per module. An air gripper on each arm grips the controls of the machine. Due to the use of lightweight materials and PAMs the mass of the arms are approximately 3Kg each. The entire unit, including valves, computational units and electric power supply has a mass of 40Kg. As multiple control levers must be operated, the arms are pre-programmed with appropriate trajectories, so an operator can switch between controls with the touch of a button. Two joysticks are then used to operate the arms and move the machine controls. The unit was installed in two separate backhoe machines and tests conducted with a user approximately 10 m away, with and without the use of cameras mounted on the backhoe. Remote control operation was only 40% less effective than the manual operation of the backhoe machines.

2.4.3 REHABILITATION DEVICES/EXOSKELETONS

Wearable devices present an interesting challenge for actuation owing to the close mechanical coupling between the device and the human operator. Exoskeletons can be used by healthy individuals to supplement the performance of the human body for particularly arduous or repetitive tasks, or for rehabilitation purposes such as prosthetics or orthosis, which assist movement of a patient's limbs. The requirements for safe operation are increased and the mass of the system must be minimised if the device is to be carried by the user. PAMs offer a potential solution due to their inherent compliance and impressive power to mass ratio [213]. They also offer performance characteristics that are comparable to that of natural muscle facilitating easier integration with biological systems. Some examples of such devices are described below and shown in Figure 2-19.

Vimieiro et al. developed a hip orthosis for patients with motor deficiency as a result of poliomyelitis [214], [215]. It consists of a polyethylene pelvic brace and a second brace on the upper thigh connected with two PAMs. A potentiometer senses the position of the joint and based on this and the anthropometric parameters of the patient, control valves contract or relax the muscle. Use of the device has been shown to improve the walking gait of patients.

Ferris et al. constructed a number of configurations of an ankle-foot orthosis. A myoelectric controller is implemented to facilitate intuitive control of the device while walking[216], [217]. Depending on the configuration one or two PAMs provide plantar flexor torque (tending to tilt the foot forward). Depending on the configuration, the foot is returned using the natural dynamics of the joint or with the assistance of an antagonistic PAM (assisting the dorsiflexor). Carbon fibre is used for the main structure helping to keep the overall mass of the system low (1.7Kg). When tested with a healthy subject the device was capable of a peak torque of 50.7Nm, 36% of that of the plantar flexor muscle. The orthosis was also adapted to provide actuation of the knee joint[218].

Costa et al. investigated an orthosis to assist both legs for patients with spinal injuries [219]. The device has 10 degrees of freedom, 8 of which are actuated. An intelligent embedded control mechanism senses hip, knee, and ankle positions, velocity, acceleration and force. This coupled with the high compliance afforded by the PAMs provides powerful yet inherently safe behaviour. The system was tested with an able bodied user and demonstrated acceptable load disturbance, muscle effort and gait tracking behaviour for use with patients with some medical conditions.

The robotic assisted upper extremity repetitive therapy (RUPERT) has been developed to provide a low cost, safe and easy-to-use, robotic-device to assist patients with upper extremity deficits [220]–[222]. Four iterations of the concept have been produced. The device reduces the stress on therapists who would otherwise manually manipulate the patient's limbs. It can also be used to assist the patient with tasks in the home such as reaching, washing and drinking, A PID based controller in combination with an iterative learning controller is implemented allows the device to adjust to different users. The orthosis has 5 actuated degrees of freedom at the shoulder, elbow, forearm and wrist. A graphite composite construction helps to reduce overall mass. Testing with six patients showed that after using the device for eight weeks, three demonstrated an improvement in reaching targets successfully, with the remaining not showing any disimprovement.

Vimieiro [215]

Ferris [217] [218]

Balasubramanian (RUPERT) [221]

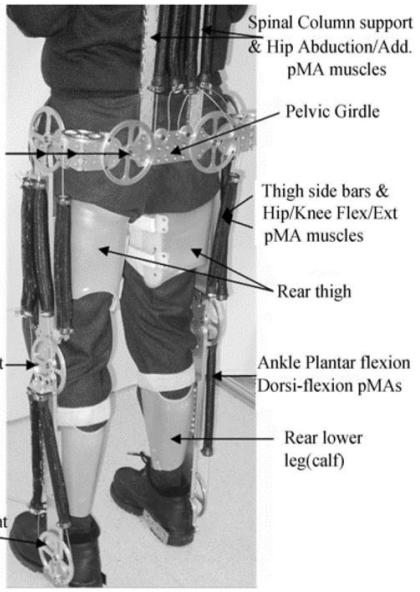

Costa [219]

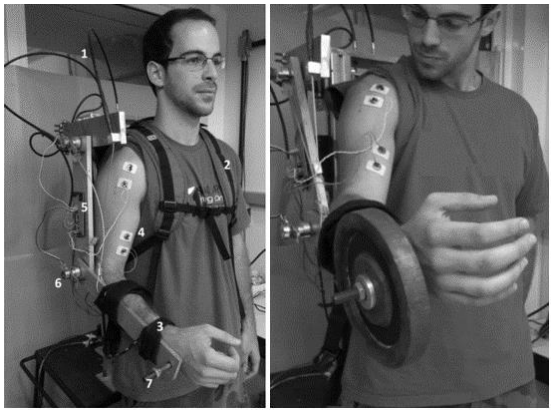

Almeida de Souza Ramos [18]

Muramatsu (Muscle Suit) [224]

Figure 2-19: A number of exoskeletons and rehabilitation orthosis which make use of PAMs.

An upper body exoskeleton to enhance human performance was proposed by Almeida de Souza Ramos et al. [18]. Surface electromyography is used to sense when the human

muscle is activated. A bank of PAMs are mounted to a frame on the users back. Force is transmitted to the joints through a system of Bowden cables. This approach means that longer muscles may be used than would be possible if the muscles were mounted directly on the linkages. Tests with a user showed much less effort was required to lift a weight while using the exoskeleton and this weight could be held statically more reliably due to the reduction in muscle fatigue.

A “Muscle Suit” is designed to assist workers who must complete manual tasks such as in nursing and types of manufacturing [223], [224]. Now in its fourth iteration, the suit uses McKibben muscles to actuate the shoulders, elbow and hip. It is suggested that in a typical application compressed air can be supplied to the suit from an overhead air line and so there is no attempt to include a compressor as part of the suit. Near infrared spectroscopy is used to indirectly measure haemoglobin in the blood and thus evaluate the level of physical effort exerted by a user. In some users this showed that the muscle suit reduced the human effort required.

2.4.4 OTHER APPLICATIONS

A number of applications of PAMs exist outside of robotics and orthosis devices. These include the industrial domain, aerospace and architecture. A sample of these are shown in Figure 2-20 and described below.

The PAM has found some use in the industrial and manufacturing sector. While the levels of uptake are not fully clear, Festo have published a report detailing the “established areas of application” for their Fluidic muscle [225]. The muscles can be used for clamping, being capable of delivering large forces in a small volume. It is also frictionless and unaffected by dirt. As an actuator for vibrating and shaking, it is capable of both low and high frequency operation (up to 150 Hz). Amplitude and frequency can be adjusted separately. When used as a pneumatic spring with an adjustable spring force, the muscle can tension belts, adjust contact force between rollers, control thread tension when winding treads etc. The Fluidic muscle has also been suggested for use as a lifting aid, for punching and to actuate an emergency stop [14].

Owing to their low mass, PAMs have been explored for use in aerospace applications. Most notable is the work by Woods et al, which focuses on the use of McKibben type PAMs

for morphing structures for wings and the control of trailing edge flaps for fixed wing and rotary air craft [226]. The use of PAMs in such applications requires a large increase in the lifetime of the actuator and this was achieved using a swaging technique [149]. PAMs were shown to be capable of operating at the required frequencies (of up to 40Hz) for such applications. Full scale whirl testing was also conducted and showed good control under aerodynamic, inertial and centrifugal loading [227]. Other examples of the use of PAMs in aerospace include that of Brown et al, who explored the use of PAMS for soft-landing parachute retraction systems[228]. Their light weight and high force output are critical for this application but their flexible nature, allowing them to be packed with a parachute when deflated, is also key. Payloads of up to 9000Kg are considered and the PAM is the link between the parachute and this load. Contraction of the muscle slows the payload just prior to ground impact. A number of tests were conducted to validate the PAM including dummy drop tests, actuated with a high pressure cylinder and pyrotechnic gas. A very large PAM (6 inch diameter, 14ft long) was constructed for larger tests and it was estimated this could produce accelerations of up to 8.8g. The affordable guided air drop system (AGAS) uses similar techniques to deform a parachute and guide it to a target [229]. Accuracies of 70 metres were achieved with 15 fully autonomous airdrops using simple circular parachutes.

A “motion seat” was developed by Pohl which uses six PAMs in a hexapod configuration for applications in simulations such as flight simulation [230], [231]. Due to the lack of stiction on pneumatic muscles, smooth, precise motions can be realised. The seat is suspended by 6 muscles which work together to realise rotations and small translations in 3 dimensions. The device was tested with flight, car racing and rollercoaster simulations.

Woods [226]

Pohl [230]

Decker [232]

Air muscle tower 2 [234]

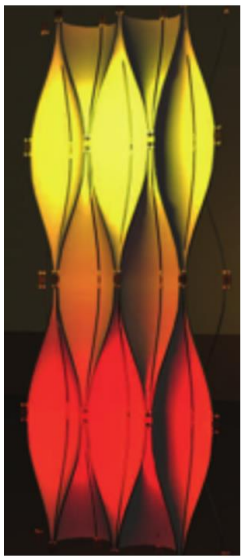

Muscle facade [234]

Figure 2-20: A number of applications of PAMs.

In order to investigate the modal parameters of bridges and other large constructions they must be excited at a range of frequencies. PAMs have been proposed as a means to accomplish this by Decker et al. [232] The advantages of PAMs in this application are compactness and speed of setup. As part of the study a bridge was excited by a Festo muscle using a linear sinesweep of 32 seconds at frequencies of 0.5 to 10 Hz. It was concluded that modal analysis was possible using a PAM, however background noise from traffic etc. masked much of the vibration so a larger muscle should be used.

PAMS have also been used in architectural structures. The term “Airtecture” was coined by Festo for such structures when they developed a warehouse museum partially supported by PAMs [233]. The soft structure could react to high winds and remain stable. Other projects looked at how structures could respond to people, as well as natural stimuli [234]. The muscle tower 1 and 2 were 1:20 models of a possible building structure. It was envisaged that the tower could adapt to external environmental conditions and usage patterns. The roof could respond to changes in solar radiation throughout the day, as well as monitoring wind speed to keep a skyscraper perfectly vertical in high winds. The morphology of the building could augment in reaction to users to suggest new ways of interacting. Use of the towers for billboard advertising could allow it to reorientate to face the most people.

The “muscle body” consisted of a Lycra skin actuated with 26 muscles [234]. There was no distinction between walls, floor and ceiling and the structure would react to occupants which entered it. A similar project, the “muscle space” was a hallway with flexible PVC walls which could move in complex ways in response to pressure sensors which tracked people through the space. The “muscle facade” was developed to break the stereotype of the facade of a building being a barrier. The shape and colour would change in response to external stimuli such as weather forecasts and feedback from sensors. If multiple buildings were constructed together they would “learn” from each other and develop complex behaviour.

2.5 MEASURING THE PERFORMANCE OF PNEUMATIC MUSCLES

In order to access the best use of PAMs in an application and to control them in an effective manner, it is necessary to characterise the behaviour of the actuator. The

manner in which the actuator is used will influence its behaviour. As such experimental evaluation must be conducted under a range of loading conditions and with different design parameters (diameter length, braid angle etc.). This can be used to generate a model of the actuator which can then be used by designers and control engineers. This section details the characteristics of PAMs which have been established through experimental evaluation.

2.5.1 FORCE PRESSURE LENGTH CHARACTERISTICS

The relationships between internal pressure, contraction and force output is paramount to understanding the fundamental characteristics of PAMs. Experiments are generally conducted holding one of these constant, controlling another and measuring how this affects the remaining quantity. As described below, it has been observed that increasing the length of PAMs gives a linear increase in absolute contraction. Therefore, in an attempt to generalise the results, the contraction is usually referred to as a percentage or ratio of the active length of the muscle in a relaxed state (nominal length) [22], [235]–[237].

A number of testing procedures have been used to establish the relationship between these three parameters.

Isometric Conditions

The muscle length is held constant and pressure is varied while the output force is measured. The muscle therefore does no external work[22]. This can be achieved, for example, with a material testing machine which holds the muscle at a specified length and measures the force output as it is pressurised [86].

Figure 2-21 shows a number of isometric tests of various muscles. From these it is clear that there exists an approximately linear relationship between muscle pressure and force output at a constant contraction ratio. When tests are repeated at different contraction ratios it is evident that at greater contraction the force output is reduced. Indeed, at low pressures and large contractions there is no force output at all. This is because at low pressures the muscle cannot contract to the specified contraction ratio even when no load is applied. This is an important consideration as it limits the overall contraction available if a low pressure source is used.

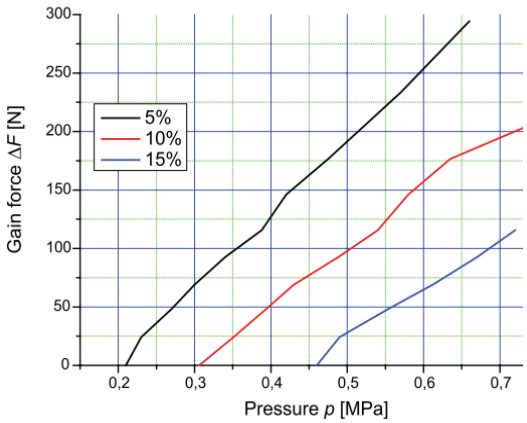

Festo Fluidic muscle 10mm diameter, 300mm long [238]

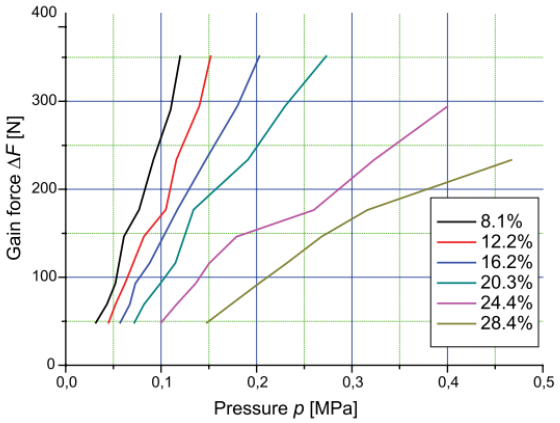

Shadow air muscle 19mm diameter, 173mm long [238] diameter, 300mm long

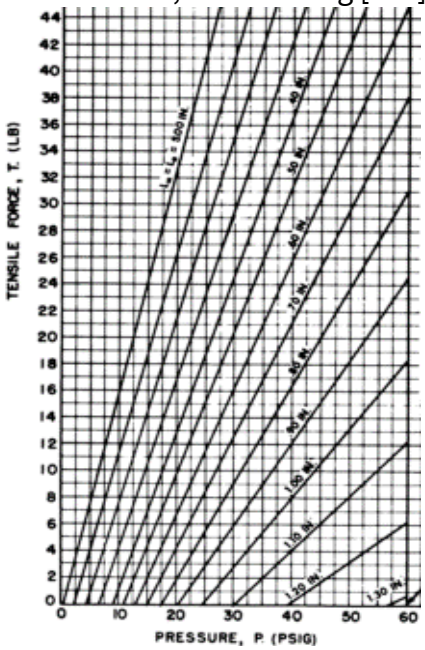

McKibben muscle diameter 24mm, length 127mm [22]

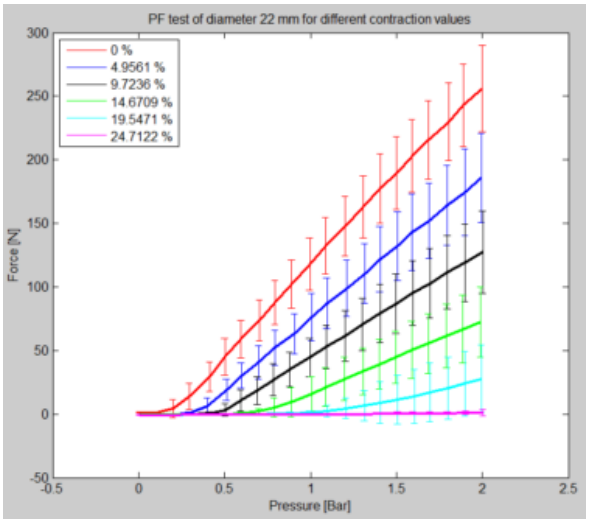

McKibben muscle diameter 22mm, length 110mm [175]

Figure 2-21: Isometric tests of several muscles in the literature.

Isotonic Conditions

The muscle force is kept constant as pressure is controlled the change in length is measured. A mass is attached to a vertically suspended muscle. Contraction is measured as the muscle is pressurised from a supply voltage. The contraction must be slow so that the inertial effects of the mass are negligible.

Figure 2-22 shows isotonic tests, graphing contraction as a function of pressure with. The graphs are approximately logarithmic in nature, though there is certainly variance depending on the muscle design tested. As the muscle shortens the relative change in

pressure required to maintain an output force increases. This is due to the braid angle approaching its limit. This information is important for design, as it will limit the range of motion which can be achieved using a PAM once the required force across the range of motion is known. For instance, if an antagonistic pair of muscles are used to actuate a joint, and a uniform torque profile is required across the full range of motion, the limiting minimum torque will be that at the extremes of travel.

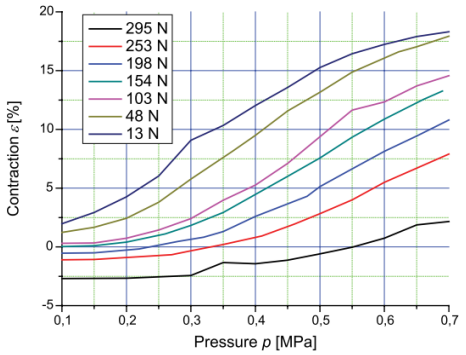

Festo Fluidic muscle 10mm diameter, 300mm long [25]

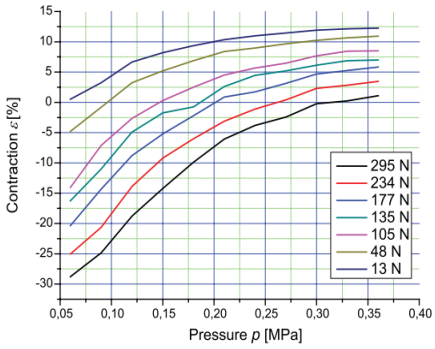

Shadow air muscle 19mm diameter, 173mm long [25]

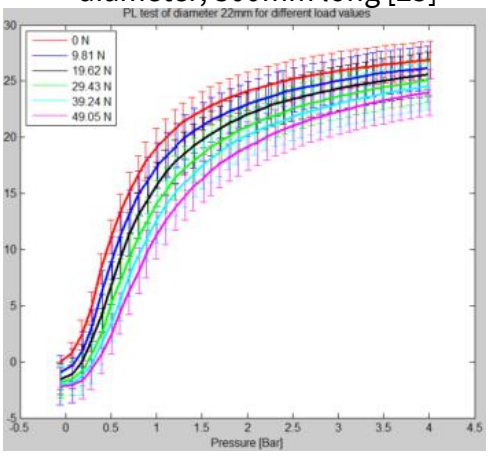

McKibben muscle diameter 22mm, length 110mm [175]

Figure 2-22: Results of isotonic muscle tests found in the literature.

Isobaric Conditions

Pressure is held constant while contraction occurs due to changes in force applied. The muscle is held in a device such as a tensile testing machine or any apparatus wherby tension may be applied to the PAM by means of a tensioner or the addition of masses. The PAM is pressurised to the test pressure. The apparatus then allows the muscle to contract. This results in an increase in muscle volume which must be accounted for if

pressure is to be held constant. A large buffer tank can render the volume/pressure change insignificant or a pressure regulator can be used. The tests may also be repeated for PAM elongation. Isobaric test results from [235]–[238] are depicted in Figure 2-23.

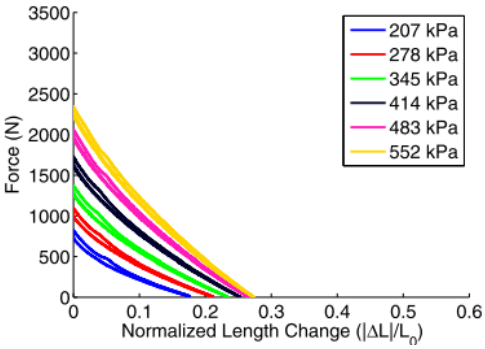

McKibben muscle diameter 25mm, length 200mm [235]

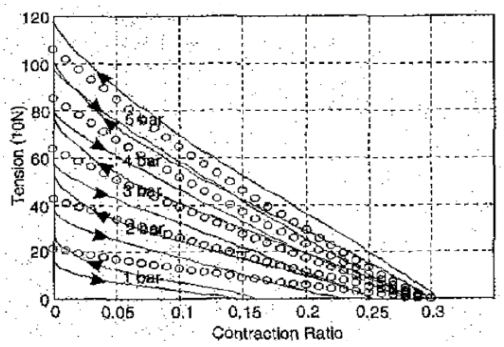

McKibben muscle diameter 14mm, length 300mm [236]

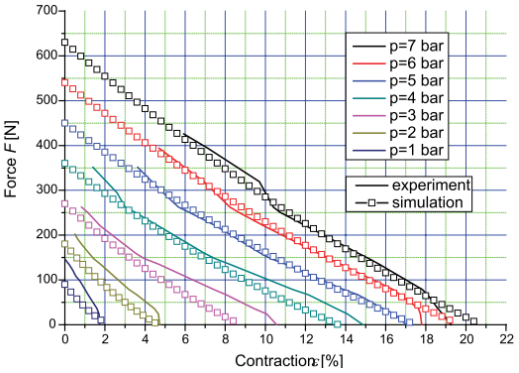

Festo Fluidic muscle 10mm diameter, 300mm long [238]

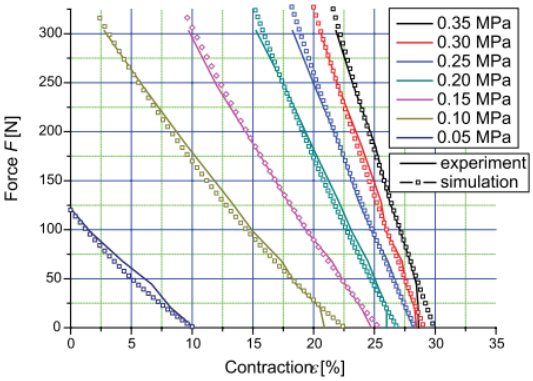

Shadow air muscle 19mm diameter, 173mm long [238]

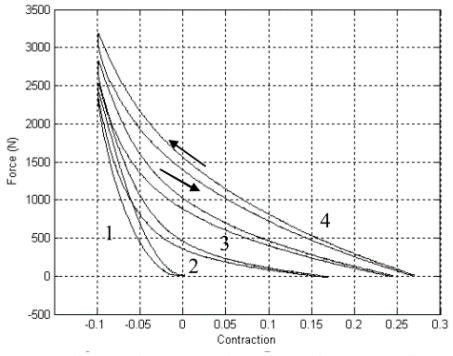

(1: 0 psi, 2: 30 psi, 3: 60 psi, 4: 90 psi)

McKibben muscle 25.4mm diameter, 89mm long [237]

Figure 2-23: Results of isobaric tests found in the literature. In all cases solid lines represent experimental results while points are theoretical.

Testing shows that at constant pressure, force output is inversely proportional to contraction. Again the exact characteristics are dependent on the PAM design with

almost linear results in [238] while the other results show a faster reduction in force output closer to the PAMs maximum length. Another reason for this may be difference in experimental procedure. In particular, the determination of when the PAM is at rest length (contraction = 0) creates some difficulty. As the deflated PAM is somewhat elastic, some authors may apply a pre-strain to the PAM (in order to ensure it is straight and there is no slack in the system) while others do not. In most cases this factor is not reported. It is also clear that at higher pressures the contraction at which force reaches zero tends to converge. This is a limit of the muscle braid as the braid angle approaches a maximum.

2.5.2 HYSTERESIS

Hysteresis is mainly observed in muscle contraction/elongation cycles, with a larger force output at a given pressure and contraction when the muscle is contracting as opposed to elongating. This is a major challenge to successfully modelling the muscle's dynamic behaviour [13]. Chou and Hannaford investigated this in some detail [136]. In their experiments the muscle internal pressure was set and maintained by a pressure regulator and buffer tank. An electric motor then provided the force to displace the muscle.

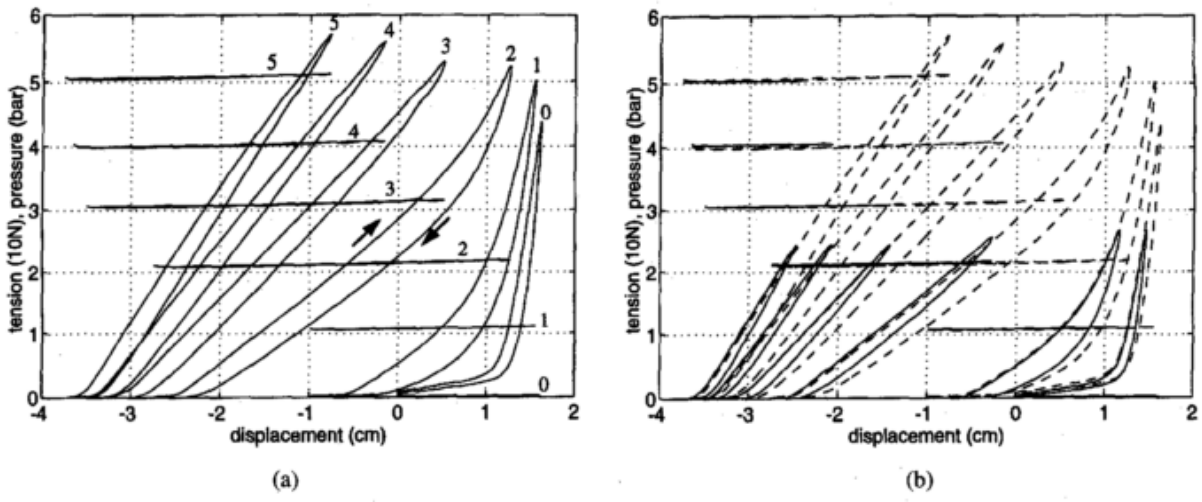

Figure 2-24: Hysteresis results under isobaric operating conditions. (a) shows the force displacement curves at several pressures when the displacement frequency is 1Hz, (b) shows higher the same test at 0.25 Hz (dashed lines) while the solid lines show 1 Hz excitation but with approximately half the displacement [136]***.***

Figure 2-24 (a) shows the hysteresis observed when the actuator is operated at 1Hz. This appears to show a decrease in hysteresis with pressure increase. Figure 2-24 (b) shows

the same test conducted at 0.25 Hz (dashed lines). This is almost identical to Figure 2-24 (a), meaning, at least at low frequencies hysteresis is independent of contraction speed, leading the authors to conclude that static coulomb friction is the main source of hysteresis. The solid lines represent the results of 1 Hz tests but with half the displacement. Significantly less hysteresis is observed, which suggests hysteresis is history dependent. This result conflicts with that of Davis and Caldwell however who found that after a short correction period, the same hysteresis loop is followed, regardless of the level of contraction achieved (Figure 2-25 (a)) [176]. Experiments conducted by Doumit also suggests hysteresis is independent of the maximum contraction during the cycle, although here an isotonic test procedure was employed, rather than isobaric as in the previous examples (Figure 2-25 (b)) [13].

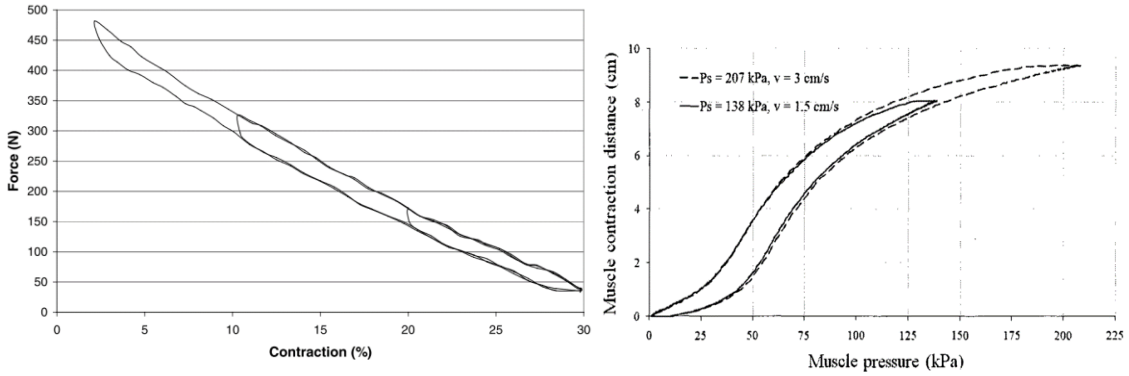

(a) (b)

Figure 2-25: Contraction cycles of a muscle with (a) 200kPa gauge pressure over multiple maximum contraction distances [176] ***and (b) contraction cycles with different pressures and velocities*** [13]***.***

2.5.3 BANDWIDTH

The bandwidth of the muscle is limited by the speed at which the internal pressure can be varied. It is therefore impossible to consider the bandwidth of a muscle without reference to the system which supplies pressure to it. For example in Figure 2-25 (b), the supply pressure was increased from 138 to 207kPa resulting in a doubling of the maximum contraction speed of the muscle, as a greater mass flow rate into the muscle is achieved.

Chou and Hannaford also examined the dynamic response of PAMs using a 14cm long 1.1cm diameter muscle with a nylon braid controlled with a Festo MPP-3-1/8

proportional pressure regulator supplied with compressed air at 5 bar [136], [239]. For their system, there was a 5ms delay from a control voltage being applied to the start of pressure increase due to the valve mechanics. Starting from a deflated muscle, under isometric conditions there is a further 7ms delay in force output as the pressure must overcome the threshold pressure of the bladder. The tension rise time (from 0 to 90%) for the maximum tension is 30ms, while the falling time (100% to 10%) is 53ms. This disparity in rise and fall time is discussed in section 2.6.7 below. During isotonic tests, the maximum average velocity was found as 41 cm/s and peak velocity 86.6 cm/s.

Reynolds also observed a delay between the application of pressure and the accompanying change in pressure, though this was attributed to stiction in the braid, rather than bladder threshold pressure [182]. Under isotonic tests, it was observed that the delay increased with applied load and decreased with pressure.

Kingsley and Quinn operated a PAM at a number of frequencies to establish the dynamic behaviour of the system [150]. The PAM used was relatively small, with a maximum length of 68mm and 11mm diameter. The valves used are not specified though it is noted that their small orifice size is the limiting factor on mass flow rate in the system. Figure 2-26 shows the results of two isotonic tests, whereby solenoid valves are used to provide a square wave pressure input. There is clearly a limit on bandwidth, whereby the contraction achieved is attenuated at higher frequencies, due to insufficient time for the required flow rate to pass through the valves. When larger forces are applied the PAM is capable of full contraction at higher frequencies. This is because, due to the applied load the muscle does not contract as much and so a smaller volume must be filled.

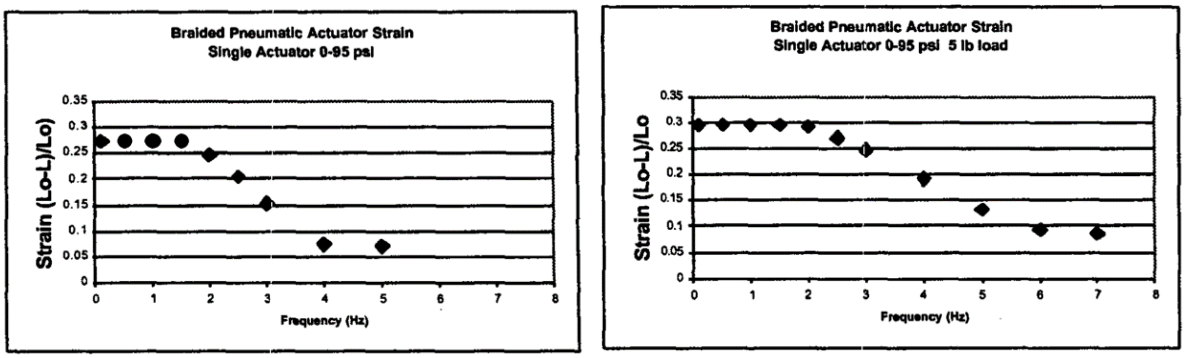

2.7Kg applied load 5.4Kg applied load

Figure 2-26: Frequency response of identical PAM systems with different applied loads [150]***.***

The bandwidths depicted in Figure 2-26 are typical of those described in the literature. It is important to remember however this is also dependent on the the pressure supply system and is not a general limitation of PAMs. The work by Woods et al show dynamic responses of PAMs at frequencies of up to 35Hz for use in aerospace applications [163]. While the pressure changes at this frequency are relatively small, substantial useful work can be achieved, moving a trailing edge flap through angles of up to 30°. A proportional spool valve (Festo MPYE-5-1/8-HF- 010-B) with a high flow rate is used to achieve this performance.

2.6 DESIGN PARAMETERS

Understanding muscle behaviour and how design of the muscle structure influences that behaviour is important for design, modelling and control of the actuator. Two main parameters are correlated with these design specifications, maximum contraction ratio and force output.

2.6.1 INITIAL LENGTH

This is the length of the active part of the muscle before it is pressurised. In some instances, the muscle may be stretched past this length during operation. In [13] muscles of length 17cm, 34cm and 51 cm with identical diameters (2.4 cm) were tested. The muscle lengths were measured when the braid angle was 20°. Their maximum contraction ratios were 23.84%, 27.7% and 27.8% respectively. The reduced contraction for the 17cm muscle was attributed to distortion of the braid near the end fittings, which occurs for each muscle, but over a more significant proportion of the length for the

shorter PAM. It was concluded that original length does not influence maximum contraction. A similar conclusion was reached by Kothera et al, [86] when muscles with a 12.5mm external diameter were tested (see Figure 2-27) and earlier by Schulte [22]. This means that absolute contraction increases linearly with muscle active length.

When maximum muscle force is compared it is approximately the same for muscles of different lengths at the same internal pressure [13], [22], [86]. This can be understood by considering that the maximum force occurs when the PAM is at its full extension and so the muscle braid angle will be the same regardless of PAM rest length. A sample of these test results are shown in Figure 2-27.

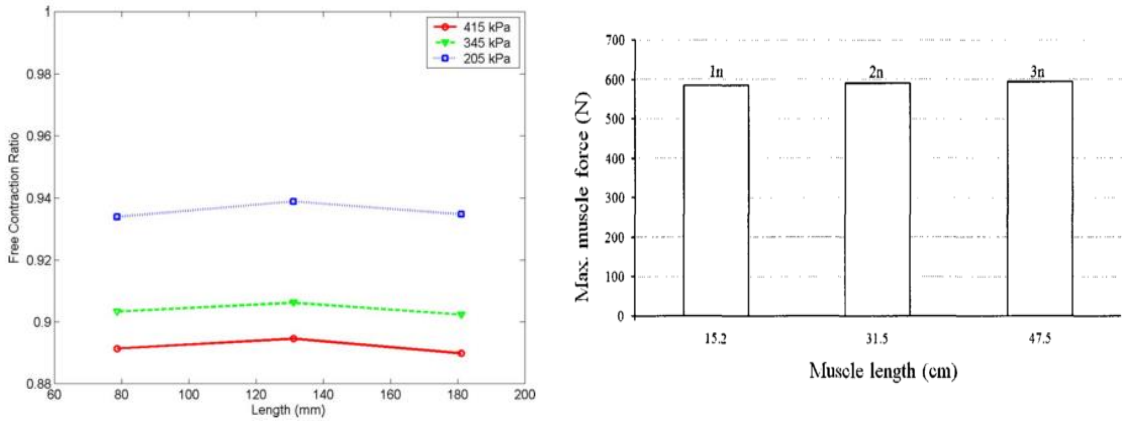

Figure 2-27: Left: free contraction ratio as a function of original length at three internal pressures [86] ***(Note contraction ratio is here defined as the current muscle length as a ratio of the original length). Right: blocked force output for three muscles of different length [13].***

2.6.2 MUSCLE DIAMETER

This can be measured as either the muscle internal diameter (inside the elastic tube), or the braid diameter. The increase in internal diameter produces an apparent quadratic increase in muscle force according to [86], although only three muscles are tested. This is supported by energy based models, such as that in the original Gaylord patent[168] where muscle force is directly proportional to the volume increase as length reduces. Doumit also found that force increases with muscle braid diameter[13]. When the braid diameter was increased from 0.9cm to 1.9cm there was a 6 fold increase in force output. Contraction was also increased from 16.97% to 29.1% with the larger diameter muscle. This assumes that the braid angle is the same when the muscles are at rest. Doumit

suggests this is due to the reduction in energy used to expand the elastic membrane for larger diameter PAMs [13]. This result is also supported by the results in [86].

Examining the performance properties published by Festo for their fluidic muscles reveals that maximum force increases for larger diameter muscles [14]. Only permissible forces are published however, likely limited by the required lifetime of the muscle and the materials used in the muscle construction. This gives a more linear increase in output force with muscle diameter.

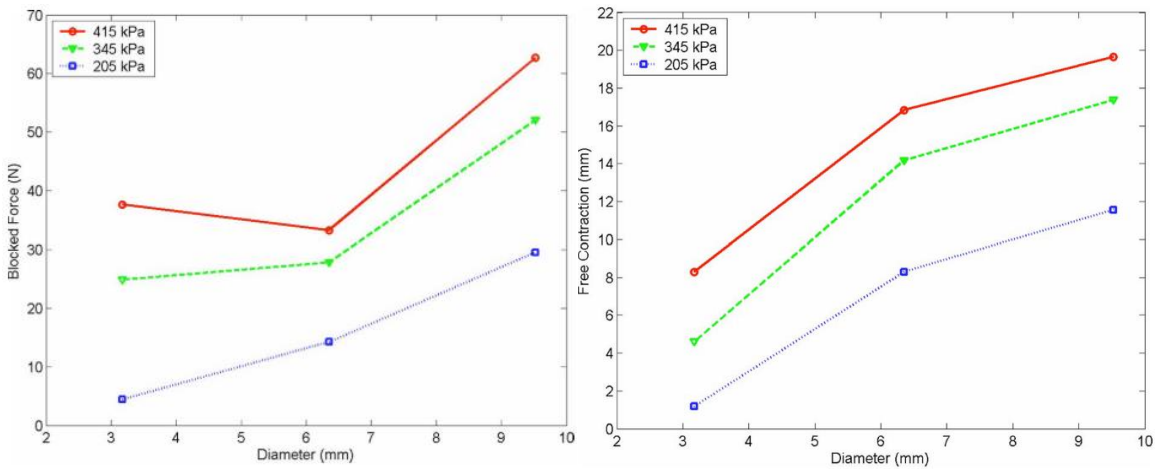

Figure 2-28: Left: the relationship between blocked force (no contraction) and PAM original diameter. Right: The relationship between free contraction and diameter. From [86].

2.6.3 MUSCLE END DIAMETER

This is the muscle diameter where it attaches to the end fitting. As the muscle cannot expand at this point, this acts as a constraint on the muscle. PAMs with a braid diameter of 1.9cm, and end fittings with 1.3cm, 1.6 and 2.5 cm diameters were tested by Doumit [13]. It was found that the muscles with smaller end fitting diameters produced a smaller force output but greater contraction. This is attributed to the curved section of the inflated muscle (shaded red in Figure 2-29) as it approaches the end fitting. The curvature here is more exaggerated for smaller end fitting diameters, and therefore results in more contraction. The increase in muscle force with larger end fitting is due to the smaller inclination angle between the braid and the end fitting as the muscle inflates (β in Figure 2-29). As the force is transmitted through the braid, if the force vector in the braid is more aligned with the direction of contraction, a greater contraction force is realised.

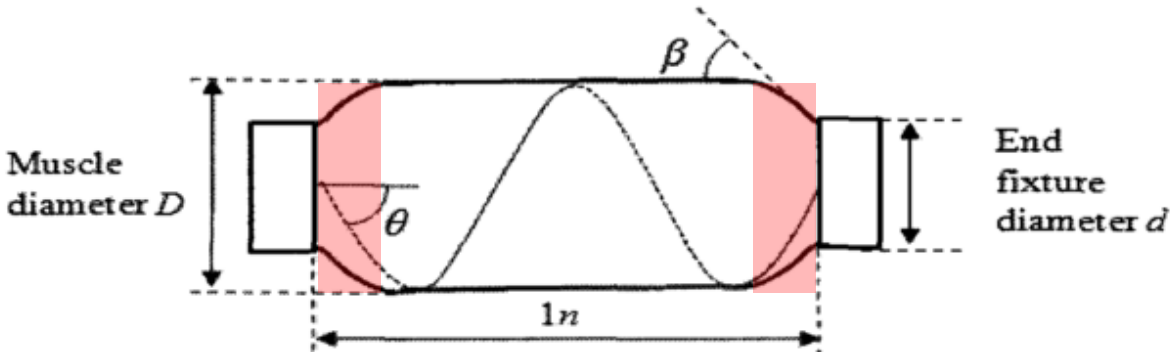

Figure 2-29: Diagram of a muscle showing the angle of inclination between the end fitting and muscle braid [13]***.***

2.6.4 BRAID PROPERTIES

The braid angle, the angle of the fibres in the muscle relative to the longitudinal axis of the muscle, increases as the muscle contracts before reaching a maximum (see Figure 2-13). While the theoretical maximum braid angle under contraction is 54.74° [22], this is not usually realisable due to friction in the braid. The initial value of the braid angle before contraction as well as the density of fibres are therefore factors which limit the maximum contraction possible.

Experimental results show a modest increase in maximum contraction when the initial braid angle is reduced from 49.1° to 28.2° [86]. There is however a large increase in blocked force (0% contraction) especially at higher pressures. At a pressure of 415 kPa there is a 6-fold increase in force output when the braid angle is reduced to 28.2°, although the effect is not as dramatic at lower pressures. Davis et al, proposed modifying the braid to decrease the minimum braid angle (when the muscle is fully extended) as the maximum braid angle cannot be modified [176]. This can be achieved by reducing the number of fibres in the braid to allow more space for them to straighten before contacting each other when the PAM is at full extension. As well as increased contraction and force output this also reduces friction in the braid and therefore hysteresis. The disadvantages of this is a greater chance of braid failure due to the increased stresses, and rupture of the bladder due to the larger gaps between the fibres. Results showed that there was a 7% increase in actuator contraction when the braid angle was reduced from 19° to 9° and a 16% increase in blocked force. Similar results showing greater contraction with lower density braids are found in [22], [136].

The braid material also plays an important role. Aramid (Kevlar) and polyethylene terephthalate (PET) are commonly used [13] as well as fiberglass and nylon [136], [240]. These fibres have high stiffness, which is important as elongation of the fibres results in reduced force output and elongation. In [13] it was suggested that owing to the high stiffness of PET, the elongation of the braid is of the order of 1.2% of the muscle contraction length and thus negligible (though this depends on the dimensions of the braid and muscle). Davis et al, found a 5% strain in the nylon braid fibres of a muscle with length 1.77m and pressure 450kPa [133]. This significantly reduced force output, and when included in the model, substantially increased accuracy.

The braid is also largely responsible for the hysteresis observed in the muscle contraction due to friction between the fibres. Tondu and Lopez argue that while there is friction between the braid and the bladder the operating principle of the muscle means these are locked together when the muscle is pressurised [236]. The nature of the braid in terms of material and geometry affect how a muscle's hysteresis will behave under these conditions. Large flat fibres have more contact area between them and so friction is increased as is hysteresis. For example in [13], flat Kevlar fibres resulted in greater hysteresis and stiction than their nylon counterparts. Cylindrically shaped PET fibres reduce the contact area, although some deformation will occur due to the large stresses and interweave [176].

2.6.5 BLADDER PROPERTIES

In general, the expansion of the elastic bladder requires energy, and so stiffer bladders reduce the output force and maximum contraction of the muscle.

Doumit examined two muscles with the same braid, but with 1.4cm and 2cm internal diameter bladders [13]. The larger bladder must expand less elastically, and thus has a larger force output and contraction. Additionally, a smaller bladder, with more elastic energy upon contraction results in greater hysteresis. The thickness to inner diameter ratio of the bladder was considered by Kothera [86]. Increasing the bladder thickness increases the energy requirement to inflate the muscle. This leads to a lower force output and shorter contractions for muscles with thicker bladders. This was shown in test results with a linear decrease in contraction ratio with bladder thickness to diameter ratio.

Similar results were observed by Pillsbury et al, who studied the bladder properties of miniature PAMS (diameter 3-4mm) [241]. They observed that muscles with larger volumes of bladder material had smaller contractions and force output. They also had a higher threshold pressure, below which the bladder does not deform elastically and so force output and contraction is severely limited.

Ball et al also showed reduced force output with bladder thickness and stated that this effect is more pronounced for smaller diameter muscles as the bladder often takes up a large percentage of the muscle overall volume [242]. Reduced hysteresis was observed with thin walled bladders. It was also shown that bladder pre-strain (that is stretching the bladder longitudinally in the muscle so it is under strain when the muscle is at its rest length) increases the force output of the muscle, as well as the contraction which is possible (contractions greater than 50% were recorded). Depending on the application this may be a useful design feature. For example, in an antagonistic pair of muscles, one may require more force than the other (perhaps working against gravity) thus pre-straining one bladder may be useful.

The material properties of the bladder also play a large role in muscle performance. More elastic materials reduce the muscle threshold pressure, and, even assuming no pre-strain, increase the contraction and force output. Viton rubber, latex and low density polyethylene (LDPE) were investigated for use as bladder materials in [138]. In the case of LDPE, the bladder did not operate elastically, but rather the diameter of the tube was less than that of the fully inflated muscle and it crumpled when the muscle was deflated. The results of these tests are shown in Figure 2-30. As Viton is stiffer than latex, it produces more contraction and force output. While LDPE performs better than either, friction is also much greater, as is hysteresis. Nonetheless use of this bladder without elastic energy storage gave an approximate 20% increase in actuator efficiency. Other materials such as bicycle tubes have also been used and were said to have a low threshold pressure [13], [182], [243]. Doumit compared silicone and butyl rubber bladders, finding that, at constant pressure, silicone gave a greater increase in stiffness with eccentric contraction testing (elongation driven by an applied load) [244]. This was

attributed to the higher threshold pressure of the silicone bladder, restricting the capacity of the material to move radially.

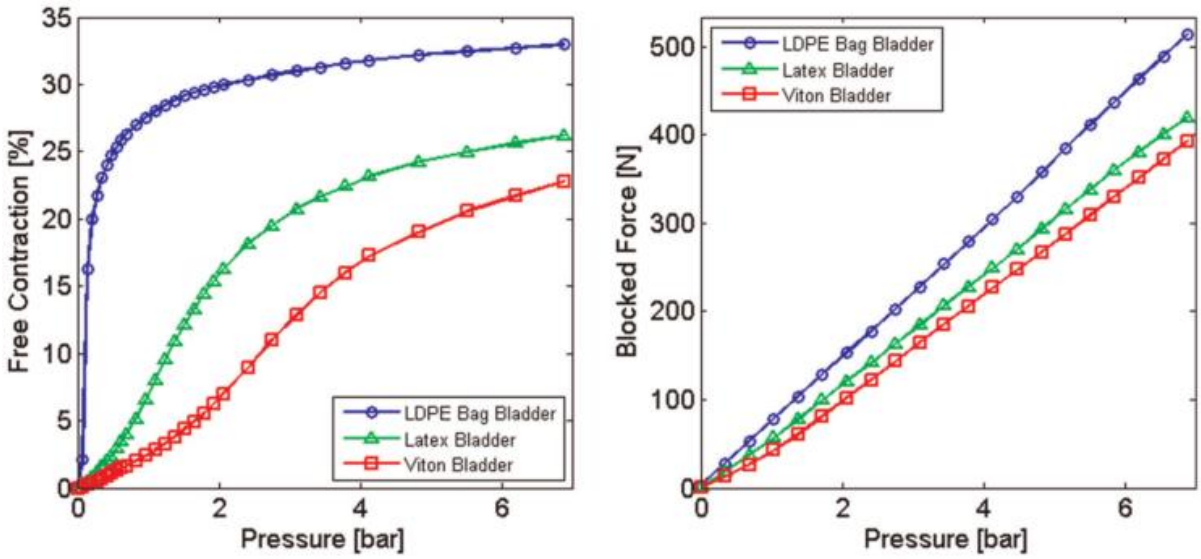

Figure 2-30: Free contraction (left) and blocked force (right) of muscles with different bladder materials [138]***.***

2.6.6 WORKING FLUID

Although technically not a pneumatic muscle if compressed air is not used, variations of the same design have been used with gasses and liquids. Indeed Joseph McKibben's initial work used compressed carbon dioxide [22]. The main variations in performance come where liquids are considered however, due to their lack of compressibility. Focci et al. quantified a number of these differences [245]. It is noted that static characteristics are identical, as the force output of an individual PAM is dependent only on the contraction and gauge pressure; the medium which applies the pressure is irrelevant. Dynamic characteristics do differ however, as the compressibility of air slows the response of the gas actuated system. Bandwidth was experimentally shown to reduce by 20% for the system using air under isometric muscle testing. It should be noted that under these conditions the volume of the muscle is constant (as it does not contract) and so this result reflects the reduction in bandwidth of the fluid supply system (valves, tubing etc.) to fill a fixed volume. Positional control under dynamic conditions showed increased overshoot when water is used, potentially due to the greater stiffness of the muscle. Adding a derivative term in the controller was postulated to improve this. The

muscle stiffness with both fluids was also examined experimentally. The results in Figure 2-31 show much larger stiffness with the water actuated muscle.

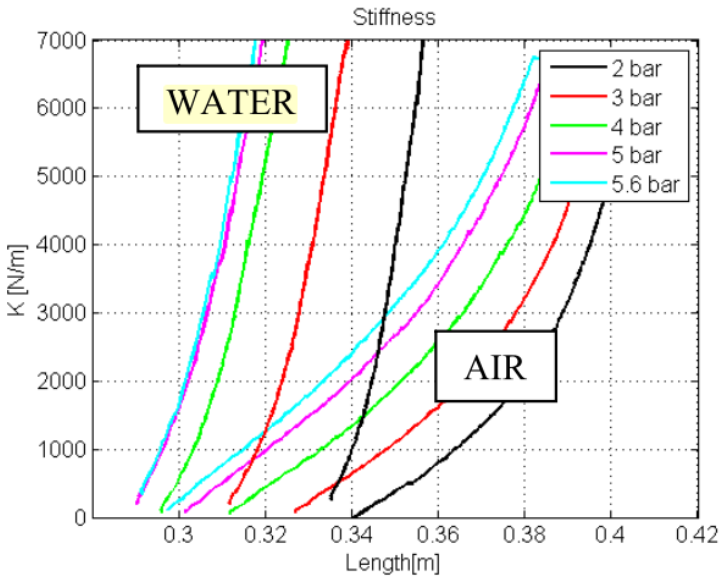

Figure 2-31: Experimental stiffness comparison of water and air actuated muscles [245]***.***

Meller compared the efficiencies of both hydraulic and pneumatic muscles [138]. It was found that as a result of the increased volume of air which must be pressurised (as a result of its compressibility), the efficiency of hydraulically actuated muscles is far superior. This is illustrated as a function of both pressure and contraction in Figure 2-32. At small contractions the difference in efficiency is most dramatic, due to the relatively large volume between the end fittings which must be filled with fluid, but which does not provide any actuation force.

Other studies looked at the possibility of using high strength water operated PAMs for under water applications [246] or for high force applications, where the muscle can be driven with a pressure of up to 7 bar[247], [248]. It is suggested that hydraulically driven PAMs are better at high pressures as air becomes less efficient and may be more dangerous should a muscle rupture.

The greater stiffness of water or oil actuated PAMs make them a less attractive option for service robots as it impacts the safety characteristics of the muscle as well as its ability to react to physical interaction with its environment. They also add more mass to the system and require that fluid exiting the muscle be returned to a reservoir rather than exhausted to the atmosphere [247].

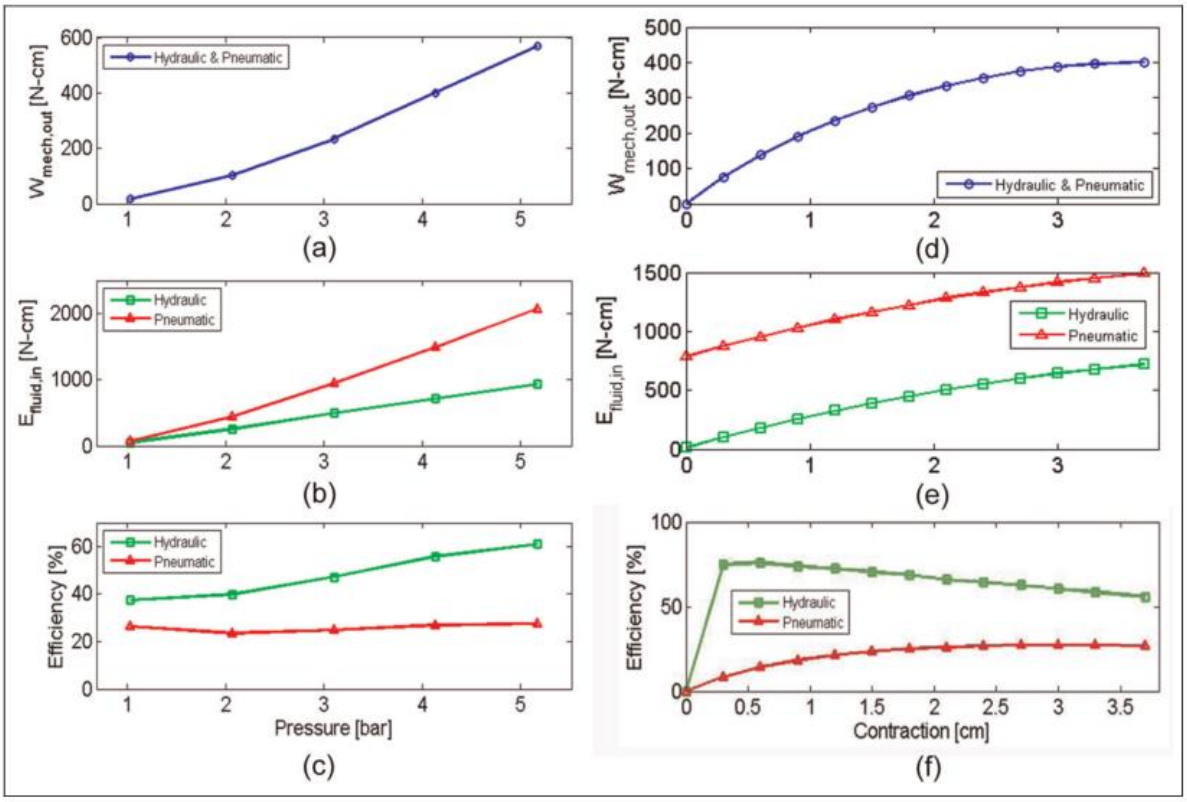

Figure 2-32: (a) Mechanical output work, (b) fluid input energy, and (c) efficiency of the latex muscle, all as a function of pressure for pneumatic and hydraulic operations. (d) Mechanical output work, (e) fluid input energy, and (f) efficiency of the latex muscle, all as a function of contraction at 4.1 bar for pneumatic and hydraulic operations [138]***.***

2.6.7 PRESSURE SUPPLY SYSTEM

A typical pneumatic system for a single muscle is shown in Figure 2-33. A compressor provides the compressed gas, which is stored in a buffer tank so that the compressor does not have to run continuously and because the compressor could not supply the muscle with air fast enough directly. A pressure regulator ensures consistent pressure in the supply line and, based on the system, may include filtration or moisture removal. A number of valve configurations are possible, but here two, 2 port 2 way valves are used to control air flow in and out of the PAM.

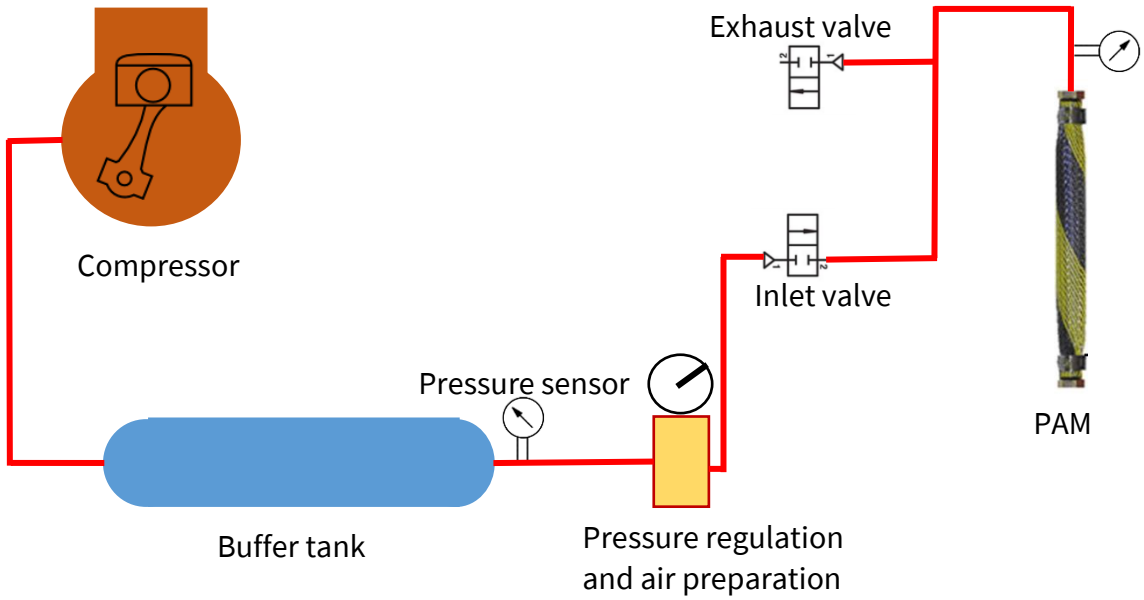

Figure 2-33: Typical pneumatic system for a single muscle.

While air supply lines cause some reduction in the mass flow rate to and from the muscle, the major factor is generally flow through the valve orifice [133], [136]. This differs for the case of supplying or discharging air from the muscle. Inflation to a set point pressure takes substantially less time than deflation. This can be understood with reference to Figure 2-34. Deflation of the muscle takes approximately twice as long as inflation, despite identical valves being used for both operations. In the case of inflation, the upstream pressure remains relatively constant and at the maximum pressure in the system (the supply pressure). Below the critical pressure ratio (P_{cr}, the transition between local sonic and subsonic flow) there is no reduction in flow rate. After this the flow rate reduces as the upstream and downstream pressures gradually equalise. In contrast, during deflation the upstream pressure (in the PAM) reduces over time, tending to atmospheric pressure. Mass flow rate drops from its initial rate almost immediately. The difference in pressure of the air entering the valves means that the density of the air passing through the valve during supply is greater than that of the air during deflation. This explains the disparity in mass flow rates across valves with the same pressure ratio. This has led some researchers to use larger or additional valves for exhausting from the muscle [85].

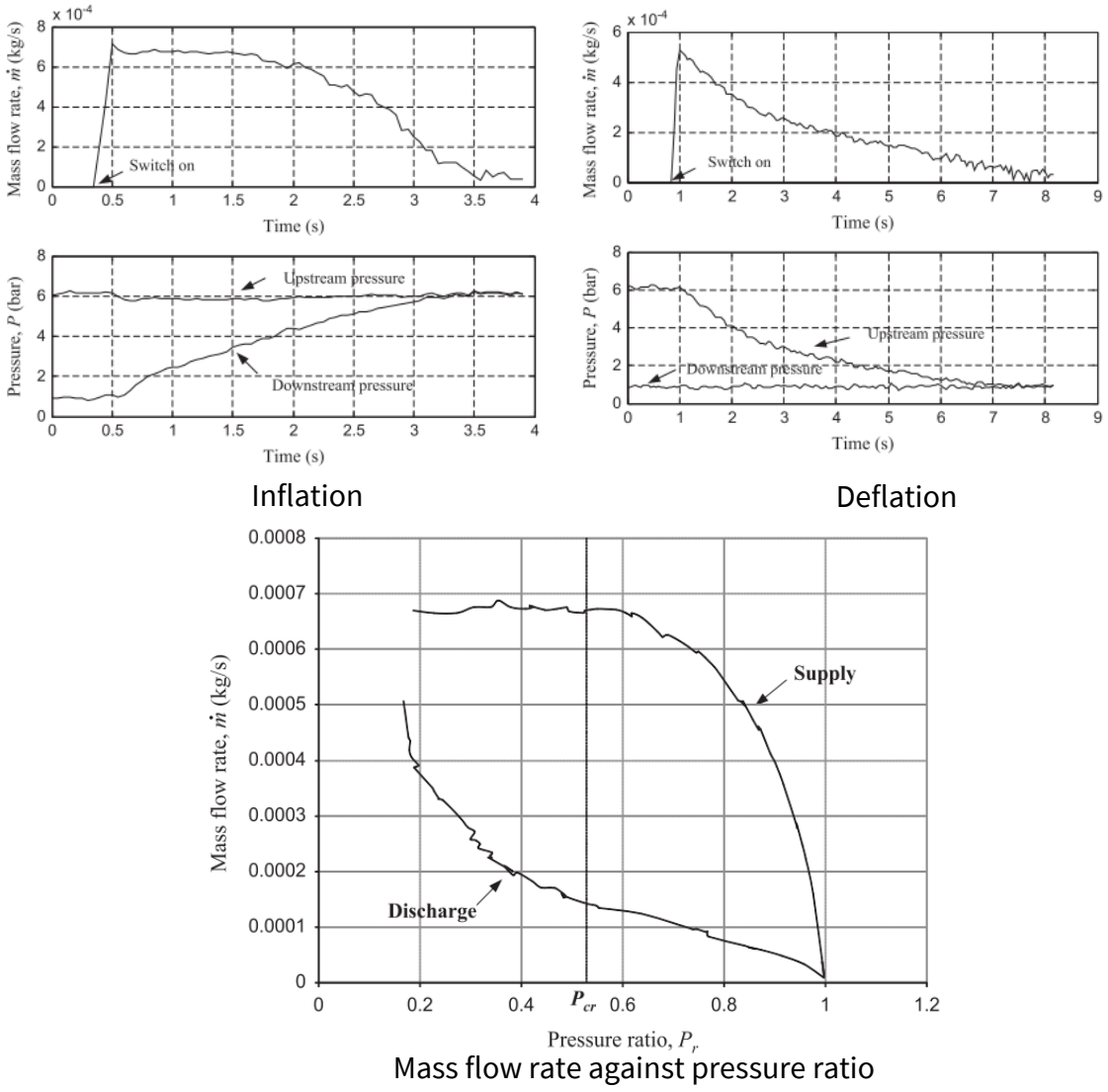

Figure 2-34: Mass flow rate as air is supplied to and exhausted from a pneumatic muscle. The pressure ratio is the ratio of upstream air pressure to downstream [249]***.***

In an effort to increase the flow rate to and from the PAM, Davis et al used multiple valves for both supply and exhaust of the muscles. This increased the maximum flow rate from 1.6 to 11 l/s [133]. For isotonic tests this gave a 400% increase in bandwidth. A number of other means were suggested to improve mass flow to and from the muscles including larger diameter but shorter supply pipelines, reduction in restrictions due to pipe connectors, increasing the supply pressure and improved design of the muscle end fitting to reduce losses here. For systems where the use of long supply pipe lines is unavoidable, additional buffer tanks may be used to store compressed air closer to where it is required by the muscle [85], [136]. A shorter distance between the valve and muscle reduces the volume which must be filled with fluid and therefore the required mass flow to actuate

the PAM. At an extreme of this Davis and Caldwell integrated a valve into the muscle end fitting. However due to a slower response time of the valve and reduced airflow as a result of the tight confines of the end cap, the bandwidth is slightly less than that of an externally located Matrix 750 valve [250].

2.6.8 MUSCLE VOLUME

The muscle volume has a large influence on the dynamic characteristics of the muscle as it defines the mass of fluid which must flow in or out of the PAM to change its internal pressure at the required level of contraction. Therefore, smaller muscles will have a faster dynamic response than larger ones. As muscle volume increases with contraction, faster responses can be expected in terms of pressure change within the muscle when the muscle is closer to its maximum length. A simple energy analysis as described by Chou and Hannaford, suggests that the force output of the muscle is proportional to the rate change of volume with length [239]. Therefore, to achieve large force outputs at large contractions, there must be as large an increase in volume as possible.

As it is a requirement for work output that muscle volume increase with contraction, efforts have focused on removing the volume which does not change with contraction or indeed that gets smaller. This is the so called “dead volume” which occupies the space between the two end fittings. A number of approaches have been investigated to achieve this. Davis et al. used a variety of filler materials to occupy the space, including a fluid (water), oval granules and a number of solid rods with a diameter equal to the internal diameter of the muscle in a relaxed state [133]. The percentage increase in bandwidth for each of these fillers under isometric conditions is illustrated in Figure 2-35. It is clear that occupying the dead volume increases bandwidth although this drops off after a certain level for granular and solid filler. This may be because air flow through the muscle is inhibited by these fillers, due to the flow around their complex shapes. The liquid filler does not have this affect as it can redistribute itself within the muscle. However, using liquid is not practical in most applications as it is possible that fluid would flow out of the muscle in some orientations, causing damage to valves etc. and causing unpredictable flow rates. A second latex bladder can be used to contain the liquid to overcome this.

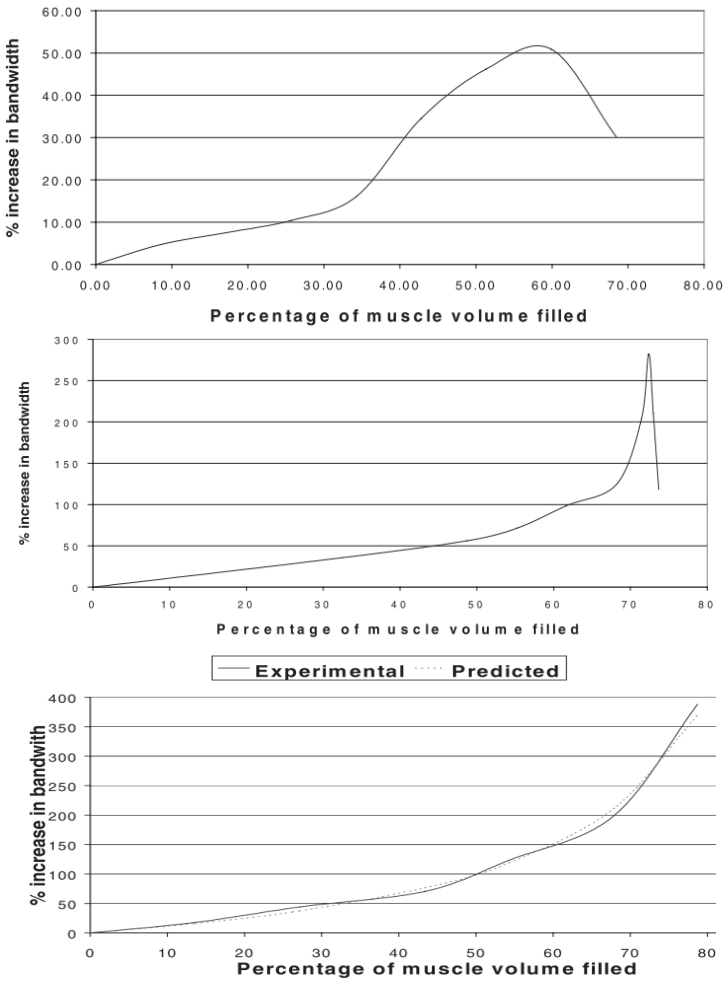

Figure 2-35: Increase in bandwidth with percentage fill of the dead volume of the muscle with various filler materials [133]***.***

2.7 MODELLING

To make use of the experimental characteristics outlined in the preceding section, models have been developed to further understand the behaviour of PAMs, facilitate design of complex systems and enable control. In general, it is the relationship between force output, gauge pressure in the muscle and contraction which is under investigation. A number of approaches have been taken to modelling these actuators as discussed below.

2.7.1 THEORETICAL

One approach to modelling a muscle is to try to estimate the forces and fundamental mechanics of its operation, relying on the geometry and material properties of the structure. This has the advantage of being applicable to different sizes and designs of

muscle, without the requirement for additional experimental data. It also validates the understanding of the muscle and how particular factors affect its operation.

Geometrical/Energy Analysis

A purely geometric analysis of the contraction mechanism of the muscle was alluded to in a patent by Gaylord[168] and described more thoroughly by Schulte et al [22]. Chou and Hannaford derived identical expressions though also made use of the virtual work principle as described below [136], [239]. Some of the relevant quantities are illustrated in Figure 2-36. Note that here the muscle is always assumed to be a cylinder which ignores the restriction on radial expansion at the end fitting.

From Figure 2-36 it is evident that

$$L = b\cos\theta \tag{2.9}$$

$$D = \frac{b\sin\theta}{n\pi} \tag{2.10}$$

where L is the active muscle length, b is the length of the individual fibres in the braid, θ is the braid angle, D is the muscle diameter and n is the number of times any fibre in the braid wraps around the muscle. L, θ and D will change as the muscle contracts, but b and n remain constant.

The volume of the muscle is therefore

$$V = \frac{1}{4}\pi D^2 L = \frac{b^3}{4\pi n^2}\sin^2\theta\cos^2\theta \tag{2.11}$$

When the muscle is pressurised, the incremental work done on the wall of the muscle is given by

$$dW_{in} = \int_0^{S_i} P' dr ds = P' dV \tag{2.12}$$

where P' is the differential pressure across the muscle wall, S is the total inner surface area of the muscle, ds is the area vector, dr is the inner surface displacement and dV is the incremental change in volume.

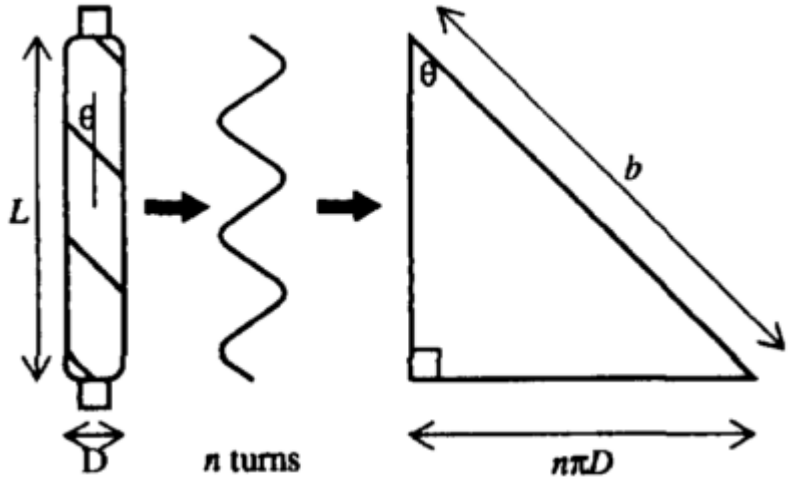

Figure 2-36: A representation of a pneumatic muscle showing a single fibre in the braid and the relevant quantities referred to in this section [239]***.***

The incremental work output done by the muscle is given by

$$dW_{out} = -FdL \tag{2.13}$$

where F is the axial force output from the muscle which is in tension. Assuming that there is no energy loss in the system, using the principle of virtual work (2.12) and (2.13) can be equated.

$$-FdL = P'dV \tag{2.14}$$

$$F = -P'\frac{dV}{dL} \tag{2.15}$$

Making use of equation (2.11), the force output may be expressed as

$$F = -P'\frac{dV}{dL} = P'\frac{\frac{dV}{d\theta}}{\frac{dL}{d\theta}} = \frac{P'b^2(2\cos^2\theta - \sin^2\theta)}{4\pi n^2} = \frac{P'b^2(3\cos^2\theta - 1)}{4\pi n^2} \tag{2.16}$$

It is generally not practical to measure the braid angle during muscle operation so using (2.9) this can be rewritten as

$$F = P'\left(\frac{3L^2 - b^2}{4\pi n^2}\right) \tag{2.17}$$

Or, in the form used by Gaylord and Schulte et al

$$\frac{P'\pi {D_{90}}^2(3\cos^2\theta - 1)}{4} \tag{2.18}$$

where D_{90} is an idealised parameter which is not physically realisable being the maximum diameter of the muscle if θ could increase to 90°.

$$D_{90} = \frac{b}{n\pi} \tag{2.19}$$

This is the simplest model which can be used to estimate the muscle force output, however in practice the accuracy is quite low (errors of 10-20%) due to energy losses and other simplifying assumptions made [176].

This has led to numerous authors proposing adaptions to the above model to correct for various factors. An expression for the additional axial force due to the bladder elasticity was derived by [22]. Improvements in the volume estimate by accounting for the bladder thickness were provided by [136]. Elastic energy storage in the bladder was considered in [148], [251]. The elasticity in the braid was included in the model developed by Davis et, al. [133] and the energy storage in the braid was included by Kothera [86]. Improvements in the expression for the shape of the muscle were proposed by Tondu and Lopez, whereby the active length of the muscle was reduced to allow for the conical shape where the braid approaches the end fitting [236]. Tsagarakis and Caldwell analysed the cylindrical and conical sections of the contracted muscle separately to account for the different geometry [252]. Doumit developed an expression accounting for the angle at which the braid meets the end fitting [13], [253]. Friction between the braid fibres is often assumed to be the major source of hysteresis in contraction. Chou [239], and Tondu and Lopez [236] used experimentally developed parameters to account for this, while Davis and Caldwell developed a friction model of the braid. However, when the number of braids in the muscle was reduced by Doumit, the hysteresis increased suggesting the interaction between braid and bladder may be more significant than originally assumed [244].

A more detailed treatment of the advances in theoretical modelling is given in Appendix C.

2.7.2 EMPIRICAL

While theoretical modelling develops an understanding of the mechanics of the muscle, there are a number of factors which are not accounted for which affect accuracy. For example, the woven nature of the braid makes the actual contact area between braids difficult to predict, the bladder may protrude somewhat through the braid affecting muscle behaviour, friction between the muscle and braid is assumed not to affect performance, nor are inconsistences in the tension of the braid due to the manufacturing processes and changes in the muscle characteristics after repeated use. This leads researchers to use experimental data to fit a model to the muscle characteristics which are observed. In these cases, no attempt is made to model the actual mechanics of the muscle, but rather the model only seeks to predict its behaviour.

To illustrate this, Zuglian et al.[254] compared experimental data to the model proposed by Tondu and Lopez [236]as described in the preceding section. This gave an average error of 9% (although the greatest error occurred when the muscle was stretched past its resting length, which the model does not account for). A process of system identification was then used to test a number of expressions to determine if they could be tuned to match the muscle's performance. The following formula was found to represent the muscle characteristics well.

$$F = \frac{c_1 P'^2 + c_2 \varepsilon^2 + c_3 P' + c_4 \varepsilon + \frac{c_5 P'}{\varepsilon} + c_6}{c_7 P' + c_8 \varepsilon} + c_9 + c_{10} e^{\varepsilon - 0.7} \qquad (2.20)$$

where ε is the PAM strain and the terms $c_1$to c_{10} must be found experimentally. Note the final term contains an exponent to capture the behaviour of the muscle when stretched. This model is then fitted to measured muscle data using the least squares technique. This gives an average percentage error of just 0.77%. Figure 2-37 shows a comparison of the error in the model by Tondu and Lopez, as well as the model proposed above.

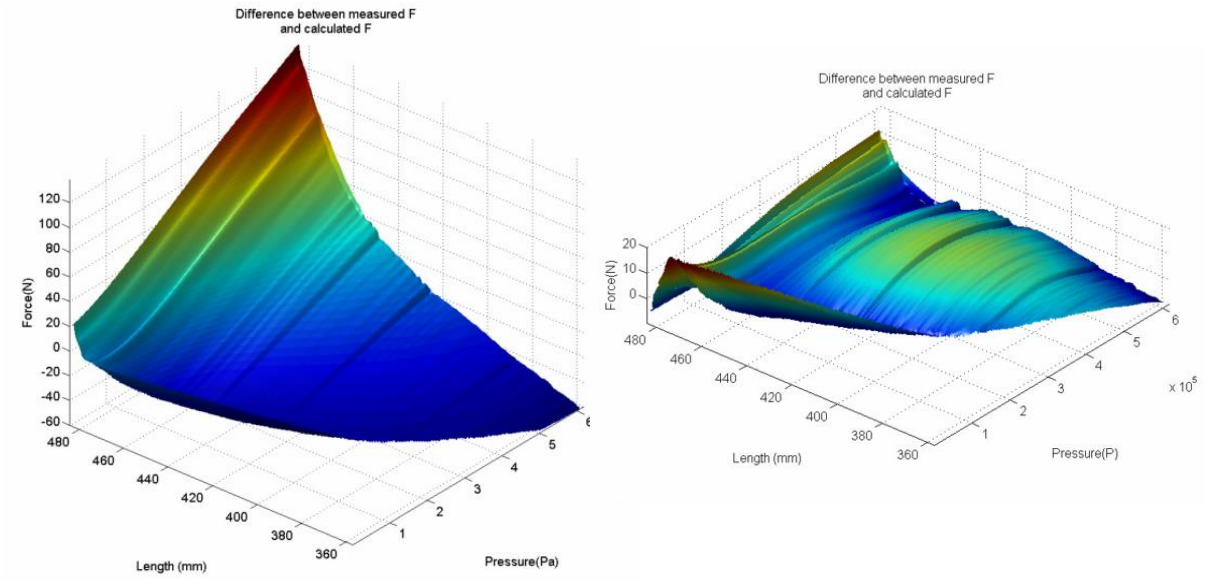

(a) (b)

Figure 2-37: The error between the model and experimental data over the range of operating condition for a 465mm long muscle using (a) the Tondu and Lopez model and (b) the empirical model developed by Zuglian et al [254]**.**

In some cases, authors have sought to build from the expressions developed through theoretical analysis of the muscle, but determining the terms in these models experimentally. It was argued by Peternel, that the model by Chou and Hannaford [136] can be treated as a second order polynomial of the form [255]

$$F = P' \sum_{i=0}^{2} a_i L^i \tag{2.21}$$

where the a terms must be identified. Chou and Hannaford determined these from energy analysis as described previously, but they can equally be determined experimentally. Hildebrandt provides further basis for this approach by suggesting that by neglecting stretch in the braid and bladder, the volume of the muscle can be represented by a third order polynomial, dependent only on muscle length [256]

$$V = \sum_{i=0}^{3} b_i L^i \tag{2.22}$$

where the b terms are determined experimentally. This can then be used in equation (2.15) to get an expression for force output. However, this approach was found to be highly prone to error. To improve this, the authors consider the $\frac{dV}{dL}$ term in equation (2.15)

as a virtual piston, the area of which is dependent on muscle length. The gauge pressure in the muscle then acts upon the virtual piston. This concept is used, with a model of a testing rig (including inertial and frictional effects) to determine the parameters for a fifth order polynomial for muscle force in the same form as equation (2.21). The same authors later modified this expression so that the virtual piston acts against a nonlinear spring [189]. This was so that the expression accounted for the elastic behaviour of the muscle materials and results in an expression for muscle force of the form

$$F = P' \sum_{j=0}^{2} a_i L^i - \left(\sum_{i=0}^{3} c_i L^i + c_4 L^{\frac{2}{3}} \right) \tag{2.23}$$

where the a and c terms are found experimentally. This model was found to give a maximum error of ±15N. Peternel modified this and combined it with the friction model of Tondu and Lopez to give [255]

$$F = P' \sum_{j=0}^{2} a_i L^i - \left(\sum_{i=0}^{4} c_i L^i + c_4 L^{\frac{2}{3}} \right) - sign(\dot{L}) \left(\sum_{k=0}^{2} d_k \dot{L}^k + d_3 e^{-\frac{|\dot{L}|}{d_4}} \right) \tag{2.24}$$

where the d terms must also be found experimentally. This equation therefore aims to account for hysteresis in the muscle. Two approaches are described by which the relevant parameters can be found; using a sine wave pressure profile and a ramp pressure profile to generate the data which can be used to tune the model constants using least squares regression. The accuracy of the models described in equations (2.21),(2.23) and (2.24) were compared in the paper with average errors of 8.76%, 1.98% and 1.34% respectively. This comparison is also illustrated in Figure 2-38.

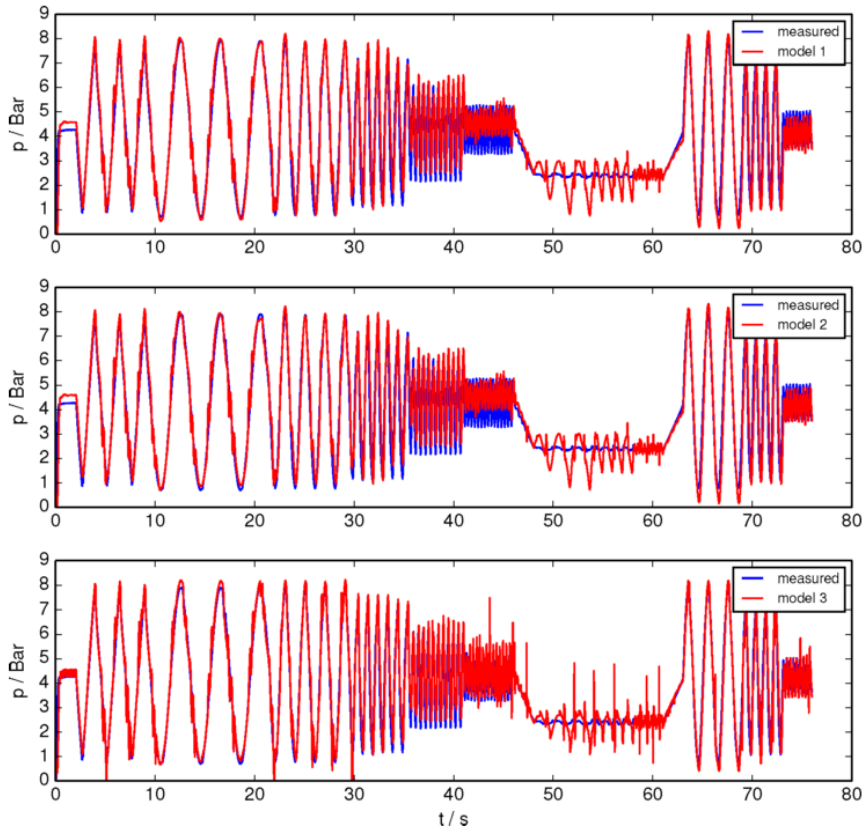

Figure 2-38: A comparison of the models described in equations (2.21)(2.23) and (2.24), corresponding to model 1, 2, 3 respectively. Note that the models were tuned using the sine wave based approach and so the training data was very similar to the test data [255]***.***

Phenomenological Models

In many cases an attempt is made to represent the muscle using well understood phenomenon, though no attempt is made to understand why the muscle behaves in this manner. This is known as phenomenological modelling and is particularly useful as a dynamic model of the PAM. Generally, the components used when modelling pneumatic muscles are springs dampers and contractile elements. This is similar to models of natural muscle such as the Hill muscle model [257]. In this three element model, the muscle is represented by a contractile element and two non-linear springs, one in series and one in parallel with the contractile element as illustrated in Figure 2-39.

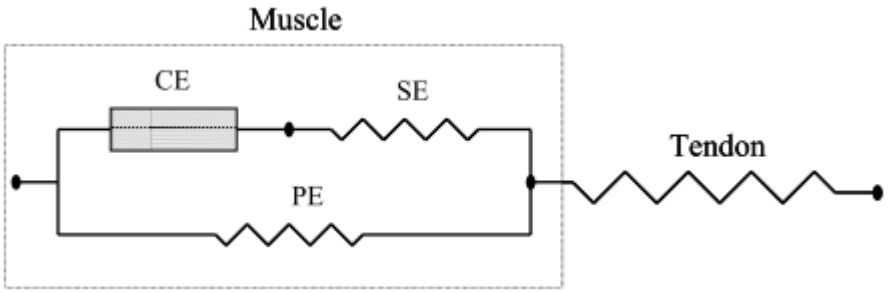

Figure 2-39: representation of the three element Hill muscle model [258].

This model has also been applied to pneumatic muscles [258], [259]. The model is normally presented as a relationship between muscle shortening velocity and its corresponding tension.

$$(\dot{L} + b_i)(F_{Hill} + a_i) = b_i(F_0 + a_i) \tag{2.25}$$

where a_i and b_i are constants determined experimentally and F_0 is the isometric force at rest length. The model is valid for isotonic contraction whereby a mass is applied to the muscle. As noted by Tondu, the force exerted by a mass under static conditions is the F_{Hill} in equation (2.25), not the instantaneous force output of the muscle [260]. Here muscles with a rayon and iron braid were modelled using the Hill model, which gave good predictions of maximum shortening velocity as illustrated in Figure 2-40. The difference in behaviour of these two braid materials is attributed to braid friction, the textile fibre exhibiting large static friction at low speeds, a stick-slip phenomenon which reduces the friction at moderate speeds, and a hydrodynamic section which increases with speed. Klute et al also use the Hill model with pneumatic muscles, to compare their response with natural muscle. It was found that an additional damping element was required to get a close match [258], [261]. Nakuma uses a similar approach for a straight fibre muscle showing the generality of the technique [21].

Siu and Xie produced a simple model by splitting the force output of the muscle into two linear spring constants based on length change and pressure change locally, for small changes in each [19]. A model is then used to predict how these local constants change over the range of muscle operating conditions and experimental data used to fit the model to the data. The final model is in the following form and a method by which to fit the model to the performance data is included.

$$F(P'L) = a_0 + a_1P' + (b_1 + b_2P')L \tag{2.26}$$

r in a slightly different form in [262]

$$F(P'\varepsilon) = c_0 - b_0\varepsilon - \frac{b_1}{2}\varepsilon^2 + a_1P' + a_2P'\varepsilon \tag{2.27}$$

This model does not consider hysteresis at all.

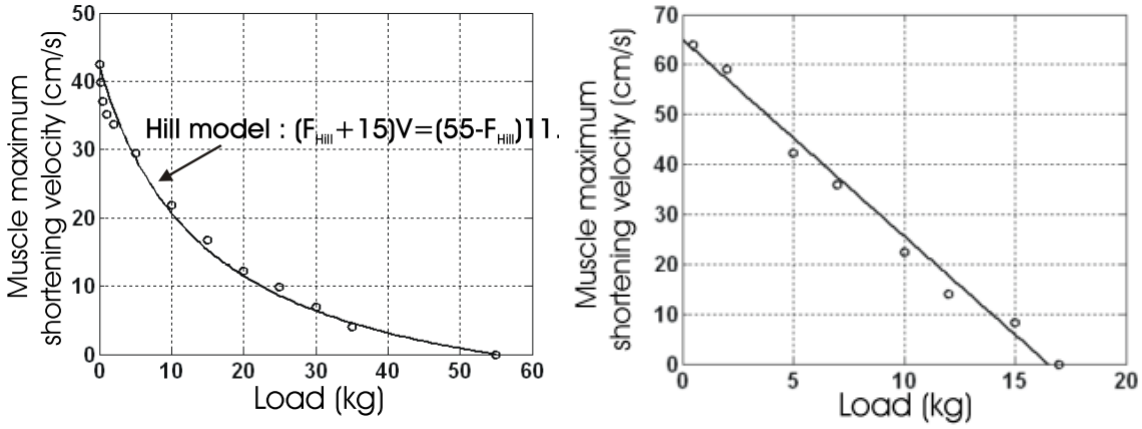

Figure 2-40: Maximum muscle shortening velocity against load for a muscle with a rayon braid (left) and an iron braid (right) [260]***.***

Repperger developed a model as illustrated in Figure 2-41 (a), with a nonlinear spring element and a viscous damping element [190], [263]. A three step methodology was designed to tune this model to a particular muscle.

1. Determine $K(x)$, the nonlinear spring constant, from steady state data ($F_{steady\ state} = K(x)x$) where x is the change in muscle length
2. Find the transient force by $F_{transient} = F_{total} - F_{steady\ state}$
3. Use regression to find $B(\dot{x})$ with the equation $F_{transient} = B(\dot{x})\dot{x}$

Using this method second order polynomials were constructed for the $K(x)$ and $B(\dot{x})$ terms at a number of pressures.

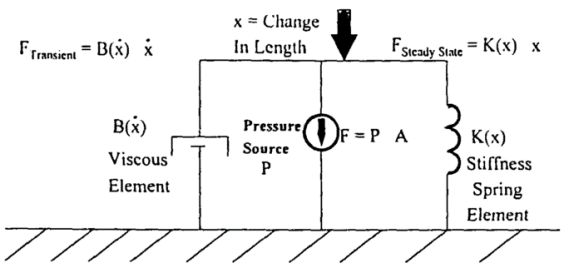

(a)

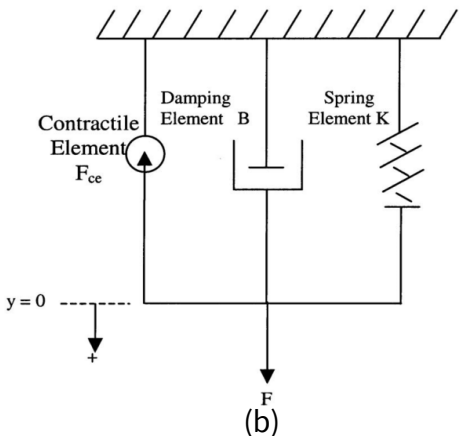

(b)

Figure 2-41: Structure of the phenomenological muscle model used by Repperger [263] ***(a) and by Reynolds*** [182], [264] ***(b).***

A number of authors have used an adapted version of the Voight viscoelastic model [265], which results in a model which is somewhat similar to that used by Repperger above. Reynolds et al. used a three element model as shown in Figure 2-41 (b) [182]. The governing equation of this model, assuming the PAM acts vertically against a mass is

$$M\ddot{y} + B\dot{y} + Ky = F_{ce} - Mg \tag{2.28}$$

where B is the damping coefficient, K is the spring coefficient, F_{ce} is a contractile element, M is the mass, which in conjunction with acceleration due to gravity, g and the acceleration of the PAM contracting constitutes the applied load (y being the muscle contraction). The contractile element acts as a constant force (F_{ce}) dependent on muscle pressure and is equal to the force output of the muscle at its rest length under static conditions. As this is the point of maximum muscle force, this means the spring element acts against the contractile element. Linear expressions (in terms of muscle gauge pressure) for the spring and damping coefficients were found using step responses. Pressure regulation maintains isobaric conditions while mass is suddenly applied to or removed from the PAM. The spring coefficient (K) is typically is found from the change in steady state contraction. The damping coefficient (B) is determined from the velocity of the response during the test. These results are shown in Figure 2-42.

There was a significant difference in damping coefficient between the muscle contracting and relaxing as illustrated in Figure 2-42. $B(P')$ is much smaller during relaxation and has an inverse relationship with pressure. This latter phenomenon suggests a non-velocity related friction. Dynamic characterisation of a festo muscle was achieved using this model by Serres [264], [266]. Here, limits were put on the maximum load for which a constant linear expression for $K(P')$ is valid, typically at approximately 70% of the muscles maximum isometric force at the same pressure. Similar approaches to modelling PAMs have been implemented in [249], [267], [268].

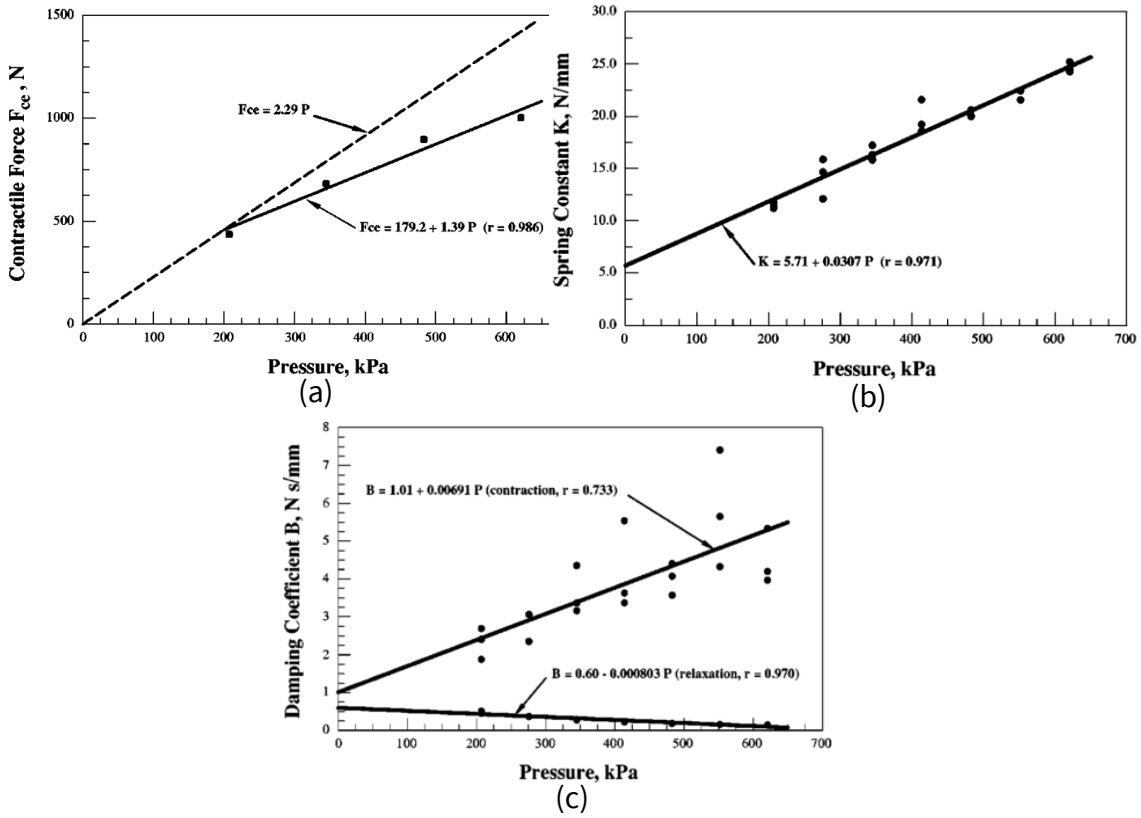

Figure 2-42: The individual components of the model proposed in [182]***, each of which is pressure dependent. The contractile force is shown in (a), the spring constant in (b) and the damping coefficient as found from a sudden removal of load from a pneumatic muscle in (c).***

Balasubramanian argued that the model by Reynolds was incomplete, as the dynamic model parameters are dependent on force applied to the muscle as well as the internal pressure [181], [269]. In addition, other dynamic parameters are needed to fully describe the muscle's dynamic behaviour. Nine muscles of varying size were tested with step pressure inputs with different loads. The displacement output with time was fitted to a second order linear model for each rise and decay (contraction and elongation) of the muscle displacement. Five parameters associated with the dynamic model of the PAM were then calculated from this model. These parameters are listed in Table 2-6. A squared error minimisation algorithm was then used to generate a second order polynomial with respect to both muscle gauge pressure and applied load for each of the five parameters. These quadratic expressions show good agreement with the experimental data.

Parameter	Description
A	The magnitude of contraction of the PMA.
ζ^{Rise}	Damping ratio of the rise response of the PMA.
ω_n^{Rise}	Natural frequency of the rise response of the PMA.
ζ^{Decay}	Damping ratio of the decay response of the PMA.
ω_n^{Decay}	Natural frequency of the decay response of the PMA.

Table 2-6: Parameters associated with a dynamic model of a PAM [269]***.***

A model by Colbrunn consists of a spring, viscous damper, and Coulomb friction all in parallel [270]. The spring force is given by the static characteristics of the muscle, which are developed partially theoretically, using a similar approach to Tondu, though an experimentally determined correction factor (called the effectiveness) is also included. A viscous damping constant is introduced to account for the "viscous effects of the fluid flow losses" and a Coulomb friction term to model the sliding losses in the shell and bladder. These were each determined experimentally.

2.8 REMARKS

The preceding review highlights that there is a clear need for service robots which can engage in meaningful physical interaction in human centric environments. Current technology is still failing to fulfil the range of requirements users expect from such devices. The present generation of general-purpose service robots are typically research platforms capable of limited interactions with their environment. They fulfil relatively simple functions, such as guiding people around a shop, carrying luggage etc. Perhaps the most concerning reason why robots have not become more ubiquitous in human environments is the inherent risk associated with such a device. Given that a major market for such robots is envisaged to be in the service of elderly or frail people, the levels of safety which must be established are significant. Actuation is key to addressing this issue. While a robot may be able to avoid collisions through sensor readings of its environment and an accompanying world model, there is always the risk that these sensors could fail or be affected by external stimuli (e.g. lighting conditions, electrical noise etc.), or the world model may be incomplete or incorrect. For this reason, designers must seek inherent safety of the system through mechanical design and low-level

control. When small actuation forces, such as those found on entertainment robots are considered, the force capacity of the actuator limits the potential harm it can cause, however, in systems requiring large actuation forces (such as delivering large pay loads, lifting people or legged robots) a different approach is required. Analysing the means by which robot safety is assessed, it is seen that the important factors that contribute to inherent safety are the mass of the robot, the speed of operation, the compliance of the cover material joint compliance and control robustness.

Pneumatic muscles present an interesting paradigm in this context. They have been repeatedly cited as being a safer alternative to other stiff actuation techniques. Rather than depending on additional apparatus to incorporate compliance, their very structure ensures compliance. This not only increases robustness but also reduces the overall mass of the system. Combined with their high power to mass ratio, this lends itself to the development of systems with low inertias while retaining large payload capacity. They can also be manufactured in virtually any size allowing compact systems to be implemented, and are relatively low cost. For unstructured environments, typical of those in which mobile service robots operate, compliance allows the robot to adapt to its surroundings directly through physical interaction.

However despite these favourable characteristics, PAMs are far from an ideal actuator for this application as is evidenced by their absence from the field. In particular:

1. PAMs are more difficult to control than standard actuation technologies such as electromechanical drives or hydraulics [238], [262], [271], [272]. Their force output is dependent on the gauge pressure in the muscle and also muscle contraction, the latter being a non-linear relationship. Muscle compliance and hysteresis also adds complexity to the control problem making modelling and accurately positioning systems actuated by PAMs challenging[130], [131]. Additionally valves and control components are required to regulate the gauge pressure of the PAMs adding to the mass and complexity of the control system [250], [273].
2. The requirement for a compressed air supply to drive the muscles is difficult to fulfil on mobile systems [111], [274], [275]. Air compressing, storage and preparation equipment is usually heavy and occupies a large volume. In addition,

compressors produce acoustic noise which is undesirable in the domestic environment.

3. Efficiency on mobile systems is always of paramount importance as all energy must be carried on board if the robot is to operate untethered. PAMs consume compressed air which is energy intensive to produce [136]. Their overall efficiency is generally less than that of electromechanical or hydraulic systems. Additionally, compressed air systems are noisy and bulky and so it should be used as conservatively as possible.
4. Similar to natural muscle, PAMs have a limited contraction ratio (approximately 25% [13], [86]). This results in the need for relatively long actuators which must be accommodated on the robot structure. Additionally, this may limit the range of motion or force output of a joint as it may be impossible to accommodate longer muscles.
5. The lifetime of a PAM is dramatically shorter than that of comparable actuation technologies[148]–[150]. This is due to the high stresses which are necessary in the PAM fibres and bladder, and the manner in which they are held in place. For complex systems, such as mobile service robots robustness is paramount to technological development and commercialisation.

A wide range of PAMs have been developed by the research community. These have been evaluated and many of these offer potential for specific applications. However, the most widely explored and general purpose of these are those popularised by McKibben, with a braided fibre structure and internal elastic bladder. Therefore, while the use of alternative PAMs is not excluded (the pleated PAM offering particularly favourable characteristics), in this research the choice has been made to work with the McKibben type muscle. This type of muscle has been frequently used in a wide range of applications, ranging from rehabilitation devices, to robotics and industrial automation. The study of these applications also highlights the diversity of ways in which the muscle can be integrated into complex systems.

In order to understand the mechanics of the PAM, a thorough investigation was conducted into its characteristic. This explored the correlation between gauge pressure,

contraction level and force output, as well as the effect of PAM design on these characteristics. Given the wide variety of designs of this type of muscle, it is perhaps not surprising that some of the identified characteristics are contradictory (such as the presence or absence of viscous friction in the muscle braid). The analysis of muscle characteristics is useful in design of PAMs as they can be better adapted for the specific requirements of their intended use. It also facilitates the development and testing of muscle models, which both enhances understanding of the physics involved and makes control possible. Where these models fail, particularly where dynamic characteristics are considered, experimentally determined empirical models can be used.

With the goal of reducing the compressed air consumption of PAMs, a new muscle design will be postulated. The basis of this design emerges from the characteristics and modelling discussed here, reducing the volume in the muscle between the end fittings and, in so doing, the force exerted by the air on the end fittings. With such a departure from the standard muscle concept, new models will be needed to describe the behaviour of the PAM, which will be developed directly from those examined in this section.

3 DESIGN OF A MCKIBBEN SLEEVE MUSCLE

While the characteristics of PAMs make them advantageous for robot actuation in close proximity and in collaboration with humans, there are still a number of challenges with the current technology. The inefficiency of the PAM is a major limitation, especially for mobile, untethered robots. A reduction in the internal volume of the muscle has been shown to improve the efficiency of the actuator [133], [179]. While a number of means have been investigated to accomplish this, perhaps the most compelling is the sleeve muscle. This also comes with a number of other advantages as described below. However, the concept has not been fully investigated, with only a limited set of performance information and designs considered. There is a need for further exploration of the topic to:

- Investigate other possible designs which could produce improved performance
- Increase the modularity of the design to make it more applicable to a wide range of use cases
- Increase the available performance data for comparison with other muscles and types of muscle
- Establish the dynamic characteristics of the sleeve PAM

To this end a sleeve muscle has been designed to investigate new concepts and enhance the body of knowledge on the performance of the actuator.

3.1 SLEEVE MUSCLE CONCEPT

The sleeve pneumatic artificial muscle, proposed by Driver and Shen [276], improves efficiency, increases force capacity, and allows the PAM to become a structural component of the system. The concept involves filling the internal cylindrical cavity of the muscle with a rigid element. The rational for this is illustrated in Figure 3-1. In the case of the traditional PAM, the internal volume of the muscle must be entirely filled with compressed air in order to produce contraction. The dead–space, the cylindrical volume between the end-fittings constitutes a significant portion of this volume but does not contribute to the contractile force. To the contrary, the air here pushes against the end fitting (similar to the driving force in a pneumatic cylinder actuator) producing a force in

opposition to contraction. This reduces the force output of the PAM as well as the contraction, as the limit of contraction occurs when the contractile force generated by the pressure acting on the braid matches that of the extensile force from the pressure acting on the end fittings rather than when the braid reaches a jamming state.

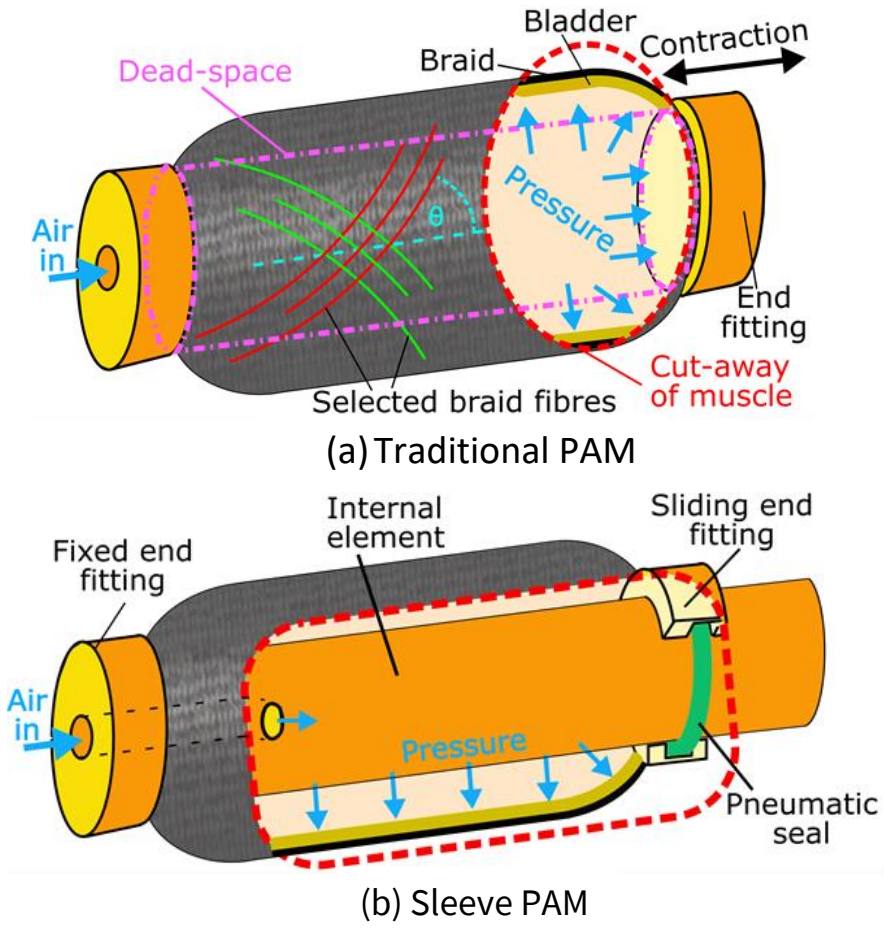

Figure 3-1: A traditional PAM is shown in (a) with the dead-space highlighted. A conceptual sleeve PAM is shown in (b).

The replaces much of the dead-space in the PAM with a rigid cylindrical element. This element is attached to the end fitting at one end of the muscle (fixed end fitting). The other end fitting has a hole, through which the element protrudes (sliding end fitting). The sliding end fitting moves along the internal element when the muscle contracts. A pneumatic seal is used to prevent air leakage. By removing the dead-volume there is an improvement in the efficiency of the PAM as the volume which must be filled with compressed air is reduced at every contraction length. An increased force output is also generated as the area of the end fitting on which the muscle pressure acts is reduced.

Contraction of the sleeve PAM is shown in Figure 3-2. The internal volume can be treated as two parts, the volume of the PAM between the end fittings (the dead-space), V_1, and the volume which increases due to the radial expansion of the braided mesh, V_2. This latter volume is unaffected by the addition of the internal element. V_1 on the other hand is reduced (ideally entirely removed, though this may be impossible for practical reasons). As the muscle contracts, some of the internal element moves out of the PAM while the proportion of the total volume which V_2 makes up increases. This means that the benefit of the sleeve PAM in terms of the volume of the PAM which must be occupied with compressed air reduces as the PAM contracts. The increase in force output of the PAM due to the sleeve adaptation is independent of contraction however as the area of the end fitting on which the pressure in the PAM would otherwise act does not change.

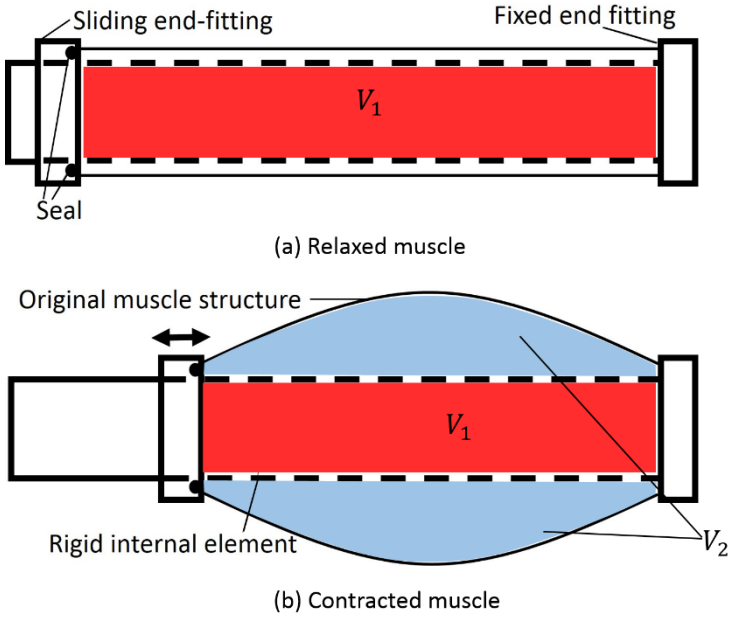

Figure 3-2: The sleeve PAM concept showing both a relaxed and contracted state.

In addition to the performance improvements delivered by the sleeve PAM, the internal element may also be used as a structural element of the robotic system. This helps to offset the additional mass of the actuator due to the rigid element and allows a more compact overall system.

3.2 PREVIOUS IMPLEMENTATIONS OF THE SLEEVE PAM

The sleeve muscle concept was first introduced by Driver and Shen [276]. Since being introduced it has only been pursued by the robotics research group in the University of Alabama. The concept, modelling and initial performance test results were outlined in this initial work. A commercially available Festo muscle was used in the research and this is shown in Figure 3-3. Testing of this sleeve muscle demonstrated a 20–37% energy saving, a greater force output across the entire contractile range (as shown in Figure 3-4), and improved stroke length.

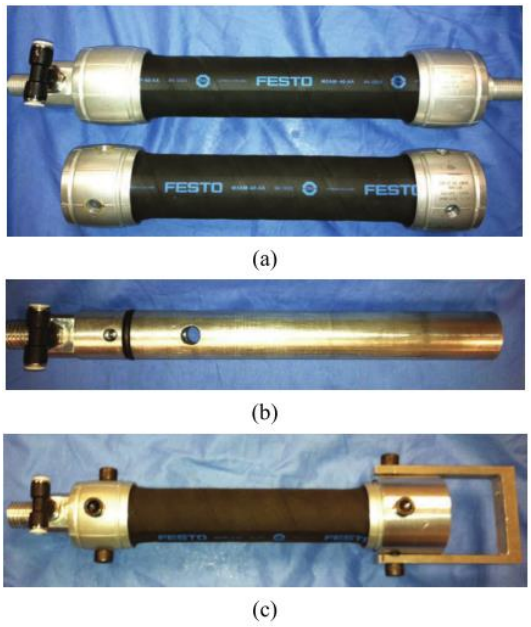

Figure 3-3: The sleeve muscle concept as implemented in [276]***.(a) shows how the end fittings have been drilled to accommodate the sleeve,(b) shows the inner sleeve and (c)shows the completed muscle.***

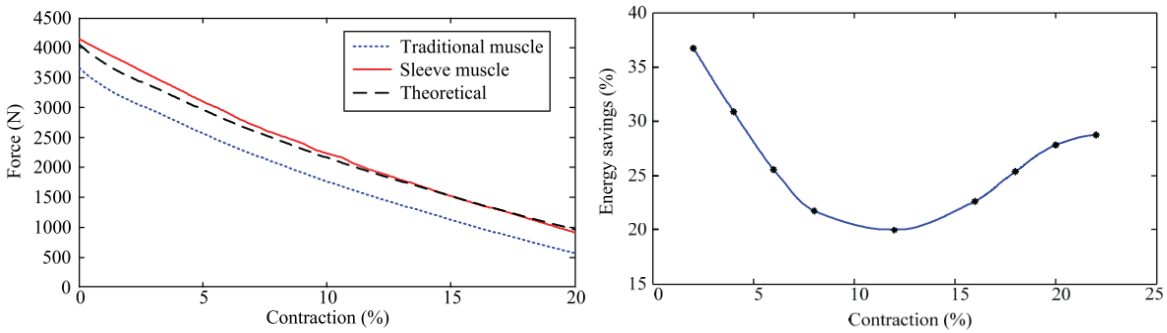

Figure 3-4: The force output of the traditional and sleeve PAMs with a gauge pressure of 414kPa is shown in (a). The energy saving achieved when comparing the sleeve PAM with the traditional PAM across a range of contractions is shown in (b) [276]***.***

Since this initial work, the sleeve muscle design has been implemented on an elbow-like joint where the structural capacity of the actuator was used as a robot link [277]. A torsional spring provided the extending torque with the sleeve muscle providing the flexion force (see Figure 3-5). A dynamic model of the system is developed which utilises a static model of the PAM with a model for fluid flow in and out of the PAM in order to control the movement of the joint using a sliding mode controller. Additionally a similar design was proposed though apparently not implemented for a knee prosthesis [278], [279].

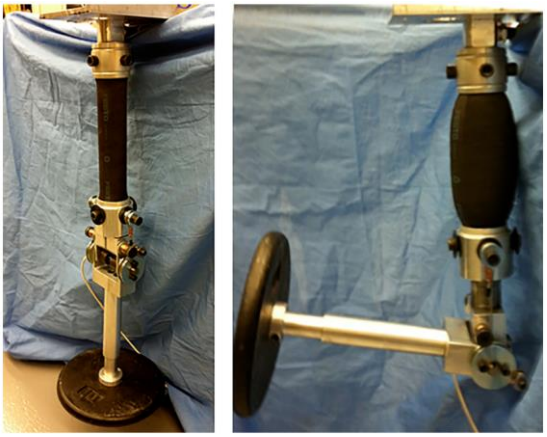

Figure 3-5: The robotic elbow developed in [277]***.***

A double-acting sleeve muscle has been proposed for use in bio-robotic systems [280]. This muscle utilizes a modified internal element containing a chamber, which can be pressurized to produce an elongating force, allowing the PAM exert forces in two directions. The structure of this double acting PAM is shown in Figure 3-6. The force profile of the two actuation directions is quite different with the extensile force being independent of muscle contraction/extension, while the contraction force reduces with contraction, though is greater than the extensile force at most contractions.

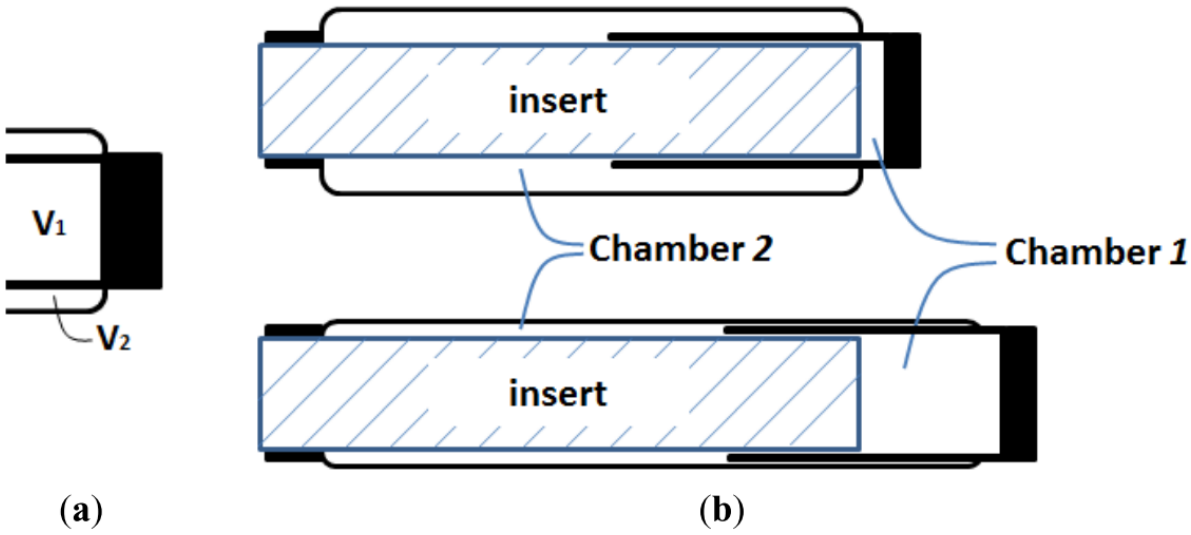

Figure 3-6: conceptual design of the double acting sleeve PAM. Pressurising chamber 1 produces an elongating force while chamber 2 produces a contractile force as before.

3.3 STATIC MODELLING OF THE SLEEVE PAM

A model of the expected performance of the sleeve muscle is useful to better understand the factors affecting its behaviour, to inform the design, and for comparison with test results. The model mentioned in the patent by Gaylord[168] and described by Schulte[22] and Chou and Hannaford [136]can be used as a basis for modelling the PAM both with and without the sleeve feature. This is similar to the approach used in [276] Energy losses including the elastic strain in the membrane and friction in the braided mesh are ignored in this model, however these factors should be identical in sleeved or standard muscles and so comparisons can still be made.

For a standard PAM, an energy analysis gives the input and output as

$$dW_{in} = P'dV \tag{3.1}$$

$$dW_{out} = -FdL \tag{3.2}$$

where P' is the gauge pressure in the muscle, dV is the internal volume change, F is the axial force and dL is the axial contraction of the muscle. Applying the principle of virtual work, equations (3.1) and (3.2) may be equated leading to:

$$F = -P'\frac{dV}{dL} \tag{3.3}$$

As noted in [276], this equation confirms that the internal volume of the muscle must increase with a contraction in length in order to generate a contractile force. It is clear

that in the case of the standard PAM, as the muscle contracts longitudinally, V_1 (see Figure 3-2) will decrease (since the end fittings move closer together) while V_2 increases. The sleeve muscle effectively removes V_1 so that there is a larger increase in the total volume as the muscle shortens.

Considering the geometric construction of the muscle braid and approximating shape of the muscle as a cylinder, even when it contracts, equation (3.4) represents the internal volume of the traditional PAM[22], [136], [168].

$$V_{TM} = \frac{L(b^2 - L^2)}{4\pi n^2} \tag{3.4}$$

where L is the current length of the muscle b represents the length of an individual fiber in the braided mesh, n is the number of times any individual fibre wraps around the muscle Differentiating equation (3.4) with respect to L and combining with equation (3.3), the force output of the muscle is given by equation (3.5)

$$F_{TM} = P'\left(\frac{3L^2 - b^2}{4\pi n^2}\right) \tag{3.5}$$

These equations can be adapted for the case of the sleeve muscle. The internal volume of the sleeve muscle is always less than that of the equivalent traditional muscle by the current length of the muscle times the cross-sectional area of the internal element. This volume is given by

$$\Delta V = -\frac{L\pi {D_1}^2}{4} \tag{3.6}$$

where D_1 is the diameter of the internal element. The volume of the sleeve muscle is therefore

$$V_{SM} = \frac{L\,(b^2 - L^2 - (\pi n D_1)^2)}{4\pi n^2} \tag{3.7}$$

Differentiating this with respect to length and again using equation (3.3), the force output of the sleeve muscle is found as

$$F_{SM} = P'\left(\frac{3L^2 - b^2}{4\pi n^2} + \frac{\pi {D_1}^2}{4}\right) \tag{3.8}$$

Therefore, the increase in force output of the sleeve muscle is

$$\Delta F = P'\frac{\pi {D_1}^2}{4} \tag{3.9}$$

The increase in output force at a given pressure is independent of the contraction of the muscle. This equation also corresponds to the area of the end fitting bordered by V_1, times the internal muscle pressure. The nature of the increase in force output of the sleeve muscle is illustrated in Figure 3-7 (a), which applies the above model to a specific sleeve implementation. The force output is increased by a constant amount across the contractile range. The maximum contraction of the muscle is also increased as force output does not reach zero until contraction is greater. Figure 3-7 (b) shows the pressure required to produce a force output of 500N across the contractile range. There is a dramatic reduction in pressure at large contraction ratios. As the force from the braid decreases with contraction while the force increase from the sleeve adaption remains constant, when the muscle is in a contracted state, the effect on the force output of the sleeve feature is more significant.

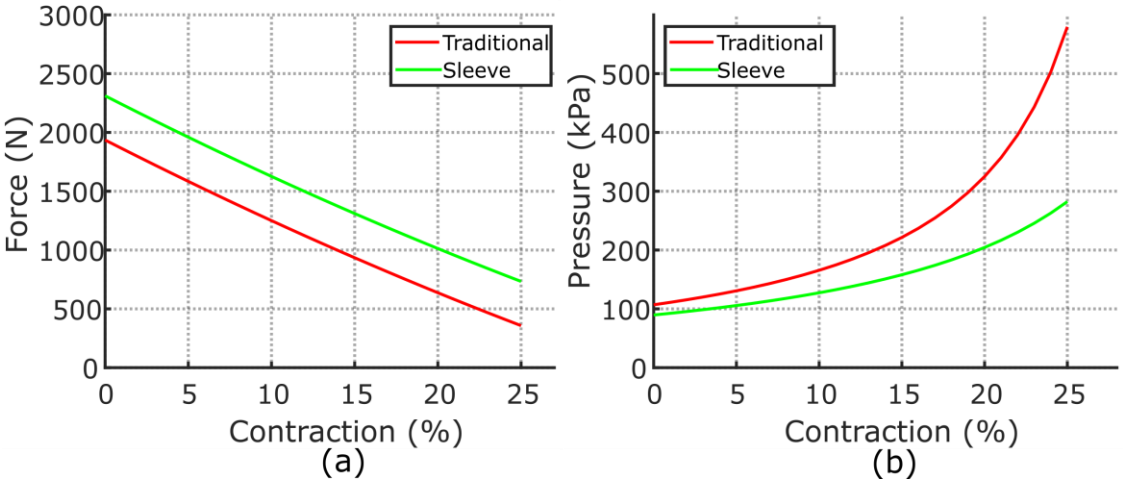

Figure 3-7: The modelled performance of a traditional and sleeve PAM over the full range of contraction. The muscle modelled has a length of 0.2m, diameter of 40mm, and central element diameter of 38mm: (a) shows the force output with a constant internal muscle pressure of 410kPa (60 psi) and (b) shows the pressure required to provide an output force of 500N over the contractile range.

Combining the reduced pressure requirement and smaller internal volume of the muscle, there is a clear reduction in energy consumption with the sleeve muscle. This can be quantified by considering the compressed gas mass consumption of the muscle and the ratio between the sleeve and standard muscle. Assuming that the compressed gas

behaves as an ideal gas and temperature changes are negligible, the mass ratio may be found using the pressure and volume ratios.

$$\frac{m_{SM}}{m_{TM}} = \left(\frac{P_{SM}}{P_{TM}}\right)\left(\frac{V_{SM}}{V_{TM}}\right) \tag{3.10}$$

Figure 3-8 shows these three ratios over the full contractile range with a constant output force. When little contraction of the muscle is allowed, the cylindrical element occupies almost the entirety of the inner volume of the muscle; hence, the volume ratio is small. PAMs output large forces when there is little contraction; therefore, the contribution of the sleeve muscle adaptation to the force output is relatively small. This is evidenced by a pressure ratio which is close to one. As the muscle contracts, it expands radially, and so the relative volume of the muscle occupied by the internal element decreases. The volume ratio therefore increases. At large contractions, the force increase from the sleeve mechanism becomes more significant in comparison with that of the muscle; thus, lower pressures are required as reflected by the lower pressure ratio. The effect of both of these phenomena is to greatly reduce the mass of air required to operate the sleeve muscle and so a substantial efficiency improvement is possible.

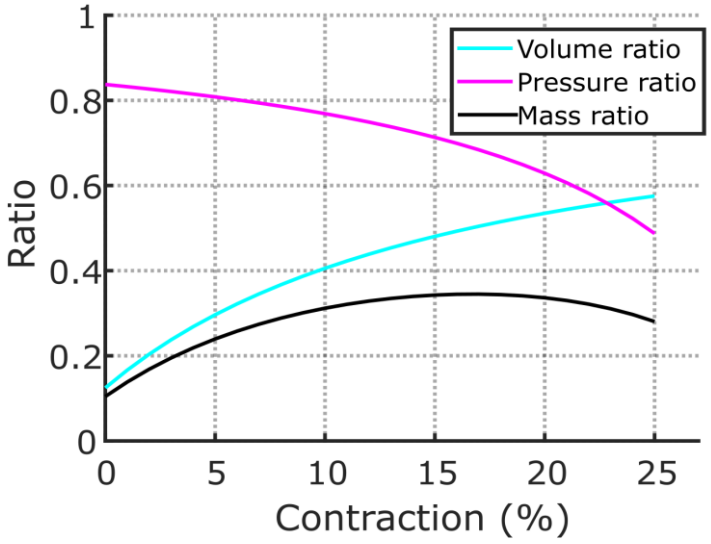

Figure 3-8: The volume, pressure, and mass ratios of a sleeve muscle in comparison with a standard muscle at constant output force.

3.4 DESIGN OBJECTIVES

3.4.1 TEST SLEEVE MUSCLE CONCEPT WITH MCKIBBEN MUSCLE

The previous implementations of the sleeve muscle have used a modified commercially available fluidic muscle developed by Festo. While the Festo muscle has been widely used in research, other muscle designs have also demonstrated favourable characteristics. The pleated pneumatic artificial muscle (PPAM), for example, has been shown to offer larger force outputs and greater contraction by removing the radial forces in the muscle [85], [281]. The sleeve muscle concept is not specific to any particular muscle design, but rather is a modification which is applicable to any muscle which retains a volume between the end fittings in a relaxed state. The McKibben and pleated muscles meet this criterion, although the ribbed nature of the PPAM may reduce the potential volume which can be removed by the sleeve. Therefore, a new sleeve muscle design which uses the McKibben muscle with distinct membrane and braid components is developed. This type of muscle is composed of readily available materials, while end fittings may be manufactured using standard workshop equipment. This means that important parameters such as muscle diameter, material, and end fitting design are at the discretion of the designer. This adaptability is more conducive to an optimized sleeve muscle design and allows better customization of the muscle to meet the needs of any particular application.

3.4.2 MAXIMISE VOLUME REDUCTION

Maximizing the proportion of the internal volume occupied by the central element of the sleeve muscle reduces the volume which would otherwise be filled with compressed gas, thus increasing efficiency. A greater reduction in the internal volume of the muscle is possible with the McKibben muscle due to greater design freedom. The larger element also allows more space for novel uses of the internal valves, for example valves, air distribution or sensors.

3.4.3 FORCE OUTPUT ALONG AXIAL CENTRAL AXIS

Previous implementations of sleeve PAMs have used mounts on either side of the sliding end fitting to transmit the muscles force. Uneven loading on these two points may lead to torsion or non-uniform force around the circumference of the muscle. Such forces are

undesirable as they can lead to increased wear between the muscle fibres, reduced force output, and unpredictable muscle performance (see Figure 3-9). Therefore, a key requirement of the design is force output along the axial central axis. This simplifies system integration as only a single mounting point is necessary. Cables are frequently used to transmit the pulling force of PAMs as the output force can easily be routed and applied as desired using pulleys or other means [18], [159], [210], [282]. Attaching a cable is greatly simplified when there is a single, central mounting point.

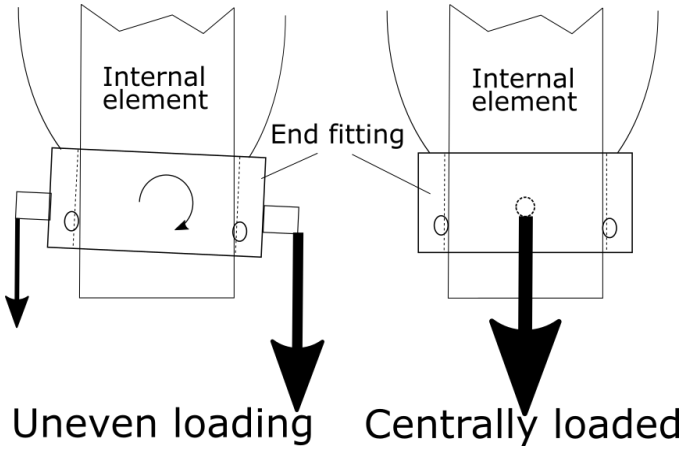

Figure 3-9: A comparison of the sliding end fitting of the sleeve PAM with two mounting points, which can result in uneven loading and with a single mounting point along the axial central axis.

3.4.4 ADAPTABILITY

The ability to configure PAMs to their application is a major advantage. Most PAMs can easily be designed and manufactured in any length, simply by cutting the muscle material (elastic bladder and braided mesh) to the appropriate length. This is not as easily achieved for the sleeve PAM as the length of the internal element is more difficult to alter. Also, based on the exact application, it may be beneficial to modify the portion of the inner element extending from the PAM (for instance for different methods of mounting to some linkage if the muscle is used structurally). Therefore, a modular, adaptable design is preferred, where many of the parts can be identical across a wide variety of use cases, with adaptions of removable parts where required.

3.4.5 CONTRACTION AMPLIFICATION

From a robotic design perspective, it is often desirable for a PAM to provide a larger contraction length, even at the expense of available force. For example, for applications

where a cable drive is necessary [18], [283], with the actuator located some distance from the join, high stresses in the cable will lead to high strain or require thicker stiffer cables. Therefore, it is advantageous to utilise cable configurations which minimise stress in the cables by increasing travel, thus transferring the same power to the joint, as achieved in [284].

Contraction amplification is also useful when direct actuation of the joint is desired. Consider the antagonistically actuated joint in Figure 3-10. This configuration makes use of the internal elements of the sleeve muscles to support the joint. If the system is to be kept as compact as possible, it is necessary to mount the muscles parallel to each other. As discussed in [79], an important consideration when using PAMs is the available space to mount the muscle on the system. In order to actuate the joint, sufficient contraction length is required to rotate the pulley over the full range of motion, necessitating a muscle of a prescribed length. For this reason, the active length should be maximised. The pulley diameter may also be reduced so as to reduce the required contraction of the muscle, however, there is a minimum distance between the muscles, which is necessary to allow the muscles to expand radially (by up to 200% at full contraction [183]). While the distance between the muscles could be greater than the diameter of the pulley and the cable from the muscle routed through a system of pulleys to the joint, this would occupy space along the length of the limb, reducing the active length of the muscle. Therefore, equation (3.11) represents the minimum size of the pulley and equation (3.12) the contraction of the muscle required to rotate the joint through an angle β_{range}.

$$D_p \geq 2D \tag{3.11}$$

$$dL = D_p \frac{\beta_{range}}{2} \tag{3.12}$$

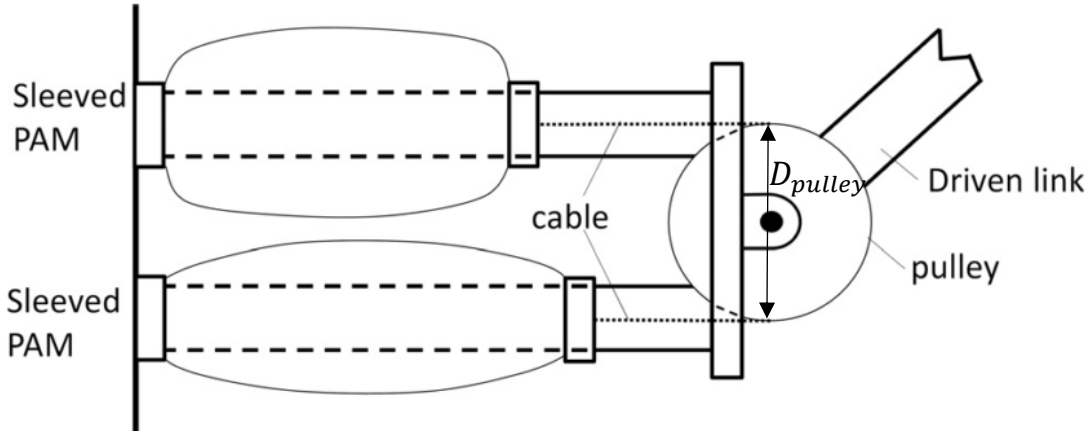

Figure 3-10: A conceptual antagonistically actuated joint using two sleeve muscles. A cable drive system is used to transfer force to the joint from the muscles and the central elements of the muscles are used to support the joint and child link.

Using this analysis, a sample application is considered, which is typical of the requirements of a robotic arm. The limb is taken to be long enough to accommodate a muscle of active length 0.25m and there is a requirement to rotate the joint through π rad. It is assumed the sleeve muscle can contract by 25% of its length. With these limitations, the maximum muscle diameter is found to be approximately 20mm if the cable is directly connected to the muscle. The alternative approach is to mount a pulley to the muscle in order to double the effective stroke length and half the force output, if losses from friction, etc., are negligible. Four potential muscle choices were analysed for this application using the model outlined in the previous section. The torque output when the muscle internal pressure is 500kPa, over the 180° range, is shown in Figure 3-11. Note that this is the maximum force that may be output and assumes the antagonistic muscle is not providing any opposing force (minimum joint stiffness). The 20 mm and 40 mm muscles represent the largest muscles possible for the directly driven and pulley driven joints, respectively. A much larger torque output is possible with the 40 mm muscle even though the force output from this muscle is halved by the addition of the internal pulley mechanism. Likewise, this means that lower pressures may be used to actuate the joint with the same torque by making use of a larger muscle, albeit that a larger volume of air is required.

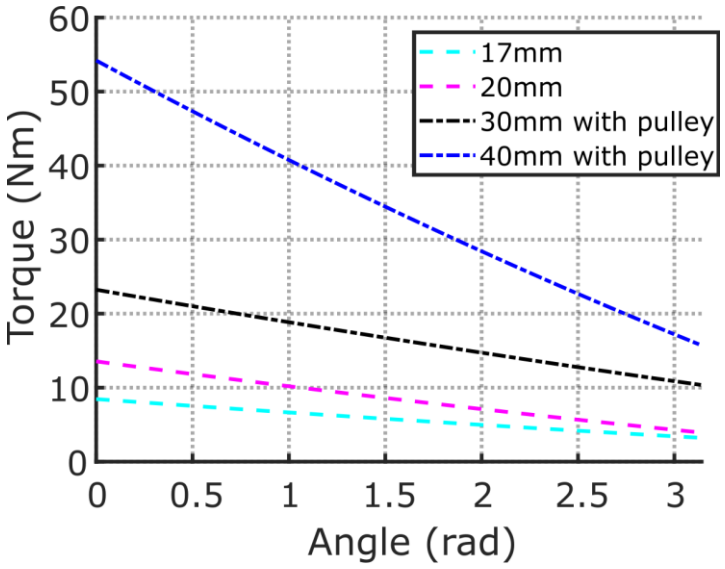

Figure 3-11: The output torque provided by four individual muscles on a joint actuated as in Figure 3-10 with an internal gauge pressure of 500kPa. In each case, a pulley that is twice the relaxed diameter of the muscle is used.

Implementation of the sleeve muscle concept is also more readily achieved using larger muscles as the structural as well as sealing components can be made larger. Additionally, the increased force output of the sleeve muscle would cause increased stress if applied directly to a joint. Limiting this force output while increasing contraction length allows the same work output while reducing the load on system components. This allows more lightweight materials to be used and reduce fatigue.

This analysis provided the motivation to construct a prototype to evaluate the inclusion of the pulley mechanism.

3.5 DESIGN REALISATION

An overview of the sleeve muscle design is shown in Figure 3-12. There are a number of elements to this design which are discussed in the subsequent section. Figure 3-13 shows the manufactured sleeve muscle with cable attached. It has a mass of 990g and active length of 0.195m. Further CAD drawings are shown in Appendix D.

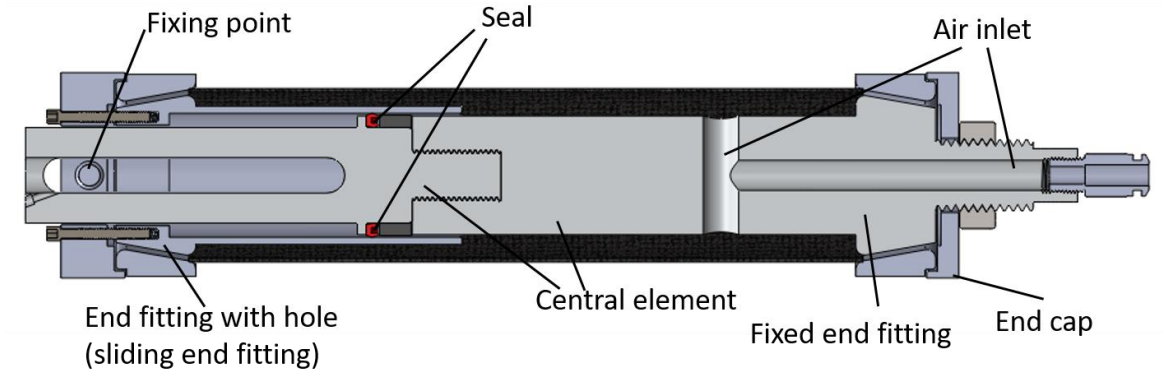

Figure 3-12: A cross section of the sleeve muscle.

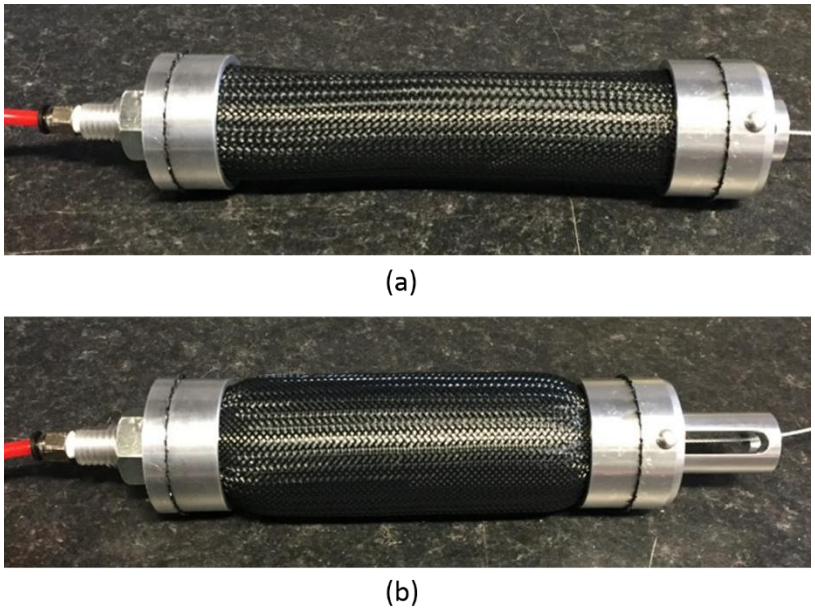

Figure 3-13: The manufactured sleeve muscle actuator in a relaxed state in (a) and a partially contracted state in (b).

3.5.1 MATERIAL SELECTION

Commercially available materials were chosen for the construction of the muscle membrane and braided mesh. Vena Technoex silicone tubing [285] was selected for the elastic membrane. While a latex membrane has been shown to provide better fatigue characteristics and lower threshold pressures, there were no commercially available products in the required diameter. A 38-mm internal diameter tube with 1mm wall thickness was chosen. Polyethylene terephthalate (PET) braided sleeves are one of the best candidates for the outer braided mesh [86] and are widely available in a range of sizes. A 40-mm diameter sleeve was chosen. Most of the rigid components were

manufactured from aluminium alloy 6082T6 as it is light weight and readily machinable. The attachment pin was made from steel as it must support significant bending stresses.

3.5.2 END FITTINGS

The main purpose of the muscle end fittings is to securely hold both the inner elastic tube (bladder) and braided mesh to ensure that air leaks are avoided. As noted, the fittings should be as low profile as possible to allow for a proportionally longer active muscle length. To achieve this, the bladder and braided mesh are both clamped in place together. The braid is then held on its own with further clamping. It has been suggested that the separation of anchoring the braid and sealing the bladder decreases the likelihood of braid pull out when the muscle is in tension [149].

To secure the braid and bladder together two conical surfaces are forced into each other with the muscle membrane and fibres between them (see Figure 3-14). This is similar to the approach proposed in[183]. The braided mesh continues past this section of the muscle and is expanded outwards to be clamped by the end cap which forces the braid around a tight radius. A single nut is used to force the conical surfaces together and secure the end cap for the fixed end fitting. Six M3 bolts are used on the sliding end to provide a uniform clamping pressure. The fixed end fitting also incorporates a pneumatic connector to allow pressurised gas in and out of the muscle.

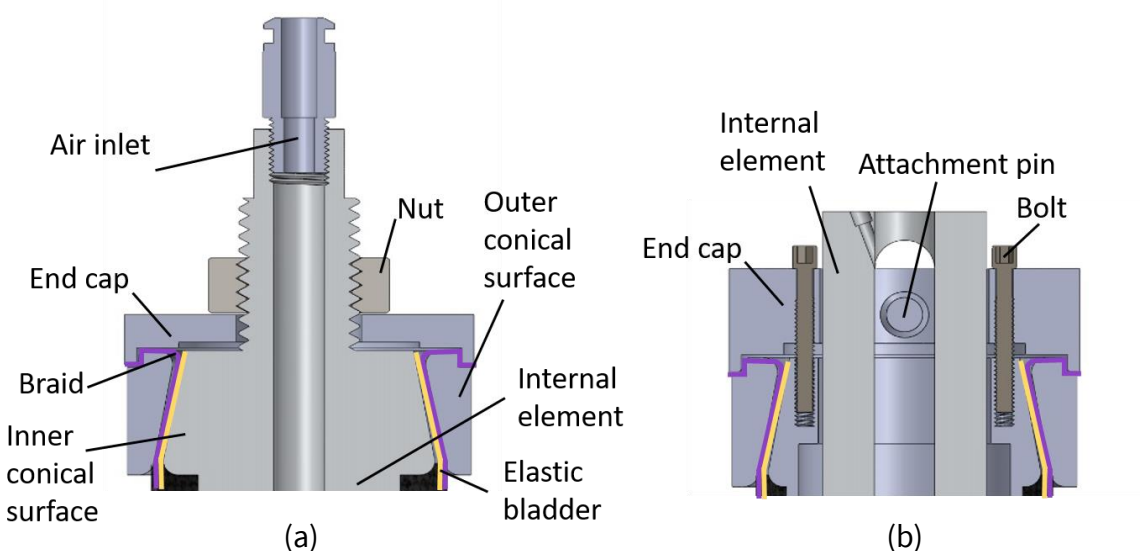

Figure 3-14: Cross section of the fixed end fitting (a), and the sliding end fitting (b).

The end fitting is also responsible for connecting the muscle to the actuated system. An M20 threaded shaft allows a variety of fittings to be attached for this purpose at the fixed end fitting. The sliding end fitting contains an attachment pin. This extends across the diameter of the end fitting, allowing connection of an external load either at the two sides of the end fitting or along the axial central axis of the muscle. The modular nature of the design allows different attachment pins to be fitted as discussed below.

3.5.3 INTERNAL ELEMENT

A modular design is implemented to allow the muscle to be adapted easily for different applications and facilitate incremental design improvements. The central element was composed of two parts which screw together, allowing the end protruding from the end fitting of the muscle to be replaced (see Figure 3-12). A slot was added to this portion of the element to allow a shaft to extend from one side of the end fitting to the other. This allows a cable or rod to be attached and transmit the contractile force of the muscle along its axial central axis. As it is not possible to create a seal along the slotted section of the central element, the end fitting is extended into the muscle and a low profile U-cup seal fitted further down the central element to ensure no gas can escape from the muscle. Extending the end fitting into the muscle has the added benefit of increasing the volume of the central element, thus reducing the mass of air required to operate the muscle. An additional advantage is the protection of the sliding surface of the seal, as this part of the central element is always covered by the muscle structure.

As this prototype is intended to operate in isolation, there is no facility to attach the protruding end of the central element to a subsequent joint. Given the modular nature of the design however, this would only require replacing the slotted portion of the central element. The diameter of the main part of the central element is 34mm while the extension of the sliding end fitting is 38mm, fully filling the relaxed diameter of the muscle in this region. Figure 3-15 shows the manufactured internal element.

Figure 3-15: The internal element before the remainder of the muscle is constructed around it.

3.5.4 PULLEY MECHANISM

The end fitting was designed so as to be easily adaptable to provide output force either directly or through a pulley mechanism housed in the end fitting and sleeve. The routing of the cable is modified as shown in Figure 3-16. Adapting the muscle to one configuration or the other requires only one component to be replaced (the attachment pin). Adopting this approach reduces the quantity of components which must be manufactured, decreasing development time. When the muscle is configured to pull directly, the fixing point of the cable is on a rod rigidly fixed to the moving end fitting, passing through the axial centre of the muscle. A hole through the rod facilitates attachment of the cable. If a pulley mechanism is desired, the rod is replaced with a different rod with a small bearing surface on which the cable can run. This acts as a pulley with the cable fixing point moved to the end of the sleeve protruding from the muscle and the other end of the cable connected to the load.

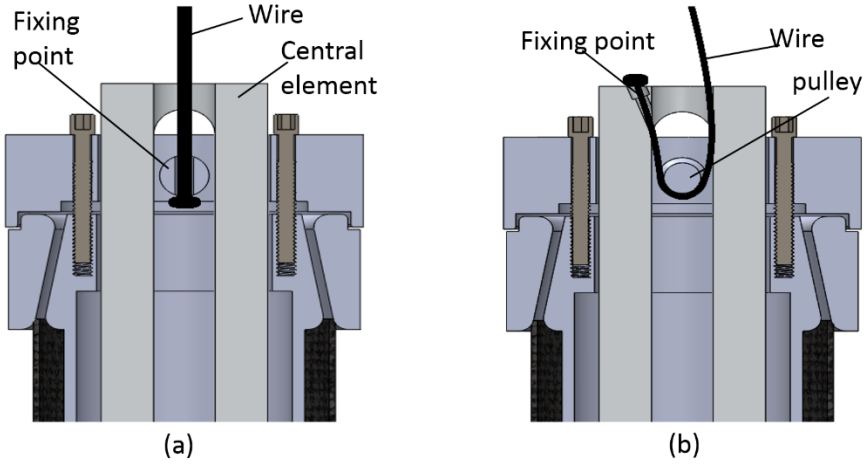

Figure 3-16: The sliding sleeve muscle end fitting with a cable configured to pull directly (a) and with the pulley mechanism (b).

3.6 UPDATED MODEL FOR SPECIFIC IMPLEMENTATION

Any implementation of the sleeve PAM will differ from the idealised model previously discussed as it will not be possible to entirely remove the dead volume in the PAM. This is for several practical reasons including the requirement to grip the PAM bladder and braid as we as accommodating the sliding seal. In the case of the muscle implemented here, the function to describe the PAM volume as the muscle contracts is complicated by the extended end fitting. The volume of the end fitting in the muscle does not change, while the volume removal due to the inner element reduces with contraction as more of it will extend outside the muscle. This is illustrated in Figure 3-17.

As a result, equation (3.7) is update to

$$V_{SM} = \frac{L\,(b^2 - L^2)}{4\pi n^2} - \frac{L_b {D_{1b}}^2 \pi}{4} - \frac{(L - L_b){D_{1a}}^2 \pi}{4} \tag{3.13}$$

The force output is dependent on the change in volume with length according to (3.3), with D_{1a} used in place of D_1 and so is unaffected by the extended end fitting or the volume reduction that this brings. This can be understood intuitively as the pressure in the muscle still pushes outwards on the fixed end cap over the area which does not have the internal element protruding from it.

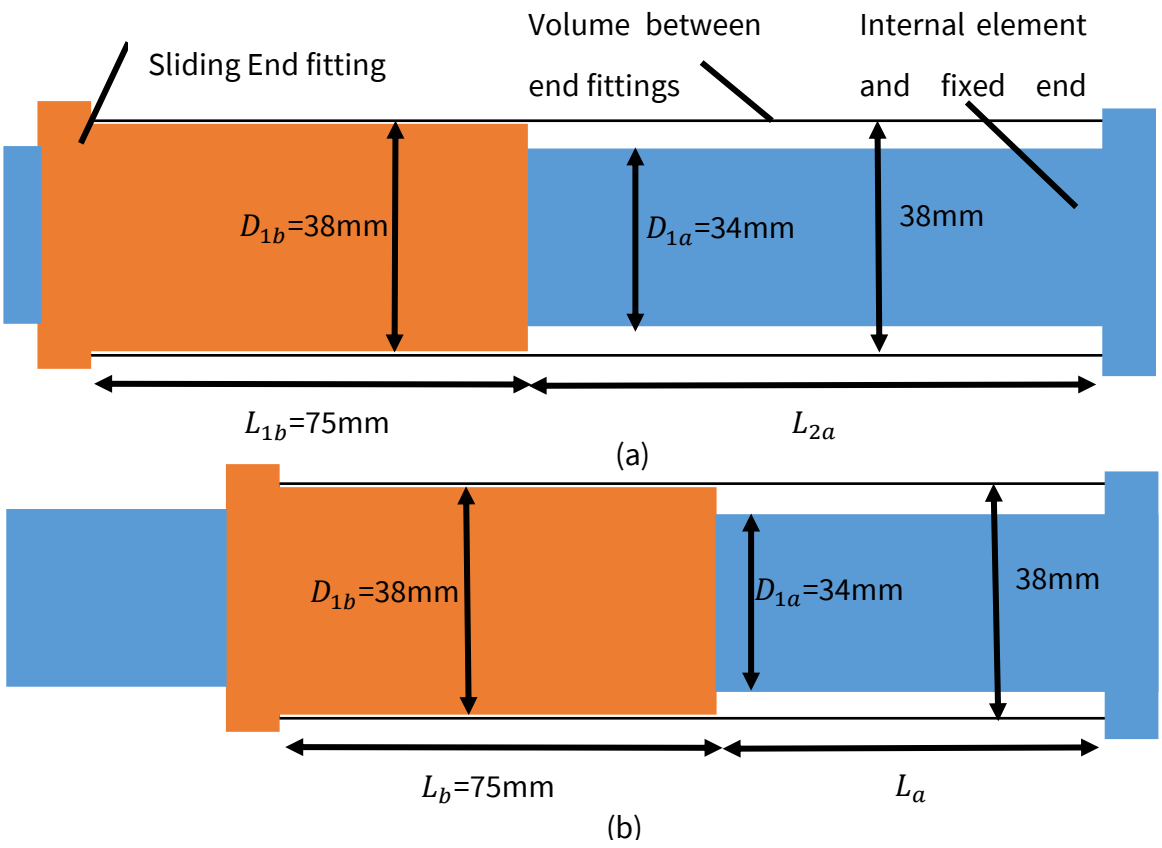

Figure 3-17: Depiction of the cylindrical volume between the end fittings as the implemented sleeve muscle contracts. (a) shows the fully extended muscles and (b) a partially contracted muscle.

3.7 TRADITIONAL PAM FOR COMPARISON

In order to evaluate the performance improvements of the sleeve muscle implementation, a traditional muscle was constructed for comparison purposes. The diameter, active muscle length and muscle materials were identical in both cases to ensure a fair comparison can be made. Additionally the manner in which the bladder and braid are held in the end fitting is identical to that of the sleeve muscle (see Figure 3-18). The mass of the actuator is 570g which is 420g less than the sleeve muscle. If the sleeve muscle is used structurally however this additional mass may be offset.

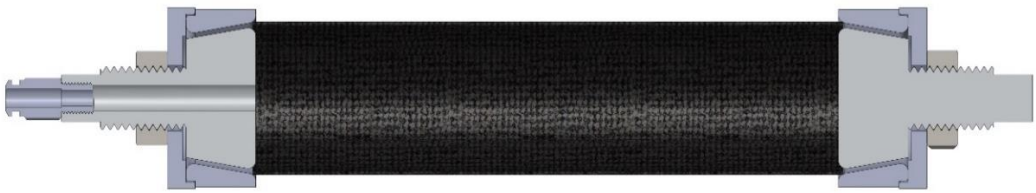

Figure 3-18: Cross section of the standard McKibben muscle.

3.8 REMARKS

In this chapter a new concept in sleeve muscles was proposed. The implemented design differs from previous research as it makes use of the McKibben type muscle. Being unconstrained by the limitations of commercially available muscles allows the actuator to be better adapted to the sleeve muscle concept by removing more of the internal volume, therefore further increasing force output and efficiency. At full extension 88% of the volume between the end fittings is occupied by the internal element and extended end fitting. Previous implementations have only achieved 78% [276]. As the muscle contracts this figure increases. A pulley mechanism was also proposed here which effectively doubles the output contraction while halving force. This is useful for integration with robot systems where it facilitates more compact actuation mechanisms.

For the proposed design to be practical, it must justify the additional complexity required for its manufacture. Given the performance increases outlined above this is arguably the case, however this will be explored further in the subsequent chapters. While the design produced here is necessarily of a defined dimension and specification, it is adaptable to many other sizes and mounting strategies making it practical for real world applications where not all actuation requirements will be identical. In particular, the design's modular nature makes adaptations for different lengths feasible. Altering PAM diameter is somewhat more difficult however, and it is likely the effectiveness of the sleeve PAM modification (in terms of internal volume reduction) would be reduced for PAMs with small diameters as there will be limitations on the size the components may be manufactured at.

The new sleeve muscle was manufactured along with a comparable traditional muscle. These muscles will be tested and evaluated in the following chapter.

4 STATIC CHARACTERISATION OF A SLEEVE PAM

To quantify the level of performance improvement of the proposed sleeve muscle design several static tests were performed on both the sleeve and standard PAM. These verify the increase in force output of the sleeve muscle as well as the increase in actuator efficiency by reducing the gas consumption. By establishing the characteristics of the sleeve muscle developed in the previous chapter comparisons, can be made with those described in the literature. Additionally, the pulley mechanism can be tested to verify its effectiveness.

4.1 TESTING APPARATUS

All tests were performed using the experimental setup shown in Figure 4-1. An Instron 3366 tensile testing machine was used to measure the force output of the muscles under different levels of contraction and a range of internal pressures. Rigid linkages were used to secure both ends of the muscle to the tensile testing machine. Compressed air was supplied using the storage tanks shown in Figure 4-2. This allowed the pressure to be adjusted and measured during tests. Honeywell TruStability HSC 150 PSI [286] pressure transducers were used to monitor the pressures in the storage tank and muscles during testing. These provide an I^2C digital output which is read by the Arduino and sent to a computer. Dynamic test conditions are not considered here, and so latency is not a concern.

1 – Gas Pressure Line
2 – Base Beam
3 – Pneumatic Muscle
4 – Load Cell
5 – Moving Crosshead
6 – PC Pressure Monitoring
7 – Testing Control

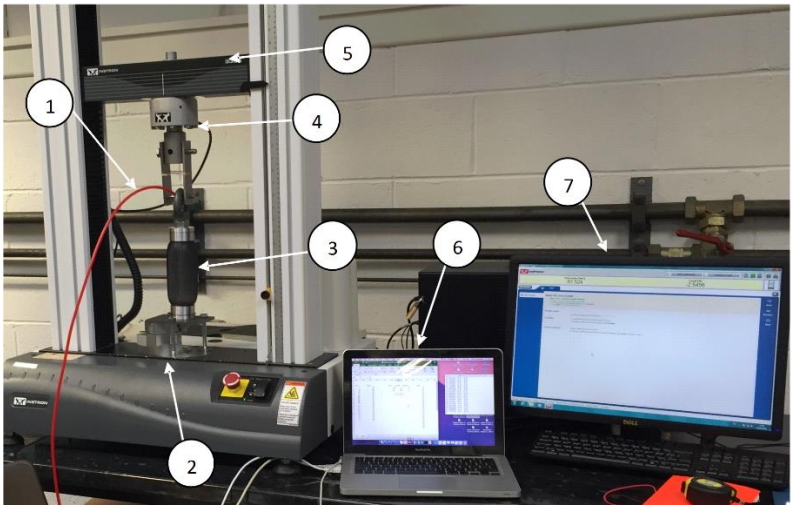

Figure 4-1: Testing apparatus.

1 – Compressed Air In
2 – Compressed Air Tanks
3 – Pressure Transducer 1
4 – Arduino Board 1
5 – Regulator
6 – Pressure Transducer 2
7 – Arduino Board 2

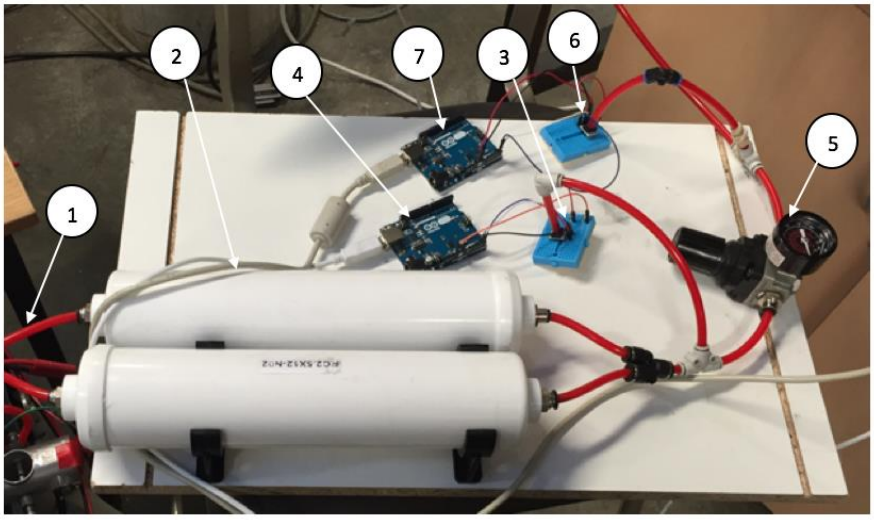

Figure 4-2: Compressed air supply with pressure sensing and regulation.

4.2 ISOMETRIC FORCE OUTPUT

The tests were conducted starting at maximum muscle length. Stretching the muscle to above its relaxed length was not considered, however a small muscle tension (40N) was applied at 0% contraction to ensure consistency between the tests on the two muscles. Pressure in the muscle was increased using the manual pressure regulator and

measurements of force output and pressure taken approximately every 35kPa. The distance between the muscle mounting points was decreased in increments of 2.5% of the active muscle length for each subsequent test. Small variations in muscle length between the sleeve and standard muscle could be accounted for by using the contraction percentage of the individual muscle rather than increments of an absolute value.

The force outputs of the standard and sleeve muscles obtained during testing are shown in Figure 4-3. Both muscles display an approximately linear relationship between force and pressure at a fixed length as is typical in the literature. It is evident from that the force output is greater at similar pressures using the sleeve muscle. In order to further illustrate this, Figure 4-4 was compiled from the results. This shows that at a given pressure the increase in output force is constant, regardless of contraction. The theoretical force output was calculated by modifying the experimental results for the standard muscle in accordance with equation (3.9). This theoretical analysis strongly agrees with the experimental results supporting the validity of the modelling approach undertaken. Figure 4-4 also confirms the reduced operating pressure required to achieve the same output force with the sleeve muscle. The difference in operating pressure between the two muscles increases with contraction. As the muscle contracts, the output force of the muscle reduces; however, the additional force from the sleeve modification remains the same and so becomes more significant. This behaviour explains the increased contraction ratio, which is possible with the sleeve muscle.

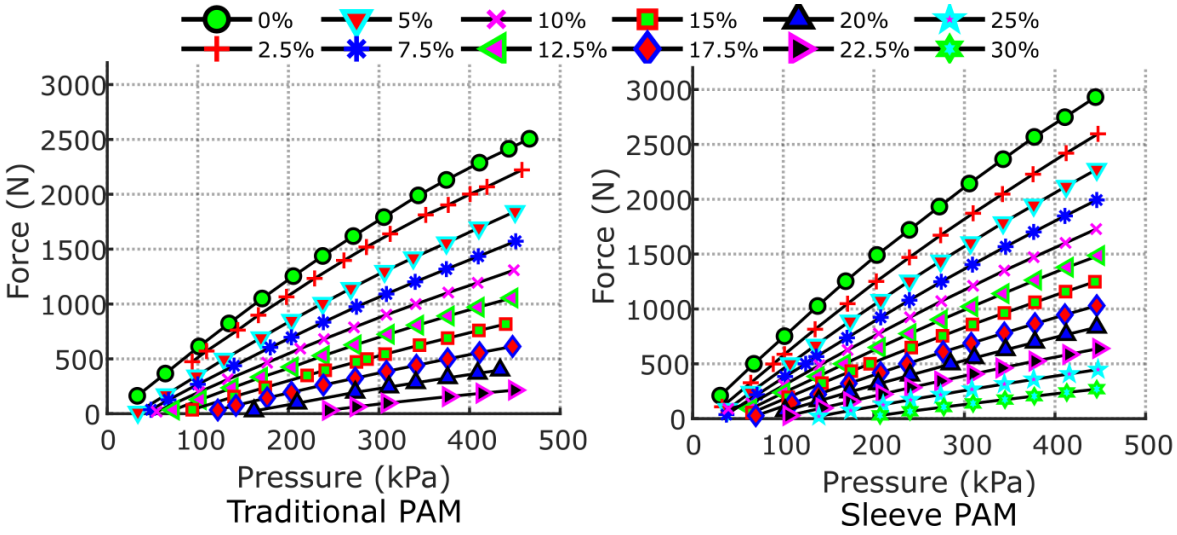

Figure 4-3: Isometric force outputs for the standard and sleeve muscle at a range of muscle internal pressures.

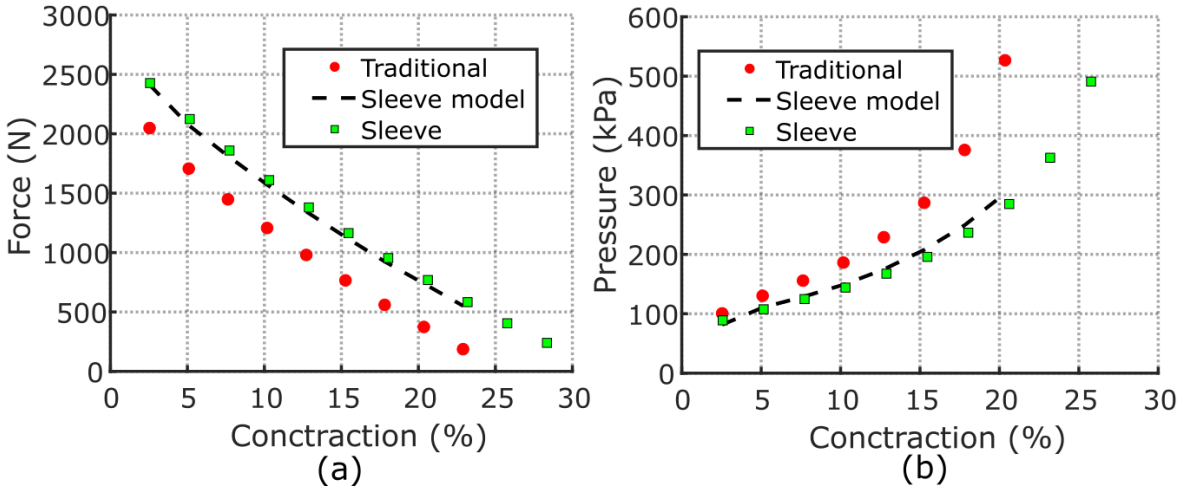

Figure 4-4: Performance of standard and sleeve muscles over the full range of contraction: (a) shows the force output with an internal muscle pressure of 410kPa and (b) shows the pressure required to provide a force of 500N.

4.3 RELATIVE EFFICIENCY

The aim of these experiments was to quantify the change in efficiency between the standard and sleeve muscle. As such an absolute measure of efficiency was not sought but rather the relative change in mass consumption. Again, isometric experiments were conducted. The supply tank was pressurised to 690 kPa. It was then sealed and no additional air added to the system as the muscle was pressurised until the force output by the PAM reached 500N. The pressure in the supply tank was monitored in order to determine the mass flow to the muscles. A similar approach is taken to that described in equation (3.10) . In this case, the pressure ratio is calculated using the reduction in

pressure in the supply tank. The volume ratio is not required as the volume of the supply tank does not change. This allows for the calculation of the mass ratio (assuming isothermal conditions), and from this, the percentage energy saving can be found using equation (4.1)

$$E_{saving} = 1 - \frac{m_{SM}}{m_{TM}} \tag{4.1}$$

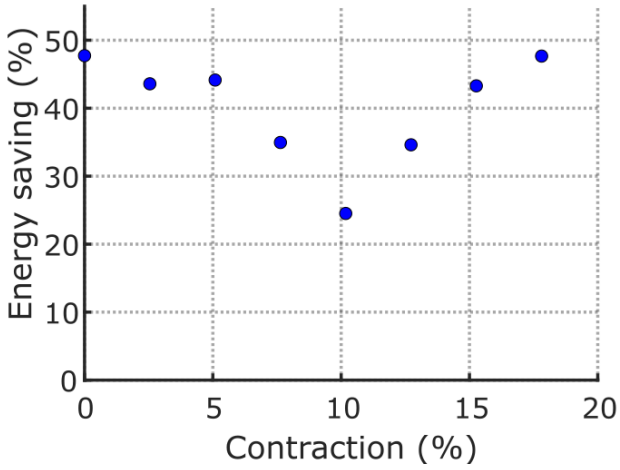

Figure 4-5 shows the percentage energy saving as a function of contraction. As expected from the theoretical analysis of mass ratio, energy saving is greatest at the two extremes of contraction, dipping around the mid-contraction point. At small contractions, a greater proportion of the internal volume of the muscle is occupied by the internal element, and so the volume reduction is at its maximum. When the contraction is large, the force output of the muscle declines, making the additional force from the sleeve adaptation more significant. This reduces the pressure requirement to a greater extent in this region. The maximum energy saving recorded was 47.7% at 0% contraction and 17.5% contraction. The minimum energy saving is 24.5% This increase in efficiency is greater than that reported by Driver and Shen, where the comparable figures vary between 37.5% and 20% [276]. This can be attributed to the greater proportion of the muscle volume, which is occupied by the internal element with this design. The general shape of the graph is rather similar however.

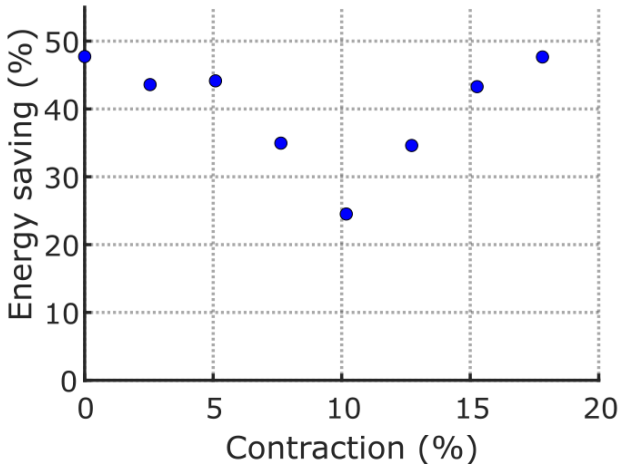

Figure 4-5: The energy saving of the sleeve muscle in comparison with the standard muscle when the output force is 500N.

4.4 HYSTERESIS

Hysteresis has been a well-known phenomenon with PAMS. As mentioned in [136], [175],this causes significant difficulty in modelling and control. The force output at a given pressure and contraction ratio is dependent on whether the muscle is contracting or elongating; being pressurised or depressurised. This is mainly due to the action of the braid and bladder and so little change was expected with the sleeve muscle, unless stiction at the U-cup seal was significant. The isometric test was extended to include the depressurisation of the muscle as well. As before, no contraction of the muscle is allowed during the test. As such it was the hysteresis with changing pressure which was tested as opposed to contraction. This is certainly not as pronounced but some hysteresis was observed. Figure 4-6 shows the results for the standard and sleeve muscle at 0% contraction. Other levels of contraction were also tested but the most significant hysteresis was observed when the muscle was at its longest. From the graphs it is confirmed that the addition of the sleeve muscle has little effect on pressure hysteresis behaviour.

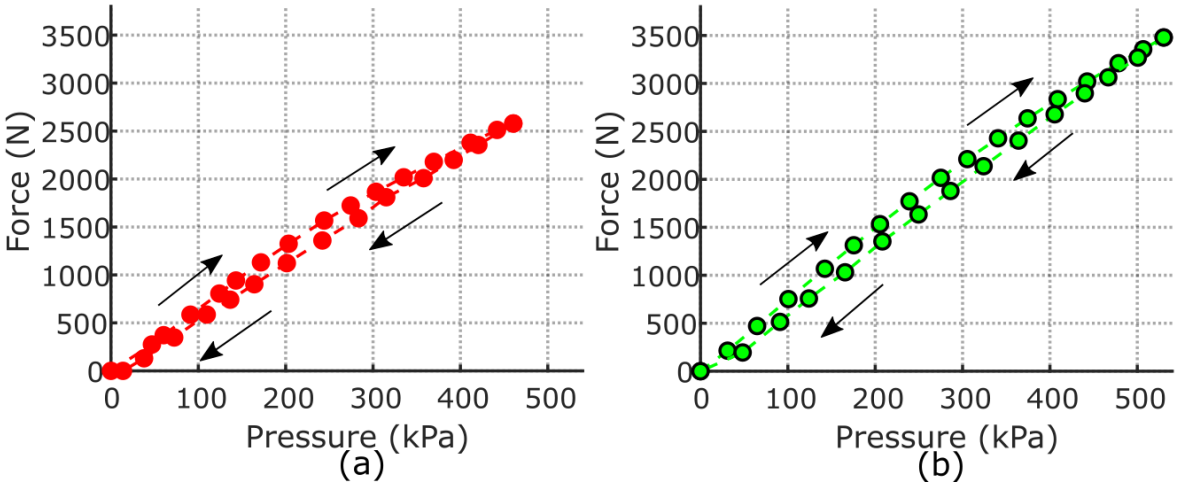

Figure 4-6: Hysteresis tests at 0% contraction. The direction of the arrows indicates the time line of the test: (a) standard PAM and (b) sleeve PAM.

4.5 PULLEY MUSCLE

The sleeve muscle in the pulley mechanism configuration was also tested using the isometric test. Unlike the previous tests, it was necessary to attach a drive cable to transfer the force from the muscle to the testing machine in order to make use of the pulley. As before, the contraction was held constant and the pressure gradually increased. The results of this procedure and comparison with the previous muscles tested are shown in Figure 4-7: Test results of the standard muscle and both direct drive and pulley configurations of the sleeve muscle at 276kPa (40 psi) operating pressure. The theoretical sleeve muscle with pulley is found by halving the force output of the sleeve muscle and doubling the contraction. The experimental results show that when using the pulley feature, the output force is considerably less than expected. This can be attributed to stretch in the drive cable, which would allow greater contraction of the muscle than desired. Rigidly attaching the end fittings to the testing machine in the previous tests avoided this issue. The increase in effective contraction ratio agreed with the predicted performance as when there is reduced force in the cable it stretches less.

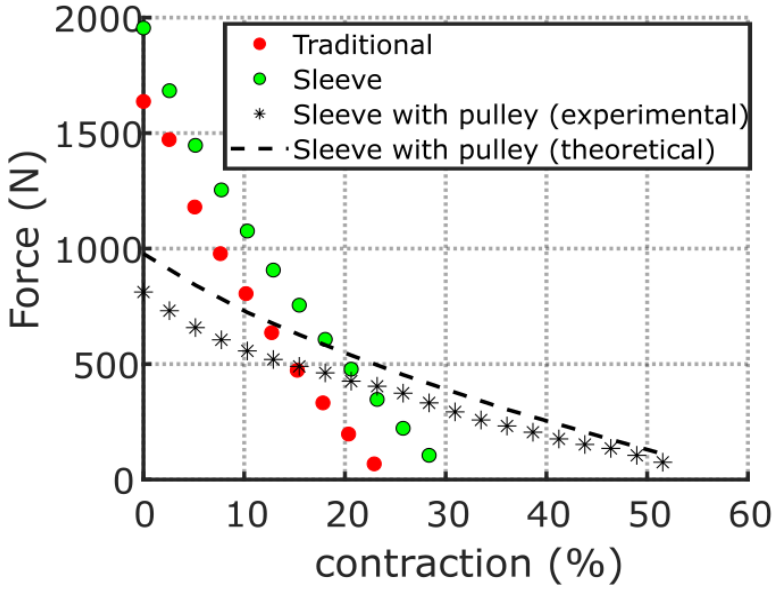

Figure 4-7: Test results of the standard muscle and both direct drive and pulley configurations of the sleeve muscle at 276kPa (40 psi) operating pressure.

4.6 REMARKS

These experimental results verify the performance improvements of the sleeve PAM. Force output is increased consistently across the contractile range. This is particularly significant at large contractions, where the muscle output force is smaller. Indeed, the maximum contraction of the muscle is extended by 5% of the active muscle length. This improves the effective operational range of the muscle which is particularly advantageous in robotic applications where a wide travel range in muscle joints is important.

Lower operating pressures can be used to achieve the same output force with the sleeve muscle, particularly at high levels of contraction. This, together with the reduced internal volume of the muscle, results in an improvement in efficiency of up to 48% in terms of mass of air consumed. For any mobile system this will be most advantageous as the power requirements are reduced.

A potential issue with the sleeve muscle concept is an increase in friction due to the sliding seal. This was not observed to be significant however, although the muscle was not tested at high speeds. Another key performance requirement of the design was reliability. Although fatigue tests were not conducted, it was noticed that there was some

sliding of the braid from the end fittings. This was particularly true when the muscle was tested without the braid extending past the silicon. The additional clamping of the braid as illustrated in Figure 3-14 reduced this somewhat but long-term use may require further clamping.

Good agreement was observed with the sleeve muscle previously implemented by Driver and Shen, however the larger volume removal resulted in greater performance improvements for the PAM implemented here, as expected. The force capability of the Festo fluidic muscle is greater than that of the McKibben muscle described here, most likely as a result of the stiff silicone used for the bladder.

The internal pulley mechanism increased the contractile range by 124% when compared to the standard muscle. This fundamentally changes the nature of the actuator from one with a large force over a short range to a more modest force over a larger contractile range. Depending on the application, this has the potential to further improve the safety of the actuator as smaller forces must be passed through the drive cable. However, limitations inherent with using cable drive methods are still observed, such as stretch in the cable.

As an actuator for use on mobile service robots, these results confirm a number of advantages. If a PAM can operate more efficiently, this reduces the energy storage requirements of on-board systems, improving the operating time and reducing the overall size of the robot. Furthermore, the reduced pressure and volume required results in a safer actuator as less potential energy is stored in the form of compressed gas in the muscle. Increasing the muscle force output opens a greater range of application areas, while the inherently compliant nature of the PAM maintains favourable safety characteristics. The demonstration of the in-muscle pulley concept facilitates more compact systems to be developed which is important where there are a large number of degrees of freedom actuated in close proximity to each other.

In order to use the sleeve muscle effectively and safely, an accurate understanding of its dynamics is necessary. This is the focus of the following chapters.

5 DYNAMIC TESTING APPARATUS

This section explores the development of a specialised testing apparatus for the characterisation of muscles under both static and dynamic conditions in a number of configurations including antagonistic actuation of a resolute joint. It also includes an account of changes made to the PAMs to improve the performance characteristics, namely the materials used and the addition of an embedded pressure sensor.

5.1 PURPOSE OF APPARATUS

While the previous section showed how an Instron tensile testing machine can be used to develop accurate characterisation of both sleeve and traditional PAMs under isometric conditions, it does not possess the capability for dynamic testing as the speed of movement of the cross beam is limited. Thus, a new testing apparatus was conceived, designed and built to achieve this goal. This apparatus was constructed to be capable of performing a wide variety of tests on as many types of muscle as possible (such as those with different lengths, diameter etc. In particular, it requires the capability to test sleeve muscles, such as those previously developed. The testing apparatus was developed with consideration for the following tests

- Isotonic testing - Whereby a single muscle is under constant load during contraction
- Isobaric testing - Where a single muscle contracts under constant pressure
- Dynamic testing - Whereby a single muscle, or antagonistic arrangement of muscles move at a speed where dynamic effects play a role. This would include tests such as
    - Pressure step responses – the muscle(s) reaction to a step change in pressure.
    - Disturbance testing -A sudden force is added or removed from the muscles
    - Stiffness testing – The muscle is deviated from its set point and the force change used to determine the muscle stiffness
- Model development and testing - The generation of data which can be used as input data for empirical models and as a means to validate these and more theoretical models.

- Longevity testing - Operation over long time periods and potentially millions of cycles to determine the robustness of muscles.

5.2 REQUIREMENTS

With the objectives of carrying out these tests as well as consideration for practical requirements, there are several features which the testing apparatus should possess.

As it is essentially the relationship between pressure, contraction and load which is of interest under different conditions in the above tests, each of these quantities must be measured independently. It must also be possible to change at least some of these in a controlled way. This must be possible for both a single muscle and in the case of a joint actuated in an antagonistic configuration.

The testing apparatus must also be easily adaptable to a wide range of tests and testing procedures, perhaps some not even envisaged at the time of construction. The capability to test both a single muscle as well as an antagonistic pair is typically not considered in testing apparatus found in the literature [13], [174], [255], [264]. For this reason, the test apparatus must be kept as reconfigurable as possible, with permanent fixtures avoided. This also lends itself to the adaptability of the system to accommodate muscles of various lengths and diameters that may be required in a robotic system. Furthermore, it may be necessary to test models of joints with different ranges of travel, but with the same muscle dimensions. Therefore it should be possible to alter the moment arm of antagonistically arranged muscles. Of course the need to facilitate the testing of sleeve muscles is a fundamental requirement of this apparatus, although as it is the force performance of the muscle which is relevant, it is considered unnecessary to use the sleeve as a load bearing structure during testing.

To reduce experimental error, the testing apparatus should be as stiff as possible. This is so that deflection of the system does not affect the validity of the measurements taken, for instance by allowing the muscle to contract by more than would be possible if the rigid assumption were true. The previous static tests suggest an approximation of the forces which may be expected, this having been quite a large muscle test. While

maintaining this rigidity, friction in the system must be minimised to reduce additional, unaccounted for forces.

In order to conduct dynamic tests, a high sampling frequency is necessary for all sensors. Examining the literature, the highest frequencies of operation of the muscle are approximately 40Hz by Woods [184]. Therefore the sampling rate should be far in excess of this value to capture the transient behaviour of the system. Also necessary for dynamic tests is a reliable, high volume, source of compressed air, capable of supplying air to the system without a reduction in pressure over time.

Finally, for practical purposes, it is desirable that the apparatus be relatively small and mobile so it can be stored when not in use.

5.3 IMPLEMENTATION

5.3.1 FRAME

The main structure of the testing apparatus is shown in Figure 5-1. In this configuration, two muscles are used antagonistically. The muscles are attached to load cells which are in turn held by the steel end plate by means of a 12mm diameter threaded bar. This allows the point of support of the muscle to be moved closer to or further from the pulley, in order to tune the apparatus for different muscle lengths, contractions, and in the case of antagonistic joints, joint rotation. A 3mm Dyneema rope runs from each muscle, around the pulley and is secured to the pulley. The use of two separate ropes allows the length of each to be adjusted independently to help in the configuration of the joint. An absolute encoder attached to the pulley shaft measures the position of the joint

For single muscle testing, where contraction is allowed and must be measured (e.g. isotonic or isobaric operation), the muscle is attached in the same way. As before, the Dyneema rope is used to attach the muscle to some load, either directly or via the pulley. A linear potentiometer can then be used to measure muscle contraction. The contraction of the muscle measured by the resulting rotation of the shaft. Alternately, when isometric tests are to be conducted, the pulley is removed and one of the steel end plates from the antagonistic setup is used to secure the other end of the muscle. The threaded bars can be used to adjust the allowable contraction of the muscle.

The frame of the test apparatus is mainly constructed from aluminium extrusions with a 40mm cross section. While aluminium does not offer as large a modulus of elasticity as steel, the construction of the extrusion helps to improve overall rigidity. Calculations of the total deflection of the beam supporting the joint showed a deflection of only 1mm when a force of 5000N is applied which was considered acceptable. Aluminium is also relatively light weight. The extrusion allows adjustable sliders to be used to secure components, making assembly more convenient, allowing the system to be tuned to particular muscles, and allowing the apparatus to be reconfigured for different experiments. Steel is used for the end plates, to which the load cells are attached. The pulley is secured with a pin, so as to make it possible to remove the pulley and replace it with a different sized alternative if required.

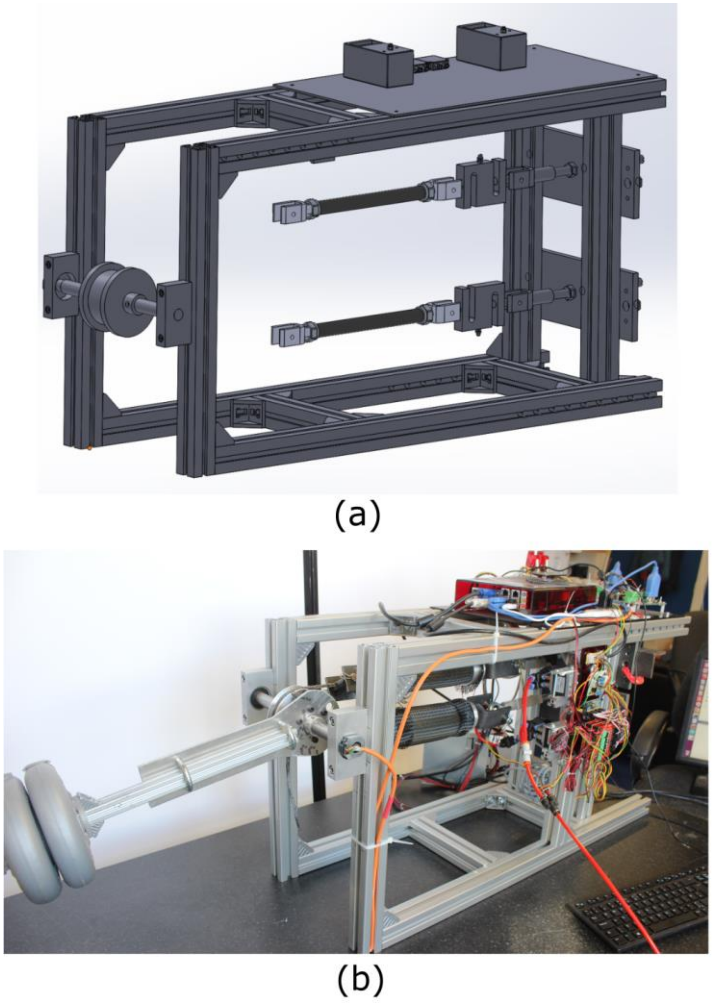

Figure 5-1: A computer rendering (a) and photograph (b) of the frame of the testing apparatus. The labelled components are: (1) load cells, (2) absolute joint encoder (3) steel end plate, (4) pulley, (5) pillow blocks supporting rotating shaft.

In its current implementation, load will be applied to the muscles by applying a mass in the single muscle configuration, or by means of a torque arm and mass in the antagonistic configuration. However the shaft to which the pulley is attached extends past the pillow block without the encoder so it may be used to connect to a motor or other device to provide the torque.

The testing apparatus possess enough mass that it does not normally need to be clamped down during operation, though given its construction, this is easily realisable. Its cuboid nature also means it can be reoriented with relative ease for different tests.

5.3.2 PNEUMATIC SYSTEM

The pneumatic system on the testing apparatus comprises of a compressor, accumulator tank, pressure regulator, tubing, valves and pressure sensors. This is illustrated for the case of an antagonistic pair of muscles in Figure 5-2. Here the compressor and accumulator tank provide the supply of compressed air, the pressure is controlled by the pressure regulator. Flow to the muscles is controlled by the inlet valves and exhausted through the exhaust valves. Pressure sensors on the air supply line and the line connected to the muscles, record the gauge pressure for characterisation and control.

The compressor used is an MGF SIL-EOl 50/100 [287] as shown in Figure 5-3. This compressor includes a 50l storage tank, which helps to regulate output pressure and supply air in short bursts faster than the compressor alone. It has a maximum pressure of 8 bar and has a flow rate of 100 l/min. It is also relatively quiet, with a noise rating of 40 dB(A), making it suitable for use in the lab environment.

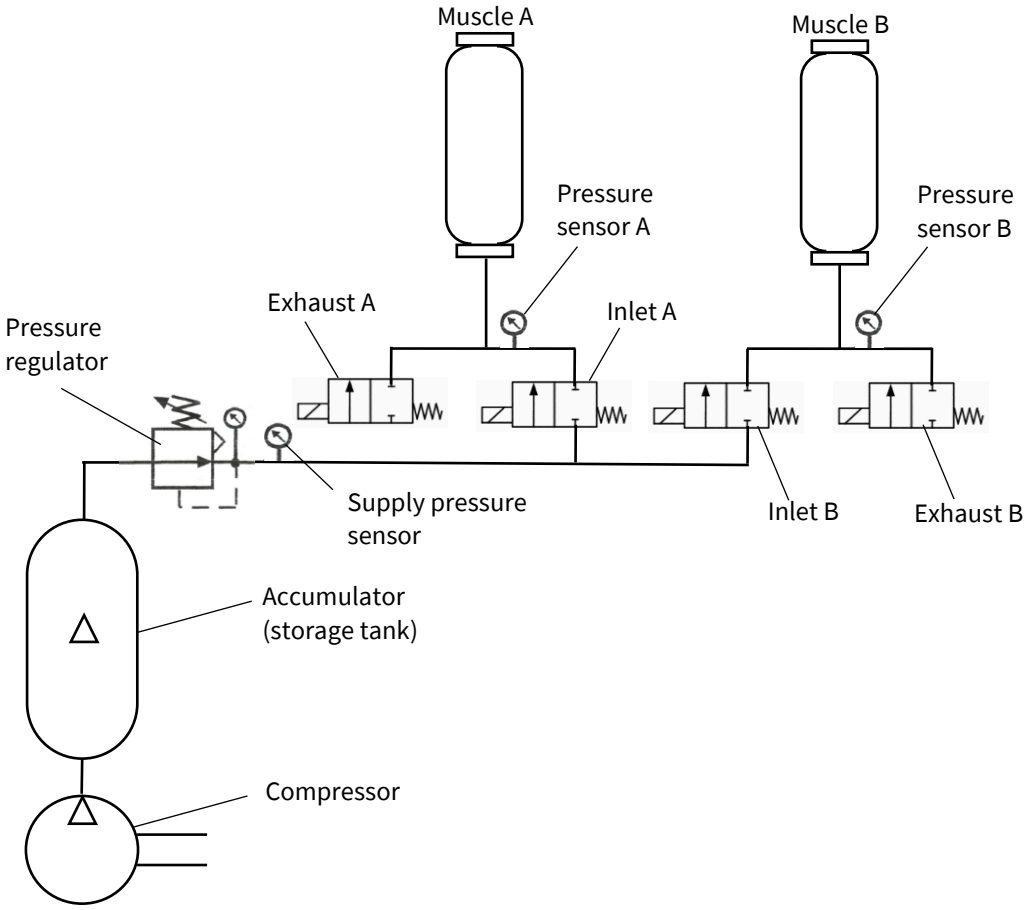

Figure 5-2: The structure of the pneumatic system required for antagonistic tests. Note that up to 3 valves are used in parallel to fulfil each inlet and exhaust function.

Connected to the output of the compressor unit is an AWG30-F02G1H filter and manual pressure regulator. This removes impurities from the air and regulates the pressure of the air leaving the tank. The regulator connects to a 9mm internal diameter hose which reduces to 4mm and finally to 2mm before connecting to the valves. After the valves the 2mm tubes connect to a 4mm tube which leads to the PAM. Push fit pneumatic connectors are used where possible to simplify reconfiguration of the system.

Figure 5-3: The MGF SIL-EOl 50/100 air compressor used in the testing apparatus, with the AWG30-F02G1H filter and manual pressure regulator attached.

Matrix BX 721 02C212 2/2 normally closed solenoid valves [288] are employed as these have fast switching times relative to other solenoid valves, making control more precise. While proportional pressure regulators would make control of the pressure in the PAMs simpler, solenoid valves offer a lower level control, necessary for some of the tests envisaged, which require the PAMs to operate as a closed system with fluctuating pressure. These valves allow 80l/min to flow at 6 bar. A minimum of two valves are required per muscle, one for intake and one for exhaust. In this case, 3 inlet and 3 exhaust valves are used in parallel to increase the flow rate. The valves are located in close proximity to the muscles so that the volume of the tubing leading to them has a minimal effect on the dynamic performance of the muscle. This is shown in Figure 5-4.

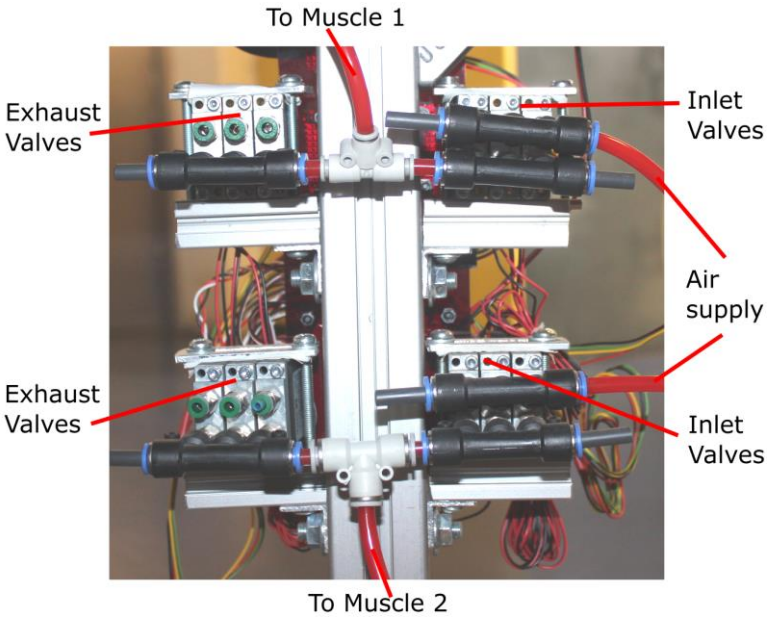

Figure 5-4: The valves on the testing apparatus arranged for an antagonistic test i.e. to control two PAMs.

5.3.3 DATA ACQUISITION AND CONTROL

In order to conduct the required testing, there are three major quantities which must be measured: muscle gauge pressure, muscle force output and muscle contraction. In the case of an antagonistic configuration, these quantities must be measured for each muscle. Additionally, up to 12 valves must be controlled. The electrical and communication system to achieve this is illustrated in Figure 5-5.

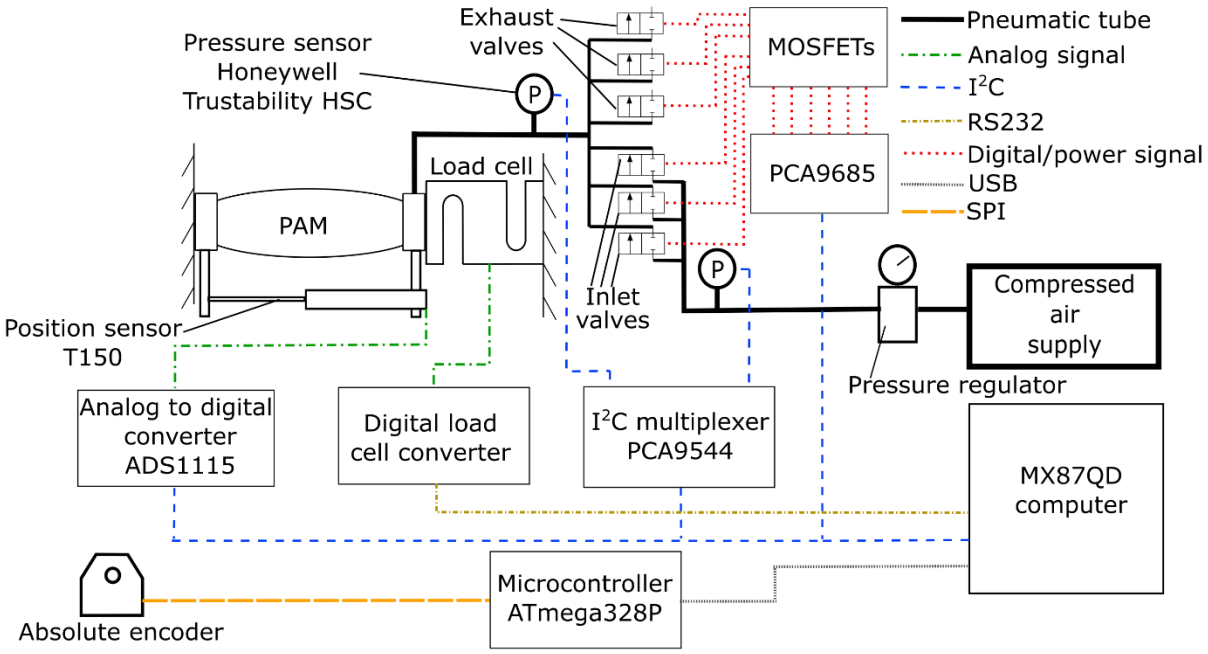

Figure 5-5: The conceptual electronics network on the testing apparatus for testing of a single PAM. This is expandable so as to be duplicated for a second PAM. Also shown is the interface for the absolute, encoder, used to measure the position of the joint for antagonistic testing.

Pressure sensing is achieved with Honeywell Tru-Stability HSCDANN150PG2A5 pressure sensors[286]. This pressure sensor operates in the 0-10 bar range, with a maximum error of 258Pa. It gives a digital output over an I²C communication bus which is temperature compensated and updated at up to 2kHz. The digital output simplifies data collection and helps to ensure high accuracy. In order to measure the pressure in the PAMs, a pressure sensor is located on the pressure supply line between the valves and the muscle. It is assumed that the pressure drop over the supply line and the orifice of the PAM is negligible. Another sensor is positioned before the valves, to measure the supply pressure. As there are a number of pressure sensors to be read an I²C multiplexer is used so all can communicate over the same I²C bus. The DVI port of the computer is used to interface with the each of the devices on the I²C bus.

Muscle force is measured by an STA-1 aluminium S type load cell [289] connected to each muscle. This is rated for up to 300 Kg. As the output of the Wheatstone bridge on the load cell is very small, dedicated hardware is required to amplify it. A Mantracourt DSC digital strain gauge to data converter is used for this purpose [290]. This can provide load readings at up to 500Hz over an RS232 connection to the computer using an RS232 to

USB converter. When two muscles are used antagonistically, they each have a load cell attached. Therefore, the torque at the joint is found using the difference between the two.

When a single PAM is being tested under conditions where the muscle length changes, the change in muscle length is read by means of a T150 Novotechnik potentiometric position transducer [291], the analogue output of which is digitized by a Texas instruments ADS1115 16 bit analogue to digital converter [292]. This connects to the computer over the I^2C communication bus.

When two muscles are arranged antagonistically their contraction/elongation is linked as when one contracts the other must elongate. This means that the change in length of both muscles can be found from a single sensor. A CUI AMT203 absolute encoder was employed to achieve this[293]. Its maximum resolution of 4096 positions per revolution was used. Given that the pulley diameter (with an allowance for the diameter of the rope) is 82mm, this gives a resolution of 0.06mm on muscle contraction. The encoder outputs its position over an SPI bus to an ATmega328P microcontroller. This in turn relays the position to the computer via USB.

To control the valves, a 12V control signal is required. To do this, a MOSFET transistor is allocated to each valve. These are in turn controlled by a PCA9685 PWM controller [294], which communicates with the computer over I^2C. In this way each of the 12 valves can be individually controlled.

A power supply unit (PSU), provides power for the system. The main computational unit is a MX87QD mini ITX format computer with an Intel i7 processor and 8 GB of RAM. This controls the valves during testing as well as logging the sensor recordings. It is also used to run the control algorithm for the system. All of the test procedures are implemented using C++.

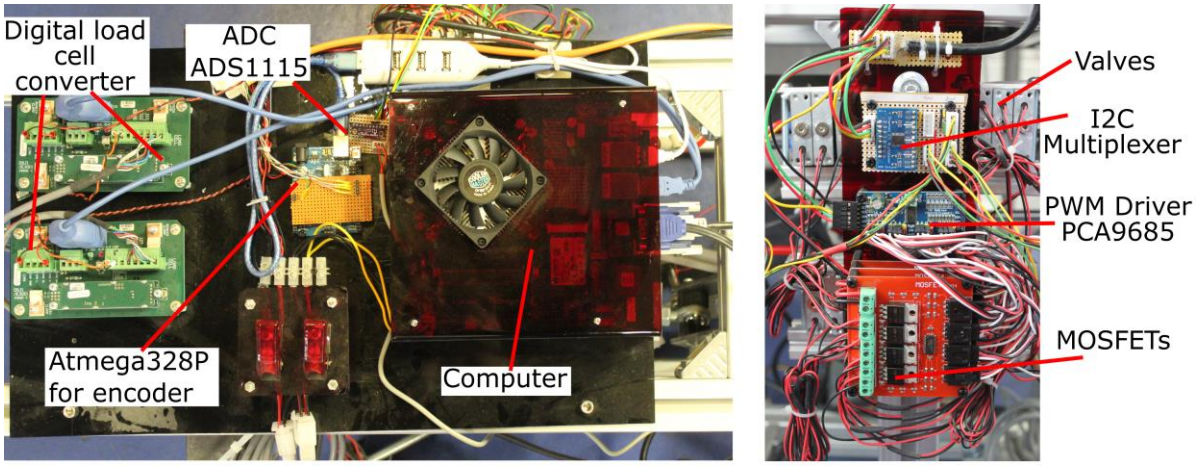

Figure 5-6: Some of the electronics on board the testing apparatus.

5.4 PAM MODIFICATIONS

5.4.1 PRESSURE SENSOR INTEGRATION

In most applications of PAMs, the pressure sensor responsible for measuring the pressure in the PAM is positioned in the pneumatic supply tubing leading to the PAM. However, resistance to flow in this tubing and the orifice entering the muscle may result in a pressure difference between the muscle and the pressure sensor. Poiseuille's law may be used to estimate the pressure drop [250], and may be expressed as

$$\frac{\Delta P}{Q} = \frac{8 L_t \eta}{\pi {r_t}^4} \tag{5.1}$$

where ΔP is the pressure difference, Q is the volumetric flow rate L_t is the length of the tubing, η is the fluid viscosity and r_t is the internal radius of the tube. This informs the important parameters which affect the pressure difference, although the dynamic nature of the pressure difference makes compensation for the pressure difference problematic. From Poiseuille's law we can surmise that using a larger diameter tube will have the greatest effect on the pressure drop, but also of importance is how close the pressure sensor is located to the PAM and the flow rate.

To this end Davis and Caldwell proposed placing the pressure sensor within the PAM itself, and this was implemented for the case of a traditional PAM, though no test results were shown [250]. Integrating the pressure sensor in the PAM also has the advantage of reducing the total volume of the system and increasing its robustness as the pressure

sensor does not have to be accommodated externally. However should a PAM fail the PAM as well as the sensor must be replaced.

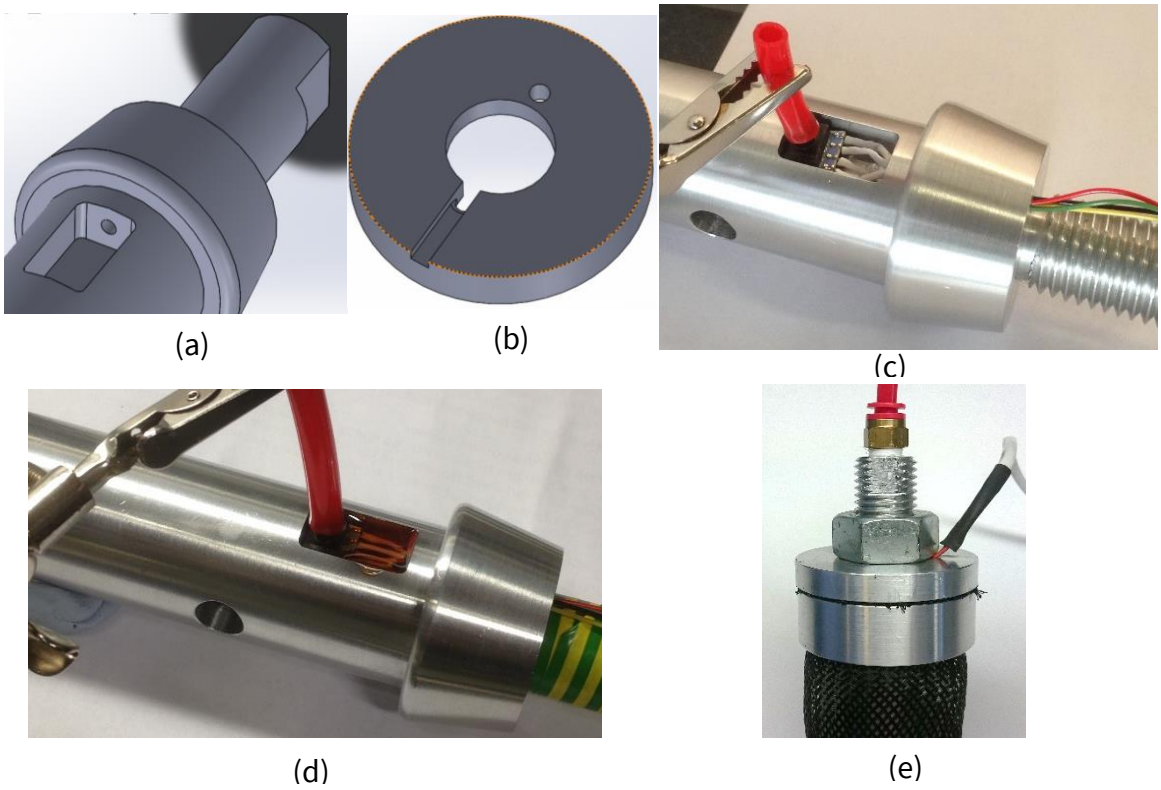

Figure 5-7: The modifications to the sleeve (a) and end cap (b) are shown from CAD files. Note that the wires exit through the slot in the end cap. The hole opposite this is used in conjunction with a pin in the end fitting to ensure the end cap does not rotate, shearing the wires during assembly. Placement of the pressure sensor is shown prior to (c) and after (d) the addition of the epoxy resin. The cables are shown exiting through the end fitting in the fully constructed muscle (e).

It was apparent that the dynamic response would be improved by the sleeve adaptation, and therefore the rate of change of pressure in the muscle will increase. This may increase the error in the measurement of muscle pressure if the pressure sensor is positioned on the tube supplying the PAM. The internal element of the PAM also simplifies sensor integration as there is a greater available space to mount the sensor. Therefore, a pocket was machined in the internal member of the sleeve muscle to house a pressure sensor. An absolute pressure sensor (Honeywell HSCSANN150PA2A5) from the same family as the pressure sensors already employed, was chosen. An absolute sensor was required as there is no available reference to atmospheric pressure in the muscle. Space was also included to allow the cable to the sensor to exit this muscle. An epoxy

resin was used to hold the sensor in place and seal the outlet for the wires to prevent air leakage. The implemented solution is illustrated in Figure 5-7.

5.4.2 MATERIALS

Before dynamic testing was conducted there were some upgrades to the materials used in the PAMs (see Figure 5-8). In particular the silicone bladder was replaced by a with a 40mm internal diameter, 1.5mm wall thickness, latex tube manufactured by ALGAM-I.A.I. S.r.l. [295]. The use of latex instead of silicone has been shown to significantly improve the lifetime of PAMs [148], which is important for testing which will require significant cyclical loading. The material properties of the bladder have been shown to have a large effect on muscle performance as previously discussed, with the greater elasticity of latex reducing the pressure required to expand it. Thus, more of the force exerted by the compressed air acts on the braided mesh resulting in greater force output and muscle contraction.

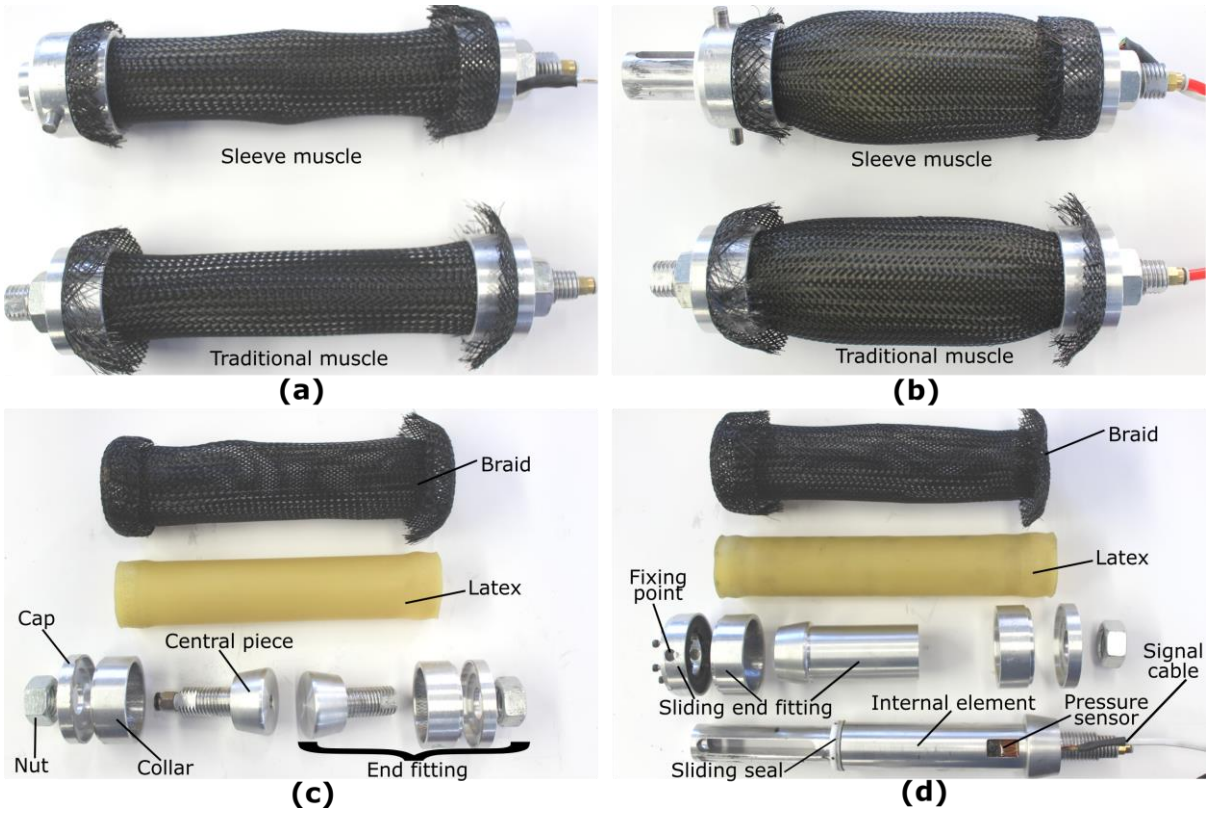

Figure 5-8: The PAMs as modified before dynamic testing. (a) shows the completed PAMs in a relaxed state, while (b) shows them pressurised to the same pressure with no load applied (free contraction). A disassembled traditional PAM is shown in (a), while a disassembled sleeve PAM is in (b).

The braided mesh used in the muscles being tested has been changed to Techflex Tight weave 2” (50.8mm) [296]. This braid has a higher density of braid fibres, with the result that the gaps between fibres as the braid expands for contraction are smaller. This reduces the stress in the latex where it bulges between the fibres, increasing the actuator lifetime [150]. Given the relatively small thickness of the latex bladder, this is particularly important for this muscle. A tighter braid may however reduce the contraction ratio which the PAM can produce.

Static testing with updated PAMs

Due to the change in the muscle materials, the static characteristics of the PAMs will be altered, and so testing is required to establish the new PAM properties. Such a comparison evaluates the importance of material selection in PAM construction and is important when considering the dynamic response of the PAMs. Isometric tests were conducted, in keeping with the testing methods employed previously. This also helps in the validation of the new testing apparatus as the results from the unaltered PAMs may be compared with those previously established in chapter 4.

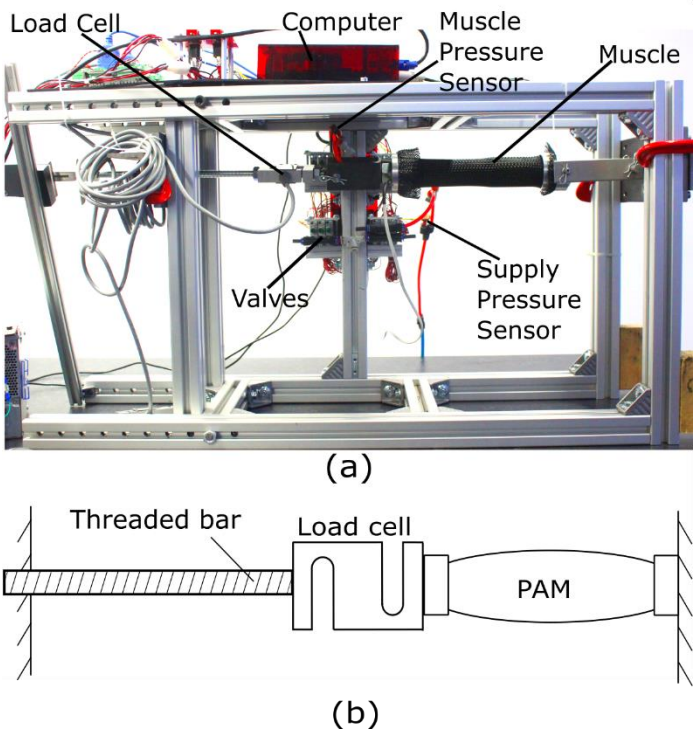

Figure 5-9: Testing apparatus configured for isometric testing in (a). A schematic representation is shown in (b).

The dynamic test apparatus was set up as in Figure 5-9. Two solenoid valves controlled the air flow in and out of the PAM while manual throttle valves were used to restrict the flow rate. The muscle was held at the test length while the pressure was slowly increased up to the maximum test pressure (415kPa gauge pressure) and then reduced to atmospheric pressure. The test was repeated for test lengths starting from no contraction until the muscle reaches its maximum contraction (in 10mm increments).

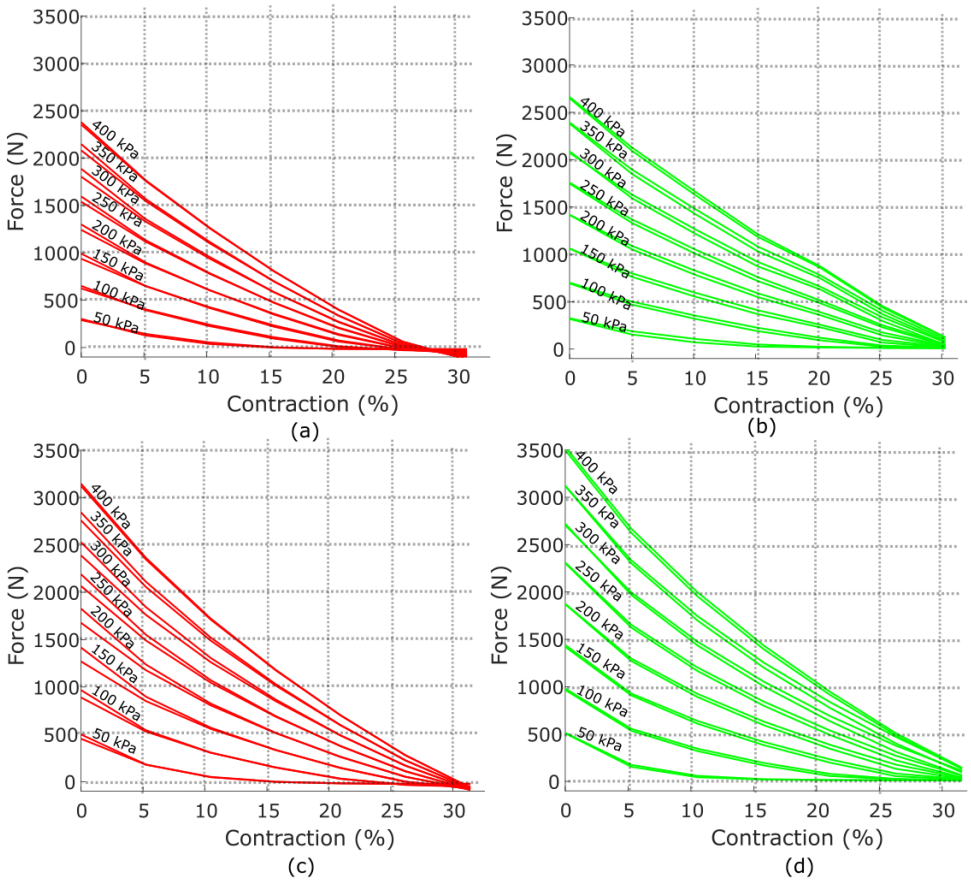

Figure 5-10: Static characteristics, under isometric test conditions, of traditional (a and c) and sleeve (b and d) muscles, with a silicone bladder (a and b) as in the previous static tests, and those with a latex bladder, (c and d,) as used throughout the remainder of this work.

Figure 5-10 illustrates the results of these static tests. Force output over the range of contraction at a number of muscle pressures is illustrated. These were generated by recording the force output during each test as the muscle pressure increases to, or decreases past, the relevant pressure ascribed to the line. As the pressure changes slowly (each test taking approximately 1 minute), dynamic effects are minimal. Particularly in the case of the traditional muscle, there is a small hysteresis at small contractions. Here

the upper line represents increasing pressure and the lower line decreasing pressure. A possible reason for this is stretch in the braid during the test cycle or realignment of the muscle braid fibres. It is not clear why this effect would be reduced for the sleeve muscle however. The increase in force output and maximum muscle contraction as a result of the use of latex instead of silicone is even greater than that for the sleeve adaptation. This underlines the importance of material selection in muscle construction.

Also of note is the close agreement between the force output recorded here for the case of the PAMs using the silicone bladder and the test results carried out on the Instron testing machine as illustrated in Figure 4-3. This supports the validity of the test results conducted on this testing apparatus albeit for a simple test.

5.5 REMARKS

The testing apparatus implemented above provides the capability to test pneumatic muscles by varying the internal pressure and load applied, and measuring the muscles reaction in terms of contraction, pressure and force output. It is reconfigurable to accommodate a wide variety of muscles and testing procedures, including isobaric tests, isotonic tests and antagonistic tests using two muscles. This enables a benchmarking of the sleeve muscle under dynamic conditions. The following chapter reports on the tests conducted using this apparatus to determine the dynamic characteristics of the sleeve PAM and how it varies from the traditional PAM.

6 DYNAMIC CHARACTERISTICS

In order to make best use of sleeve muscle technology it is necessary to accurately account for the changes in dynamic performance in both the design of the PAM system and its control. From the literature, and particularly the work of Davis [133], [179], it is known that occupying the internal volume of the muscle increases the actuator bandwidth, as less mass of air is required to increase the pressure in the muscle. However, the additional benefit of reducing the force the pressurised air exerts on the end fittings should further improve the dynamic response, as lower pressures are required for the same force output. It is unclear however, if the addition of friction at the seal will have an appreciable effect on the muscle dynamics. The test apparatus developed in the previous chapter was therefore used to compare the dynamic characteristics of traditional and sleeve PAMs.

6.1 ISOMETRIC RESPONSE

The dynamic response of traditional and sleeve PAMs under isometric conditions is investigated in this section. Isometric testing was employed as testing involving the contraction of the muscle under load would require a second control system to control the applied load (as simply using a weight to apply the force would result in significant dynamic forces), thus increasing errors in the measured PAM response. The rate at which each PAM can respond to changes in the valves controlling the PAM was examined for both the pressure and force response. These responses are dependent on the entire pneumatic system (the supply pressure, the valves used, the pneumatic tubing and other losses in the system) as well as the PAM itself. Therefore, the purpose of these tests was to compare the performance of the two PAM designs rather than to conclude a theoretical maximum bandwidth. Indeed greater operating bandwidths for PAMs have previously been reported using smaller PAMs and valves capable of greater flow rates [149].

6.1.1 PRESSURE RESPONSE

The first set of tests measure the time taken for a PAM to inflate and deflate from three test pressures (140kPa, 275kPa and 415kPa) under isometric conditions and across the

full range of contraction. In all cases the supply pressure is 500kPa. The testing apparatus was configured as in Figure 5-9. The PAMs were tested from 0% contraction to their contraction limit in 10mm increments. A pretension of 100N was applied at 0% contraction for consistency between the tests. It is assumed that the valves, having a much smaller orifice size (1.3mm diameter) than any other components in the system, are what limits flow rate. Using multiple valves in parallel has been shown to effectively increase the dynamic response of PAM systems [133]. It can also be used to balance the flow rate in and out of the muscle so the rate of change of muscle pressure is similar for inflation and deflation [85]. The exhaust from the muscle typically has a lower flow rate than the inlet flow as the pressure upstream of the valve is always greater for the inlet valve. For this reason, testing was conducted using one, two and three valves in parallel for inflation and deflation so the response of both PAMs to each could be compared.

The tests consisted of inflating the PAM to the desired test pressure using the selected number of inlet valves and closing the valve(s). After four seconds the exhaust valve(s) were opened to release the pressure in the muscle to the atmosphere. Sample test results for a traditional and sleeve muscle are shown in Figure 6-1. There is clearly a drop in pressure after the inlet valve is closed. As the pressure sensors are positioned upstream of the muscle, it could be postulated that this is due to pressure differences between the muscle (which constitutes the majority of the system volume) and the pressure sensor. However, the pressure sensor located in the sleeve muscle (“internal” in Figure 6-1) also records this drop in pressure, suggesting that there is little pressure difference between these two points. It is therefore more likely due to temperature stabilization in the system. The greater mass of air in the traditional muscle means this effect is more pronounced. The internal element in the sleeve PAM will also act as a thermal mass reducing the change in air temperature in the muscle during inflation. The greater volume is also responsible for the longer inflation and deflation times of the traditional muscle as a greater mass of air must flow through the valves.

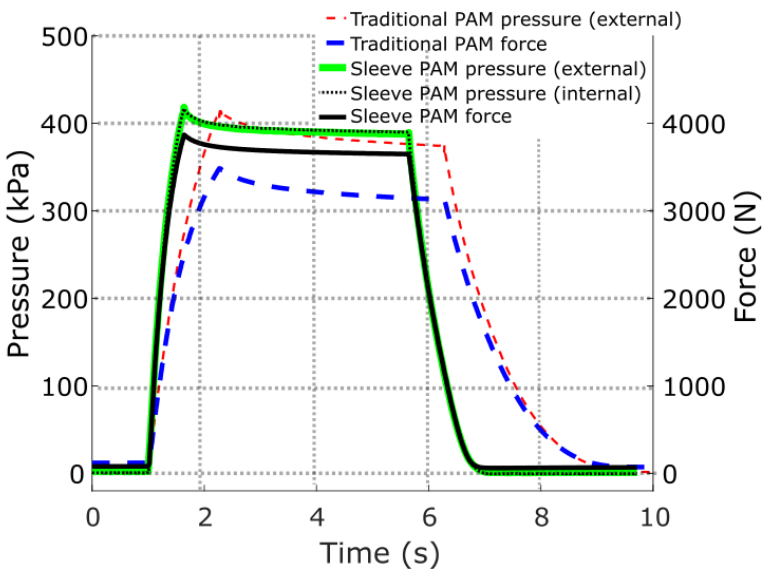

Figure 6-1: Pressure and force response of a traditional and sleeve PAM during inflation and deflation under isometric conditions at rest length (no contraction). One inlet and one exhaust valve were used in this test. For the sleeve muscle, two pressures are given, with "internal" that which is recorded by the sensor mounted in the muscle and "external" that in the pneumatic supply tube.

When this test is repeated across the range of contraction and at the three test pressures, the time of inflation and deflation can be measured. As can be seen from Figure 6-1, as the muscle deflates the rate at which pressure changes gradually reduces as pressure approaches atmospheric pressure. For this reason, the muscle is considered deflated when the pressure drops below 10kPa. Figure 6-2 presents the results of these tests. In each case the test was run for the two traditional and two sleeve muscles, the results of the nominally identical muscles agree very closely and are almost indistinguishable in most tests. The sleeve muscle has a faster pressure response than the traditional muscle under all conditions, however at greater contractions the effect is less significant. The volume of the muscle increases as the muscle contracts, while, in the case of the sleeve muscle, more of the internal element is moved outside of the muscle internal volume. This means the difference in muscle volume due to the sleeve adaptation, reduces with contraction, diminishing its effect on bandwidth. It is also evident that the addition of parallel valves increases the rate at which all the muscles respond and seems to affect the response of each muscle similarly. Importantly, the time to deflate the muscle is typically approximately twice that of inflation time with the same number of valves. This is because the upstream pressure is consistently greater for the inlet valve.

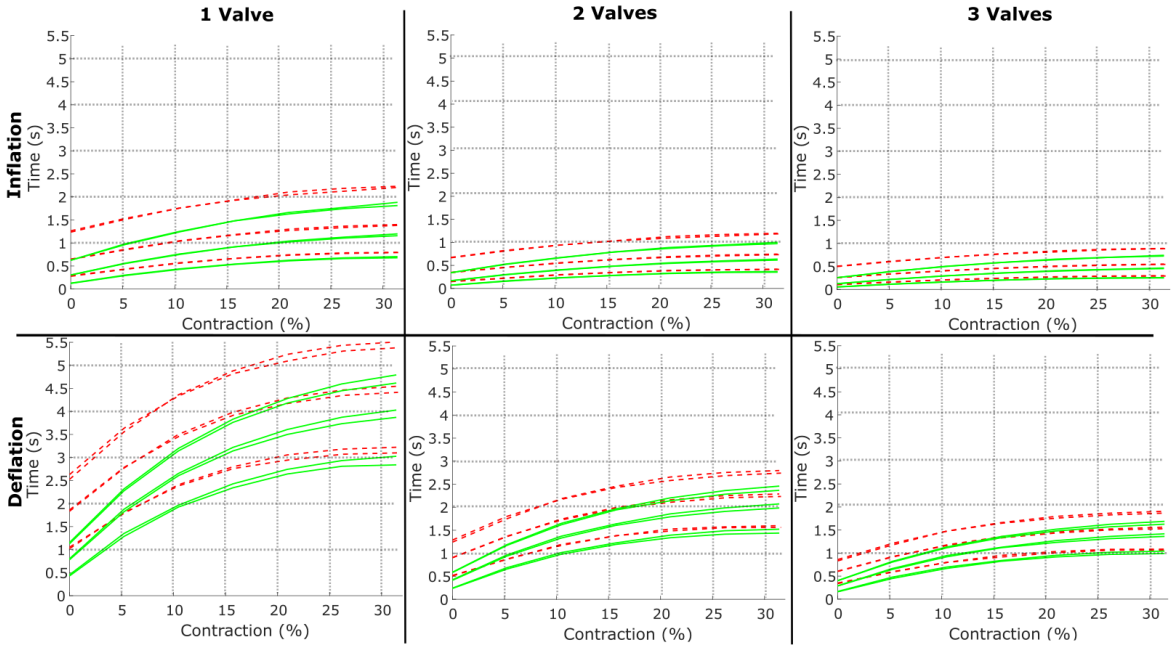

Figure 6-2: The time taken to inflate and deflate the traditional (dashed lines) and sleeve (solid lines) PAMS. The test is repeated with the muscles being inflated to 140kPa, 275kPa and 415kPa represented by the lower, centre and higher line for each muscle respectively.

Figure 6-3 illustrates the response of the sleeve PAM as a proportion of that of the traditional PAM. At zero contraction, the time required for the sleeve PAM to inflate or deflate to all of the test pressures is approximately half that of the traditional muscle. This improvement declines as contraction increases. There is also a dependence on pressure, as the reduction in time with the sleeve muscle is less significant at 140kPa than when the muscle is inflated to greater pressures.

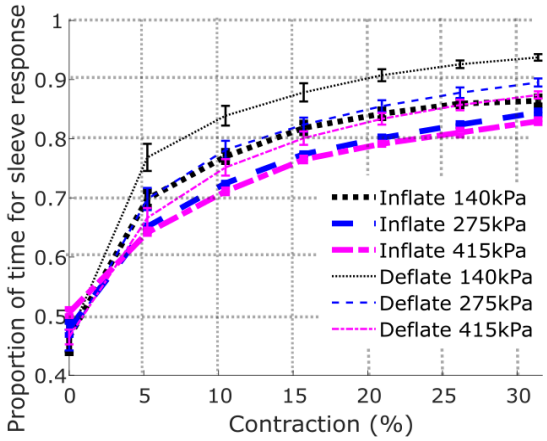

Figure 6-3: The time for the sleeve PAMs to inflate to and deflate from 140kPa, 275kPa and 415kPa relative to that of the traditional PAMs. The data here is averaged over the response when one, two or three valves are used, and multiple tests. The variation is indicated by the error bars.

6.1.2 PRESSURE BANDWIDTH

A comparison of the isometric pressure bandwidth of the traditional and sleeve muscle was also conducted. The valves are controlled so as to alternate the gauge pressure between 100kPa and 400kPa. This range maintains at least a 100kPa pressure differential across both the inlet and exhaust valves. The frequency with which the pressure alternates is gradually increased, past the point where there is not enough time to reach 400kPa. This procedure is repeated for both sets of traditional and sleeve muscles, across the range of contractions and with different combinations of inlet and exhaust valves.

A relatively simple control procedure was implemented in this test. The PAM was first pressurized to 400kPa. As the frequency at which the muscle was tested increased, the period of time for each cycle correspondingly decreased. The exhaust valve(s) were opened at the start of this period. Once the pressure reduced to 100kPa the exhaust valve(s) were closed and the inlet valve(s) opened increasing the pressure. The inlet valves were closed when the muscle pressure reached 400kPa or when the period for the test frequency elapsed. The exhaust valve(s) opened again at the start of the next period. This control sequence produced some overshoot as the valve states are not modified until the pressure set point was reached and recorded. A control signal must then be sent to the valves which will take a further 2-5ms to respond. Test results show that this overshoot was, in practice, relatively small and the simplicity of the procedure aids an intuitive understanding and consistency of testing which may be more difficult to guarantee if a model of air flow was used to close the control valves before the pressure limit was reached. Furthermore, in the case that the muscle was not capable of reaching the upper pressure bound, it is time alone that dictates when the valve states change, thus reducing error from this source.

Figure 6-4 shows examples of the pressure readings from such tests for a traditional and sleeve PAM. There is a distinct frequency at which the muscle is no longer able to fully complete the pressure cycle. For the sleeve muscle, this occurs at a higher frequency than the traditional muscle. The pressure reached during the cycle then reduces further as the frequency increases.

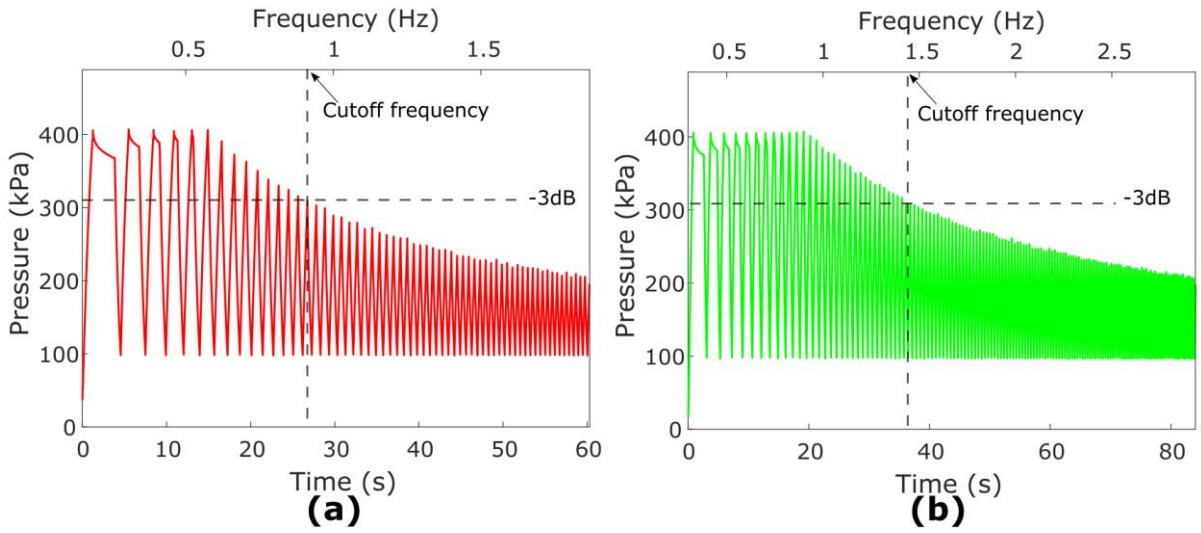

Figure 6-4: Example isometric pressure bandwidth tests. (a) shows the pressure response of a traditional PAM at 10.5% contraction using one inlet valve and two exhaust valves. (b) is the corresponding test for a sleeve PAM.

The cutoff frequency is the frequency of operation of the muscle when the amplitude of the measured response is reduced by 3dB. Using this metric, the bandwidth of the traditional and sleeve PAMs can be compared across the range of contractions. A number of valve configurations were tested with both types of PAM and with the two test muscles for each. The cutoff frequency for the combinations of valves tested are shown in Figure 6-5. Clearly the sleeve muscle produces quite a significant improvement in bandwidth, particularly at small contractions. Adding additional valves will increase the useful bandwidth of the actuators.

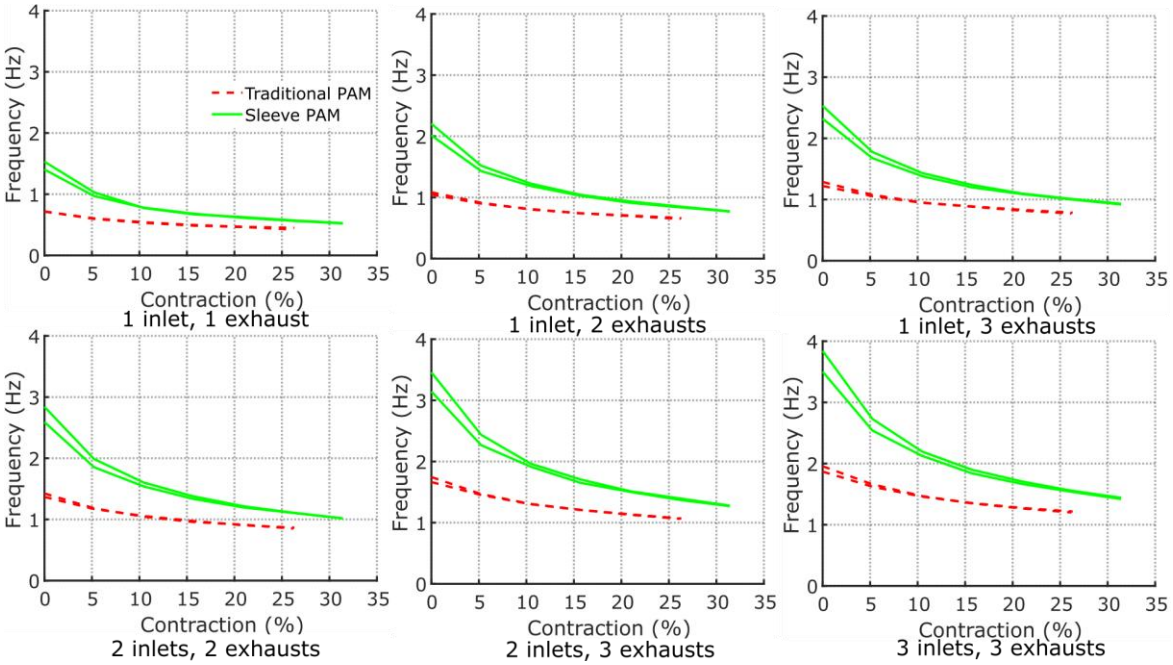

Figure 6-5: The cutoff frequency of the traditional and sleeve PAMs for the valve configurations tested. The tests were repeated with the two traditional and two sleeve PAMs.

The percentage increase in cutoff frequency with the sleeve muscle, when compared to the same valve configuration using traditional PAMs is plotted in Figure 6-6.This illustrates that the improvement in dynamic performance of the sleeve muscle is consistent, regardless of the number of valves used.

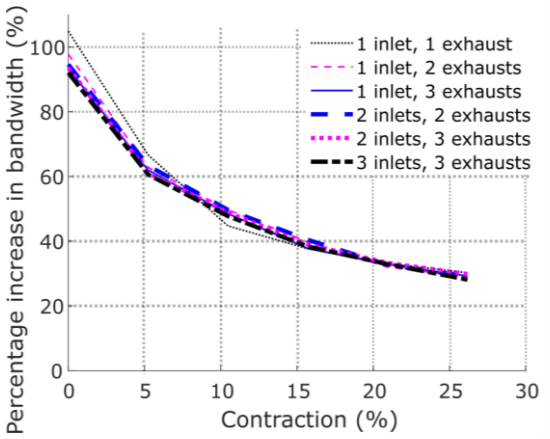

Figure 6-6: The percentage increase in bandwidth (as measured using the cutoff frequency) of the sleeve muscle for the valve c0mbinations tested.

6.1.3 FORCE BANDWIDTH

As the force output of the sleeve PAM is greater than that of the traditional PAM at all pressures, it is expected that the increase in force bandwidth due to the sleeve muscle

adaptation would be greater than that of the pressure bandwidth. This has been tested by conducting isometric bandwidth tests identical to those for pressure, but using force as the relevant output. The force output of the muscle was alternated between 120N and four test forces (600N, 1000N, 1400N and 1800N). Feedback for the control procedure was provided by the load cell. These tests were performed using two inlet and two exhaust control valves. Figure 6-7 shows an example force and pressure response for a traditional and sleeve muscle. Overshoot in these experiments is more significant as muscle force slightly lags pressure. The overshoot is more pronounced for the sleeve muscle due to the faster response, with an overshoot of up to 100N. Due to the greater force output of the sleeve muscle, it operates at lower pressures and with a smaller change in pressure than the traditional muscle.

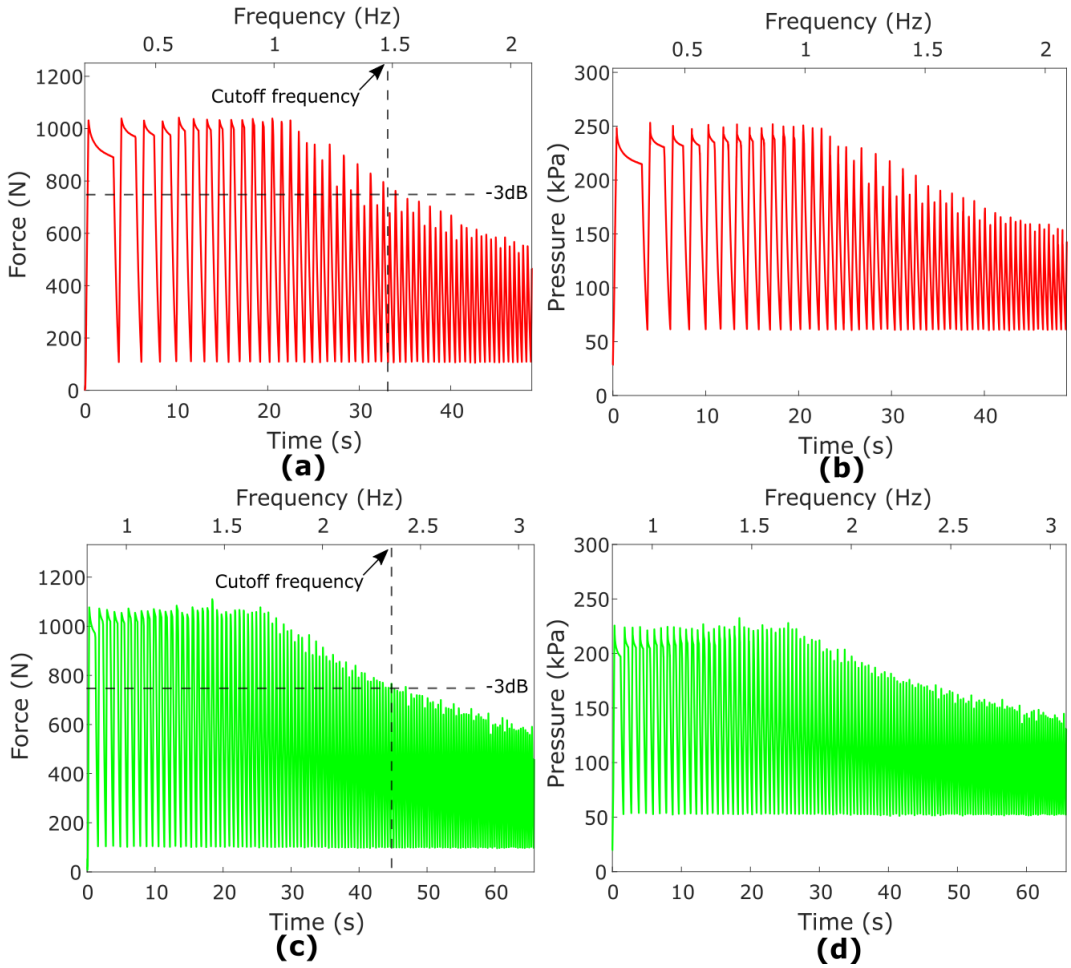

Figure 6-7: Sample force bandwidth tests for muscle contraction of 10% and a test force of 1000N. The traditional muscle response is shown in (a) and (b) in terms of force and pressure respectively. (c) and (d) show the force and pressure response of the sleeve muscle.

As with the pressure response, the cutoff frequency for each test can be established. This is indicated in Figure 6-8 across the range of contraction for each test force. The pressure required to generate larger forces is greater, so bandwidth reduces as the test force increases. As would be expected, at greater contractions the bandwidth is lower, as a larger volume must be filled to a higher pressure in the PAM to produce the same force output. The sleeve PAM once again is capable of greater bandwidth across all contractions but especially when the muscle operates close to its maximum length. To further illustrate this, Figure 6-9 shows the percentage increase in bandwidth of the sleeve PAM in these tests, when compared to the same tests using a traditional muscle. It is apparent that the increase in force bandwidth due to the sleeve adaptation is considerably greater than that of pressure bandwidth. This is a property of the sleeve PAM which comes as a result of the increased force output which is attained with the adaptation and is not produced when a filler is used as in [179].

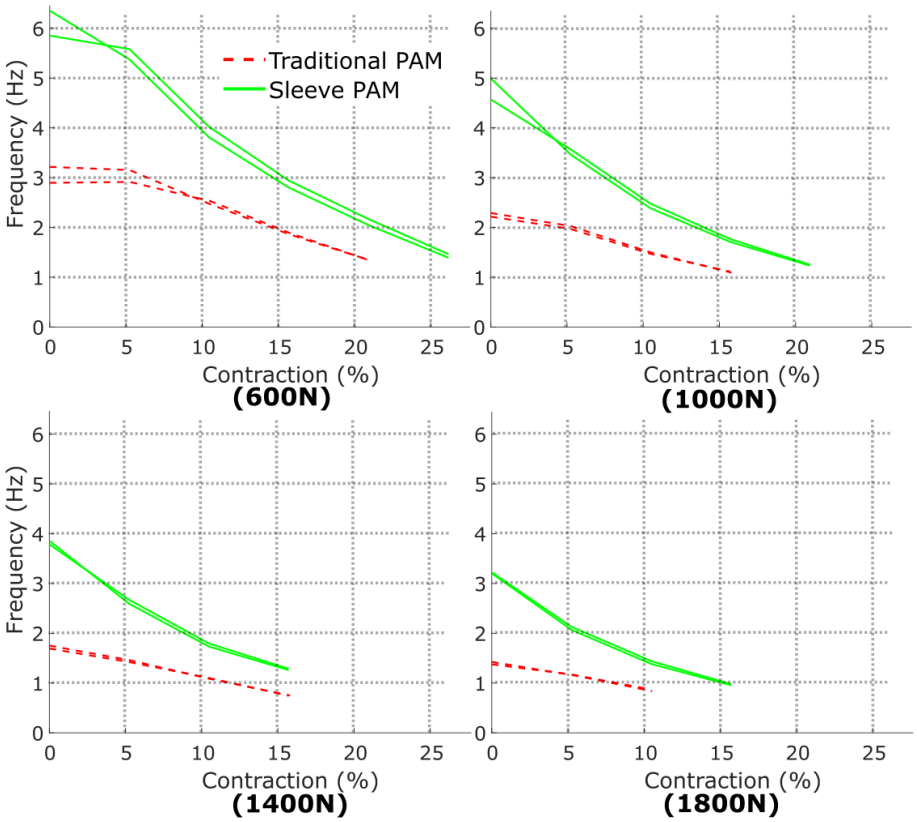

Figure 6-8: The cutoff frequencies for the two sleeve (solid lines) and two traditional (dashed lines) muscles as measured by their force response with two inlet and two exhaust valves. The range for each test was between 120N and the test force on each graph. For higher forces the muscles could not produce the necessary force output at large contractions.

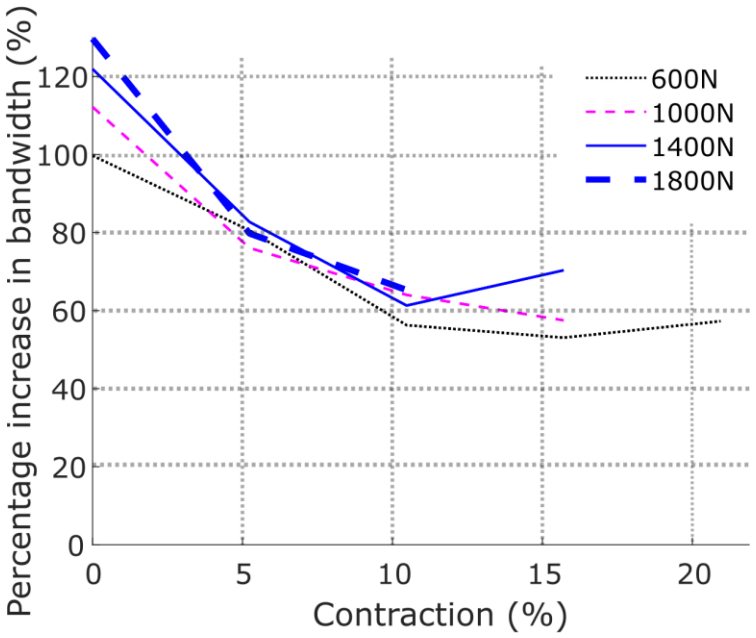

Figure 6-9: Percentage increase in force bandwidth (as measured by the increase in cutoff frequency) of the sleeve PAM when compared to the same tests using a traditional muscle.

6.2 CONSTANT FORCE PROFILE

Isometric tests are an instructive benchmark to compare the performance of pneumatic muscle systems, however, as no contraction of the muscle occurs during the test, it is not representative of typical operating conditions. Indeed, no useful work is done by the muscle as it does not change length. Isotonic tests (constant force) are also used to characterize these conditions. The most common way to achieve this is to mount the muscle vertically with an attached mass before increasing and decreasing the PAM pressure. Assuming accelerations are small the force on the PAM can be considered constant. For dynamic tests at high frequencies this can create difficulties as the motion of the mass muscle system may be erratic and inertial effects will be significant. Therefore, a different approach is adopted here whereby the muscle acts against a spring (as in Figure 6-10). This provides a linear force profile rather than a constant force, but is capable of maintaining stable operation at higher frequencies. Here it is assumed that the mass of the muscle end fitting and spring is negligible, and the only force applied to the muscle is that of the spring.

Testing was conducted using springs with a spring constant of 1 N/mm and 8 N/mm (measured using the testing apparatus), with an initial tension (at 0% contraction) of 110N and 200N respectively. Retaining some tension at no contraction increased the load

applied by the spring at all contractions. The PAMs were cycled between an initial contraction and progressively larger contractions with three inlet and three exhaust valves. As with the previous tests, the frequency of these cycles continued to be increased past the point where the full commanded contraction could be reached. The cutoff frequency was calculated for each of the four muscles. This is illustrated in Figure 6-11 (a) and (c) for initial contractions of 2.5%, 10.5% and 18.5 %. To give a greater understanding of the muscle operation, Figure 6-11 (b) and (d) show the force applied by the spring across the range of contraction (as predicted by its spring constant and verified during testing) and the pressure readings from the muscles for a test with an initial contraction of 2.5%. As the force profile is the same for each test with the same spring, these pressures are indicative of all experiments. These figures illustrate the difference between these tests and those conducted under isometric conditions which result in the same final state regarding contraction and force output. In isometric tests, the change in pressure occurs at a single contraction ratio and therefore muscle volume, while in these tests, the muscle volume changes as the muscle pressure increases leading to significantly different responses.

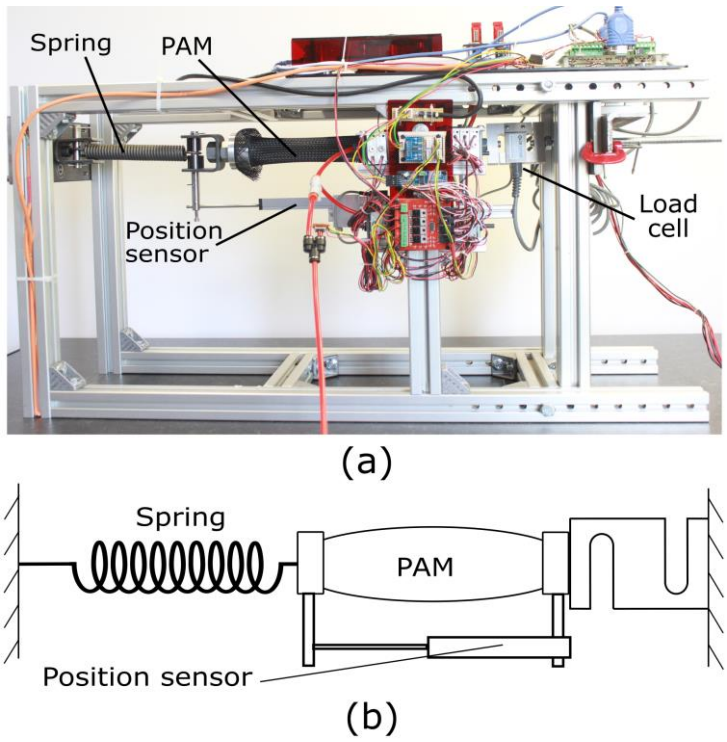

Figure 6-10: The testing apparatus configured with a PAM acting against a spring, thereby operating against a constant force/contraction profile. (b) represents this schematically.

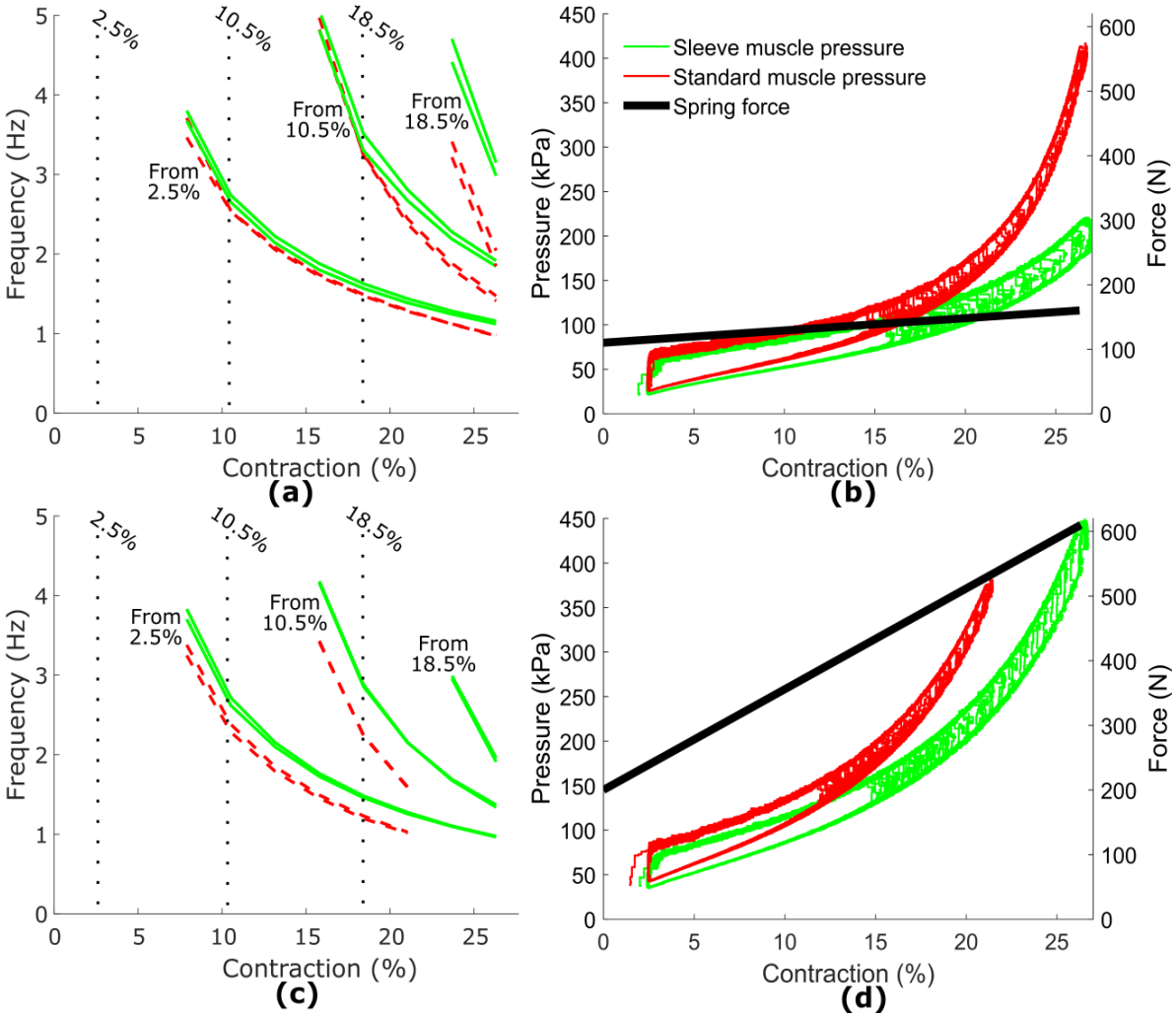

Figure 6-11: Constant force profile bandwidth tests. The cutoff frequency with respect to contraction for tests with springs with a spring constant of 1 N/mm and 8 N/mm are shown in (a) and (c) respectively. The solid line represents the sleeve muscles and the dashed line the traditional muscles. The muscles cycle between contractions of 2.5%, 10.5% and 18.5% and the test contraction (x-axis value). Note that the traditional muscle was not capable of reaching the full range of testing contractions in (c). The force applied by the springs as a function of muscle contraction for the tests in (a) and (c) is shown in (b) and (d) respectively. The muscle pressure readings for tests with the greatest contraction magnitude is also illustrated for a traditional and sleeve muscle.

As would be expected, those tests which require a shorter contraction had a higher cutoff frequency. A number of other factors affect the bandwidth. Higher pressures increase the bandwidth as there is a larger pressure gradient across the system during the exhaust part of the cycle, increasing the mass flow rate during exhaust. For tests with small contractions and low forces, the muscle pressures (see Figure 6-11 (b) and (d)) are such that the time to exhaust will be the limiting factor on bandwidth. In Figure 6-11 (a) and (c), contractions operating from 10.5% have a higher cutoff frequency than those which

operate from 2.5%, when contractions of the same distance are considered. This is despite the fact that the volume of the muscles are larger, and therefore a greater mass flow is required to increase the pressure at larger contractions. Indeed, towards the limits of contraction, the increased volume and the reduction in force capacity of the muscles reduce the bandwidth, as is seen in the case of the contractions from 18.5%. These factors are even more apparent with the larger applied force in Figure 6-11(c). It is at these large contractions, and applied forces, that the main increase in performance is seen with the sleeve muscle. These conditions have the greatest difference in pressure between the two muscle designs due to the increase in force capacity of the sleeve muscle. At small contractions and with smaller applied loads (and so with a lower muscle pressure) there is little difference between the two muscle designs even though this is when the greatest disparity in volume is seen. The difference in performance between traditional and sleeve muscles is least at low pressures. This is consistent with the results illustrated in Figure 6-3, where it was shown that the difference in time to change the pressure in a traditional or sleeve PAM was least at lower pressures.

6.3 RESULTS OF PRESSURE SENSOR INTEGRATION

The placement of the pressure sensor in the sleeve PAM rather than on the pneumatic supply line leading to the PAM should give a truer reflection of the actual PAM pressure as it is not effected by pressure losses in the pneumatic supply line or at the PAM orifice. In practice however, in the testing discussed in this section, there was no significant difference between the two measurements, even for the cases which would typically result in the largest pressure differences across the system. These are the cases where the maximum number of valves with the greatest pressure difference (in this case 3 valves as air is allowed into the PAM) and with the largest volume in the PAM (largest contraction). The pressure response of the sleeve PAM at 31.5% contraction using 3 valves and inflating to 415kPa is shown in Figure 6-12 (a). While there is a small initial difference in the pressure recorded between the two sensors, in general both agree very closely.

In subsequent testing however, where 6 inlet valves are used (described in detail in section 7.2) a significant spike is observed in the pressure recorded in the supply line

which is not apparent from the sensor mounted within the PAM (Figure 6-12 (b)). In these tests the PAM operates against a spring so as to provide a constant force profile. Therefore initially the PAM operates at its rest length, meaning the volume of the PAM is small. Operating at larger contractions would exacerbate the difference in the recorded pressures as a greater air flow is required to increase PAM pressure. Therefore the benefit of positioning pressure sensors in the PAM for the purposes of increasing the accuracy of the pressure readings obtained is dependent on the operating conditions envisaged.

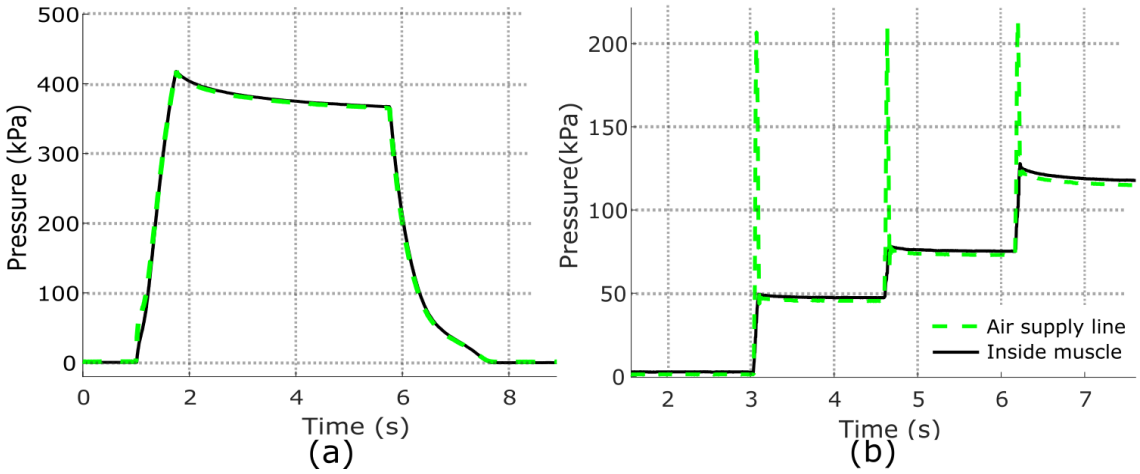

Figure 6-12: Pressure recorded by sensors in the supply line leading to the sleeve muscle and inside the muscle. (a) is from the testing conducted to determine the pressure response (section 6.1.1), with the sleeve PAM held at 31.5% contraction and using 3 inlet and 3 exhaust valves. (b) is from testing conducted using 6 inlet valves, being opened for short periods, as the PAM operates against a spring. The procedure is described in detail in section 7.2.. The measurements from inside the PAM are taken with an absolute pressure sensor but here have been adjusted to gauge pressure.

6.4 REMARKS

The improvements in dynamic performance of the sleeve muscle have been analysed under a number of operating conditions. Muscles operating isometrically at small contractions showed the greatest increase in bandwidth, with an almost 100% increase in dynamic response when muscle pressure is considered. Comparing this result with those using a solid filler to occupy the “dead space” in the PAM, this corresponds to approximately 60% of the volume of the muscle being occupied [133]. As the muscle contracts, the relative difference in volume with the sleeve muscle reduces as does the improvement in dynamic performance.

When force output is considered, again under isometric conditions, the improvement in the dynamic performance of the sleeve muscle is further improved. The greater force output of the sleeve muscle means a smaller change in pressure is required to complete the force cycle. This contributes approximately 20% further increase in bandwidth over the isometric pressure tests. As using a filler alone to decrease the muscle volume does not contribute any additional muscle force, this can be considered the increase in performance over that approach.

Under conditions which allow contraction of the muscle, the increase in bandwidth when using the sleeve muscle is more modest. A fundamental reason for this may be the low pressures which were used at small contractions in these tests, as at higher contractions, with greater muscle pressure, the improvement when using the sleeve muscle is much more significant.

The performance of a pressure sensors embedded in the sleeve PAM was also analysed. There were significant improvements in the validity of the pressures measured by the pressure sensor in this location over that in the pneumatic supply tubing when there are large flow rates. Depending on the nature of the application this may be a significant advantage, although this must be offset against the additional design complexity associated with sensor integration.

7 DYNAMIC MODELLING OF TRADITIONAL AND SLEEVE PAMS

In order to predict the dynamic behaviour of a system utilizing either traditional or sleeve PAMs, a model is required. In this section a phenomenological model of both PAM types is developed to capture their response to pressure changes in the muscle. However, for a system controlled with solenoid valves, it is the valve positions rather than pressure which is the input to the system. To this end, an empirical model for the internal volume of both PAM types as they contract is also proposed. This is combined with an established model of air mass flow through pneumatic components to predict the pressure in the PAMs.

7.1 PAM VOLUME MODEL

The volume of the muscle as it contracts can be modelled as a cylinder, the diameter of which increases uniformly with contraction. If the length of the fibres in the muscle are known as well as the initial braid angle the diameter of this cylinder can be calculated as the muscle contracts. However, the diameter of the PAM adjacent to the end fittings does not change and so as the PAM contracts the cylindrical assumption is increasingly erroneous. Experimental procedures have therefore been suggested to determine the change in PAM volume with contraction. These typically involve the use of an incompressible fluid, either as the working fluid as in [138], or submerging the muscle in a fluid as in [297] and measuring the displacement of the fluid as the muscle contracts or lengthens. Approximating the volume of the muscle at full extension as a cylinder, the volume at any contraction can then be determined.

An alternative experimental procedure was employed here which does not require any additional equipment past an antagonistically actuated joint. The testing apparatus was arranged as in Figure 7-1. The PAM to be tested was connected with Dyneema cable around a pulley to an agonist muscle. Using the linear potentiometer attached rigidly to the end fittings of the test muscle to measure its contraction ensured stretch in the cable did not affect the accuracy of the results. The muscles were configured so that when the test muscle is at its maximum contraction, the agonist muscle was fully extended, though not imparting any force. The test muscle was inflated to the test pressure and allowed to contract to its maximum (i.e. no force applied). The valves controlling the PAM were then

closed, maintaining the mass of air in the muscle for the remainder of the test. The pressure in the agonist muscle was slowly increased, causing the PAM to contract. This applied a force on the test PAM, resulting in its elongation and consequently increasing the pressure in the PAM. The agonist was cycled to its maximum pressure and back to atmospheric pressure.

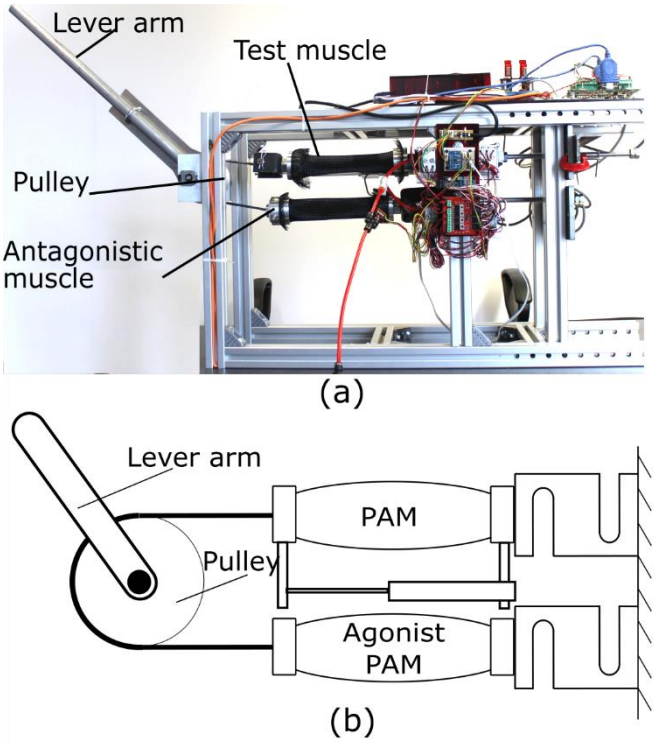

Figure 7-1: Testing apparatus arranged as an antagonistic joint, with no weights attached to the lever arm

The results of this procedure, in terms of pressure in the test PAM, are shown in Figure 7-2. The tests were repeated at multiple start pressures so that the full range of contraction can be attained. There is considerable hysteresis in these tests, likely due to realignment of the braid in the PAMs.

The volume of the PAM at the zero point of contraction is calculated assuming it is a cylinder. In the case of the sleeve muscle, the volume of the internal element is subtracted. Using the pressure at the zero point of contraction, the volume throughout the cycle can be related to the pressure using Boyle's law, assuming temperature changes are negligible.

$$PV = constant \tag{7.1}$$

where the constant dependent on the mass and temperature of the gas in the system as well as its chemical composition. As the cycle happens slowly the isothermal assumption is a realistic approximation.

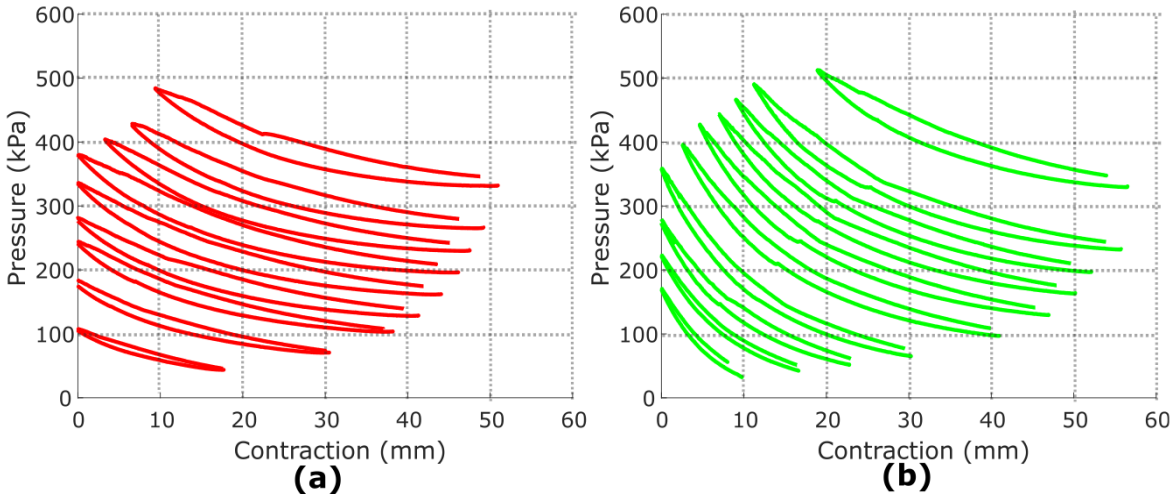

Figure 7-2: Pressure measurements as the (a) traditional and (b) sleeve muscles are elongated and allowed to contract with a constant mass of air. The test is repeated at multiple starting pressures. The upper line on each cycle is the elongation stroke.

While it has been assumed that the braid fibres are inelastic, this is a source of error, especially when the muscle exerts the largest forces, under high pressure. Therefore, measurements of the diameter of the muscle were taken under these conditions to improve the accuracy of the volume of the PAM at rest length. It was found that the diameter was approximately 46mm (as opposed to the nominal 45mm) and so this was used for the volume calculation, assuming a cylindrical shape. Figure 7-3 shows the results of this calculation across the range of contraction. In the case of tests which did not reach full elongation, the volume at the greatest elongation attained was determined from the model fitted to previous tests.

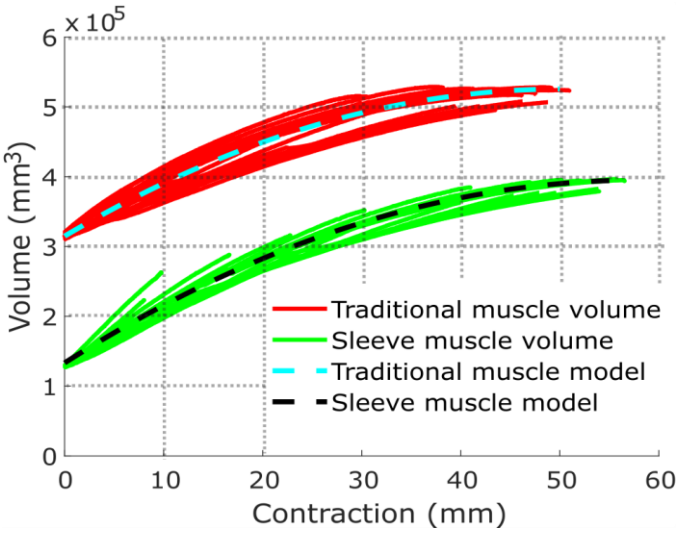

Figure 7-3: Volume of the traditional muscle and sleeve muscles as determined from the test results in Figure 7-2. The dashed lines fitted to the data are the models used for volume for each muscle.

The polynomials fitted to the volumes of the traditional and sleeve muscles in Figure 7-3 are:

$$V_{TM} = 3.148 \times 10^5 + 8395y - 83.62y^2 \quad (7.2)$$

$$V_{SM} = 1.332 \times 10^5 + 9026y - 77.79y^2 \quad (7.3)$$

These equations also include the volume of the supply tubing between the valve and muscle. While the volume of the sleeve muscle is always less than that of the traditional muscle, the difference between the two reduces with contraction as part of the internal element moves out of the muscle volume. The coefficient of determination (R^2) for the traditional and sleeve muscle polynomial fits are 0.957 and 0.971 respectively. The better agreement of the sleeve muscle with the model is likely due to the smaller mass of air involved.

7.2 PHENOMENOLOGICAL MODELLING OF TRADITIONAL AND SLEEVE PAMS

A phenomenological model, first described by Reynolds et al. [182] and widely used in the literature is employed here. This has been described in section 2.7.2. The muscle is represented as an elastic element, a damper and a contractile element in parallel (see Figure 7-4). The governing equation is

$$B\dot{y} + Ky = F_{ce} - F_A \quad (7.4)$$

where B is the damping coefficient, K is the spring coefficient, F_{ce} is a contractile force, F_A is the applied load and y is the muscle contraction. Previously F_{ce}, K and B have been

modelled as being linearly proportional to pressure. In order to better fit the experimental data recorded here, a dependence on contraction is introduced for the spring constant. This helps the model better match the experimental data. It does however increase the complexity of the model.

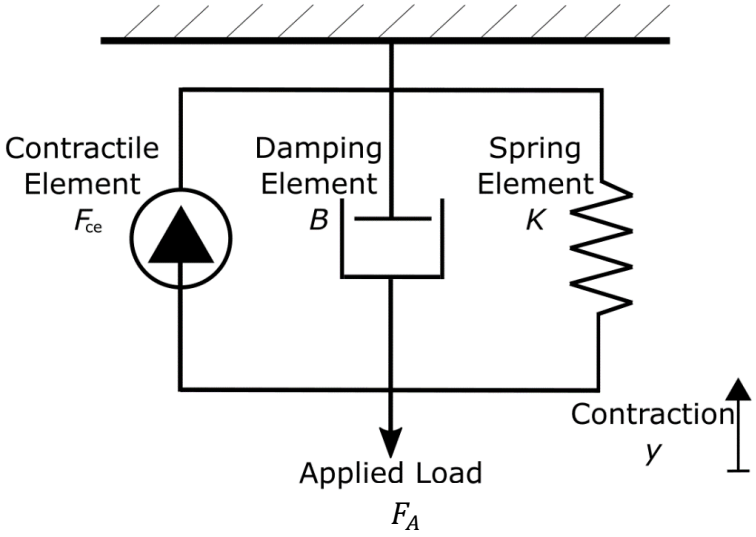

Figure 7-4: Graphical representation of the phenomenological model of a pneumatic artificial muscle.

7.2.1 STATIC TESTS

The method by which a phenomenological model is produced is identical for both traditional and sleeve PAMs as the modelling does not rely on a fundamental understanding of the working principle of the muscle. Tests were conducted to establish the relevant constants for each model. These testing procedures differ considerably from those presented by other authors [182], [264], [268] to suit the testing apparatus used in this work.

Examining equation 7.4, the only parameter which depends on the dynamic response of the muscle is the damping coefficient. Under static conditions the equation becomes

$$F_A = F_{ce} - Ky \tag{7.5}$$

Therefore it is appropriate to determine F_{ce} and K using static characteristics. To this end, isobaric tests were conducted whereby the muscle elongated and contracted slowly so that $\dot{y}$ can be considered negligible. When a muscle elongates due to the applied load being greater than the force generated by the PAM this is known as eccentric contraction

[244]. If the PAM contracts due to the force generated by the PAM being greater than the applied load, this is known as concentric contraction.

The testing apparatus was arranged as in Figure 7-1. The procedure is similar to that employed to determine the muscle volume. After inflating the test muscle to the test pressure, the agonist muscle slowly increases the force it applies to the test muscle. In this case, the valves controlling the pressure in the test muscles maintain the test pressure (to within 5kPa) during the operation. Depending on the test pressure, the agonist muscle may not be able to exert enough force to cause the test muscle to reach its full length. If this was the case additional force was applied manually using the lever arm until the muscle reached its maximum length or the muscle force reached 3000N. The test muscle was then allowed to contract again. These tests were repeated at six muscle pressures.

The results of these tests for a traditional and sleeve muscle are presented in Figure 7-5. Values of F_{ce} and K are determined by fitting a model to this data using the least squares method. As with previous studies, F_{ce} is assumed to be linearly proportional to pressure. Examining the test data, it is observed that the force is not linearly proportional to contraction. Due to this, and in a departure from previous implementations of this model, K is modelled as being proportional to contraction as well as pressure. The model is graphed in Figure 7-5 and relevant equations for the traditional muscle were found to be:

$$F_{ce_{TM}} = 212 + 9.463P' \quad (7.6)$$

$$K_{TM} = 33.92 + 0.176P' - 0.593y \quad (7.7)$$

While those for the sleeve muscle are:

$$F_{ce_{SM}} = 170.4 + 10.22P' \quad (7.8)$$

$$K_{SM} = 29.78 + 0.165P' - 0.479y \quad (7.9)$$

In each case pressure is in kPa and contraction in mm.

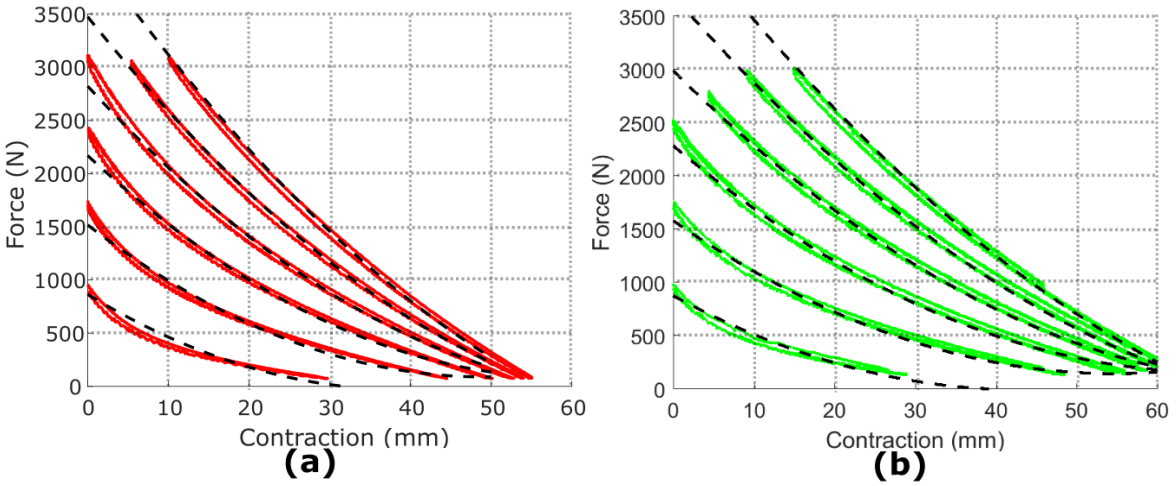

Figure 7-5: Static characteristics based on isobaric conditions for a traditional muscle (a) and a sleeve muscle (b). Solid lines are experimental results; dashed lines are the model which was fitted to this data. The experiments shown were conducted at six pressures (69kPa, 138kPa, 207kPa, 276kPa, 345kPa, 414kPa).

From this model it is seen that F_{ce} is greater for the sleeve muscle for all pressures in excess of 55kPa although this effect is relatively small. The larger difference is seen in the value for K which is substantially smaller for the sleeve muscle. This implies that, under isobaric conditions, while the sleeve muscle only marginally increases the force at full extension it does not diminish as quickly with contraction. No attempt is made to model the hysteresis effect observed here as the magnitude of this error is relatively small, and, for the purposes of control, could be considered a disturbance in the system. The model in general appears to capture the static behaviour of the muscle well, although some errors are seen at low pressures and in particular at small contractions. This may be a similar effect to that observed in [264] where the value of K is modeled with a dependence on the applied load when this load is above a threshold value. As muscle force is greatest at small contractions it is difficult to differentiate between these effects.

The isobaric test results differ substantially from those observed in the isometric tests presented in Figure 5-10 which also recorded the force output across a range of pressures and contractions. The difference in test method apparently affected the muscle force output showing that the muscle force is dependent on the contraction history of the muscle. This is likely due to the alignment of the braid fibres. Other factors which affected the results could include degradation of the muscle fibres as the isometric tests were one of the first tests conducted while the isobaric tests occurred after many bandwidth tests.

Indeed it was observed that the general shape of the muscle under contraction changed somewhat over the course of the tests, with the central portion of the muscle having a reduced density of fibres. Additionally, the muscle length for the isometric tests was measured manually before the muscle applied any contractile force, while the length of the muscle during isobaric tests was continually measured. This means the isometric tests have an additional error from any deflection in the testing apparatus.

7.2.2 DYNAMIC TESTS

Previous studies have determined the value of the damping coefficient under isobaric conditions, and the muscle's response to a step change in the applied load (by manually removing a mass acting on the muscle as quickly as possible). The control system here makes it difficult to maintain isobaric conditions under dynamic operation, therefore step changes in the mass of air in the muscle are instead considered. This operating condition is also more typical of the majority of PAM movements whereby it is a controlled change in the muscle pressure rather than a change in applied load which causes the length to change. The test apparatus was configured as in Figure 6-10, with the muscle acting against a spring. In order to produce a sufficient change in the mass of air in the muscle in as short a time as possible, the valves were configured with 6 inlet and 6 exhaust valves. The supply pressure was also increased to 690kPa. When the test commenced, the inlet valves were opened very briefly (for less than 100ms), increasing the mass of air in the muscle and therefore the pressure, causing the muscle to contract. This was repeated until the muscle reached full contraction. The exhaust valves were then used in a similar manner to reduce the mass of air in the muscle in steps. The results of such a test are illustrated in Figure 7-6.

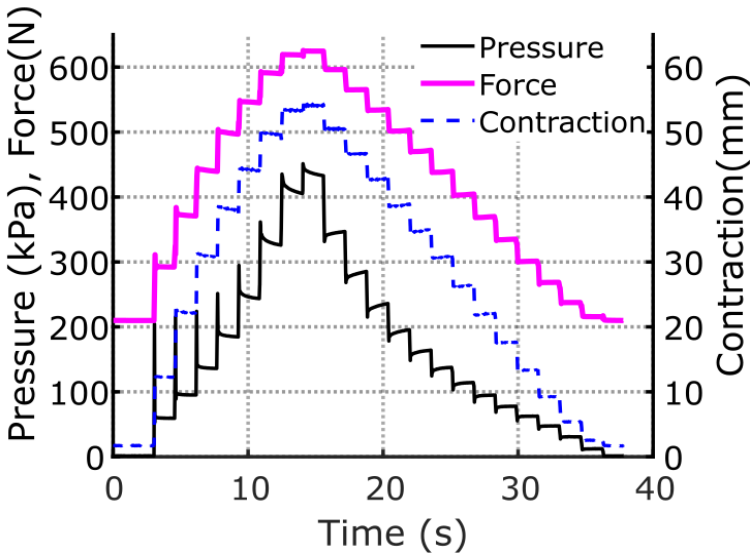

Figure 7-6: Response of the traditional muscle to step changes in pressure when acting against a linear spring.

To determine a value of B, equation 7.4 is arranged in the following form

$$B = \frac{F_{ce} - Ky - F_A}{\dot{y}} \tag{7.10}$$

Muscle performance is evaluated at the midpoint of contraction for each step change. The velocity is considered constant at this point and a linear function fitted to contraction against time yields $\dot{y}$. With constant velocity, the only force applied to the muscle is that from the spring (F_A), assuming the mass of the muscle end fitting and spring have a negligible effect. This force is the average of the static force before and after the contraction as the spring force is linear. The static force being exerted by the muscle at the midpoint of contraction ($F_{ce} - Ky$) is found using the model previously developed (equations 7.6 to 7.9). As evidenced by Figure 7-6 the pressure reading during the contraction is unstable and so there is a large potential for error if a value in this region is used. As there is a step increase in the mass of air in the PAM at the beginning of the contraction and no further change in the mass of air thereafter, the pressure at the midpoint of contraction may be approximated using the muscle pressure at steady state after contraction using the ratio of muscle volumes. Assuming adiabatic conditions (as the contraction occurs quickly, with little time for heat dissipation), this can be written as

$$P_m = P_e \left(\frac{V_e}{V_m}\right)^{\alpha} \tag{7.11}$$

Where subscripts m and e refer to the midpoint and end of contraction/elongation respectively, P is absolute pressure and V is the muscle volume, calculated using equation (7.2) or (7.3) as appropriate. α is the ratio of specific heats, which is 1.4 for air under adiabatic conditions. Using this approach a value of B can be found for each step at a corresponding pressure and contraction.

The experiment was repeated with the spring under different initial extensions so as to vary the force at the same muscle contraction. The results are shown in Figure 7-7. From these test results there is no discernible trend for the damping coefficient with regard to pressure. Similarly no dependence on contraction or applied force was found. This is in contrast to other studies [182], [298] which found a dependency on muscle pressure, albeit with much variance in the recorded values of B due to experimental difficulties in measuring this quantity, as with the results here. The difference in muscle design, as well as experimental procedure is likely the reason for this deviation. For the purposes of modelling, an average value of B for each muscle is used, 2.07Ns/mm for the traditional muscle, and 2.41 Ns/mm for the sleeve muscle. The larger value for the sleeve muscle is likely attributable to friction at the pneumatic sliding seal.

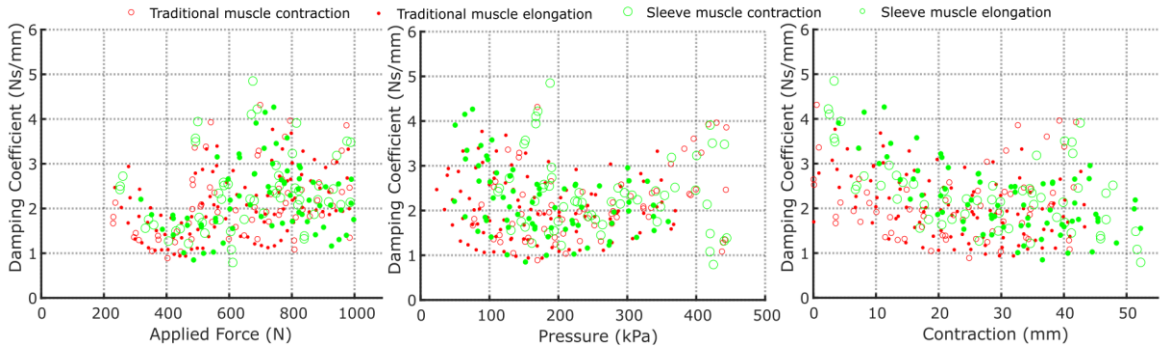

Figure 7-7: Damping coefficient for the traditional and sleeve muscles

Therefore the total model of the PAMs is

$$F_{mus} = a_1 + a_2 P' - (a_3 + a_4 P' + a_5 y)y - a_6 \dot{y} \tag{7.12}$$

Where the constants a_1 - a_5 are determined from static tests and a_6 from dynamic tests and these constants are shown in Table 7-1 for the traditional and sleeve PAMs.

		Traditional PAM	Sleeve PAM
$\boldsymbol{F_{ce}}$	a_1	212	170.4
	a_2	9.463	10.22
$\boldsymbol{K}$	a_3	33.92	29.78
	a_4	0.176	0.165
	a_5	-0.593	-0.479
$\boldsymbol{B}$	a_6	2.07	2.41

Table 7-1.: Summary of the models fitted to the traditional and sleeve PAMs, for use with equation 7.12. For these values the gauge pressure should be in kPa, the contraction in mm and the velocity in mm/s.

7.3 VALVE MASS FLOW MODEL

It is assumed that the main restriction in flow in and out of the muscle is the valve orifice and so other losses are not considered here. As these are solenoid valves they may only be in either an open or closed state and it is assumed they move between these states instantaneously. The mass flow rate through the valves when they are open can be modelled using the well accepted method described in ISO6358 [299]. This is formulated as:

$$\dot{m} = \begin{cases} C\rho_0\sqrt{\dfrac{T_0}{T_{up}}}P_{up}, & \dfrac{P_{down}}{P_{up}} \leq b_p \\ C\rho_0\sqrt{\dfrac{T_0}{T_{up}}}P_{up}\sqrt{1-\left(\dfrac{\frac{P_{down}}{P_{up}}-b_p}{1-b_p}\right)^2}, & \dfrac{P_{down}}{P_{up}} > b_p \end{cases} \tag{7.13}$$

Where C is the sonic conductance of the valve, ρ_0 and T_0 are the density and temperature respectively of air under standard reference atmosphere, T_{up} and P_{up} are the absolute temperature and pressure upstream of the valve, P_{down} is the absolute pressure downstream of the valve and b_p is the critical back-pressure ratio of the valve. The first equation represents a choked flow while the second describes a subsonic flow. The upstream and downstream conditions will change depending on the direction of flow. For the inlet valve, the compressed air supply constitutes the upstream conditions and the downstream conditions are those in the PAM, while for the exhaust valve, the upstream conditions are those in the PAM and downstream is atmospheric conditions.

Values of C and b_p for the Matrix BX721 valves used here were calculated using flow rate data provided by the manufacturer [300] and the procedure described in [299]. C was found to be 2.028X10^{-9} m^3/sPa while b_p was 0.31. It is assumed that adding additional valves in parallel will cause a linear increase in mass flow rate. While this is a simplification, the experiments conducted in chapter 6 support this hypothesis for up to 3 valves. Using this model alone assumes pressure losses in the air supply lines and fittings do not affect flow and so may overestimate the flow rate.

7.4 PRESSURE MODEL

In order to make use of estimates of the mass flow of air and the volume of the PAMs it is necessary to relate these to the change in pressure of a PAM. Such a relationship was derived in [301] for the case of a pneumatic cylinder which is similar to a PAM in this respect. This approach has since been used with success for predicting PAM behaviour [163]. The derivation assumes air behaves as a perfect gas, temperature and pressure changes occur homogenously and kinetic and potential energy in the gas is negligible when compared to pressure energy of the air. Using the ideal gas law, conservation of mass and conservation of energy, the rate change of pressure can be formulated as

$$\dot{P} = \frac{RT_{up}}{V}(\alpha_{in}\dot{m}_{in} - \alpha_{out}\dot{m}_{out}) - \alpha_{vol}P\frac{\dot{V}}{V} \tag{7.14}$$

Where R is the individual gas constant for air (287.05 J/Kg·K) , $\dot{m}_{in}$ and $\dot{m}_{out}$ are the mass flow rates in and out of the muscle and V is the muscle volume. $\alpha_{in}, \alpha_{out}$ and α_{vol} are specific heat ratios for inflation, deflation and volume change. The values of specific heat ratios depend on the nature of the processes, which occur between isothermal conditions (α=1) and adiabatic conditions ($\alpha = 1.4$). The values suggested in [301] are $\alpha_{in} = 1.4, \alpha_{out} = 1$ and $\alpha_{vol} = 1.2$, however this proved to greatly overestimate the pressure increase during inflation in this case and so isothermal conditions were assumed in all cases. This is likely due to the lower operating frequency in this study, allowing more time for heat dissipation.

7.5 MODEL VALIDATION

Using the modelling approaches outlined, the operation of a pneumatic muscle system can be simulated. This is done in discrete time steps. The initial contraction and pressure

of the PAM is known. At each step the volume of the PAM and the rate at which it is changing is calculated using the modelled parameters from the previous iteration. The mass flow rate through the valves is then estimated if either inlet or exhaust valves are open using the most up to date estimate of pressure. The pressure model (equation 7.14), is used to calculate the rate change of pressure in the model and the new pressure. Using the phenomenological model of the muscle (with the modelled pressure and contraction as inputs) together with a model of the system being actuated the contraction velocity, over the time step can be calculated, which is in turn used to find the contraction/elongation of the PAM. This process is illustrated in Figure 7-8.

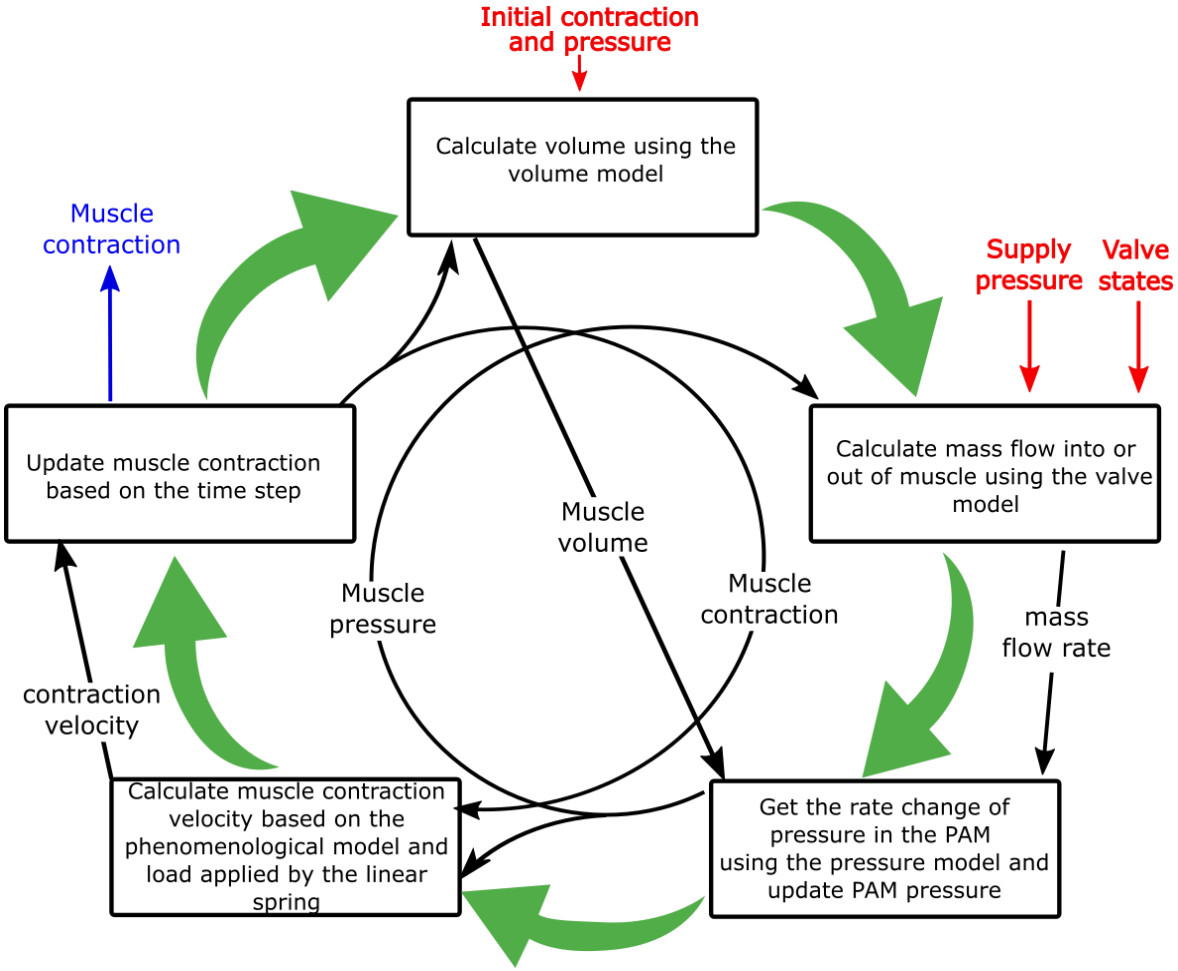

Figure 7-8: Illustration of the computation which occurs at each time step in order to model the behaviour of the PAM/spring system. Those quantities in red are taken as inputs from the experimental data, while the muscle contraction (in blue) is the output of the model.

To test the validity of the models developed here, sample tests were conducted with a traditional and sleeve muscle in which the muscle operated against a linear spring as in

Figure 6-10. One inlet and two exhaust valves were used to cycle the muscle through multiple contractions. The applied load is easily modelled as a linear spring (with a spring constant of 8.1N/mm) allowing the contraction of the PAM to be predicted and compared to experimental measurements. The initial pressure in the muscle, the initial contraction, the valve positions during the test and the supply pressure were all inputs to the model. A time step of 0.01s was used for the simulation.

A comparison between the model and the experimental results is presented in Figure 7-9. The model of muscle pressure is quite accurate for the sleeve muscle though less so for the traditional PAM. This may be due to the greater volume and hence mass of air required to pressurize the traditional muscle which increases the sensitivity to error in the mass flow rate model. The model used here does not predict the initial spike and gradual reduction in pressure after the inlet valve is closed. As isothermal conditions are assumed any increase in temperature during the inflation of the muscle is not considered, nor is any gradual elongation in the muscle braid fibres which would influence the muscle volume. Both the traditional and sleeve muscle models agree well with the experimentally measured muscle contraction, with the largest errors being approximately 5mm during portions of the test with the most rapid movements.

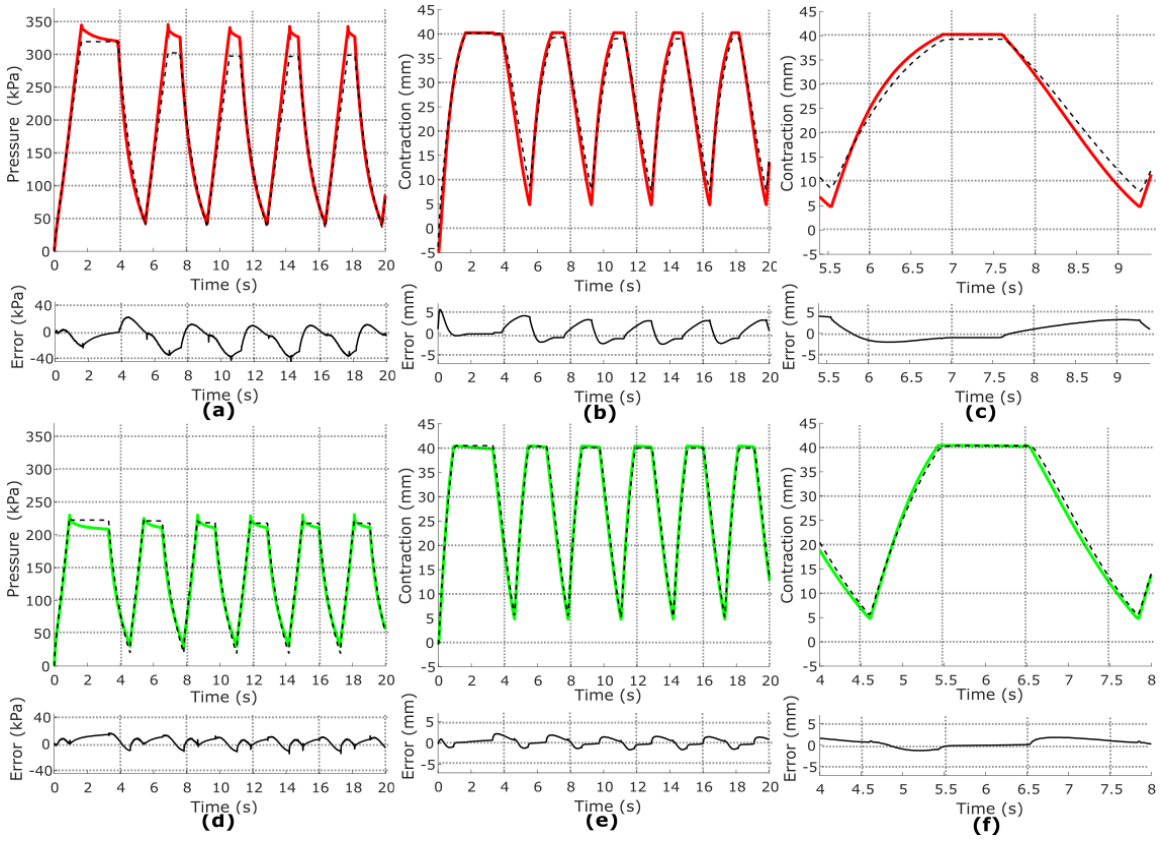

Figure 7-9: Comparison of the model and experimental data for a traditional muscle (a-c) and sleeve muscle (d-f). Muscle pressure is compared in (a) and (d), while muscle contraction is compared in (b) and (e) over a 20s period. (c) and (f) compare a single contraction cycle in greater detail.

7.6 REMARKS

This section built a model of a PAM actuated system which predicts the dynamic response of the PAM from the valve positions. This is useful for both design and control purposes. It was demonstrated that the same methods which can be used to tune the phenomenological model for a traditional PAM can also be employed for a sleeve PAM.

The procedure used to establish the phenomenological model for the muscles is considerably revised from that used in previous work. The difference in testing procedure undoubtedly influences the model constants developed. In particular, the results for viscous damping in the system appear to have no dependence on pressure or contraction. Additionally, K is modelled as having a dependence on muscle contraction to account for the nonlinearity observed in isobaric contraction and elongation, improving the accuracy of the model but increasing the computational complexity.

A new method to determine the internal volume of the muscles was also presented. This relied on measuring the pressure change in the PAM while its length/volume for changed under closed system conditions. This relatively simple testing procedure requires little additional equipment and so is practical for a wide range of use cases. A volume hysteresis which is rarely discussed in the literature is observed which is likely due to realignment of the fibres in the braid.

When combined with an established model of mass flow through inlet and exhaust valves and a pressure model the simulation of the PAM system matched that of experimental results within reasonable bounds. The model for both traditional and sleeve muscles was developed in the same way and both showed reasonable accuracy given that the operating conditions were considerably different to those used to develop the model. The sleeve PAM model was somewhat more accurate than the traditional PAM model, perhaps due to the reduction in the mass of air required to operate the muscle, limiting the effect of inaccuracies in the pressure model. One source of inaccuracy was the change in PAM pressure due to temperature change of the air in the PAM due to inflation/deflation. As this occurs relatively slowly it can be treated as a minor disturbance by a control system.

8 SLEEVE PAMS FOR ANTAGONISTIC ACTUATION

There are a number of means by which PAMs may be configured to actuate a joint. For a revolute joint, the fact that PAMs can only impart a tensile force means that some other restoring force is required to operate the joint in the opposite direction. This can be achieved using standard mechanical springs, as in [201], [277], however this means it is impossible to alter the joint stiffness as the spring stiffness is fixed. This capability is desirable in order to alter the dynamics of the system to optimize energy storage (for example during walking) and for safety characteristics, by using low stiffness during high speed traversals and high stiffness when fine control is required (see Figure 2-9). Indeed, without the ability to modify joint stiffness it is possible to argue that the low mass property of PAMs is unjustified. In a comparison between electric motors and PAMs, Tavakoli et al. found that electric motors can be lighter than PAMs under most operating conditions [79]. However, controllable joint stiffness is not considered here, and whereas the joint actuated with two PAMs is inherently compliant, achieving same with a joint actuated by an electric motor requires an additional controllable degree of freedom (for example to control the effective length of a spring between the drive train and the joint), hence more mass must be added if this is a requirement.

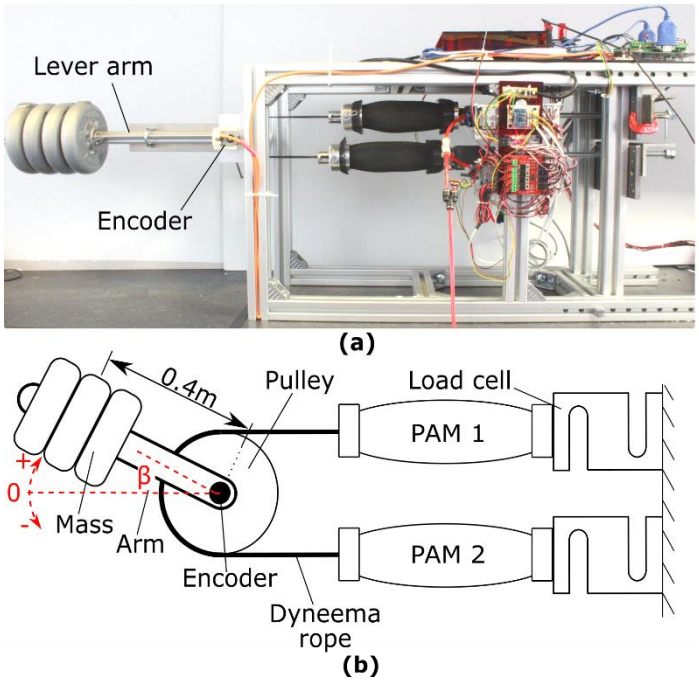

Figure 8-1: Testing apparatus as configured for antagonistic operation. (b) shows the configuration schematically.

In this chapter the sleeve PAM is applied to an antagonistically actuated joint and compared to a joint actuated with traditional PAMs. Torque, range of rotation, joint stiffness, damping and energy consumption are compared. A combination of modelling and experimental results are used to make these comparisons with the testing apparatus arranged as in Figure 8-1.

8.1 MODELLING

The phenomenological models of the traditional and sleeve PAMs (equations 7.6 to 7.9) developed in the previous chapter can be applied to the case of an antagonistically actuated joint. For an antagonistically actuated joint using a pulley to transmit the force between the muscles and the joint, the torque output is

$$\tau = r_p(F_1 - F_2) \tag{8.1}$$

where r_p is the radius of the pulley and F_1 and F_2 are the forces exerted by the two PAMs. The contraction of each PAM can be related to the angle of the joint (β, in radians). Labelling the muscles 1 and 2 this can be expressed as

$$y_1 = r_p\left(\frac{\beta_{range}}{2} + \beta\right), \qquad y_2 = r_p\left(\frac{\beta_{range}}{2} - \beta\right) \tag{8.2}$$

Here, β_{range} is the total range of rotation of the joint. This range is limited by the maximum extension of the PAMs and is altered by moving the PAM closer to, or further from the pulley. Combining these equations with the PAM phenomenological model, and assuming that the operating conditions are such that both muscles apply a tensile force, the torque of the joint can be related to β and expressed as:

$$\tau = r_p\left((P'_1 - P'_2)\left(a_2 - a_4 r_p \frac{\beta_{range}}{2}\right) - \beta r_p\left(2a_3 + a_4(P'_2 + P'_1) + 2a_5 r_p \beta_{range}\right) - 2a_6 \dot{\beta} r_p\right) \tag{8.3}$$

From this it is evident that the joint torque is dependent not just on the pressure in the PAMs but also on joint position. This gives a more complex torque profile than other actuation techniques such as an electric motor which produces the same torque at any point in the joints rotation and in either direction. Due to the reduction in the force exerted by PAMs with contraction, the maximum torque will vary based on the joint position and the direction in which torque is required. At the limits of rotation, the muscle acting to rotate the joint away from the limit will be close to full extension, and hence is

capable of large forces in that direction. In contrast the muscle pulling the joint towards the limit is close to full contraction and consequently can only offer a small torque in that direction.

The stiffness of the joint is the derivative of equation 6 with respect to β (without the effect of the damper).

$$\frac{d\tau}{d\beta} = -{r_p}^2\left(2a_3 + a_4({P'}_2 + {P'}_1) + 2a_5 r_p \beta_{range}\right) \tag{8.4}$$

While the torque is dependent on both the PAM pressures and the joint angle, joint stiffness only depends on the combined pressure in the PAMs. However, as the torque and angle dictate the difference in pressure between the PAMs, the maximum stiffness at an angle is limited by the maximum operating pressure.

8.2 JOINT CONFIGURATION

The choice of pulley diameter and the point of rotation at which the muscles reach their full extension will alter the operating characteristics of PAM actuated joints. A smaller pulley means that for the same PAM contraction there is greater joint rotation but also a smaller torque. If the PAMs are configured so that when one PAM is at full extension the other is fully contracted, the joint will have a large range of rotation, but relatively low force in the direction of the contracted muscle when compared with a joint where the maximum contraction of the muscles is limited due to the other reaching full extension at a smaller angle. In this work, an 80mm diameter pulley is used for all tests.

As an example configuration, the traditional PAMs are arranged so that the joint can rotate by ±0.6rad while maintaining a torque of at least 15Nm in both directions at the limits of rotation at the maximum operating pressure. Two comparable joint configurations using sleeve PAMs are evaluated, both using the same pulley. The first (configuration A), aims to increase the operating range of the joint, while maintaining the torque available across the range of rotation. This is achieved by moving both muscles closer to the pulley. As the sleeve PAM is capable of greater contraction than the traditional PAM this allows the joint to rotate further before reaching the maximum extension of the antagonistic muscle. The second (configuration B) aims to maintain the same range of rotation as the joint actuated with traditional PAMs, but utilize the

increased force output of the sleeve PAM to increase torque. Here the sleeve PAMs are positioned so that they reach maximum extension at the same limits of rotation as the joint actuated with the traditional PAMs.

8.3 JOINT TORQUE AND ISOBARIC STIFFNESS

In order to characterize the torque profile of the joint, the torque which can be applied by each muscle is considered, using equation 7.12, at six test pressures. This is shown for both directions of rotation and each joint configuration in Figure 8-2.Stretch in the Dyneema cable was accounted for, with testing showing an extension of 0.0017mm/N over the 30 cm length of each cable.

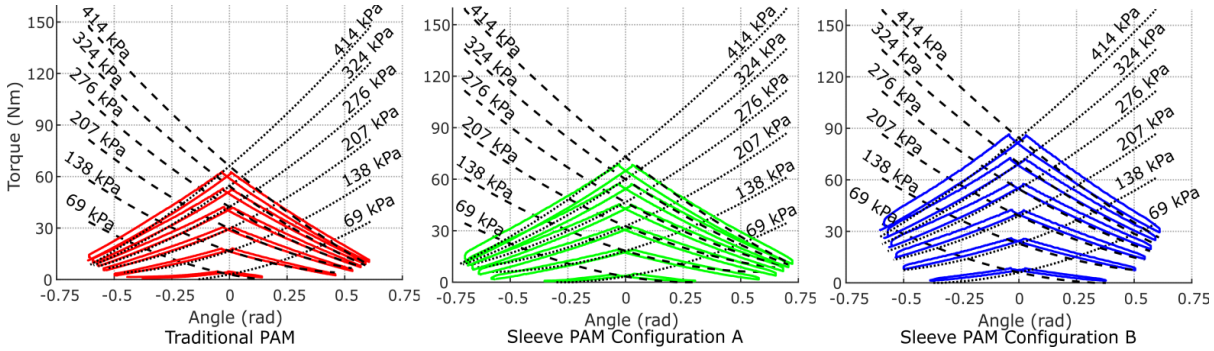

Figure 8-2: The torque developed by PAMs operating an antagonistically actuated joint for the case of traditional PAMs and the two sleeve PAM configurations. The dotted line is the modelled torque towards the negative angle, while the dashed line is the modelled torque towards the positive angle. The solid line represents the experimental testing in each case.

To verify the model experimentally, the arm and mass were removed from the joint so that there is no output torque. The two PAMs then act against each other only while rotating the joint. The test sequence maintains one PAM at the test pressure while the other PAM's pressure is slowly increased to change the joint position. When both PAMs are at the same pressure (which occurs at 0 radians as there is no output torque) their roles reverse and the pressure in the PAM which was maintained at the test pressure is slowly reduced until it reaches atmospheric pressure. The procedure is then repeated in reverse so that the joint rotates back to its original position.

The results of these tests for six test pressures are shown in Figure 8-2. The torques represented here are those exerted by the PAM at the test pressure and align with those generated by the model. From this it is seen that in configuration A at the same pressure

and position the torque is always equal to or slightly greater than the joint actuated by traditional PAMs while also giving an additional 14% of rotation past the original limits of the joint. For configuration B, the range of rotation is approximately the same as that of the joint actuated using traditional PAMs, while the torque is at least 25% greater, rising to over 100% at the limits of contraction. There is significant hysteresis observed as the joint moves in one direction or the other, with this being more significant for the sleeve PAM configurations. This is likely due to the added friction at the sliding seal.

8.4 ISOBARIC STIFFNESS

Maximum isobaric stiffness, as calculated using the joint model is shown in Figure 8-3 for each joint configuration. Three different applied torques are considered. While equation 8.4 shows no dependence of torque on joint angle, the sum of the pressures in the PAMs is limited by the required difference in the PAM pressures to maintain the joint position and torque. For example, when no output torque is required, and the joint is at an angle of 0rad both PAMS can be inflated to their maximum operating pressure. However, to move from this position one of the PAMs must reduce their pressure thus reducing the joint stiffness. The point in the rotation where maximum stiffness occurs is moved depending on the joint torque, but occurs where both PAMs can be inflated to their maximum pressure. The traditional PAMs have the greatest maximum stiffness, however this reduces more quickly as the joint moves away from this angle. The configuration of the sleeve PAMS also affected the maximum stiffness with the joint capable of greater torque also showing the greater stiffness.

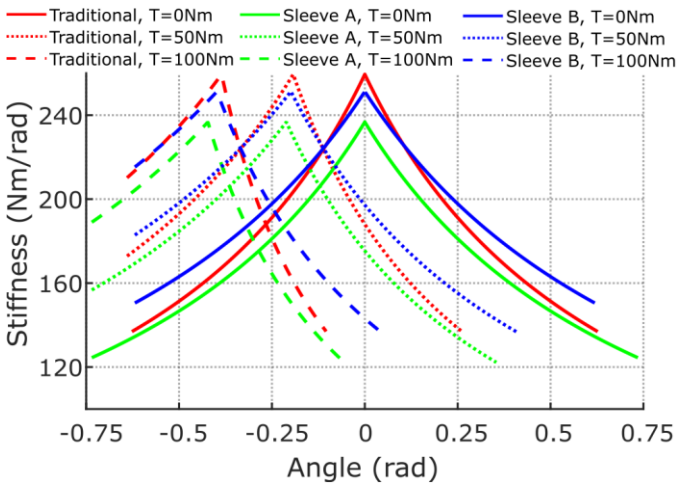

Figure 8-3: The maximum stiffness of the three joint configurations with three different output torques as modelled using equation 8.4.

8.5 CLOSED SYSTEM STIFFNESS

As the volume of PAMs change with length, if the mass of air in the PAM is held constant (by not opening the valves) this will cause the pressure in the PAM to change with joint angle. This would be the case for a collision in which there is insufficient time or inadequate sensing for the control system to react. It could also be used as a control strategy, as a means by which to increase the effective stiffness of the joint.

To evaluate this property, the testing apparatus was arranged as in Figure 8-1 with between 0 and 4 masses attached. The loading associated with each of these testing configurations is shown in Table 8-1. The valves were controlled to move the joint to a test angle and adopt a specified force on the antagonistic PAM. The joint was then manually displaced from the set point position by 0.052, 0.087 or 0.14 radians (3°, 5° or 8°) during which time the valves remained closed. The change in the output torque of the joint (measured as the difference between the torque exerted by the agonist and antagonist PAMs) was approximately linear, even for larger deflections as illustrated for example tests in Figure 8-4. Therefore, the slope of a linear regression fitted to the torque/deflection curve yields the joint stiffness. The change in pressure of both PAMs is also illustrated in Figure 8-4, for each PAM. The upper PAM increases its pressure and the lower PAM decreases due to the direction of the deflection. The increase in pressure is larger than the corresponding decrease as the volume of the PAM changes faster when it operates closer to full elongation.

Number masses	Static torque (Nm)	Moment of inertia (Kgm^2)
0	1.15	0.05
1	6.1	0.26
2	11.1	0.47
3	15.7	0.7
4	20.6	0.95

Table 8-1: The joint loading configurations tested. With 0 masses applied only the mass of the arm itself acts on the joint. The static torque refers to that when the joint is in the 0 radian position, i.e. the arm is horizontal.

An aggregation of the results of these tests is shown in Figure 8-5 for the tests with 0 to 4 masses on the arm. The position set point and the direction in which the joint was displaced from the set point is also indicated. The error bars indicate the maximum and minimum values attained for the three displacements tested. The values of stiffness recorded here are greater than those in the isobaric case, particularly for the joints actuated by sleeve PAMs. This can be understood from the result of the pressure change which occurs in the PAM as the joint deviates from the set point. The increase in pressure per unit joint rotation ($dP/d\beta$, the slope of the pressure/deflection graphs in Figure 8-4) is larger for the case of the sleeve PAMs. Furthermore, it is apparent that in each case the change in pressure with rotation is greater in the B configuration of the sleeve PAM actuated joint, consequently leading to a greater stiffness for this setup. The results with different numbers of masses on the arm are very similar, albeit for a slight increase in stiffness with mass acting on the joint.

These results are significant as they point to an operating mode which substantially increases the apparent stiffness of the joint in the case of sleeve PAMs. While the increase in stiffness over the isobaric case for the traditional PAMs is minimal, the increase in the sleeve PAM stiffness can be as much as a factor of three in the case of configuration B. This effect may therefore be exploited in control to give a greater effective stiffness for the joint which could be desirable for operations at human like bandwidths. For comparison, while the stiffness of human joints is contentious [284], a value of approximately 350Nm/rad for the elbow is suggested in [302].

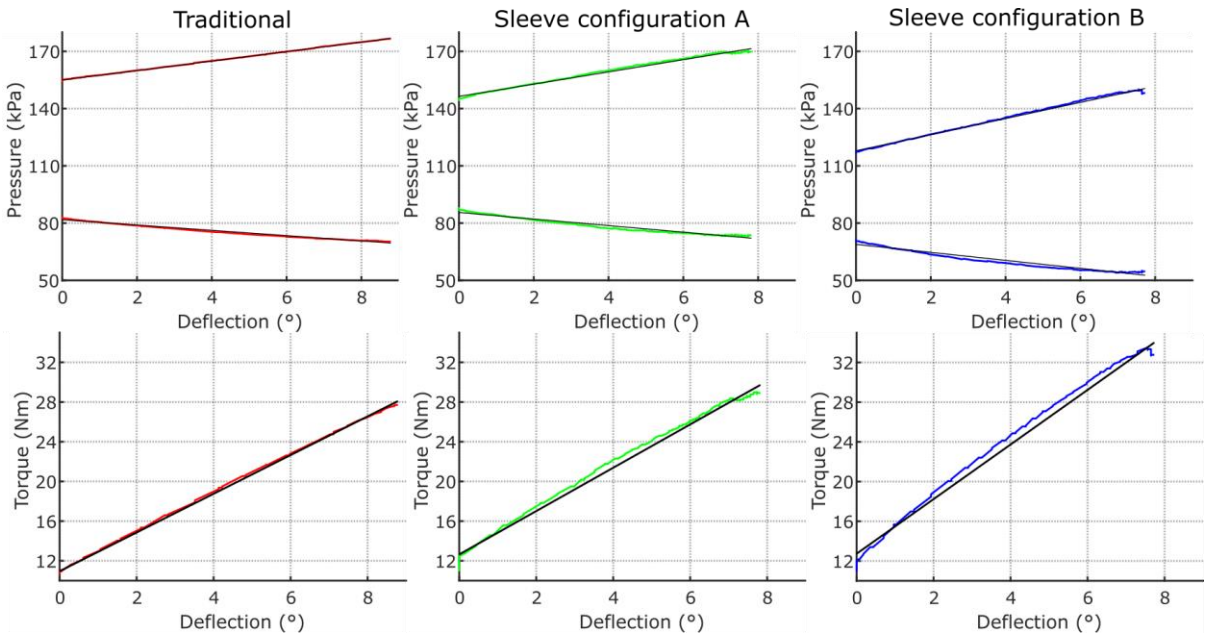

Figure 8-4: A sample of the responses of the joint while it is deviated from the set point in terms of change in pressure in the PAMs (both PAMs shown) and torque. In these cases, the joint has a set point of 0 radians with the minimum isobaric stiffness values shown in Figure 8-5 and there is 8° of deflection. In each graph the black line represents the linear model fitted to the response.

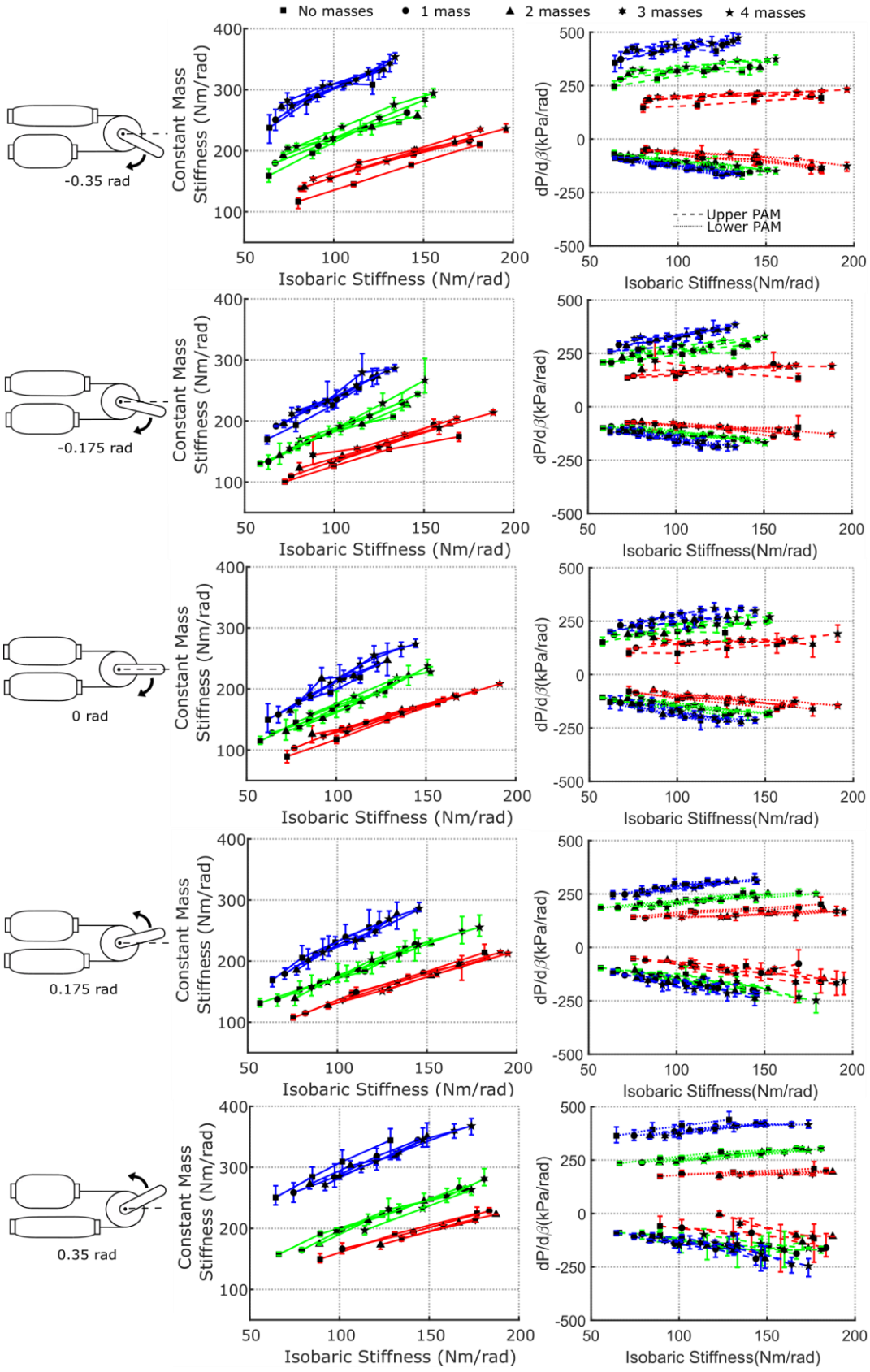

Figure 8-5: Closed system stiffness (centre column) and pressure changes (right). Joint position and direction of rotation is shown on the left. Traditional PAM is red, Sleeve A is green and Sleeve B is blue.

As a part of the testing procedure described for closed system stiffness, after the arm had been displaced, it was released and allowed to oscillate freely. The dynamic response allowed an assessment of damping in the system following the same approach as in [303], where a PAM actuated rotational joint, supporting a mass on an arm was modelled as a linear spring,-mass-damper system. In the following calculation, the action of the two PAMs is treated as a rotational spring and damper (see Figure 8-6 (a)).

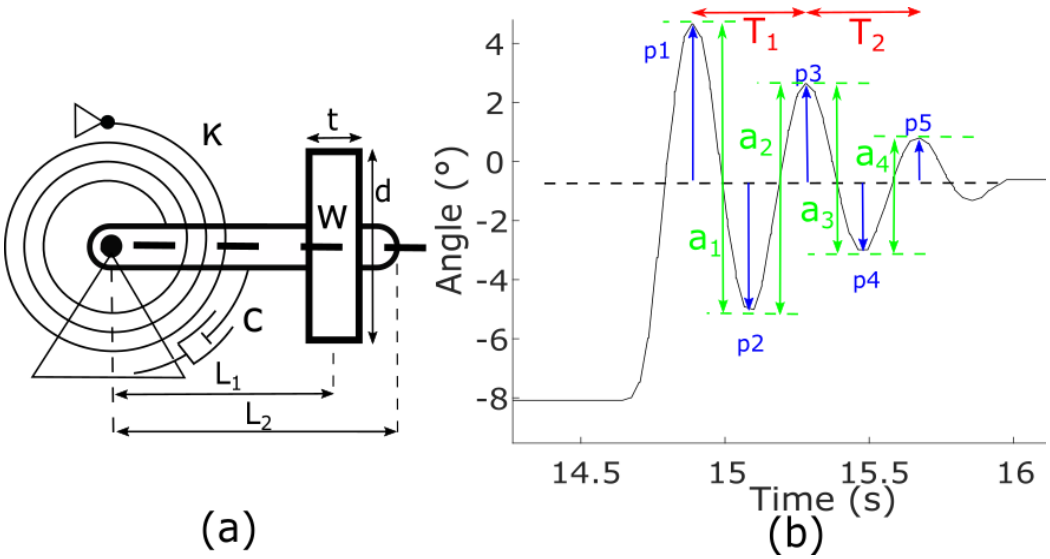

Figure 8-6: The premise of the modelling approach used to estimate damping is shown schematically in (a), while (b) graphs the response of the joint after being released with relevant quantities indicated. In this case it is the response of the joint actuated using traditional PAMs with an isobaric stiffness of 88Nm/rad with 2 masses atttached whn the joint set point is 0 radians.

The system is assumed to be under damped with each oscillation resulting in a smaller amplitude than the preceding one. The logarithmic decrement of the decay is defined as

$$\delta = ln\frac{p_1}{p_n} \tag{8.5}$$

where p_n is the amplitude of the nth peak or trough. As noted in [303], the equilibrium position during oscillation can be difficult to establish and so an alternative formulation utilizing the total travel between successive peaks and troughs is used instead (see Figure 8-6 (b)).

$$\delta = \frac{2}{n-1} ln\left(\frac{a_1}{a_n}\right) \tag{8.6}$$

where a_n is the n^{th} peak/trough. Using δ the damping ratio can be found using

$$\zeta = \sqrt{\frac{\delta^2}{4\pi^2 + \delta^2}} \tag{8.7}$$

For a rotational system, the viscous damping coefficient, can be related to the damping ratio by

$$c = 2\zeta\sqrt{\kappa J_0} \tag{8.8}$$

where J_0 is the moment of inertia of the arm about the pivot point and κ is the rotational stiffness. Simplifying the arm to a slender beam with a cylindrical mass attached (the weights) this is given by

$$J_0 = \frac{w_1 L_1}{3} + \left(\frac{w_2 d^2}{16} + \frac{w_2 t}{12}\right) + m_2 {L_2}^2 \tag{8.9}$$

where w_1 is the mass of the arm without the weights attached, l_1 is its length, w_2 is the mass of the weights, l_2 is the distance from the pivot to the centre of the weights and t is the combined thickness of the weights.

The damping coefficient of the arm is shown in Figure 8-7. In some of these tests, particularly those with the sleeve PAMs, there were insufficient oscillations to determine δ. In all cases there were more oscillations with the traditional PAMs, improving the accuracy of these values of c. While they vary considerably, it is observed that the damping of both sleeve actuated joints is similar, while that actuated with traditional PAMs is substantially lower. Varying the joint stiffness does not have a significant effect on damping, nor does the operating angle. This is consistent with the findings for a single PAM (section 7.2.2) which also found greater damping with the sleeve muscle. When more mass is added to the arm the damping increases, perhaps due to additional friction at the joint bearing.

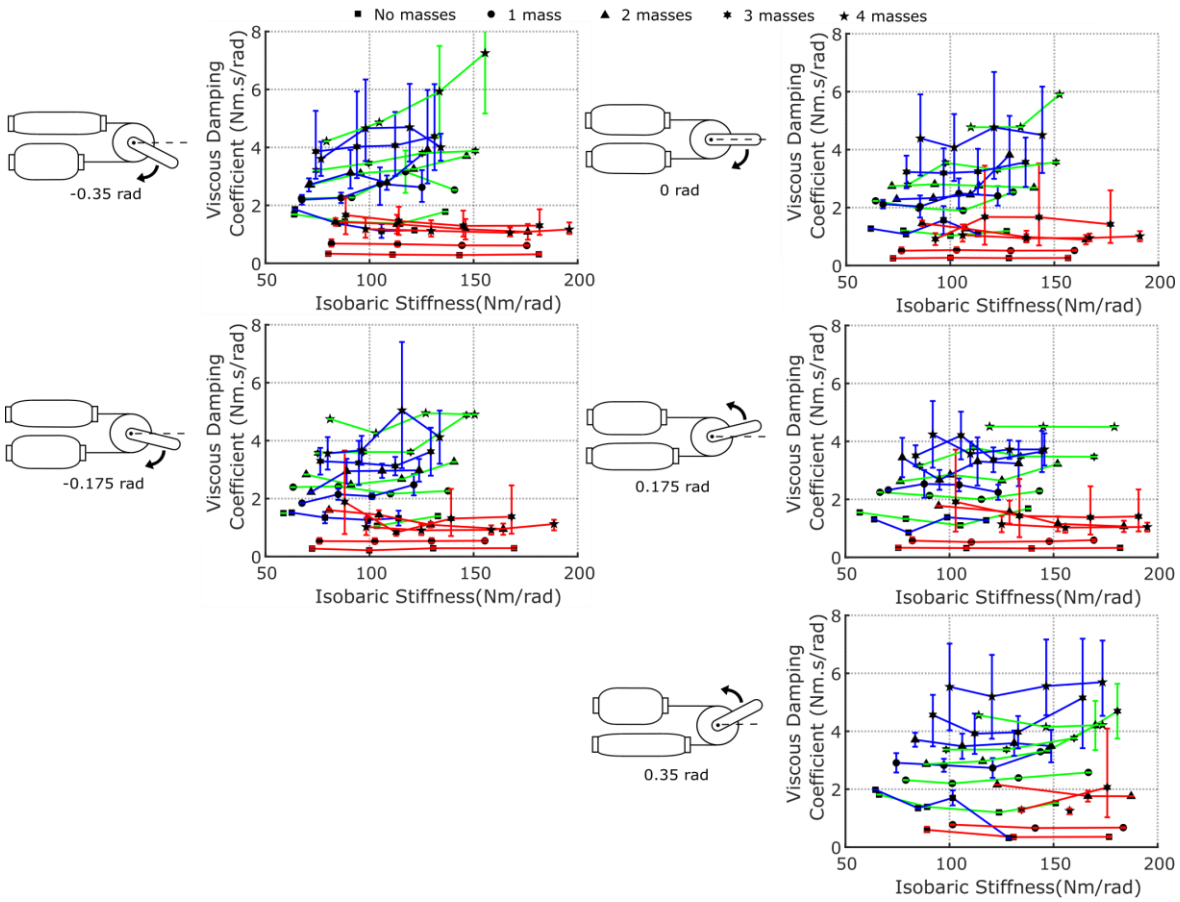

Figure 8-7: Viscous damping coefficient for the antagonistically actuated joint. Joint position and direction of rotation is shown to the left of each graph. Traditional PAM is red, Sleeve A is green and Sleeve B is blue.

8.6 ENERGY EFFICIENCY

The energy usage of the joints can be evaluated theoretically. An approach similar to that in [136] is employed, whereby an idealized compressor is the source of compressed air to a PAM. In this work, the volume of the compressor cylinder is such that it holds the mass of air, at ambient pressure, required to increase the pressure in the PAM to the pressure and contraction of interest. The energy required to drive the piston is the energy required to operate the system. This analysis assumes air behaves as a perfect gas, all operations occur isothermally, and ignores dynamic effects at the joint and PAMs.

While in [136] the air is first compressed before the muscle contracts isobarically using a single stroke of the compressor, here the movement of the joint is modelled in discrete steps, with a compressor stroke in each, to allow the methodology to be used for any arbitrary series of joint movements. At each step, the volume of an ideal compressor

required to change the pressure in the PAM (allowing for the required changes in muscle length, volume and force output) is calculated. The model of PAM volume developed previously is used for this purpose. The piston then acts upon this volume of air increasing its pressure to that within the PAM. A valve linking the compressor to the PAM is then opened, and the piston completes its stroke, acting upon the total volume as the PAM length changes in response to the pressure and torque. Mathematically, the work done by the piston can be represented as:

$$W = -\int_{V_{c1}}^{V_{c2}} (P - P_{atm})dV - \int_{V_{c2}+V_{m1}}^{V_{m2}} (P - P_{atm})dV \quad (8.10)$$

Where P is the absolute pressure in the cylinder, P_{atm} is the ambient pressure, V_{c1} is the initial volume of the cylinder, V_{c2} is the volume after the pressure in the cylinder has been increased to that in the PAM, and V_{m1} and V_{m2} are the initial and final volumes of the muscle respectively. Making use of the ideal gas law this becomes

$$W = -\Delta m RT\, ln\frac{V_{c2}}{V_{c1}} - P_{atm}(V_{c1} - V_{c2}) - (\Delta m + m_1)RT\, ln\left(\frac{V_{m2}}{V_{c2} + V_{m1}}\right) - P_{atm}((V_{c2} + V_{m1}) - V_{m2}) \quad (8.11)$$

Where m_1 is the initial mass of air in the PAM and Δm is the change in this mass during the operation.

An example of the use of this methodology is shown in Figure 8-8, where the stiffness of the joint is varied. In this case the joint moves in a sinusoidal motion of amplitude 0.2rad while applying a torque of 20Nm for one cycle. As the compressed air which is exhausted from the PAMs is typically lost to the atmosphere, only energy input to the PAM is considered. The joint actuated using the traditional PAM requires a greater energy input to achieve the same result. There is also considerable difference between both sleeve muscle configurations, with configuration A requiring the PAMs to operate in a more contracted state, thus increasing the required PAM pressure and volume and therefore energy requirement.

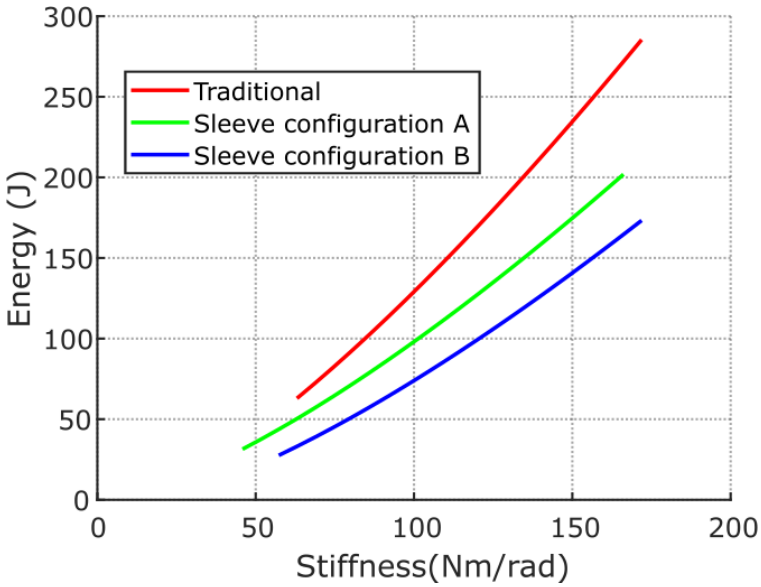

Figure 8-8: Energy consumption of the joint in order to move from the 0 angle sinusoidally at an amplitude of 0.2 rad, exerting 20Nm.

Due to the assumptions in this analysis, these results can only be seen as indicative of the true energy consumption. In reality the energy consumption of a compressor is complicated by temperature changes and most systems operate using a buffer tank requiring all the gas used to be pressurized to some operating pressure before being used to operate the PAMs

8.7 REMARKS

Using sleeve PAMs for antagonistically actuated joints can provide significant improvements in performance. The operating range and/or the available joint torque can be increased as demonstrated. The stiffness behaviour of the joint is quite different also, especially for the case of closed system operation. This operating condition is not frequently considered in the literature, though is an important safety characteristic as it is the stiffness which will be observed upon initial impact during a collision. Here it was found that the stiffness of the sleeve PAM actuated joint can be more than three times greater than the isobaric case due the pressure change in the PAMs. This effect is less pronounced when traditional PAMs are considered as the internal PAM volume is substantially larger. Using this operating condition may lead to systems with a greater apparent stiffness through adaptation of the control approach.

Damping in the joint was found to be greater when sleeve PAMs were used. Although these tests were conducted under closed system conditions, little change was observed with stiffness and so it is likely these results are comparable to those under a broader set of operating conditions. Finally, the theoretical energy consumption of the joint undertaking a simple operation was quantified. There was a significant reduction in energy use for both joint configurations using the sleeve PAMs at all stiffnesses. The procedure used here, while theoretical, may be applied to any arbitrary operation to give an indication of energy consumption.

The importance of the configuration of the joint, not just in terms of pulley diameter, but also the point of rotation at which the PAMs reach full extension, is also highlighted. While only two sleeve PAM configurations were investigated, they provided substantially different operating characteristics. This is an important factor in the design of such systems and their capability.

9 CONCLUSION

Evaluating the requirements of actuators for human-friendly service robots, the suitability of PAMs becomes apparent. Their low mass and high power to mass ratio reduces the inertia of robotic systems directly, while still allowing direct actuation of the joints. Their inherent compliance acts to decouple robot links from the overall system reducing further the apparent inertia on impact, while also providing advantages for operation in unstructured environments. They are also relatively low cost, can be manufactured in a range of sizes and can operate in compact configurations. However, a number of challenges have restricted their use in this field, particularly on mobile platforms. PAMs are relatively inefficient and require a compressed air supply which is typically bulky. Their low bandwidth means for many applications they may operate too slowly to be practically useful. Control is also made more difficult by their compliant nature, making accurate manipulation difficult.

A scientific understanding of the operation of PAMs is developed through analysis of their working principle and a review of the modelling techniques used to capture their performance. From this it is seen that several aspects of PAM design limit their performance. As the PAM internal pressure acts upon the end-fittings, an elongating force is exerted in opposition to the contraction of the PAM. It is also noted that the compressed air between the end fittings does not contribute to the radial expansion of the PAM and therefore muscle contraction. Eliminating this volume of air would therefore increase force output and contraction while reducing the volume of compressed air required to actuate the PAM. A reduced volume will also increase the bandwidth of the actuator as the pressure may be changed at a faster rate.

The sleeve PAM addresses a number of these shortcomings and so advancement of this actuator in terms of design, characterisation and modelling was pursued in this thesis. The sleeve muscle concept was applied to the McKibben type PAM with a design which is more adaptable, and which offers greater improvements to the muscle's capabilities than the previously implemented designs. The modular nature of the proposed solution makes it possible to configure the muscle to particular operating conditions such as the manner by which force is to be transmitted to the robot joint. This adaptability is key for

mobile service robots as it affords the designer the opportunity to better configure each joint for its particular role. The low-profile end fittings maximise the active length of the muscle, providing increased contraction for a muscle of the same overall length. A novel method to increase the effective contractile range of the muscle is also tested in the form of a pulley housed internally in the muscle again making the PAM more suitable for a greater range of applications.

When static operating characteristics are tested they are found to agree well with the modelled performance improvements because of the reduction in muscle volume and reduced area on which the muscle pressure acts on the end fitting. When compared with a traditional PAM the load capacity is increased across the full range of operation, but most especially at larger contractions. This also means the total contraction of the PAM is greater than a traditional PAM facilitating greater joint mobility. The efficiency of the sleeve muscle is found to be superior to that of the traditional muscle and previous sleeve muscle implementations. The increase in the proportion of the dead space occupied by the internal element when compared to previous sleeve PAM designs provides a greater reduction in compressed air consumption which is necessary for mobile platforms. The increase in stroke length and force output allows smaller PAMs to be used, thus decreasing the volume occupied on the robot by the actuators and potentially facilitating a greater range of motion. The internal pulley mechanism worked effectively, however frictional losses, were large.

In order to test the dynamic capabilities of the muscle, a testing apparatus was designed and implemented. This allowed both traditional and sleeve PAMs to be investigated under a range of operating conditions including isometric, isobaric, closed system and antagonistic actuation of a rotational joint. Testing on this apparatus revealed dramatically improved dynamic response using the sleeve muscle. Under isometric conditions the bandwidth of the sleeve PAM can be up to 100% greater than that of the traditional PAM when pressure is considered, or up to 120% greater if force is considered. An improvement in bandwidth for constant load profile conditions was also observed, though this was more modest. This result is important if PAMS are to deliver the speed of operation required for effective operation on service robots. In particular, productivity is

paramount in industrial applications. Attaining safe operation at such speeds is challenging; inherently compliant actuators are therefore a compelling option if their performance can be improved.

Static and dynamic testing allowed the application of an existing phenomenological PAM model to the case of a sleeve PAM. While phenomenological models are specific to the PAM for which the model is tuned, the results here showed that both the traditional and sleeve PAMs could be modelled using the same procedure with comparable accuracy. The testing procedure is considerably adapted from previous approaches found in the literature. Static testing, whereby the PAM is forced to elongate and contract at constant pressure by an agonist PAM is used to determine the static constants. A model of PAM volume is also produced in a similar manner but keeping the mass of air in the PAM constant, using the change in air pressure to relate the PAM volume. The dynamic performance is evaluated with step changes in pressure as the PAM acts against a spring. This approach simplifies the testing procedure, thus making it more practical for tuning a large number of PAMs to a model as would be necessary for a complex service robot. As the performance of PAMs are known to change with use, it may also be useful to be able to recalibrate the PAMs static model in place. This is useful in order to develop robust control strategies for sleeve PAMs, a requirement for any human-friendly system.

Finally, traditional and sleeve PAMS were compared for antagonistic actuation. The previously used phenomenological model was adapted so as to be applicable for this case and showed close agreement with experimentally measured torque values. Two stiffness regimes were investigated, that of isobaric operation and closed system operation. There was little difference between the joints' stiffness under isobaric conditions. However, the joints operating with sleeve PAMs saw a large increase in stiffness under closed system conditions due to the change in PAM pressure. Due to the larger internal volume of the traditional PAMs, this effect is less pronounced here. This result raises interesting possibilities as a means of increasing the stiffness of PAM actuated systems. This could also facilitate higher bandwidth operation. A theoretical method to determine the energy efficiency of joints operated antagonistically using PAMs is also presented. This builds upon previously proposed methods to estimate PAM energy

usage but discretises the operation into multiple steps, thus allowing arbitrary joint movements to be analysed. While the nature of the analysis requires many simplifying assumptions, it does highlight the increased efficiency of joints actuated using sleeve PAMs. As joints actuated antagonistically with PAMs offer variable stiffness, this configuration is the most useful for general purpose robots in human centric environments, therefore a detailed understanding of the operation of sleeve PAMs in this regard is necessary

From the study of mobile human-friendly service robots and their actuation requirements, it is evident that the sleeve muscle, as demonstrated here is a much more compelling actuator than the traditional PAM. Most critically it has been demonstrated that the sleeve PAM is dramatically more efficient, a key requirement for actuators on mobile systems. The improved force output and contraction ratio can also improve the dexterity and payload of actuated systems. It also means smaller actuators may be used, facilitating more compact, complex robotic systems. The use of the structural capabilities of the sleeve muscle, though not demonstrated here, can also decrease the spatial foot print of the robotic system.

While it has been noted that speed of operation is not as critical in service robots when compared with their industrial counterparts, they must nonetheless be fast enough to be useful, and bandwidth has been identified as a major limitation of PAM actuation. A thorough understanding of the dynamic behaviour of the actuator is also important to ensure their safe operation in human centred environments. This aspect of the sleeve PAM characteristics has not been analysed in the literature. The faster operating speed observed with sleeve PAMs can facilitate smaller, more efficient pneumatic networks while still delivering the required performance.

In terms of safety, the sleeve modification differs somewhat from the traditional PAM. The higher stiffness under closed system conditions increases the effective inertia of the actuated system should a collision. However, this can be somewhat negated by operating at a lower isobaric stiffness, thus further reducing energy consumption. While the sleeve PAM is necessarily heavier than the traditional PAM, thus increasing its inertia, this effect may be eliminated if the actuator is used structurally. Due to the internal

volume reduction in sleeve PAMs, there is less compressed fluid and therefore stored energy on the system, making it safer in the case of a failure where this energy is released (e.g. PAM rupture).

Ultimately it is only through demonstration of sleeve PAMs on mobile human-friendly robots that their suitability and practicality for this application can be verified. The work presented here goes some way to meeting the challenges which this presents, preserving the favourable characteristics inherent in PAMs while addressing some of their shortcomings. Further work will however be required if the possibilities which PAMs possess to contribute to human-friendly robot technology are to be realised.

9.1 FUTURE WORK

While the capabilities of the sleeve PAM and the advantages it offers over the traditional design have been investigated here, there is clearly much work remaining if the sleeve PAM is to be viewed as a favourable actuator for use on human-friendly mobile service robots. Foremost in this regard is the investigation of pneumatic sources for mobile platforms. The use of more efficient actuators such as sleeve PAMs may reduce the performance required of the pneumatic supply, however the need still remains. While air compressors are a convenient means to produce a stable source of compressed air for testing and characterisation purposes, they are quite large and heavy. Other possible solutions include high pressure tanks on board the robot which can be replenished at a docking station or the use of chemical reactions to produce pressurised gas. The use of these systems on complex mobile platforms is necessary.

Additionally, the valve technology used for pneumatic systems on robots presents several difficulties. They tend to consume a relatively large amount of energy, are heavy, bulky and noisy. New technologies such as piezoelectric valves offer many advantages as well as offering proportional control. Additionally, the cost of such systems must be reduced through economies of scale for PAMs to be practical in a wide range of applications. An interesting approach pressure control, could be to place the pneumatic source in the internal element of the sleeve PAM, thus further reducing the overall volume of the system and removing losses in compressed air distribution. Novel pneumatic sources such as hydrolysis or other chemical reactions may prove useful in this regard.

Robust control of sleeve PAM systems is clearly a required step not investigated in this work. In particular, the aspects of control for which the sleeve PAM differs from traditional PAMs must be investigated. These include the additional damping observed with sleeve PAMS and the faster response to flow in/out of the PAM. The stability of sleeve PAMs in terms of control may also be improved. Their smaller internal volume and the addition of a thermal mass in the PAM reduces the influence of thermal effects on PAM performance. Of particular interest is the greater stiffness of sleeve PAMs under closed system conditions. Considering this effect in control may be useful in developing higher stiffness and faster operation.

In this work a particular sleeve PAM implementation was demonstrated. While this design was modular in order to facilitate adaption to different use cases, it is certainly not suitable in all cases. In particular the diameter of the PAM is large relative to other PAMs investigated in the literature and produced commercially. A sleeve PAM implementation which could be produced in a smaller size (of the order of 5mm to 20mm diameter) would be useful for applications such as robot hands and light arms.

If PAM or other dynamic systems are to be made practical for pHRI all safety considerations arising from the use of compressed air must be addressed. Compressed air is a store of potential energy in a form which allows the energy to be released quickly. Safe guarding users from accidents involving the rupture of pneumatic supply lines or storage tanks is vital. However, the use of sleeve PAMs potentially reduces the pressure required in the system as well as the volume of compressed air which must be stored due to greater efficiency. Other human factors must also be addressed such as noise produced, mainly by valves and the flow of fluid through orifices.

Finally, actuators are only a small part of what is required to make human-friendly service robot s a reality. Greater reliability in sensing and the way a robot builds up a model of its surroundings is crucial to their safe and effective integration in any environment. Further, the robot must be able to interact effectively with people, most compellingly in a social way, so non-expert users can take advantage of them. This requires much to be accomplished in HRI. In order to carry out other complex operations, such as product assembly, fine manipulation etc., new high-level control procedures must be developed.

References

[1] A. De Santis, B. Siciliano, A. De Luca, and A. Bicchi, “An atlas of physical human-robot interaction,” *Mech. Mach. Theory*, vol. 43, no. 3, pp. 253–270, 2008.

[2] T. S. Tadele, T. J. A. De Vries, S. Stramigioli, and S. Member, “Safety in Domestic Robotics : A Survey,” pp. 1–8, 2014.

[3] A. Ajoudani, A. M. Zanchettin, S. Ivaldi, A. Albu-Schäffer, K. Kosuge, and O. Khatib, “Progress and prospects of the human–robot collaboration,” *Auton. Robots*, vol. 42, no. 5, pp. 957–975, 2018.

[4] J. Forlizzi and C. DiSalvo, “Service robots in the domestic environment,” *Proceeding 1st ACM SIGCHI/SIGART Conf. Human-robot Interact. - HRI ’06*, p. 258, 2006.

[5] R. W. Hicks II and E. L. Hall, “A Survey of Robot Lawn Mowers,” *Spie*, vol. 4197, pp. 262–269, Oct. 2000.

[6] R. Nickerson, “Pioneering the personal robotics industry,” *2009 IEEE Int. Conf. Technol. Pract. Robot Appl.*, vol. 5, pp. 179–185, Nov. 2009.

[7] H. Tanaka, M. Yoshikawa, E. Oyama, Y. Wakita, and Y. Matsumoto, “Development of Assistive Robots Using International Classification of Functioning , Disability , and Health : Concept , Applications , and Issues,” vol. 2013, 2013.

[8] J. M. Hollerbach, I. Hunter, and J. pd. Ballantyne, “A comparative analysis of actuator technologies for robotics,” *The Robotics Review*, vol. 2. pp. 299–342, 1991.

[9] M. Zinn, O. Khatib, B. Roth, and J. K. Salisbury, “Towards a human-centered intrinsically-safe robotic manipulator.,” *IEEE Robot. Autom. Mag.*, vol. 11, no. 2, pp. 12–21, 2004.

[10] F. Daerden and D. Lefeber, “Pneumatic artificial muscles: actuators for robotics and automation,” *Eur. J. Mech. Environ. Eng.*, vol. 47, no. 1, pp. 11–21, 2002.

[11] G. Andrikopoulos, G. Nikolakopoulos, and S. Manesis, “A Survey on applications of Pneumatic Artificial Muscles,” *19th Mediterr. Conf. Control Autom.*, pp. 1439–1446, 2011.

[12] B. Tondu *et al.*, “A Seven-degrees-of-freedom Robot-arm Driven by Pneumatic Artificial Muscles for Humanoid Robots,” *Int. J. Rob. Res.*, vol. 24, no. 4, pp. 257–274, 2005.

[13] M. D. Doumit, “Characterization, modeling and design of the braided pneumatic muscle,” University of Ottawa, 2009.

[14] Festo, “DMSP Fluidic Muscle DMSP / MAS,” 2016.

[15] D. G. Caldwell, N. Tsagarakis, D. Badihi, and G. a. Medrano-Cerda, “Pneumatic muscle actuator technology: a light weight power system for a humanoid robot,” *Proceedings. 1998 IEEE Int. Conf. Robot. Autom. (Cat. No.98CH36146)*, vol. 4, no. May, pp. 3053–3058, 1998.

[16] D. G. Caldwell, A. Razak, and M. J. Goodwin, “Braided Pneumatic Muscle

Actuators," *IFAC Conf. Intell. Auton. Veh.*, pp. 507–512, 1993.

[17] B. Ugurlu, P. Forni, C. Doppmann, and J. Morimoto, "Torque and variable stiffness control for antagonistically driven pneumatic muscle actuators via a stable force feedback controller," *IEEE Int. Conf. Intell. Robot. Syst.*, vol. 2015-Decem, pp. 1633–1639, 2015.

[18] M. A. Almeida de Souza Ramos, João Luiz Meggiolaro, "Use of Surface Electromyography To Control an Active Upper Limb Exoskeleton Actuated By Pneumatic Artificial Muscles and Optimized With Genetic Algorithms," in *22nd International Congress of Mechanical Engineering (COBEM 2013)*, 2013, vol. 6, no. Cobem, pp. 5376–5387.

[19] L. M. Sui and S. Q. Xie, "A Model of Pneumatic Muscle Actuated Joint Using Linearized Method," *Int. Conf Mechatronics Mach. Vis. Pract.*, no. 1, pp. 414–419, 2012.

[20] N. Saga, J. Nagase, and T. Saikawa, "Pneumatic artificial muscles based on biomechanical characteristics of human muscles," *Appl. Bionics Biomech.*, vol. 3, no. 3, pp. 191–197, 2006.

[21] T. Nakamura, N. Saga, and K. Yaegashi, "Development of a Pneumatic Artificial Muscle based on Biomechanical Characteristics," in *Industrial Technology, 2003 IEEE International Conference on*, 2003, vol. 2, pp. 729–734.

[22] H. F. Schulte, D. F. Adamski, and J. R. Pearson, "Characteristics of the Braided Fluid Actuator," 1961.

[23] C. J. Bowler, D. G. Caldwell, and G. a Medrano-Cerda, "Pneumatic Muscle Actuators: Musculature for an Anthropomorphic Robot Arm," *IEE Colloq. Actuator Technol. Curr. Pract. New Dev.*, pp. 1–8, 1996.

[24] International Standards organisation, "ISO 8373: Robots and robotic devices — Vocabulary," 2012.

[25] International Federation of Robotics, "Executive Summary - World Robotics (Service Robots) 2017," 2017.

[26] U. Reiser, "Robots as Multifunctional gentlemen," 2015.

[27] Franhofer IPA, "Care-O-bot 4," 2017. [Online]. Available: http://www.care-o-bot.de/en/care-o-bot-4.html. [Accessed: 02-Mar-2017].

[28] Franhofer IPA, "Care-O-bot® 4 celebrates its première as shopping assistant," 2016.

[29] F. IPA, "Care-O-Bot 4: Technical Data Sheet," 2015.

[30] C. Jiang, Y. Nakatomi, and S. Ueno, "Optimal Control of Holding Motion by Nonprehensile Two-Cooperative-Arm Robot," *Math. Probl. Eng.*, vol. 2016, 2016.

[31] RIKEN, "ROBEAR Research Platform." [Online]. Available: http://rtc.nagoya.riken.jp/ROBEAR/#spec. [Accessed: 02-Mar-2017].

[32] RIKEN, "The strong robot with the gentle touch | RIKEN." [Online]. Available: http://www.riken.jp/en/pr/press/2015/20150223_2/. [Accessed: 03-Mar-2017].

[33] S. Cousins, “ROS on the PR2,” *IEEE Robot. Autom. Mag.*, vol. 17, no. 3, pp. 23–25, 2010.

[34] Willow Garage, “PR2 Robot for Research and Innovation.” [Online]. Available: http://www.willowgarage.com/pages/pr2/overview. [Accessed: 03-Mar-2017].

[35] Willow garage, “Hardware and Software Platform for Mobile Manipulation R&D,” 2015. [Online]. Available: http://www.willowgarage.com/pages/pr2/design. [Accessed: 06-Mar-2017].

[36] W. Garage, “PR2 User Manual,” 2012.

[37] W. Garage, “PR2 Pricing & Open Source Discount,” 2010. [Online]. Available: http://www.willowgarage.com/blog/2010/09/07/pr2-pricing-and-open-source-discount. [Accessed: 06-Mar-2017].

[38] Y. Sakagami, R. Watanabe, C. Aoyama, S. Matsunaga, N. Higaki, and K. Fujimura, “The intelligent ASIMO: system overview and integration,” *IEEE/RSJ Int. Conf. Intell. Robot. Syst.*, vol. 3, no. October, pp. 2478–2483, 2002.

[39] J. Chestnutt, P. Michel, J. Kuffner, and T. Kanade, “Locomotion among dynamic obstacles for the Honda ASIMO,” *IEEE Int. Conf. Intell. Robot. Syst.*, pp. 2572–2573, 2007.

[40] Honda, “All-New ASIMO Extends Danish Trip to Inspire Local Children,” 2015. [Online]. Available: http://world.honda.com/worldnews/2015/c150417ASIMO-Trip-Danish.html. [Accessed: 06-Mar-2017].

[41] Honda, “ASIMO to Welcome Visitors Arriving at Narita International Airport,” 2016. [Online]. Available: http://world.honda.com/news/2016/c160322eng.html. [Accessed: 06-Mar-2017].

[42] “2011 Evolution of ASIMO - Key Specifications,” 2017. [Online]. Available: http://world.honda.com/ASIMO/technology/2011/specification/index.html. [Accessed: 06-Mar-2017].

[43] T. Yoshikawa and O. Khatib, “Compliant humanoid robot control by the torque transformer,” *2009 IEEE/RSJ Int. Conf. Intell. Robot. Syst. IROS 2009*, pp. 3011–3018, 2009.

[44] A. Bicchi and G. Tonietti, “Fast and ‘soft-arm’ tactics: Dependability in Human-Friendly Robots,” *IEEE Robot. Autom. Mag.*, vol. 11, no. 2, pp. 22–33, 2004.

[45] J. Heinzmann and A. Zelinsky, “Quantitative Safety Guarantees for Physical Human-Robot Interaction,” *Int. J. Rob. Res.*, vol. 22, no. 7–8, pp. 479–504, 2003.

[46] M. van Damme *et al.*, “The safety of a robot actuated by pneumatic muscles-a case study,” *Int. J. Soc. Robot.*, vol. 2, no. 3, pp. 289–303, 2010.

[47] R. Alami *et al.*, “Safe and dependable physical human-robot interaction in anthropic domains: State of the art and challenges,” *IEEE Int. Conf. Intell. Robot. Syst.*, no. 1, 2006.

[48] B. Group, “BSI Standards Publication Robots and robotic devices — Safety requirements for personal care robots,” 2014.

[49] A. Fetzner, C. Frese, and C. Frey, “A 3D Representation of Obstacles in the Robot’s Reachable Area Considering Occlusions,” *Int. Symp. Robot. Ger. Conf. Robot.*, pp. 85–92, 2014.

[50] B. Schmidt and L. Wang, “Depth camera based collision avoidance via active robot control,” *J. Manuf. Syst.*, vol. 33, no. 4, pp. 711–7118, 2014.

[51] L. Wang, B. Schmidt, and A. Y. C. Nee, “Vision-guided active collision avoidance for human-robot collaborations,” *Manuf. Lett.*, vol. 1, no. 1, pp. 5–8, 2013.

[52] H. Iwata, H. Hoshino, T. Morita, and S. Sugano, “Force detectable surface covers for humanoid robots,” *IEEE/ASME Int. Conf. Adv. Intell. Mechatronics*, no. July, pp. 1205–1210, 2001.

[53] A. Bicchi *et al.*, “Physical human-robot interaction: Dependability, safety, and performance,” *Int. Work. Adv. Motion Control. AMC*, vol. 1, pp. 9–14, 2008.

[54] M. Van Damme *et al.*, “The Role of Compliance in Robot Safety,” *IARP Work. Tech. Challenges Dependable Robot. Hum. Environ.*, no. 231554, pp. 65–71, 2010.

[55] A. L. Edsinger, “Robot Manipulation in Human Environments,” Massachusetts Institute of Technology, 2007.

[56] S. Haddadin, A. Albu-Schäffer, and G. Hirzinger, “Safe Physical Human-Robot Interaction: Measurements, Analysis & New Insights,” *Robot. Res.*, vol. 66, pp. 395–407, 2011.

[57] K. Ikuta, H. Ishii, and M. Nokata, “Safety Evaluation Method of Design and Control for Human-Care Robots,” *Int. J. Rob. Res.*, vol. 22, no. 5, pp. 281–297, 2003.

[58] K. Ikuta and M. Nokata, “General evaluation method of safety for human-care robots,” *Proc. 1999 IEEE Int. Conf. Robot. Autom. (Cat. No.99CH36288C)*, vol. 3, no. May, pp. 2065–2072, 1999.

[59] H. I. Christensen, “Intelligent Home Appliances,” *Robot. Res.*, no. 6, pp. 319–330, 2003.

[60] A. Bicchi, S. Lodi, and G. Toniet, “Compliant design for intrinsic safety: General issues and preliminary design,” in *International Conference on Intelligent Robots and Systems*, 2001, pp. 1864–1869.

[61] E. Acome *et al.*, “Hydraulically amplified self-healing electrostatic actuators with muscle-like performance,” *Science (80-.).*, vol. 359, no. 6371, pp. 61–65, 2018.

[62] S. Hunt, T. G. McKay, and I. A. Anderson, “A self-healing dielectric elastomer actuator,” *Appl. Phys. Lett.*, vol. 104, no. 11, p. 113701, Mar. 2014.

[63] A. Miriyev, K. Stack, and H. Lipson, “Soft material for soft actuators,” *Nat. Commun.*, vol. 8, no. 1, pp. 1–8, 2017.

[64] R. A. Bilodeau, A. Miriyev, H. Lipson, and R. Kramer-Bottiglio, “All-soft material system for strong soft actuators,” *2018 IEEE Int. Conf. Soft Robot. RoboSoft 2018*, pp. 288–294, 2018.

[65] N. Li *et al.*, “New twist on artificial muscles,” *Proc. Natl. Acad. Sci.*, vol. 115, no. 11,

p. 201802492, 2018.

[66] S. H. Kim *et al.*, “Harvesting temperature fluctuations as electrical energy using torsional and tensile polymer muscles,” *Energy Environ. Sci.*, vol. 8, no. 11, pp. 3336–3344, 2015.

[67] J. Cui *et al.*, “Combinatorial search of thermoelastic shape-memory alloys with extremely small hysteresis width,” *Nat. Mater.*, vol. 5, no. 4, pp. 286–290, 2006.

[68] B. Holschuh, E. Obropta, and D. Newman, “Low spring index NiTi coil actuators for use in active compression garments,” *IEEE/ASME Trans. Mechatronics*, vol. 20, no. 3, pp. 1264–1277, 2015.

[69] T. Xie, “Tunable polymer multi-shape memory effect,” *Nature*, vol. 464, no. 7286, pp. 267–270, 2010.

[70] S. Popi and B. Miloradovi, “Light Weight Robot Arms – An overview,” vol. 14, no. March, pp. 818–822, 2015.

[71] O. Khatib, “Inertial Properties in Robotic Manipulation:An object-Level Framework,” *Int. J. Rob. Res.*, vol. 14, no. 1, pp. 19–36, 1995.

[72] S. Haddadin, a. Albu-Schaffer, and G. Hirzinger, “Requirements for Safe Robots: Measurements, Analysis and New Insights,” *Int. J. Rob. Res.*, vol. 28, no. 11–12, pp. 1507–1527, 2009.

[73] D. G. Caldwell, N. Tsagarakis, and G. A. A. Medrano-Cerda, “Bio-mimetic actuators: Polymeric Pseudo Muscular Actuators and pneumatic Muscle Actuators for biological emulation,” *Mechatronics*, vol. 10, no. 4, pp. 499–530, Jun. 2000.

[74] J. E. Huber, N. A. Fleck, and M. F. Ashby, “The selection of mechanical actuators based on performance indices,” *Proc. R. Soc. A Math. Phys. Eng. Sci.*, vol. 453, no. 1965, pp. 2185–2205, 1997.

[75] A. Festo, “Standard cylinders DSNU/DSNUP/DSN/ESNU/ESN, ISO 6432,” 2013.

[76] B. Hannaford and J. M. Winters, *Actuator properties and movement control: biological and technological models. In Multiple Muscle Systems*. Springer-Verlag, 1990.

[77] D. G. Caldwell, G. a. Medrano-Cerda, and M. J. Goodwin, “Braided pneumatic actuator control of a multi-jointed manipulator,” *Proc. IEEE Syst. Man Cybern. Conf. - SMC*, pp. 423–428, 1993.

[78] D. H. Plettenburg, “Pneumatic actuators: A comparison of energy-to-mass ratio’s,” *Proc. 2005 IEEE 9th Int. Conf. Rehabil. Robot.*, vol. 2005, pp. 545–549, 2005.

[79] M. Tavakoli, L. Marques, and A. T. De Almeida, “A comparison study on pneumatic muscles and electrical motors,” in *IEEE International Conference on Robotics and Biomimetics, ROBIO*, 2008, pp. 1590–1594.

[80] G. Yang, S. K. Mustafa, S. H. Yeo, W. Lin, and W. Bin Lim, “Kinematic design of an anthropomimetic 7-DOF cable-driven robotic arm,” vol. 6, no. 1, pp. 45–60, 2011.

[81] J. Ma, Y. Li, and S. S. Ge, “Adaptive control for a cable driven robot arm,” *2012 IEEE*

Int. Conf. Mechatronics Autom. ICMA 2012, pp. 1074–1079, 2012.

[82] M. Zinn, B. Roth, O. Khatib, and J. K. Salisbury, "A New Actuation Approach for Human Friendly Robot Design," *Int. J. Rob. Res.*, vol. 23, no. 4, pp. 379–398, 2004.

[83] D. Shin, I. Sardellitti, and O. Khatib, "A hybrid actuation approach for human-friendly robot Design," *Proc. - IEEE Int. Conf. Robot. Autom.*, pp. 4369–4374, 2009.

[84] S. Jörg, M. Nickl, A. Nothhelfer, T. Bahls, and G. Hirzinger, "The computing and communication architecture of the DLR Hand Arm System," *IEEE Int. Conf. Intell. Robot. Syst.*, pp. 1055–1062, 2011.

[85] B. Vanderborght, "Dynamic stabilisation of the biped Lucy powered by actuators with controllable stiffness," Vrije Universiteit Brussel, 2007.

[86] C. S. Kothera, M. Jangid, J. Sirohi, and N. M. Wereley, "Experimental Characterization and Static Modeling of McKibben Actuators," *J. Mech. Des.*, vol. 131, no. 9, p. 091010, 2009.

[87] G. J. M. Tuijthof and J. L. Herder, "Design, actuation and control of an anthropomorphic robot arm," *Mech. Mach. Theory*, vol. 35, no. 7, pp. 945–962, 2000.

[88] Sanyo Denki, "Stepping Motors 56Mm Sq. (2.20 Inch Sq.)," 2009.

[89] Crouzet, "DCmind Brush Motors," 2012.

[90] S. Haddadin, K. Krieger, N. Mansfeld, and A. Albu-Schaffer, "On impact decoupling properties of elastic robots and time optimal velocity maximization on joint level," *IEEE Int. Conf. Intell. Robot. Syst.*, pp. 5089–5096, 2012.

[91] W. Wang, R. N. K. Loh, and E. Y. Gu, "Passive compliance versus active compliance in robot- based automated assembly systems," vol. 25, no. 1, pp. 48–57, 1998.

[92] S. Haddadin, A. Albu-schäffer, and G. Hirzinger, "Safety evaluation of physical human-robot interaction via crash-testing," 2007.

[93] A. Albu-Schaffer *et al.*, "Soft robotics," *IEEE Robot. Autom. Mag.*, vol. 15, no. 3, pp. 20–30, 2008.

[94] S. Wolf *et al.*, "Variable Stiffness Actuators: Review on Design and Components," *IEEE/ASME Trans. Mechatronics*, vol. 21, no. 5, pp. 2418–2430, 2016.

[95] A. M. Dollar and R. D. Howe, "Towards grasping in unstructured environments: grasper compliance and configuration optimization," *Adv. Robot.*, vol. 19, no. 5, pp. 523–543, 2005.

[96] A. M. Dollar, "Design principles for robust grasping in unstructured environments," Harvard University, 2006.

[97] D. Leidner, C. Borst, A. Dietrich, M. Beetz, and A. Albu-Schaffer, "Classifying compliant manipulation tasks for automated planning in robotics," *IEEE Int. Conf. Intell. Robot. Syst.*, vol. 2015-Decem, pp. 1769–1776, 2015.

[98] B. Dadashzadeh, M. J. Mahjoob, M. N. Bahrami, and C. Macnab, "Compliant leg architectures and a linear control strategy for the stable running of planar biped robots," *Int. J. Adv. Robot. Syst.*, vol. 10, pp. 1–13, 2013.

[99] M. Li, X. Wang, W. Guo, P. Wang, and L. Sun, “System design of a cheetah robot toward ultra-high speed,” *Int. J. Adv. Robot. Syst.*, vol. 11, no. 1, pp. 1–11, 2014.

[100] J. E. Pratt and B. T. Krupp, “Series Elastic Actuators for legged robots,” *Proc. SPIE 5422, Unmanned Gr. Veh. Technol. VI*, vol. 5422, pp. 135–144, 2004.

[101] G. K. Hari *et al.*, “Performing Explosive motions using a multi-joint arm actuated by pneumatic muscles with quasi-DDP optimal control,” in *Control Applications (CCA), 2016 IEEE Conference on*, 2016, vol. 1104, no. 1, pp. 1104–1110.

[102] P. Cherelle, A. Matthys, V. Grosu, B. Vanderborght, and D. Lefeber, “The AMP-Foot 2.0: Mimicking intact ankle behavior with a powered transtibial prosthesis,” *Proc. IEEE RAS EMBS Int. Conf. Biomed. Robot. Biomechatronics*, pp. 544–549, 2012.

[103] D. Braun, M. Howard, and S. Vijayakumar, “Optimal variable stiffness control: Formulation and application to explosive movement tasks,” *Auton. Robots*, vol. 33, no. 3, pp. 237–253, 2012.

[104] S. Wolf, G. Hirzingher, and G. Hirzinger, “A New Variable Stiffness Design: Matching Requirements of The Next Robot Generation,” in *International Conference on Robotics and Automation*, 2008, pp. 1741–1746.

[105] B. Misgeld and K. Gerlach-Hahn, “Control of Adjustable Compliant Actuators,” *Machines*, pp. 134–157, 2014.

[106] V. R. Ham, T. G. Sugar, B. Vanderborght, K. W. Hollander, and D. Lefeber, “Compliant actuator designs: Review of actuators with passive adjustable compliance/controllable stiffness for robotic applications,” *IEEE Robot. Autom. Mag.*, vol. 16, no. 3, pp. 81–94, 2009.

[107] M. G. Catalano *et al.*, “VSA-CubeBot: A modular variable stiffness platform for multiple degrees of freedom robots,” *Proc. - IEEE Int. Conf. Robot. Autom.*, pp. 5090–5095, 2011.

[108] A. Enoch, A. Sutas, S. Nakaoka, and S. Vijayakumar, “BLUE : A Bipedal Robot with Variable Stiffness and Damping,” in *International Conference on Humanoid Robots*, 2012, pp. 487–494.

[109] S. Collins, “Efficient Bipedal Robots Based on Passive-Dynamic Walkers,” *Science (80-.).*, vol. 307, no. 5712, pp. 1082–1085, 2005.

[110] B. Vanderborght *et al.*, “Exploiting Natural Dynamics to Reduce Energy Consumption by Controlling the Compliance of Soft Actuators,” *Int. J. Rob. Res.*, vol. 25, no. 4, pp. 343–358, 2006.

[111] B. Vanderborght *et al.*, “LUCY, a Bipedal Walking Robot with Pneumatic Artificial Muscles,” *Mechatronics*, 2004.

[112] N. G. Tsagarakis, S. Morfey, G. Medrano Cerda, Z. Li, and D. G. Caldwell, “COMpliant huMANoid COMAN: Optimal joint stiffness tuning for modal frequency control,” *Proc. - IEEE Int. Conf. Robot. Autom.*, pp. 673–678, 2013.

[113] F. Y. Hsu and L. C. Fu, “Intelligent robot deburring using adaptive fuzzy hybrid position/force control,” *IEEE Trans. Robot. Autom.*, vol. 16, no. 4, pp. 325–335, 2000.

[114] B. Vanderborght *et al.*, "Variable impedance actuators: A review," *Rob. Auton. Syst.*, vol. 61, no. 12, pp. 1601–1614, 2013.

[115] G. A. Pratt and M. M. Williamson, "Series elastic actuators," *1995 IEEE/RSJ Int. Conf. Intell. Robot. Syst. 'Human Robot Interact. Coop. Robot.*, vol. 1, no. 1524, pp. 399–406, 1995.

[116] S. A. Migliore, E. A. Brown, and S. P. DeWeerth, "Biologically Inspired Joint Stiffness Control," in *International Conference on Robotics and Automation*, 2005, no. April, pp. 4508–4513.

[117] K. W. Hollander, R. Ilg, T. G. Sugar, and D. Herring, "An Efficient Robotic Tendon for Gait Assistance," *J. Biomech. Eng.*, vol. 128, no. 5, p. 788, 2006.

[118] C. E. English and D. Russell, "Mechanics and stiffness limitations of a variable stiffness actuator for use in prosthetic limbs," *Mech. Mach. Theory*, vol. 34, no. 1, pp. 7–25, 1999.

[119] K. Koganezawa, T. Inaba, and T. Nakazawa, "Stiffness and angle control of antagonistially driven joint," *Int. Conf. Biomed. Robot. Biomechatronics*, vol. 2006, pp. 1007–1013, 2006.

[120] H. Seki, A. Takada, Y. Kamiya, M. Hikizu, and H. Nomura, "Development of a robot joint mechanism with variable compliance by rotating a leaf spring," in *Japan/USA Flexible Automation Conference*, 2000.

[121] S. Kawamura *et al.*, "Development of passive elements with variable mechanical impedance for wearable robots," *IEEE Int. Conf. Robot. Autom.*, vol. 1, no. May, pp. 248–253, 2002.

[122] T. Morita and S. Sugano, "Development of an anthropomorphic force-controlled manipulator WAM-10," *Adv. Robot. 1997. ICAR '97. Proceedings., 8th Int. Conf.*, pp. 701–706, 1997.

[123] K. W. Hollander, T. G. Sugar, and D. Herring, "Adjustable Robotic Tendon using a ` Jack Spring'TM," in *International Conference on Rehabilitation Robotics*, 2005, pp. 1–6.

[124] R. Van Ham, B. Vanderborght, M. Van Damme, B. Verrelst, and D. Lefeber, "MACCEPA, the mechanically adjustable compliance and controllable equilibrium position actuator: Design and implementation in a biped robot," *Rob. Auton. Syst.*, vol. 55, no. 10, pp. 761–768, 2007.

[125] M. Marônek, J. Bárta, and J. Ertel, "Inaccuracies of industrial robot positioning and methods of their correction," *Teh. Vjesn. - Tech. Gaz.*, vol. 22, no. 5, pp. 1207–1212, 2015.

[126] CEA Technologies Inc, "Electric Motors - Energy Efficiency Reference Guide," 2007.

[127] A. Hošovský, J. Piteľ, K. Židek, M. Tóthová, J. Sárosi, and L. Cveticanin, "Dynamic characterization and simulation of two-link soft robot arm with pneumatic muscles," *Mech. Mach. Theory*, vol. 103, pp. 98–116, 2016.

[128] M. Van Damme, B. Vanderborght, B. Verrelst, R. Van Ham, F. Daerden, and D.

Lefeber, “Proxy-based Sliding Mode Control of a Planar Pneumatic Manipulator,” *Int. J. Rob. Res.*, vol. 28, no. 2, pp. 266–284, 2009.

[129] R. M. Robinson, C. S. Kothera, R. M. Sanner, and N. M. Wereley, “Nonlinear Control of Robotic Manipulators Driven by Pneumatic Artificial Muscles,” *IEEE/ASME Trans. Mechatronics*, vol. 21, no. 1, pp. 55–68, 2016.

[130] T. V. Minh, T. Tjahjowidodo, H. Ramon, and H. Van Brussel, “Non-local memory hysteresis in a pneumatic artificial muscle (PAM),” *2009 17th Mediterr. Conf. Control Autom.*, pp. 640–645, 2009.

[131] V. Jouppila and A. Ellman, “Position Control of Pwm-Actuated Pneumatic Muscle Actuator System,” *ASME Int. Mech. Eng. Congr.*, pp. 393–404, 2012.

[132] K. K. Ahn and H. P. H. Anh, “Comparative study of modeling and identification of the pneumatic artificial muscle (PAM) manipulator using recurrent neural networks,” *J. Mech. Sci. Technol.*, vol. 22, pp. 1287–1298, 2008.

[133] S. Davis, N. Tsagarakis, J. Canderle, and D. G. Caldwell, “Enhanced modelling and performance in braided pneumatic muscle actuators,” *Int. J. Rob. Res.*, vol. 22, no. 3, pp. 213–227, 2003.

[134] G. Belforte and S. Mauro, “New developments and new trends in pneumatics,” in *The 6th International Symposium on Flow Control, Measurements and Flow Visualization*, 2000.

[135] C. M. Burt, X. Piao, F. Gaudi, B. Busch, and N. F. Taufik, “Electric Motor Efficiency under Variable Frequencies and Loads,” *J. Irrig. Drain. Eng.*, vol. 134, no. 2, pp. 129–136, 2008.

[136] C.-P. Chou and B. Hannaford, “Measurement and modelling of McKibben pneumatic artificial muscles,” *Robot. Autom. IEEE Trans.*, vol. 12, no. 1, pp. 90–102, 1996.

[137] M. A. Meller, M. J. Bryant, and E. Garcia, “Energetic and Dynamic Effects of Operating Fluid on Fluidic,” in *Conference on Smart Materials, Adaptive Structures and Intelligent Systems*, 2013, pp. 1–8.

[138] M. a. Meller, M. Bryant, and E. Garcia, “Reconsidering the McKibben muscle: Energetics, operating fluid, and bladder material,” *J. Intell. Mater. Syst. Struct.*, vol. 25, no. 18, pp. 2276–2293, 2014.

[139] T. Nozawa, “[JSAP] Tokai University Unveils 100W DC Motor with 96% Efficiency - Nikkei Technology Online,” 2009. [Online]. Available: http://techon.nikkeibp.co.jp/english/NEWS_EN/20090403/168295/. [Accessed: 27-Jun-2017].

[140] Microchip, “Brushless DC (BLDC) Motor Fundamentals -AN885,” 2003.

[141] M. Murray, “Total System Efficiency,” *Power Transm. Eng.*, pp. 16–23, 2010.

[142] Harmonic Drive LLC, “Harmonic Planetary - Precision Gearing and Motion Control.”

[143] J. W. Sensinger and J. H. Lipsey, “Cycloid vs. harmonic drives for use in high ratio,

single stage robotic transmissions," *Proc. - IEEE Int. Conf. Robot. Autom.*, vol. 60611, pp. 4130–4135, 2012.

[144] "Compressed Air Energy Efficiency Reference Guide," 2007.

[145] P. V. Ramana and D. Rambabu, "Experimental Compaison of Single and Multistage Air Compressor Efficiencies Under the same Receiver Tank Pressure," *Anveshana's Int. J. Res. Eng. Appl. Sci.*, vol. 1, no. 6, pp. 28–37, 2016.

[146] G. Liu, "Control of robot manipulators with consideration of actuator performance degradation and failures," *Int. Conf. Robot. Autom.*, vol. 3, pp. 2566–2571, 2001.

[147] G. Clark-Derby, "Prolonging a robot's life expectancy," *Ind. Robot An Int. J.*, vol. 22, no. 2, pp. 16–17, 1995.

[148] G. K. Klute and B. Hannaford, "Fatigue characteristics of McKibben artificial muscle actuators," *Int. Conf. Intell. Robot. Syst.*, vol. 3, no. October, pp. 1776–1781, 1998.

[149] B. K. Woods, M. F. Gentry, C. S. Kothera, and N. M. Wereley, "Fatigue life testing of swaged pneumatic artificial muscles as actuators for aerospace applications," *J. Intell. Mater. Syst. Struct.*, vol. 23, no. 3, pp. 327–343, 2012.

[150] D. A. Kingsley and R. D. Quinn, "Fatigue life and frequency response of braided pneumatic actuators," *Proc. 2002 IEEE Int. Conf. Robot. Autom. (Cat. No.02CH37292)*, vol. 3, no. May, pp. 2830–2835, 2002.

[151] B. J. Chalmers, *Electric Motor Handbook*. Butterworths, 1988.

[152] Radionics, "8981A1-3 (15Nm) | Crouzet DC Geared Motor, Brushed, 24 V dc, 15 Nm, 9 rpm, 20 W | Crouzet." [Online]. Available: http://ie.rs-online.com/web/p/dc-geared-motors/7893039/. [Accessed: 05-Jul-2017].

[153] Festo, "DMSP Fluidic Muscle with press-fitted connection." [Online]. Available: https://www.festo.com/cat/en-gb_ie/products_DMSP. [Accessed: 05-Jul-2017].

[154] R. Niiyama and Y. Kuniyoshi, "A Pneumatic Biped with an Artificial Musculoskeletal System," *4th Int. Symp. Adapt. Motion Anim. Mach.*, pp. 80–81, 1998.

[155] R. Niiyama, A. Nagakubo, and Y. Kuniyoshi, "Mowgli: A bipedal jumping and landing robot with an artificial musculoskeletal system," *IEEE Int. Conf. Robot. Autom.*, no. April, pp. 2546–2551, 2007.

[156] Hoerboger, "Proportional Pressure Regulation - Pneumatic Proportional Valve." [Online]. Available: https://www.hoerbiger.com/en-0/pages/534. [Accessed: 05-Jul-2017].

[157] V. Jouppila, S. A. Gadsen, and A. Ellman, "Modeling and Identification of a Pneumatic Muscle Actuator System Controlled By an on / Off Solenoid Valve," *7th Int. Fluid Power Conf.*, pp. 1–11, 2010.

[158] Festo, "Valves VUVS-VUVS-LK20-M32C-AD-G18-1C1-S." [Online]. Available: https://www.festo.com/cat/en-gb_ie/products_VUVS_S. [Accessed: 05-Jul-2017].

[159] Shadow Robotics, "Shadow Dexterous Hand Technical Specifications," 2013.

[160] R. Walker, "Shadow Dextrous Hand Research Systems Dextrous Hand system ,

model C6M," vol. 44, no. 3308007, pp. 1–6, 2009.

[161] D. Shin, I. Sardellitti, Y. L. Park, O. Khatib, and M. Cutkosky, "Design and Control of a Bio-inspired Human-Friendly Robot," in *Springer Tracts in Advanced Robotics*, 2009, vol. 54, pp. 43–52.

[162] T. Lens, J. Kunz, O. Von Stryk, C. Trommer, and A. Karguth, "BioRob-Arm : A Quickly Deployable and Intrinsically Safe , Light- Weight Robot Arm for Service Robotics Applications . Service Robotics for SMEs," in *International Symposium on Robotics and German Conference on Robotics*, 2010, no. Isr, pp. 905–910.

[163] B. K. S. Woods, C. S. Kothera, G. Wang, and N. M. Wereley, "Dynamics of a pneumatic artificial muscle actuation system driving a trailing edge flap," *Smart Mater. Struct.*, vol. 23, no. 9, p. 095014, 2014.

[164] J. Marcincin and A. Palko, "Negative pressure artificial muscle - an unconventional drive of robotic and handling systems," *Trans. Univ. Kosice*, pp. 350–334, 1993.

[165] C. R. Johnson and R. C. Pierce, "Expansible Cover," US2238058, 1941.

[166] H. De Haven, "Tensioning device for producing a linear pull," US2483088, 1949.

[167] A. H. Morin, "Elastic Diaphram," 2642091, 1953.

[168] R. H. Gaylord, "Fluid actuated motor system and stroking device," US2844126, 1958.

[169] W. Gurstelle, "Chapter 9: Joseph McKibben and the Air Muscle," in *ReMaking History, Volume 3*, 1st ed., 2017.

[170] M. Ozkan, K. Inoue, K. Negishi, and T. Yamanaka, "Defining a neural network controller structure for a rubbertuator robot," *Neural Networks*, vol. 13, no. 4–5, pp. 533–544, 2000.

[171] P. van der Smagt, F. Groen, K. Schulten, and P. van der Smagt, "Analysis and control of a rubbertuator arm," *Biol. Cybern.*, vol. 75, no. 5, pp. 433–440, 1996.

[172] R. T. Pack, J. L. Christopher, and K. Kawamura, "A rubbertuator-based structure-climbing inspection robot," *Int. Conf. Robot. Autom.*, no. April, pp. 1869–1874, 1997.

[173] S. Robotics, "Shadow Air Muscle - Specifications," *Manual*, pp. 1–11, 1996.

[174] K. L. Hall, "Dynamic Control for A Pneumatic Muscle Actuator to Achieve Isokinetic Muscle Strengthening," Wright State University, 2011.

[175] K. Mortier, "Braided pneumatic muscles for rehabilitation apparatus," Universiteit Gent, 2014.

[176] S. Davis and D. G. Caldwell, "Braid Effects on Contractile Range and Friction Modeling in Pneumatic Muscle Actuators," *Int. J. Rob. Res.*, vol. 25, no. 4, pp. 359–369, 2006.

[177] G. Krishnan, J. Bishop-Moser, C. Kim, and S. Kota, "Kinematics of a Generalized Class of Pneumatic Artificial Muscles," *J. Mech. Robot.*, vol. 7, no. November, pp. 1–9, 2015.

[178] D. G. Caldwell, G. a. Medrano-Cerda, and C. J. Bowler, "Investigation of bipedal

robot locomotion using pneumatic muscle actuators," *Int. Conf. Robot. Autom.*, vol. 1, 1997.

[179] S. Davis, J. Canderle, P. Artrit, N. Tsagarakis, and D. G. Caldwell, "Enhanced Dynamic Performance in Pneumatic Muscle Actuators," *Proc. 2002 IEEE Int. Conf. Robot. Autom.*, vol. 3, no. May, pp. 2836–2841, 2002.

[180] M. A. Oliver-Salazar, D. Szwedowicz-Wasik, A. Blanco-Ortega, F. Aguilar-Acevedo, and R. Ruiz-González, "Characterization of pneumatic muscles and their use for the position control of a mechatronic finger," *Mechatronics*, vol. 42, pp. 25–40, 2017.

[181] S. Balasubramanian, H. Huang, and J. He, "Quantification of dynamic property of pneumatic muscle actuator for design of therapeutic robot control," *Annu. Int. Conf. IEEE Eng. Med. Biol. - Proc.*, pp. 2734–2737, 2006.

[182] D. B. Reynolds, D. W. Repperger, C. A. Phillips, and G. Bandry, "Modeling the dynamic characteristics of pneumatic muscle," *Ann. Biomed. Eng.*, vol. 31, no. 3, pp. 310–317, 2003.

[183] J. Murillo, "Design of a Pneumatic Artificial Muscle For Powered Lower Limb Prostheses," University of Ottawa, 2013.

[184] B. K. S. Woods, C. S. Kothera, and N. M. Wereley, "Whirl Testing of a Pneumatic Artificial Muscle Actuation System for a Full-Scale Active Rotor," *J. Am. Helicopter Soc.*, vol. 59, no. 2, pp. 1–11, 2014.

[185] F. Daerden, "Conception and Realization of Pleated Pneumatic Artificial Muscles and their Use as Compliant Actuation Elements," p. 176, 1999.

[186] D. G. Caldwell, G. A. Medrano-Cerda, and M. Goodwin, "Control of pneumatic muscle actuators," *IEEE Control Syst. Mag.*, vol. 15, no. 1, pp. 40–48, 1995.

[187] D. Shin, X. Yeh, and O. Khatib, "Circular pulley versus variable radius pulley: Optimal design methodologies and dynamic characteristics analysis," *IEEE Trans. Robot.*, vol. 29, no. 3, pp. 766–774, 2013.

[188] G. Waycaster, S.-K. Wu, T. Driver, and X. Shen, "Design and control of a compact and flexible pneumatic artificial muscle actuation system: Part two - robust control," *ASME 2011 Dyn. Syst. Control Conf. Bath/ASME Symp. Fluid Power Motion Control. DSCC 2011*, vol. 2, pp. 471–478, 2011.

[189] A. Hildebrandt, O. Sawodny, R. Neumann, and A. Hartmann, "Cascaded control concept of a robot with two degrees of freedom driven by four artificial pneumatic muscle actuators," *Am. Control Conf.*, vol. 1, pp. 680–685, 2005.

[190] D. W. Repperger, K. R. Johnson, and C. A. Phillips, "Nonlinear feedback controller design of a pneumatic muscle actuator system," *Am. Control Conf.*, vol. 3, no. June, pp. 1525–1529, 1999.

[191] D. Bergemann, B. Lorenz, and A. Thallemer, "Actuating Means," US 6,349,746 B1, 2002.

[192] D. A. Kingsley, "A cockroach robot with artificial muscles," Case Western Reserve

University, 2005.

[193] R. Walker, “Shadow Project: Shadow Biped,” 2000. [Online]. Available: http://www.shadow.org.uk/projects/biped.shtml. [Accessed: 05-Feb-2017].

[194] David Buckley, “Shadow Biped Walker,” 2007. [Online]. Available: http://davidbuckley.net/DB/ShadBiped.htm. [Accessed: 01-Aug-2017].

[195] B. Verrelst, R. Van Ham, B. Vanderborght, F. Daerden, D. Lefeber, and J. Vermeulen, “The pneumatic biped ‘lucy’ actuated with pleated pneumatic artificial muscles,” *Auton. Robots*, vol. 18, no. 2, pp. 201–213, 2005.

[196] R. Van Ham, F. Daerden, B. Verrelst, D. Lefeber, and J. Vandenhoudt, “Control of Pneumatic Artificial Muscles with Enhanced Speed Up Circuitry,” in *International conference on Climbing and Walking Robots and the Support Technologies for Mobile Machine*, 2002.

[197] R. Van Ham, B. Verrelst, F. Daerden, and D. Lefeber, “Pressure control with on-off valves of Pleated Pneumatic Artificial Muscles in a modular one-dimensional rotational joint.,” *Int. Conf. Humanoid Robot. Karlsruhe Munich*, p. abstract p. 35 + CDROM, 2003.

[198] R. Niiyama and Y. Kuniyoshi, “Design of a Musculoskeletal Athlete Robot: A Biomechanical Approach,” *Mobile Robitcs: Solutions and Challenges, Proc. of the 12th Int. Conf. on Climbing and Walking Robots (CLAWAR 2009)*. pp. 173–180, 2009.

[199] R. Niiyama, S. Nishikawa, and Y. Kuniyoshi, “Athlete robot with applied human muscle activation patterns for bipedal running,” *2010 10th IEEE-RAS Int. Conf. Humanoid Robot. Humanoids 2010*, pp. 498–503, 2010.

[200] X. Wang, M. Li, W. Guo, P. Wang, and L. Sun, “Design and development of a cheetah robot under the neural mechanism controlling the leg’s muscles,” *IEEE Int. Conf. Intell. Robot. Syst.*, pp. 2749–2755, 2012.

[201] D. A. Kingsley, R. D. Quinn, and R. E. Ritzmann, “A Cockroach Inspired Robot with Artificial Muscles,” in *International Conference on Intelligent Robots and Systems*, 2006, pp. 659–666.

[202] I. Boblan and A. Schulz, “A Humanoid Muscle Robot Torso with Biologically Inspired Construction,” *41st Int. Symp. Robot. 6th Ger. Conf. Robot.*, pp. 1–6, 2010.

[203] Festo, “Humanoid Muscle-Robot,” 2006.

[204] Festo, “Airic’s_arm Airic’s_arm Robot arm with Fluidic Muscles,” 2007.

[205] A. Festo, “AirArm,” 2009.

[206] M. Eichhorn *et al.*, “Modelling of the 4-Axis Kinematic Manipulator AirArm Driven by Pneumatic Muscle Actuators,” in *International Conference on Control and Automation*, 2009, vol. 100565, pp. 1301–1307.

[207] C. Ament and M. Eichhorn, “Model-based control design of the compliant robot arm ‘AirArm,’” *Proc. IEEE Int. Conf. Control Appl.*, pp. 334–337, 2010.

[208] “RoboThespian | Engineered Arts Ltd,” 2016. [Online]. Available:

https://www.engineeredarts.co.uk/robothespian/. [Accessed: 08-Aug-2017].

[209] Festo, “RoboThespian: fascinating interaction | Festo Corporate,” 2016. [Online]. Available: https://www.festo.com/group/en/cms/11921.htm. [Accessed: 04-Aug-2017].

[210] D. Shin, F. Seitz, O. Khatib, and M. Cutkosky, “Analysis of torque capacities in hybrid actuation for human-friendly robot design,” *Proc. - IEEE Int. Conf. Robot. Autom.*, pp. 799–804, 2010.

[211] T. Sasaki, T. Nagai, and K. Kawashima, “Remote control of backhoe for rescue activities using pneumatic robot system,” *Proc. - IEEE Int. Conf. Robot. Autom.*, vol. 2006, no. May, pp. 3177–3182, 2006.

[212] T. Sasaki and K. Kawashima, “Remote control of backhoe at construction site with a pneumatic robot system,” *Autom. Constr.*, vol. 17, no. 8, pp. 907–914, 2008.

[213] M. A. M. Dzahir and S. Yamamoto, “Recent Trends in Lower-Limb Robotic Rehabilitation Orthosis: Control Scheme and Strategy for Pneumatic Muscle Actuated Gait Trainers,” *Robotics*, vol. 3, no. 2, pp. 120–148, 2014.

[214] B. G. Do Nascimento, C. B. S. Vimieiro, D. A. P. Nagem, and M. Pinotti, “Hip orthosis powered by pneumatic artificial muscle: Voluntary activation in absence of myoelectrical signal,” *Artif. Organs*, vol. 32, no. 4, pp. 317–322, 2008.

[215] C. B. S. Vimieiro, B. G. do Nascimento, D. A. P. Nagem, and M. Pinotti, “Development of a Hip Orthosis Using Pneumatic Artificial Muscles,” *Technol. Meets Surg. Int.*, pp. 2–6, 2005.

[216] D. P. Ferris, K. E. Gordon, G. S. Sawicki, and A. Peethambaran, “An improved powered ankle-foot orthosis using proportional myoelectric control,” *Gait Posture*, vol. 23, no. 4, pp. 425–428, 2006.

[217] K. E. Gordon, G. S. Sawicki, and D. P. Ferris, “Mechanical Performance of Artificial Pneumaic Muscles to Power an Ankle-foot Orthosis,” *J. Biomech.*, vol. 2, no. c, pp. 4–6, 2006.

[218] G. S. Sawicki and D. P. Ferris, “A pneumatically powered knee-ankle-foot orthosis (KAFO) with myoelectric activation and inhibition.,” *J. Neuroeng. Rehabil.*, vol. 6, p. 23, 2009.

[219] N. Costa, M. Bezdicek, M. Brown, J. Gray, D. Caldwell, and S. Hutchins, “Joint motion control of a powered lower limb orthosis for rehabilitation,” *IEEE Int. J. Autom. Comput.*, vol. 3, pp. 271–281, 2006.

[220] S. Balasubramanian, R. Wei, and J. He, “RUPERT closed loop control design,” *Conf Proc IEEE Eng Med Biol Soc*, vol. 2008, pp. 3467–3470, 2008.

[221] S. Balasubramanian *et al.*, “Rupert: An exoskeleton robot for assisting rehabilitation of arm functions,” *2008 Virtual Rehabil. IWVR*, pp. 163–167, 2008.

[222] T. G. Sugar *et al.*, “Design and control of RUPERT: A device for robotic upper extremity repetitive therapy,” *IEEE Trans. Neural Syst. Rehabil. Eng.*, vol. 15, no. 1, pp. 336–346, 2007.

[223] Y. Muramatsu, H. Umehara, and H. Kobayashi, “Improvement and quantitative performance estimation of the back support muscle suit,” *Proc. Annu. Int. Conf. IEEE Eng. Med. Biol. Soc. EMBS*, pp. 2844–2849, 2013.

[224] Y. Muramatsu and H. Kobayashi, “Assessment of local muscle fatigue by NIRS-development and evaluation of muscle suit-,” *ROBOMECH J.*, vol. 1, no. 19, pp. 623–626, 2014.

[225] Festo, “Fluidic Muscle Established areas of application.”

[226] N. M. Wereley, C. S. Kothera, E. Bubert, B. Woods, M. Gentry, and R. Vocke, “Pneumatic artificial muscles for aerospace applications,” *50th AIAA/ASME/ASCE/AHS/ASC Struct. Struct. Dyn. Mater. Conf.*, no. May, pp. 1–11, 2009.

[227] B. K. S. Woods, “Pneumatic Artificial Muscle Driven Trailing Edge Flaps For Active Rotors,” *ProQuest Diss. Theses*, vol. 3517579, p. 358, 2012.

[228] G. Brown, R. Haggard, and R. Benney, “Parachute retraction soft-landing systems using Pneumatic Muscle Actuators,” *Model. Simul. Technol. Conf.*, no. c, 2000.

[229] S. Dellicker *et al.*, “Steering a Flat Circular Parachute – They Said It Couldn’t Be Done,” *17th AIAA Aerodyn. Decelerator Syst. Technol. Conf. Semin.*, no. May, pp. 1–8, 2003.

[230] M. Pohl, “A motion seat using pneumatic membran actuators in a hexapod system structur,” *Beitrag REM Annecy, Fr.*, 2005.

[231] Festo AG & Co, “Festo Airmotion Simulator,” *Info*.

[232] K. Deckers, P. Guillaume, D. Lefeber, G. De Roeck, and E. Reynders, “Modal testing of bridges using low-weight pneumatic artificial muscle actuators,” *IMAC_XXVI Conf. Expo. Struct. Dyn.*, pp. 1–7, 2008.

[233] C. Dickey, “Air Power,” *Wired*, 2001. [Online]. Available: https://www.wired.com/2001/08/festo/. [Accessed: 15-Aug-2017].

[234] K. Oosterhuis and N. Biloria, “Interactions with proactive architectural spaces,” *Commun. ACM*, vol. 51, no. 6, p. 70, 2008.

[235] T. E. Pillsbury, Q. Guan, and N. M. Wereley, “Comparison of contractile and extensile pneumatic artificial muscles,” *IEEE/ASME Int. Conf. Adv. Intell. Mechatronics, AIM*, vol. 2016-Septe, pp. 94–99, 2016.

[236] B. Tondu and P. Lopez, “Modeling and control of McKibben artificial muscle robot actuators,” *IEEE Control Syst. Mag.*, vol. 20, no. 2, pp. 15–38, 2000.

[237] B. S. Kang, C. S. Kothera, B. K. S. Woods, and N. M. Wereley, “Dynamic modeling of mckibben pneumatic artificial muscles for antagonistic actuation,” *Proc. - IEEE Int. Conf. Robot. Autom.*, pp. 182–187, 2009.

[238] J. E. Takosoglu, P. A. Laski, S. Blasiak, G. Bracha, and D. Pietrala, “Determining the Static Characteristics of Pneumatic Muscles,” *Meas. Control (United Kingdom)*, vol. 49, no. 2, pp. 62–71, 2016.

[239] C.-P. Chou and B. Hannaford, “Static and dynamic characteristics of McKibben

pneumatic artificial muscles," *Proc. 1994 IEEE Int. Conf. Robot. Autom.*, no. 3, pp. 281–286, 1994.

[240] B. Hannaford, J. M. Winters, C. P. Chou, and P. H. Marbot, "The Anthroform Arm: A System for the Study of Spinal Circuit," *Ann. Biomed. Eng. L. Stark Spec. Issue*, vol. 23, pp. 399–408, 1995.

[241] T. E. Pillsbury, C. S. Kothera, and N. M. Wereley, "Effect of bladder wall thickness on miniature pneumatic artificial muscle performance," *Bioinspir. Biomim.*, vol. 10, 2015.

[242] E. Ball and E. Garcia, "Effects of Bladder Geometry in Pneumatic Artificial Muscles," *J. Med. Device.*, vol. 10, no. 4, p. 041001, 2016.

[243] J. H. Lilly and L. Yang, "Sliding mode tracking for pneumatic muscle actuators in opposing pair configuration," *IEEE Trans. Control Syst. Technol.*, vol. 13, no. 4, pp. 550–558, 2005.

[244] M. Doumit and J. Leclair, "Development and testing of stiffness model for pneumatic artificial muscle," *Int. J. Mech. Sci.*, vol. 120, no. November 2016, pp. 30–41, 2017.

[245] M. Focchi *et al.*, "Water/air performance analysis of a fluidic muscle," *IEEE/RSJ 2010 Int. Conf. Intell. Robot. Syst. IROS 2010 - Conf. Proc.*, pp. 2194–2199, 2010.

[246] Z. Zhang, J. Hou, D. Ning, X. Gong, and Y. Gong, "Modeling and experiments on the drive characteristics of high-strength water hydraulic artificial muscles," *Smart Mater. Struct.*, vol. 26, no. 5, p. 055023, 2017.

[247] K. Iwata, K. Suzumori, and S. Wakimoto, "A method of designing and fabricating Mckibben muscles driven by 7 MPa hydraulics," *Int. J. Autom. Technol.*, vol. 6, no. 4, pp. 482–487, 2012.

[248] M. Mori, K. Suzumori, S. Seita, M. Takahashi, T. Hosoya, and K. Kusumoto, "Development of very high force hydraulic McKibben artificial muscle and its application to shape-adaptable power hand," *2009 IEEE Int. Conf. Robot. Biomimetics, ROBIO 2009*, pp. 1457–1462, 2009.

[249] K. C. Wickramatunge and T. Leephakpreeda, "Empirical modeling of dynamic behaviors of pneumatic artificial muscle actuators," *ISA Trans.*, vol. 52, no. 6, pp. 825–834, 2013.

[250] S. Davis and D. Caldwell, "Pneumatic Muscle Actuators for Humanoid applications - Sensor and Valve Integration," *2006 6th IEEE-RAS Int. Conf. Humanoid Robot.*, pp. 456–461, 2006.

[251] G. K. Klute and B. Hannaford, "Accounting for Elastic Energy Storage in McKibben Artificial Muscle Actuators," *J. Dyn. Syst. Meas. Control*, vol. 122, no. 2, p. 386, 2000.

[252] N. Tsagarakis and D. G. Caldwell, "Improved modelling and assessment of pneumatic muscle actuators," *Proc. 2000 ICRA. Millenn. Conf. IEEE Int. Conf. Robot. Autom. Symp. Proc. (Cat. No.00CH37065)*, vol. 4, pp. 3641–3646, 2000.

[253] M. Doumit, A. Fahim, and M. Munro, "Analytical modeling and experimental

validation of the braided pneumatic muscle," *IEEE Trans. Robot.*, vol. 25, no. 6, pp. 1282–1291, 2009.

[254] G. Zuglian, L. Corrêa, and G. Geremia, "Static Modeling of Mckibben Pneumatic Muscle," *ABCM Symp. Ser. Mechatronics*, vol. 4, pp. 914–922, 2009.

[255] L. Peternel, B. Ugurlu, J. Babic, and J. Morimoto, "Assessments on the improved modelling for pneumatic artificial muscle actuators," *Proc. 17th Int. Conf. Adv. Robot. ICAR 2015*, pp. 34–39, 2015.

[256] A. Hildebrandt, O. Sawodny, R. Neumann, and A. Hartmann, "A Cascaded Tracking Control Concept for Pneumatic Muscle Actuators," *2003 Eur. Control Conf.*, pp. 2517–2522, 2003.

[257] V. Hill, "The heat of shortening and the dynamic constants of muscle," *Philos. Trans. R. Soc. London*, 1938.

[258] G. K. Klute, J. M. Czerniecki, and B. Hannaford, "Artificial muscles: Actuators for biorobotic systems," *Int. J. Rob. Res.*, vol. 21, no. 4, pp. 295–309, 2002.

[259] J. Pitel and M. Tóthová, "Dynamics of Pneumatic Muscle Actuator: Measurement and Modeling," in *International Carpathian Control Conference (ICCC)*, 2011, pp. 1–4.

[260] B. Tondu and S. D. Zagal, "McKibben artificial muscle can be in accordance with the Hill skeletal muscle model," *First IEEE/RAS-EMBS Int. Conf. Biomed. Robot. Biomechatronics*, no. 3, pp. 714–720, 2006.

[261] G. K. Klute, J. M. Czerniecki, and B. Hannaford, "McKibben artificial muscles: pneumatic actuators with biomechanical Intelligence," *1999 IEEE/ASME Int. Conf. Adv. Intell. Mechatronics (Cat. No.99TH8399)*, pp. 1–6, 1999.

[262] L. Sui and S. Xie, "Modelling of pneumatic muscle actuator and antagonistic joint using linearised parameters," *Int. J. Biomechatronics Biomed. Robot.*, vol. 2, no. 2/3/4, pp. 67–74, 2013.

[263] D. W. Repperger, K. R. Johnson, and C. A. Phillips, "A VSC Position Tracking System involving a large Scale Pneumatic Muscle Actuator," *IEEE Conf. Decis. Control*, vol. 4, no. December, pp. 4302–4307, 1998.

[264] J. L. Serres, D. B. Reynolds, C. A. Phillips, M. J. Gerschutz, and D. W. Repperger, "Characterisation of a phenomenological model for commercial pneumatic muscle actuators.," *Comput. Methods Biomech. Biomed. Engin.*, vol. 12, no. 4, pp. 423–30, 2009.

[265] Y. C. Fung, *Biomechanics Mechanical Properties of Living Tissues*. Springer, 1993.

[266] J. L. Serres, "Dynamic Characterization of a Pneumatic Muscle Actuator and its Application to a Resistive Training Device," Wright State University, 2008.

[267] S. W. Chan, J. H. Lilly, D. W. Repperger, and J. E. Berlin, "Fuzzy PD+I learning control for a pneumatic muscle," *12th IEEE Int. Conf. Fuzzy Syst.*, vol. 1, pp. 278–283, 2003.

[268] V. Sakthivelu, S. H. Chong, M. H. Tan, and M. M. Ghazaly, "Phenomenological modeling and classic control of a pneumatic muscle actuator system," *Int. J.*

Control Autom., vol. 9, no. 4, pp. 301–312, 2016.

[269] S. Balasubramanian, J. Ward, T. Sugar, and J. He, "Characterization of the Dynamic Properties of Pneumatic Muscle Actuators," *IEEE 10th Int. Conf. Rehabil. Robot.*, vol. 00, no. c, pp. 764–770, 2007.

[270] R. W. Colbrunn, G. M. Nelson, and R. D. Quinn, "Modeling of braided pneumatic actuators for robotic control," *IEEE Int. Conf. Intell. Robot. Syst.*, vol. 4, no. February, pp. 1964–1970, 2001.

[271] B. Tondu, "Modelling of the McKibben artificial muscle: A review," *J. Intell. Mater. Syst. Struct.*, vol. 23, no. 3, pp. 225–253, 2012.

[272] S. Ganguly, A. Garg, A. Pasricha, and S. K. Dwivedy, "Control of pneumatic artificial muscle system through experimental modelling," *Mechatronics*, vol. 22, no. 8, pp. 1135–1147, 2012.

[273] P. Scarfe and E. Lindsay, "Air muscle actuated low cost humanoid hand," *Int. J. Adv. Robot. Syst.*, vol. 3, no. 1, pp. 139–146, 2006.

[274] D. Majoe, L. Widmer, and J. Gutknecht, "Pneumatic air muscle and pneumatic sources for light weight autonomous robots," *Proc. - IEEE Int. Conf. Robot. Autom.*, pp. 3243–3250, 2011.

[275] T. Kitamori, A. Wada, H. Nabae, and K. Suzumori, "Untethered Three-Arm Pneumatic Robot using Hose-free Pneumatic Actuator," pp. 543–548, 2016.

[276] T. Driver and X. Shen, "Sleeve Muscle Actuator: Concept and Prototype Demonstration," *J. Bionic Eng.*, vol. 10, no. 2, pp. 222–230, 2013.

[277] T. Driver and X. Shen, "Design and Control of a Sleeve Muscle-Actuated Robotic Elbow," *J. Dyn. Syst. Meas. Control*, vol. 136, no. July 2014, p. 041023, 2014.

[278] H. Zheng and X. Shen, "Sleeve Muscle Actuator and Its Application in Transtibial Prostheses," in *IEEE Int Conf Rehabil Robot.*, 2013, vol. 18, no. 11, pp. 1492–1501.

[279] T. A. Driver, "Innovation for powered prostheses utilizing pneumatic actuators," The University of Alabama, 2012.

[280] H. Zheng and X. Shen, "Double-Acting Sleeve Muscle Actuator for Bio-Robotic Systems," *Actuators*, vol. 2, no. 4, pp. 129–144, 2013.

[281] D. Villegas, M. Van Damme, B. Vanderborght, P. Beyl, and D. Lefeber, "Third–Generation Pleated Pneumatic Artificial Muscles for Robotic Applications: Development and Comparison with McKibben Muscle," *Adv. Robot.*, vol. 26, no. 11–12, pp. 1205–1227, 2012.

[282] R. W. Colbrunn, G. M. Nelson, and R. D. Quinn, "Design and control of a robotic leg with braided pneumatic actuators," Case Western Reserve University, 2000.

[283] D. Buchler, H. Ott, and J. Peters, "A lightweight robotic arm with pneumatic muscles for robot learning," *Proc. - IEEE Int. Conf. Robot. Autom.*, vol. 2016-June, pp. 4086–4092, 2016.

[284] Y. J. Kim, "Design of low inertia manipulator with high stiffness and strength using

tension amplifying mechanisms," *IEEE Int. Conf. Intell. Robot. Syst.*, vol. 2015-Decem, pp. 5850–5856, 2015.

[285] V. Technoex, "Vena® technoex," p. 2014, 2014.

[286] Honeywell, "TruStability Board Mount Pressure Sensors HSC Series—High Accuracy, Compensated/Amplified," 2014.

[287] MGF, "Silent Car Lubricated from 100 LT, SIL-EOL 50/100 CAR."

[288] Matrix SpA, "Solenoid Valves 720 series 2/2 3/2," 2017.

[289] LCM Systems Ltd, "STA-1 Aluminium S Type Tension & Compression Load Cell," 2015.

[290] Mantracourt Electronics Ltd., "DSC Digital Strain Gauge to Data Converter," 2011.

[291] Novotechnik U.S Inc., "Position Transducer potentiometric up to 150 mm Series T / TS," 2014.

[292] Texas Instruments, "ADS111x Ultra-Small, Low-Power, I2C-Compatible, 860-SPS, 16-Bit ADCs With Internal Reference, Oscillator, and Programmable Comparator," 2018.

[293] CUI Inc., "Series : Amt20," 2016.

[294] adafruit, "PCA9685 - product data sheet," 2015.

[295] M. Sirotti, "Tubo in lattice 'DRELAX' (TDS 1416)," 2016.

[296] Techflex, "Flexo Tight Weave - General Purpose Technical Data Sheet," 2018.

[297] E. A. Bubert, "Highly Extensible Skin for a Variable Wing-Span Morphing Aircraft Utilizing Pneumatic Artificial Muscle," University of Maryland, 2009.

[298] J. L. Serres, D. B. Reynolds, C. A. Phillips, D. B. Rogers, and D. W. Repperger, "Characterisation of a pneumatic muscle test station with two dynamic plants in cascade," *Comput. Methods Biomech. Biomed. Engin.*, vol. 13, no. 1, pp. 11–18, 2010.

[299] ISO, "ISO6358 -Pneumatic fluid power - Determination of flow-rate characteristics of components using compressible fluids," 2014.

[300] Matrix SpA, "CURVE di porta BX721 serie." p. 7, 2018.

[301] E. Richer and Y. Hurmuzlu, "A High Performance Pneumatic Force Actuator System: Part II—Nonlinear Controller Design," *J. Dyn. Syst. Meas. Control*, vol. 122, no. 3, p. 426, 2000.

[302] K. P. Tee, E. Burdet, C. M. Chew, and T. E. Milner, "A model of force and impedance in human arm movements," *Biol. Cybern.*, vol. 90, no. 5, pp. 368–375, 2004.

[303] M. Sekine, R. Kokubun, and W. Yu, "Investigating the Effect of a Mechanism Combined with a Speed-Increasing Gear and a Pneumatic Artificial Muscle," *Actuators*, vol. 7, no. 2, p. 22, 2018.

APPENDIX A: EVALUATING ROBOT IMPACTS

This section reports on the ways in which to evaluate the severity of different types of robot impacts with humans.

BLUNT UNCONSTRAINED IMPACTS

In order to establish the severity of collisions and the risk of injury a number of performance metrics have been proposed, though none has been universally accepted[1]. By far the most popular is the Head Injury Criterion (HIC) [2]–[7] used for unconstrained blunt impacts. This empirical formula was developed by the automotive industry to correlate head acceleration and the severity of the impact as a predictor for skull fracture and brain injury. It is defined as:

$$HIC_{\Delta t} = max_{t1,t2}\left[\Delta t\left(\frac{1}{\Delta t}\int_{t1}^{t2} a(t)dt\right)^{\frac{5}{2}}\right] \quad \text{(A.1)}$$

Where Δt is the time over which the impact occurs ($t2$ - $t1$) and $a(t)$is the acceleration of the head (measured in "g"= 9.81m/s^2) during this time. Therefore this criteria accounts for both the magnitude of the acceleration and its duration. This allows for the fact that the head may be exposed to relatively large accelerations so long as it is for a short period of time [8]. It should be noted that the HIC itself does not directly correspond to head injury, but rather it can be correlated with the Abbreviated Injury Scale (AIS) which ranks injuries from 0 (no injury) to 6 (fatal) [9], [10]. The HIC index may then be used to quantify the potential for head injury. A simple two degree of freedom mass spring model can be used to predict the head acceleration caused by an impact [2]. This allows the identification of parameters which increase the likelihood of injury. Equation (A.2) shows the result of this (in SI units) [4].

$$HIC_{15} = 0.00433\left(\frac{K_{conv}}{M_{oper}}\right)^{\frac{3}{4}}\left(\frac{M_{rob}}{M_{rob}+M_{oper}}\right)^{\frac{7}{4}} v^{\frac{5}{2}} \quad \text{(A.2)}$$

Where K_{conv} is the stiffness of the material on the arm at the point of collision, M_{oper} is the operator mass (usually of the head), M_{rob} is the effective inertia of the

robot composed of the mass of the link and the reflected rotor inertia (coming from the actuator moving the joint) and v is the velocity of the robot.

The most significant component is the actuator velocity, but the effective mass of the actuator and the compliance of the material covering the robot can also be altered [5]. Several authors have studied the use of padding on the robot to improve safety characteristics, but this is largely irrelevant to actuation. The robot's effective mass can also be reduced. The most obvious way to do this is to reduce the robot's mass [3], [11]–[13]. This can be accomplished by using lightweight materials for the robot's construction, including the systems used for actuation. Figure A1 demonstrates the effect of altering the robot's mass. The HIC value for small masses is much reduced, however for large masses the HIC value reaches a maximum. This saturation effect is explained intuitively in [13]. If a very heavy robot collides with a person at 2m/s this would be equivalent to a person walking into a rigid wall at 2 m/s.

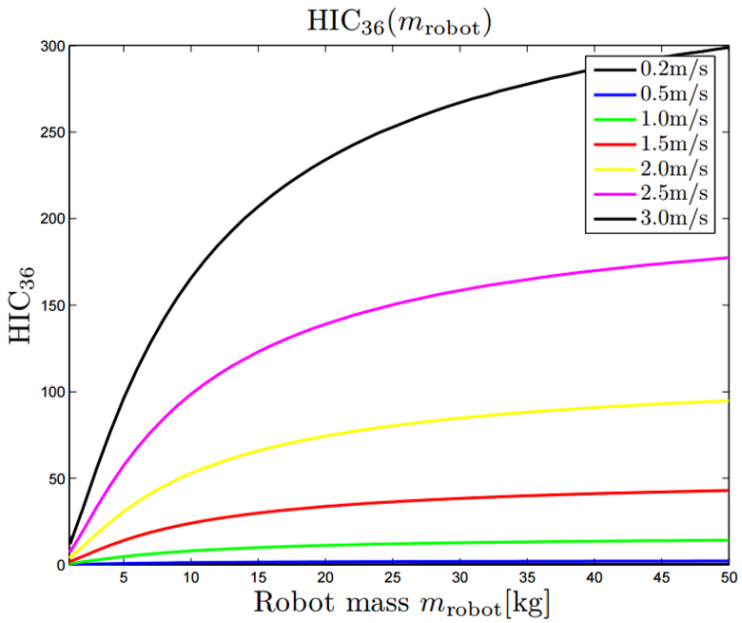

Figure A1: HIC values from simulation for a 1 degree of freedom robot with varying robot link mass and velocity [8]***.***

Further reductions in effective mass can be achieved by introducing compliance to the system. By reducing the stiffness with which limbs are attached to their actuators, the reflected inertia through the actuator can be significantly reduced

as the joint is partially decoupled from the actuator. The robot mass from equation (A.2) becomes[5], [14]:

$$M_{rob} = M_{link} + \left(\frac{K_{transm}}{K_{transm} + \gamma}\right) M_{rot} \qquad \text{(A1.3)}$$

Where M_{link} is the mass of the robot link, γ is the stiffness of the rigid coupling, K_{transm} is the stiffness of the introduced compliance and M_{rot} is the rotor inertia of the actuator. Figure A2 shows the effect of joint stiffness on HIC. The effect is most noticeable at high speeds.

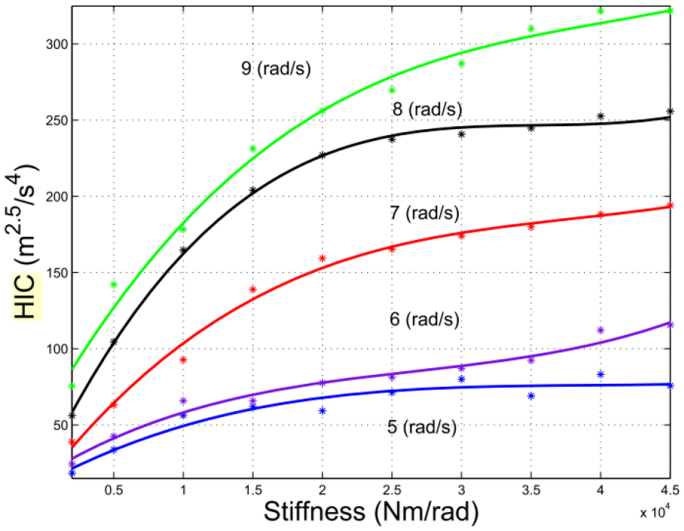

Figure A2: Experimental HIC results for a one degree of freedom system at various speeds. The arm is actuated by a variable stiffness actuator (VSA) which allows the stiffness of the interface between actuator and limb to be altered. Note the units are different to that usually associated with HIC as m/s² are used as acceleration instead of g. This gives a multiplication factor of approximately 300 of the numeric values [15].

While the HIC has been used extensively in the literature and helps identify methods to improve the safety of robots [3], [14], [16], it has been found to be unsuitable for actually assessing the injury caused by robots as the HIC values calculated or measured are too small to cause head injuries[13]. This is due to the relatively low speeds (typically up to 2 m/s) involved in these interactions, as opposed to those typical in automotive scenarios. This means that the HIC values are typically of the order of 2-60s [10]. As Figure A3 shows, this is not nearly enough to cause a brain injury, though they may of course cause other injuries. The reason why this metric became so popular may be due to an error in a number of

publications such as [2], [3], [5], [14] whereby the acceleration in terms of m/s^2 was used instead of g, leading to a much higher numeric HIC value. This lead to an overestimation of the potential for injury in these publications as this was not accounted for [4], [17]. Despite this criticism the metric still provides a basis to identify factors which affect safety and compare levels of safety [15], [18]. As noted in [18], "there is still a long way to go between "unlikely to be life-threatening" and "suitable for physical human-robot interaction""

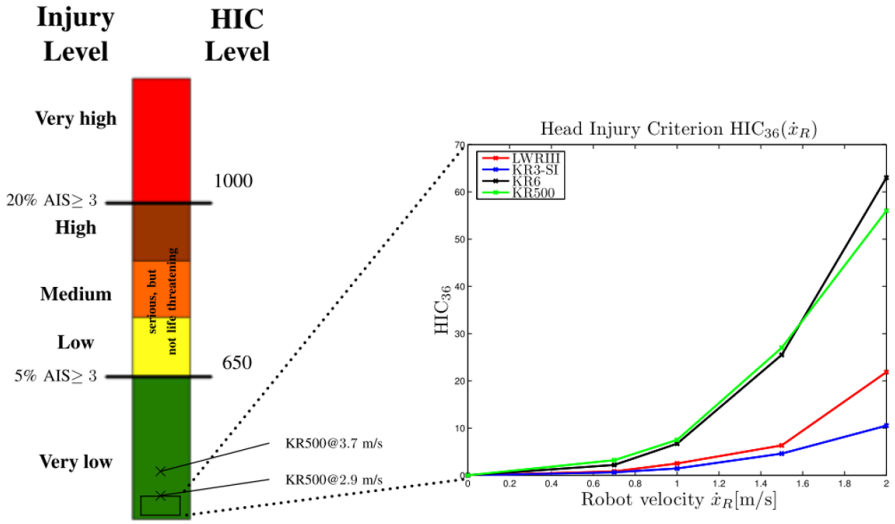

Figure A3: Experimental HIC_{36} values for a number of robots with different operating speeds [10]***. All values rate quite low on the AIS scale.***

Due to the unsuitability of HIC as an "absolute" measure of safety, other metrics have been suggested. A number of these come from the automotive industry and have been applied both experimentally and in simulation. Table A1 details indices which were experimentally applied in a crash testing facility for a number of robots of varying mass and construction [17]. Where appropriate the European New Car Assessment Programme (EuroNCAP) safety rating was used to evaluate the AIS from these indices. Similar approaches are discussed in [8], [10], [13], [19]. There are also some robot specific criteria such as Safety Index for Robotics (SIR),the New Safety Index for Robotics (NIR)[20], [21], and the Manipulator Safety Index (MSI) [16], which are all based on the HIC. While the metrics differ from the HIC in how they are applied and evaluated, the requirements they identify for safe pHRI are

similar; that is, low inertia (both through low mass and compliant joints), a suitable compliant covering and restricted velocity.

Severity Index	Body part	Symbol	EuroNCAP
Contact force	head	$F_{\text{ext}}^{\text{frontal}}$	No
Contact force	head	$F_{\text{ext}}^{\text{mandible}}$	No
Head Injury Criterion	head	HIC_{36}	Yes
Maximum res. acceleration	head	$a_{\text{max}}^{\text{head}}$	Yes
3 ms criterion	head	$a_{3\text{ms}}^{\text{head}}$	Yes
Shearing neck force	neck	F_x	Yes
Shearing neck force	neck	F_y	Yes
Tension/compression force	neck	F_z	Yes
Flexion neck torque	neck	$M_{y,OC}^{\text{Flex}}$	No
Extension neck torque	neck	$M_{y,OC}^{\text{Ext}}$	Yes
Contact force	chest	$F_{\text{ext}}^{\text{chest}}$	No
Compression Criterion	chest	CC	Yes
Viscous Criterion	chest	VC	Yes
3 ms Criterion	chest	$a_{3\text{ms}}^{\text{chest}}$	No

Table A1: evaluated injury indices in [80]. Note not all of these are applicable for unconstrained impacts as discussed below.

BLUNT CONSTRAINED IMPACTS

Constrained impacts are a far less studied cause of injury in robotics. It relates to instances where a human is caught between the robot and a fixed object or another part of the robot producing a clamping effect. It is perhaps most thoroughly considered by Haddadin [10]. Here dynamic clamping, where the robot is moving at speed and traps a human against a rigid object is analysed. It is necessary to assume that the robot can detect and react to collisions as the industrial robots tested would certainly have the capacity to injure a human if their full force was applied without restriction. The DLR- Lightweight Robot III (LWRIII), which is designed to operate safely with humans (being lightweight and possessing torque sensing) was compared against a range of industrial robots of varying sizes in simulation in constrained chest impacts. The LWRIII results were also verified using a Hybrid III Dummy. The results for chest impacts are summarised in [17]. Three indices are used here. The compression criterion (CC) is the amount by which the chest is compressed and quantifies the risk of injury by crushing. This is supplemented by the viscous criterion (VC) which assesses the risk of soft tissue

injury by a rate-dependent viscous injury mechanism [22]. In both cases the results are correlated with the AIS using the EuroNCAP (green being very low chance of injury, and red fatal). The contact force is also provided. Clearly the likelihood of injury from this kind of collision is much greater than that for unconstrained collisions. Crushing type injuries also seem to be dominant rather than acceleration dependant mechanisms. Similar analysis is found in [13], [17], [19]. The main robot parameters which increase the severity of injury in these cases are speed and mass, though it is clear that the compliance of the robot/human interface material as well as the joint compliance will also play a role.

ROBOT	CC[mm]	VC[m/s]	F^x_{ext}[N]
LWRIII	14.4(0.0)	0.035	741.6(1.3)
KR3 (Cat.0)	31.2(0.0)	0.1	851.9(1.4)
KR6 (Cat.0)	65.5(2.0)	0.25	2836.1(2.7)
KR6 (Cat.1)	66.6(2.1)	0.25	2904.6(2.7)
KR500 (Cat.0)	228.0(6.0)	0.84	14282.0(6.0)
KR500 (Cat.1)	245.0(6.0)	0.89	15491.0(6.0)

Table A2: A summary of simulation results for chest impacts of a human restrained in a seat, impacted by a robot travelling at 2 m/s. These are correlated with the EuroNCAP rating for injury severity. In the case of the industrial robots (KR3, KR6 KR500), the number represents the approximate payload in Kg [22].

Static blunt impacts have also been considered in the literature. The most dangerous scenario here is when a person is impacted close to a singularity [17] (as depicted in Figure A4) In this configuration the robot arm is theoretically capable of infinitely large forces, though the velocity is quite low. The contact force was used as an indicator of injury, being compared to the force required to break the frontal bone of the skull (approximately 4kN). For the LWRIII robotic arm the measured forces were considerably less than that required to fracture the skull (Figure A4, right). This is due to a low level system which limits joint torque on the joints, even when the robot does not actively respond to the collision. Other

approaches which limit output force, such as compliant actuation could also be suitable here.

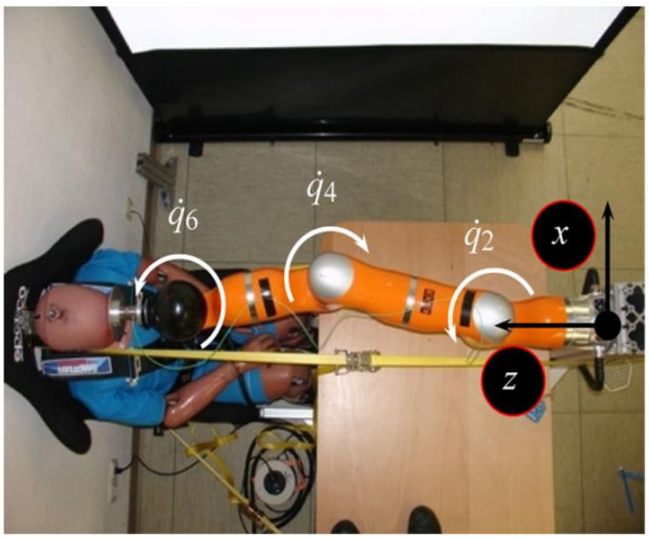

Exp. Nr.	Robot	Strategy	d_s [mm]	$F_{\max}^{\text{static}}$ [N]	$F_{\max}^{\text{peak}}$ [N]
*L*13	LWR-III	0	10	0	✓692
*L*14		0	10	674	✓1244
*L*15		1	10	277	✓540
*L*16		2	10	0	✓590
*L*19		0	5	0	✓1593
*L*17		1	5	256	✓505
*L*18		2	5	0	✓617

Figure A4: DLR LWRIII impacting a crash test dummy (left). The arm is close to a singularity here, making in capable of large forces. The results of testing for impacts in this configuration are also shown (right). Strategy 0 denotes the robot does not react to the impact, strategy 1 stops the robot immediately and strategy 2 switches to torque control with gravity compensation. [17]

NON-BLUNT IMPACTS

For practical applications it may be desirable that robots operate tools, such as when cutting bread or preparing meals. These can often make the robot more dangerous as they can introduce sharp edges as well as reduce the capacity of sensing, especially tactile sensing. Again injury arising from this kind of pHRI is poorly studied, perhaps due to the complexity of the interactions given the number of tools which could be considered. A worst case situation was examined by Haddadin with the LWRIII, where a stabbing motion with a range of sharp implements was considered [19], [23]. Pig specimens were used to simulate human tissue (Figure A5), though it is acknowledged that this is not a perfect representation. It was found that even with the LWRIII, if collision detection is not used, the robot will penetrate deeply into the flesh with tools such as a steak knife, scissors, kitchen knife and scalpel even at velocities as low as 0.16 m/s. With

collision detection this is drastically improved, with no penetration at this speed in all but the case of the scalpel, and very small penetration at faster speeds.

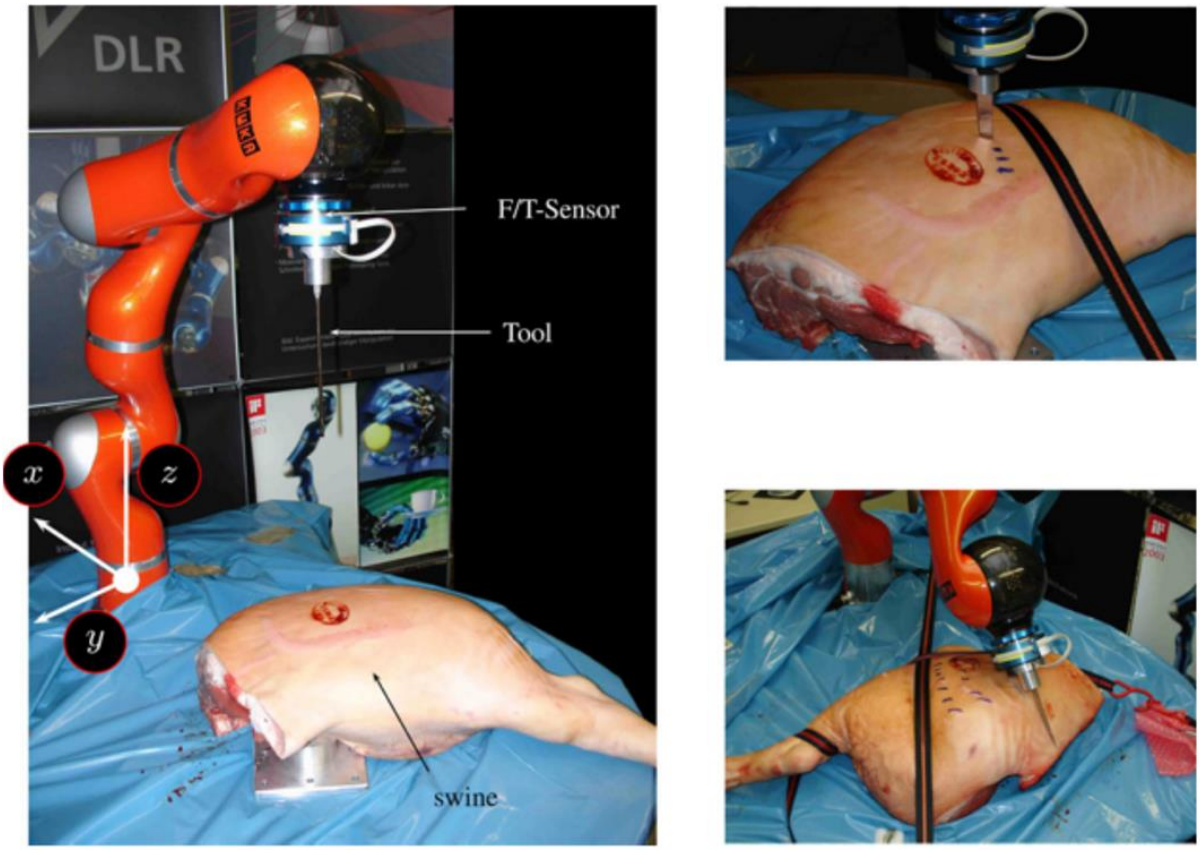

Figure A5 Testing with sharp objects with pig specimens [23]

Subsequently, in [24] a comprehensive range of tests is conducted to evaluate the effect of a number of factors including shape of the end effector on injury severity. Again pig specimens are used. The AO (Arbeitsgemeinschaft für Osteosynthesefragen [25]) scale is used to quantify the severity of soft tissue injuries. This scale classifies the injury based on the level of damage itself, rather than the potential for injury as is the case for other indices such as the HIC. Drop tests were conducted to establish safe operating speeds for a range of different shapes and masses of object. This allowed safety curves to be developed which place an upper limit of the speed of operation of robots which feature or carry objects of this type. This is correlated against effective mass of the robot which is dependent on the mass and compliance of the system.

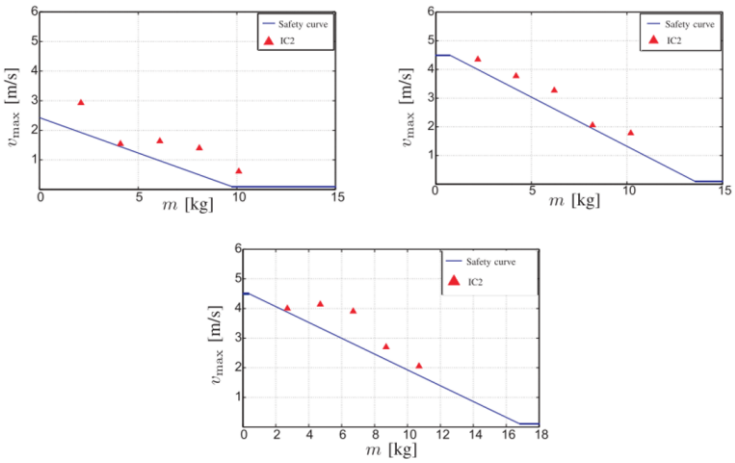

Figure A6: Safety curves for a 5mm radius sphere (top left), 12.5mm sphere (top right) and 45 wedge bottom. These curves remain below the IC2 injury level defined as contusion without skin opening [24]***.***

REFERENCES

[1] T. S. Tadele, T. J. A. De Vries, S. Stramigioli, and S. Member, “Safety in Domestic Robotics : A Survey,” pp. 1–8, 2014.

[2] M. Zinn, O. Khatib, B. Roth, and J. K. Salisbury, “Towards a human-centered intrinsically-safe robotic manipulator.,” *IEEE Robot. Autom. Mag.*, vol. 11, no. 2, pp. 12–21, 2004.

[3] M. Zinn, B. Roth, O. Khatib, and J. K. Salisbury, “A New Actuation Approach for Human Friendly Robot Design,” *Int. J. Rob. Res.*, vol. 23, no. 4, pp. 379–398, 2004.

[4] D. Gao and C. W. Wampler, “Assessing the Danger of Robot Impact,” no. December, pp. 13–16, 2009.

[5] A. Bicchi and G. Tonietti, “Fast and ‘soft-arm’ tactics: Dependability in Human-Friendly Robots,” *IEEE Robot. Autom. Mag.*, vol. 11, no. 2, pp. 22–33, 2004.

[6] D. Gao and C. W. Wampler, “Head injury criterion,” *IEEE Robot. Autom. Mag.*, vol. 16, no. 4, pp. 71–74, 2009.

[7] S. Haddadin, A. Albu-Schäffer, and G. Hirzinger, “Approaching Asimov’s 1st law: The impact of the robot’s weight class,” *Robot. Sci. …*, pp. 1–6, 2007.

[8] S. Haddadin, A. Albu-schäffer, and G. Hirzinger, “Safety evaluation of physical human-robot interaction via crash-testing,” 2007.

[9] O. Ogorodnikova, “Human Robot Interaction : The Safety Challenge (An integrated frame work for human safety), PhD dissertation,” p. 114, 2010.

[10] S. Haddadin, M. Frommberger, and G. Hirzinger, “The Role of the Robot Mass and Velocity in Physical Human-Robot Interaction - Part I: Non-constrained Blunt Impacts,” no. 011838, pp. 1339–1345, 2008.

[11] J. Heinzmann and A. Zelinsky, “Quantitative Safety Guarantees for Physical Human-Robot Interaction,” *Int. J. Rob. Res.*, vol. 22, no. 7–8, pp. 479–504, 2003.

[12] N. Sporer, M. Hdmle, R. Krenn, a Pascucci, and M. Schedl, “DLR’s torque-controlled light weight robot,” *Mechatronics*, no. May, pp. 1710–1716, 2002.

[13] S. Haddadin, a. Albu-Schaffer, and G. Hirzinger, “Requirements for Safe Robots: Measurements, Analysis and New Insights,” *Int. J. Rob. Res.*, vol. 28, no. 11–12, pp. 1507–1527, 2009.

[14] A. L. Edsinger, “Robot Manipulation in Human Environments,” Massachusetts Institute of Technology, 2007.

[15] A. Bicchi *et al.*, “Physical human-robot interaction: Dependability, safety, and performance,” *Int. Work. Adv. Motion Control. AMC*, vol. 1, pp. 9–14, 2008.

[16] M. Zinn, O. Khatib, B. Roth, and J. K. Salisbury, “Playing it safe: Dependability in Human-Friendly robots,” *IEEE Robot. Autom. Mag.*, vol. 11, no. 2, pp. 12–21, 2004.

[17] S. Haddadin, A. Albu-sch, M. Frommberger, and G. Hirzinger, “The ‘ DLR Crash Report ’: Towards a Standard Crash-Testing Protocol for Robot Safety - Part II : Discussions,” pp. 272–279, 2009.

[18] M. Van Damme *et al.*, “The Role of Compliance in Robot Safety,” *IARP Work. Tech. Challenges Dependable Robot. Hum. Environ.*, no. 231554, pp. 65–71, 2010.

[19] S. Haddadin, A. Albu-Schäffer, and G. Hirzinger, “Safety analysis for a human-friendly manipulator,” *Int. J. Soc. Robot.*, vol. 2, no. 3, pp. 235–252, 2010.

[20] J. EchÃ¡varri *et al.*, “Towards a safety index for assessing head injury potential in service robotics,” *Adv. Robot.*, vol. 27, no. 11, pp. 831–844, 2013.

[21] C. A. Cordero, G. Carbone, M. Ceccarelli, J. Echávarri, and J. L. Muñoz, “Experimental tests in human-robot collision evaluation and characterization of a new safety index for robot operation,” *Mech. Mach. Theory*, vol. 80, pp. 184–199, 2014.

[22] L. Ian and V. David C., “The viscous criterion - Bases and applications of an

injury severity index for soft tissues," Oct. 1986.

[23] S. Haddadin, A. Albu-Schaeffer, F. Haddadin, J. Rossmann, and G. Hirzinger, "An Experimental Safety Study for Stab/Puncture and Incised Wounds," *iEEE Robot. Autom. Mag.*, no. December, pp. 20–34, 2011.

[24] S. Haddadin *et al.*, "On making robots understand safety: Embedding injury knowledge into control," *Int. J. Rob. Res.*, vol. 31, no. 13, pp. 1578–1602, 2012.

[25] T. P. Ruedi, R. E. Buckley, and C. G. Moran, *AO Principles of Fracture Management. second expanded ed*. 2007.

APPENDIX B: TYPES OF PAM

In this section, for reasons of brevity, only muscles which produce primarily a contractile force are considered. While pneumatic muscle like actuators do exist which are designed to supply an extensile force (for example [1], [2]), these usually cannot exert large forces as the lack of a structural element causes them to buckle. However they can be made to have much larger stroke lengths [3]. Extensile muscles are primarily used in soft robotics, while contractile muscles are more applicable to traditional robot morphologies which maintain a structural frame.

STRAIGHT FIBRE MUSCLES

Rather than a double helix arrangement of the load carrying fibres, muscles with fibres running straight between the end-fittings have been developed. In general they make use of an elastic membrane to enclose the air and act on these fibres. The operating principle of the straight fibre PAM is simpler than that of the McKibben muscle. The elastic bladder, when inflated pushes out on the fibres and the radius of the structure increases. As the fibres are inelastic, this pulls the end fittings closer together.

Baldwin suggests straight fibre muscles can provide increased force output, improved efficiency, less hysteresis and a lower threshold pressure than McKibben type muscles as there is no friction between the muscle fibres [4]. Pressure is however limited due to the wide, unsupported spans of the elastic membrane as the muscle inflates. However, even at pressures as low as 100 kPa forces of up to 1600N were reported as well as a fatigue life of up to 30,000 cycles.

A mathematical description of the forces in straight fibre muscles is given in [5]. Using this model the geometric properties of the muscle are analysed such as the original length and radius. It is shown that there is a limit on the initial length of the muscle for a given radius. As this length is increased the strain in the elastic muscle membrane, when the muscle is inflated, exceeds that admissible by the material properties of the membrane [5] (in the case of the study, 450%).

This issue, as well as the large volume occupied by this type of actuator when inflated were addressed by researchers who used solid rings to restrict the muscles expansion. This effectively breaks the muscle up into multiple muscles operating in series. Nakamura et.al. developed a new manufacturing process for the straight fibre muscle by embedding the fibres directly into a latex rubber membrane which was built up in layers from liquid latex [6]. The muscle developed was 70mm long with a diameter of 13mm. It was possible to achieve contraction ratios as high as 27%. Experiments were conducted to establish the number of containing rings for optimal muscle performance. With one containing ring in place at the centre of the muscle, the contraction can be increased to 35%. The addition of two rings only provided 23% contraction at the same pressure, and so a single ring for a muscle with this length and radius is deemed appropriate. Later a muscle with the same design, but using Silicone instead of latex was used for a robotic arm by the same research group [7]. This muscle was tested to 200 kPa, produced 20.5 % contraction (the muscle was 50mm long), had a maximum force output of 350N and had a mass of 45g. Kamo built upon these results, creating longer actuators with more supporting rings, and using them in a 6DOF arm [8]. A further mathematical analysis of this type of muscle is given in [9], where the shape of the cross section of the muscle in the longitudinal direction (along a plane which cuts both the end fittings) is considered as a catenary rather than circular as was previously assumed. The contraction and force output showed better agreement with experimental data than previous models.

Bertetto conducted a comparison between McKibben muscles and straight fibre muscles using a combination of finite element analysis and experimentation [10]. It was found that at similar pressures, at zero contraction, the straight fibre muscle could produce five times more force than the McKibben muscle. However contraction ratios with the McKibben is greater the straight fibre muscle only achieving 4.5% contraction owing to is greater radial deformation. This result stands in contrast however to the previously discussed results where far larger contractions were demonstrated.

Wirekoh[11] presents an interesting adaptation of the straight fibre PAM in the form of a flat pneumatic muscle. Silicone is formed in a flat rectangular piece with internal cavities which may be filled with fluid. Kevlar fibres are positioned in the silicone running the length of the muscle. When the internal cavities are inflated, they push the fibres outwards, contracting the muscle. Contraction of up to 18% is realised and forces up to 32 N with a 60mmx20mm muscle. Failure of the muscles occurred at 138 kPa

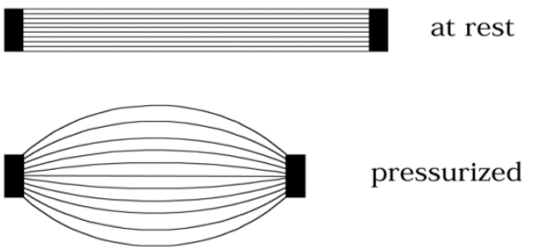

Baldwin[4]

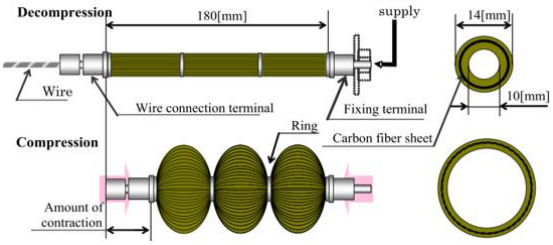

Kamo [8]

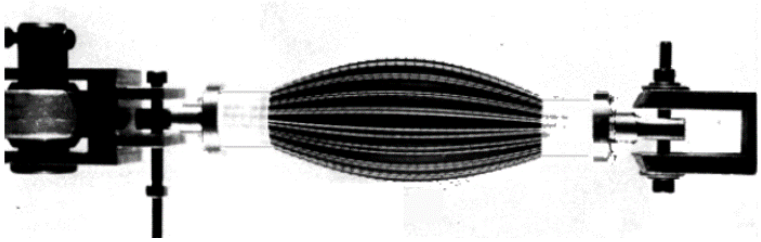

Ferraresi [5]

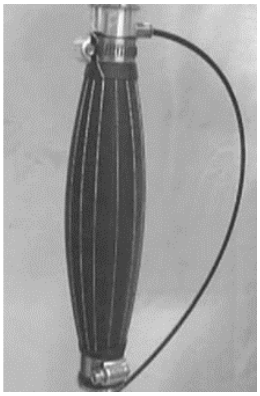

Bertetto [10]

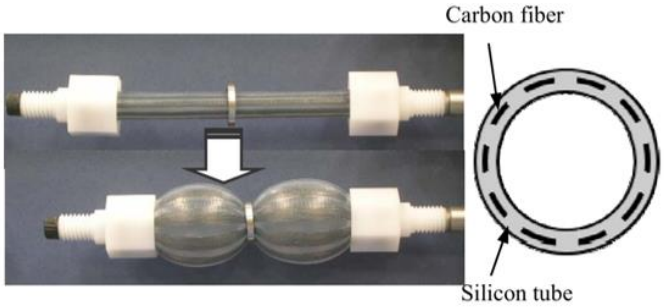

Nakamura, Saga[7]

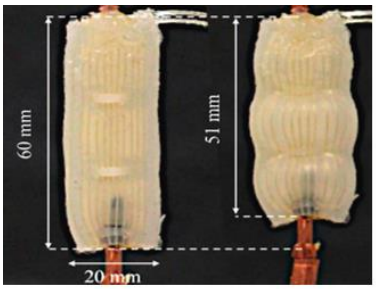

Wirekoh [11]

Figure B1: A variety of straight Fibre PAMs

PLEATED PAM

The Pleated Pneumatic artificial muscle (PPAM) is a special case of the straight fibre PAM. While straight fibre PAMs make use of an elastic bladder, the pleated

muscle instead uses a flexible but inelastic membrane. This is pleated to allow it to expand radially, unfolding as it does so. Load is transmitted either through the fabric which makes up the membrane, or by additional fibres running over this membrane (similar to the straight fibre muscle). The main advantage of this over the standard straight fibre muscle design is the removal of radial stresses. This effectively eliminates the threshold pressure required to start the muscle expanding and improves efficiency, there being virtually no energy required to deform the membrane [12]. It also removes friction related hysteresis.

The PPAM was proposed by Daerden [13] and the majority of the research on this actuator has been conducted at Vrije Universiteit Brussel. The main motivation for the work was the removal of the effects of friction in previous muscle designs. A detailed mathematical model of the muscle is also provided based on a pressurised axisymmetric membrane. This is an idealised case of the muscle, assuming an infinite number of infinitely narrow pleats. With this model force output, contraction, total volume and other geometric requirements were developed. It was shown that a muscle with higher slenderness, that is the ratio of muscle length to radius at rest (l/R), is a major contributor to the achievable contraction. The theoretical limit of contraction is 54.3% but this is not realistically achievable. For a PPAM with l/R=10 a contraction ratio of 45.5% can theoretically be achieved [14].

In order to practically realise the actuator a finite number of pleats must be designed in the membrane. Necessarily, the radius at the top of the ridges in the pleats will be greater than the radius at the bottom. As the muscle expands the difference in these radii reduces as the muscle approximates a circular cross section. As the relative change in radius is different for these two regions, stresses are developed in the membrane. It is desirable to minimise these stresses in order to minimise stress concentrations, improve force output and work transferred. Therefore the pleats are arranged so as to be as shallow as possible with as little movement of material in the circumferential direction as possible. The preferred implementation is therefore a cartridge pleated method, whereby the end fittings

hold the membrane as in Figure B2 (a). The end-fittings were therefore designed with the greatest practical number of pleats while maintaining slenderness. The result is shown in Figure B3.

A high-tensile stiffness, para-aramid fibre, fabric (Kevlar and Twaron) was chosen for the membrane due to its high strength and low elongation. This was formed into a cylinder before being pleated by gluing a sheet of material back on itself. A polypropylene film was used to seal the fabric, and this was bonded to the fabric with a rubber resin adhesive. An epoxy resin was used to bond the membrane to the aluminium end fittings. The developed prototype had an active length of 10cm, radius of 1.25cm at rest and weighed 58.3g.

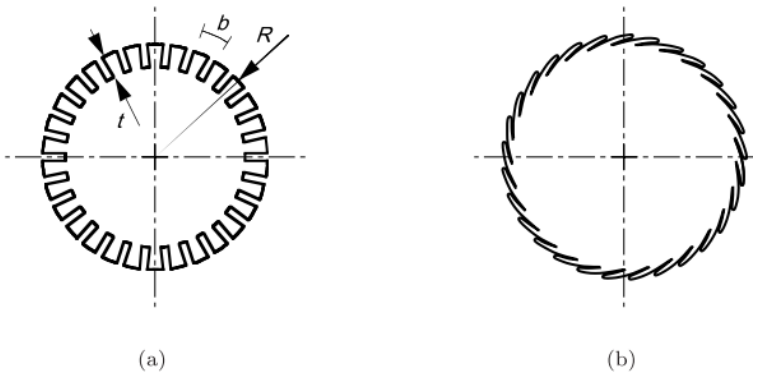

Figure B2: Two considered methods of holding the pleated muscle at the end fitting. (a) is the preferred cartridge pleated method while (b) would result in greater membrane stress [13]***.***

First generation PPAM [15]

Second generation PPAM [15]

Third generation PPAM [21]

Figure B3: The three generations of pleated pneumatic muscles

Testing of the prototype showed very good agreement with the model although contraction was somewhat less than predicted. The threshold pressure of the muscle was found to be 10kPA, as below this pressure non-uniform bulging occurred. Muscle forces up to 3500N were recorded though the pressure was restricted so as not to damage the muscle (300KPa). The prototype was used to actuate a revolute joint and a controller is described.

While this research showed that a PPAM was possible, the actuator had a very limited lifetime, and was therefore unsuited for use on most robots [15]. Therefore a second generation was developed. In order to improve muscle lifetime, the fabric material was made of an already tubular structure so there was no joining. The membrane layout itself was also changed with high tensile fibres being added at the bottom of the pleats to take the load while a more flexible membrane was used to contain the air. This was to avoid the non-uniform bulging observed in the original prototype. Manufacturability was also improved by removing the aluminium toothed ring which held the pleats in place, replacing it with a “basin”

in which an epoxy resin holds the pleats approximately in place. The prototype was manufactured using a polyester fabric with a polymer liner for the main membrane and Kevlar for the load carrying fibres. Figure B3 shows the second generation PPAM.

These changes allowed the muscle to lift 130Kg with a pressure between 1 and 3 bar for 400,000 cycles without failure. A modified model is also presented though the outcome yields little difference from the original model, provided a large number of load bearing fibres are used. This type of PPAM has been used the most in documented applications, including the biped robot Lucy [16]–[18] a lightweight robot manipulator designed for safe use in close proximity to humans [19], and a lower limb exoskeleton device for rehabilitation [20]. In the latter two instances, restraining rings were used on the muscle in order to allow longer muscles, with greater contraction to be used (in a similar fashion to the rings placed on the straight fibre muscle).

In order to further improve manufacturability, a third generation PPAM was developed [21], [22]. The build time for a single muscle was reduced from 8 hours to 2 hours. The major change was in the end-fittings of the muscle. Fused deposition modelling was used to produce complex parts which held the pleats in place in a similar way to the first generation muscle. This was supported by metal components for strength. Dyneema rope was used as the load carrying fibre as this allowed for a continuous length to be used rather than many individual lengths as in the second generation PPAM. These two changes greatly simplified the assembly of the PPAM. The PPAM 3.0 is shown in Figure B3. It should be noted however that hysteresis in the muscle was increased to approximately ±10%.

A comparison between the third generation PPAM and Festo Fluidic muscles is given in [21]. The PPAM is shown to have many desirable qualities. The force output at a given contraction ratio is dependent on the slenderness for a PPAM, but mainly dependent on radius alone (if braid angle is not changed) for a Festo or McKibben type muscle. This must be accounted for in any comparison as depicted in Figure B4. The first graph shows actual measured values and clearly demonstrates the

larger contraction capable with the PPAM. Force values are also generally greater than even the largest diameter Festo muscle. The PPAM is not tested at forces greater than 3500N due to failure concerns. This limits the pressures tested to 4 bar. The Festo muscle can be used up to 8 bar and so larger forces are possible. The remaining 3 graphs show scaled versions of the PPAM output force with different initial lengths. The dependence on slenderness suggests that, while greater force capacity is possible with the PPAM, where a shorter actuator is needed the Festo muscle may be more appropriate. PPAMs with a slenderness higher than 3 will reach higher contractions than Festo muscles. Also evident in Figure B4 is the inability of the PPAM to be stretched due to its straight fibres, whereas the Festo muscle can be.

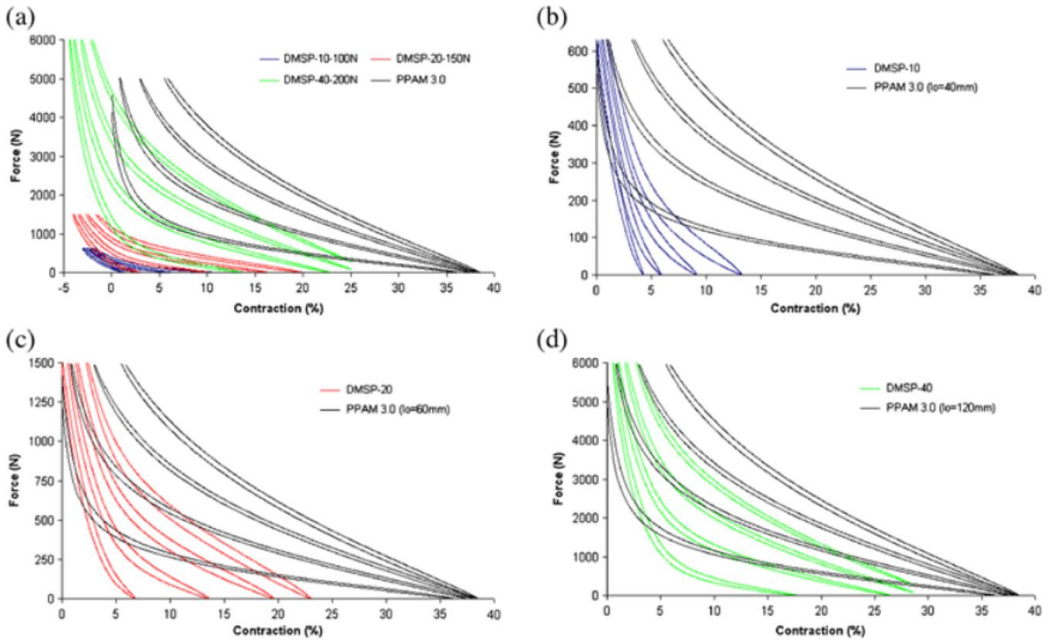

Figure B4: (a) Measured forces as a function of contraction for PPAM 3.0 (with length 110mm, l/R=9.56)and Festo products: DMSP-10-100N (10mm diamter muscle), DMSP-20-150N (20mm diameter muscle), and DMSP-40-200N (40mm diameter muscle) at pressure levels 1–4 bar, (b) measured forces for Festo DMSP-10 and scaled measured forces for PPAM 3.0 of l=40mm as a function of contraction at pressure levels 1–4 bar, (c) same as, (b) but for Festo DMSP-20 and l=60 mm; and (d) same as (b) but for Festo DMSP-40 and l =120 mm [21]

A potential disadvantage of the PPAM is the relatively large increase in diameter associated with contraction [21]. This means muscles cannot be positioned as

densely as the fluidic muscles which may restrict the feasible number of degrees of freedom which can be implemented on a compact system.

The force to mass and energy to mass ratios were also compared. These show the PPAM far outperforming the festo muscle. This is largely due to the mass of the end fittings and materials. Given the construction of the Festo muscle it is difficult to imagine that it has been optimised for mass. More lightweight end-fittings have been developed by other researchers [23].

A summary table of the comparison between the two types of pneumatic muscle is shown in Table B1. While this paper details many comparrisons between the two muscles, many of which favour the PPAM, fatigue is not addressed. This has already been established as a potential issue[15], [22]. The lack of testing of the PPAM to perform at higher pressures is also a concern in this regard. Recently the use of self-healing polymers in the membrane of these muscles has been proposed, though this has only been demonstrated at low pressures (up to 0.25 bar) [24]. Nontheless the PPAM represents an interesting departure from the more established pneumatic muscle designs and it is curious that other research groups have not attempted to make use of the actuator. This is likely due to the more complex manufacturing process.

		Festo Fluidic Muscle			PPAM (lo/R=9,56)		
Properties	Units	DMSP-10	DMSP-20	DMSP-40	lo=40mm	lo=60mm	lo=120mm
Max Tension	N	630	1500	6000	660	1487	5950
Max Diameter	mm	20.7	39	75.4	35.4	53	106.1
Max contraction (4 bar)	%	13	22.8	28.3	1 mod - 38.2 5 mod – 34.7 10 mod – 34.3 20 mod – 34.1	1 mod - 38.2 4 mod – 36.0 8 mod – 35.6 15 mod – 35.4	1 mod - 38.2 2 mod - 37.4 3 mod – 37.0 4 mod - 36.8
Tension intesity @ max contraction	kN/m^2	1516.3	1255.6	1473,6	618.2	618.2	618.2
Force to Mass	kN/kg	lo=40mm - 8	lo=60mm - 7.1	lo=120mm - 7.4	1 mod - 9.8	1 mod - 19.7	1 mod - 50.2
Energy to Mass	Nm/kg	lo=40mm - 14.6	lo=60mm - 38.7	lo=120mm - 108.1	1 mod - 72.7	1 mod - 218,5	1 mod - 1112
Energy to Volume	Nm/l	268.5	159.1	227.8	1 mod - 287.1	1 mod - 287.1	1 mod - 287.1

Table B1: Summary table of the comparison between Festo Fluidic muscles and the pleated muscle [21]

NETTED MUSCLES

This are quite similar in construction to the McKibben or straight fibre muscles, but the density of the braid is much larger. This means the membrane can be forced out through it more readily, reducing the realisable operating pressure before failure. Several of these muscles are shown in Figure B5.

The operating principle to the Yarlott muscle is similar to that of the pleated PAM [25]. It is composed of load bearing fibres that run between two end fittings as with a straight fibre muscle. The bladder is composed of an elastomer but this is reinforced in the radial direction by a number of inelastic strands which are embedded in the elastomer to prevent elastic expansion. The lack of elastic expansion reduces energy losses. The muscle is designed to work at low pressures (as low as 1.7 kPa are quoted). While the Yarlott muscle is similar to the PPAM, the number of pleats is much less and the manner in which the pleats are held in place is less precise. This actuator was commercialised under the name Ampflex by Trish Energetics Inc. [26]. A Neoprene filler with a polyester web formed the membrane. It was quoted as having negligible hysteresis, could operate at up to 15Hz and had a lifetime of over 10 million cycles, although this was contested by other authors [27]. It was patented for use in a spray coating apparatus[28]. Trish Energetics was later taken over by the Dynacycle Corporation (established by Henry Paynter, who developed a number of muscle designs discussed below).

The RObotic Muscle Actuator (ROMAC) was patented in 1990 by Kukolj and Immega[29]. Again it makes use of a non-elastic membrane, and this is surrounded by a very coarse mesh, composed of linked cables. The inelastic membrane protrudes through this considerably to form a “plurality of (convex polyhedral) protrusions”. The inflation of these protrusions separates the mesh, causing it to contract longitudinally. The actuator is capable of contraction of up to 50% and very large forces (up to 19,620N for an actuator with a mass of 0.3Kg) [30]. However this comes at a cost, as the muscle’s large volume results in a long filling time and reduced efficiency. It was also used in a one degree of freedom arm [31].

The Kukolj muscle is very similar to the McKibben muscle, except the braided sleeve is more similar to a net [32]. An elastic membrane deforms when inflated to push outwards on the net causing a contractile affect. A version with straight fibres is also included in the patent.

A quite different type of netted muscle is the Paynter hyperboloid muscle [33] . When the muscle is elongated, it forms a hyperboloid shape. The end fittings on this muscle are of quite a large diameter. Stiff fibres run between them in a straight line but to a different point on the circumference of the other end fitting (see Figure B5). When the muscle is inflated it pushes out on these fibres, approximating a sphere and contracting the muscle.

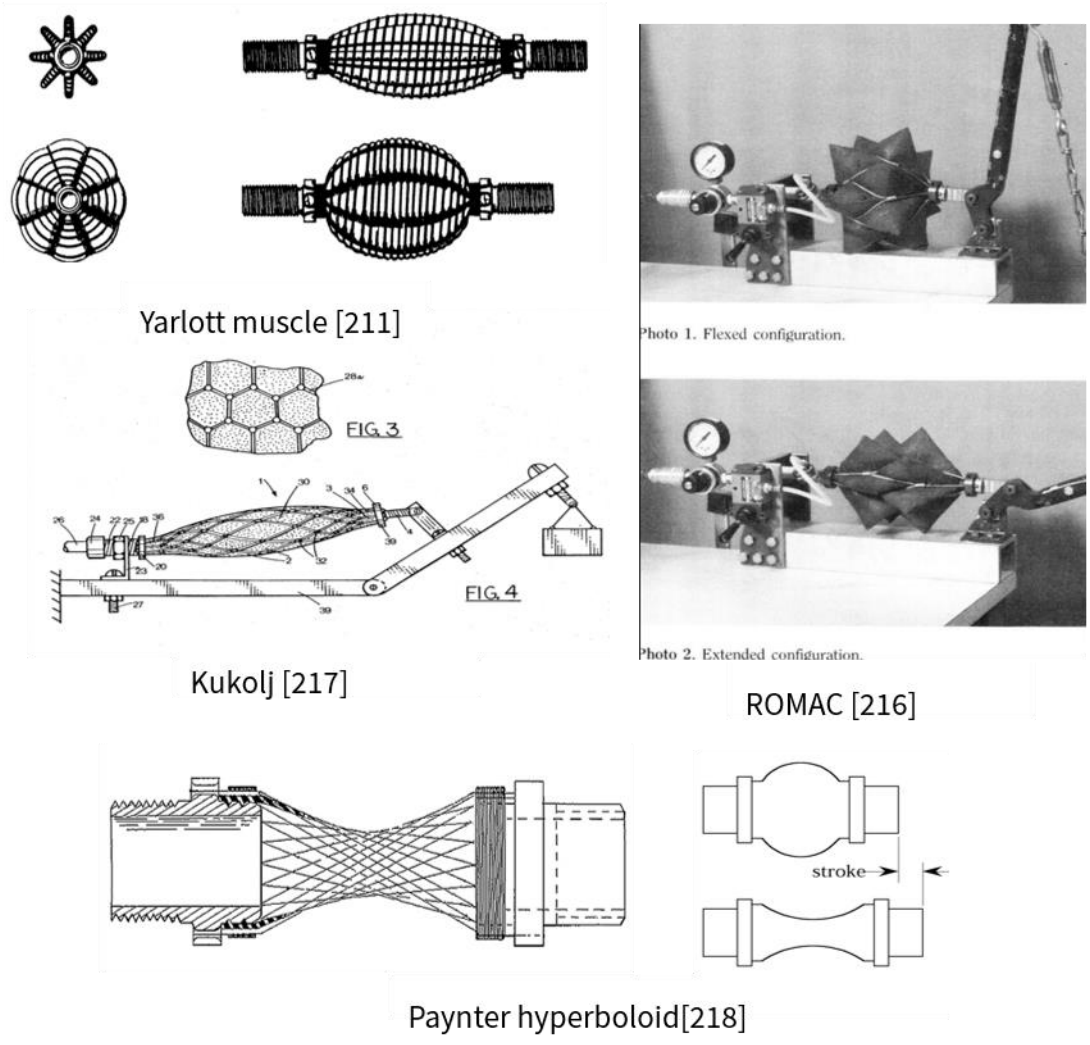

Figure B5: A variety of netted muscles

KNITTED MUSCLE / TEXTILE MUSCLE

The Knitted muscle is quite similar to the straight fibre muscle, but the elastic bladder is completely surrounded by a loosely knitted fabric sheath. Figure B6 illustrates the stockinette stitch employed in the fabric which forms a cylinder around the muscle. This knit material is bonded to the bladder, which prevents the fibres sliding in the stiches when the muscle is expanded. Instead, the stiches form longitudinal lines of reinforcement between the two end caps.

The muscle described in the patent awarded to Paynter makes use of a resilient, hollow tubular bladder [27]. It was designed to overcome some of the problems with the Yarlott muscle, namely the non-uniform stresses in the membrane and "tumble off" problems where with the helically wound fibres are attached to the end fitting. Here the helically wound fibres are pulled away from the longitudinal fibres upon inflation, leading to early failure. The Paynter muscle sleeve (made of a stiff fibre such as Dacron or Kevlar) provides an outer limit to radial expansion and reinforces the bladder, allowing larger pressures to be used (800kPa). When inflated the muscle forms an approximately spherical shape. The stiches in the centre of the muscle are made looser to facilitate this. It is suggested that the muscle can be operated for hundreds of thousands of cycles without failure. The Dynacycle corporation commercialised the design, marketed as the Dynaflex linear tension actuator [34]. A number of models were produced with a maximum force of up to 12,900 N. They were used to make a radial motor which used a number of the actuators to rotate a shaft in a similar way to a crank shaft in an internal combustion engine (albeit with contractile force, rather than compressive force input from a piston) [35]. These were commercially available in a range of sizes.

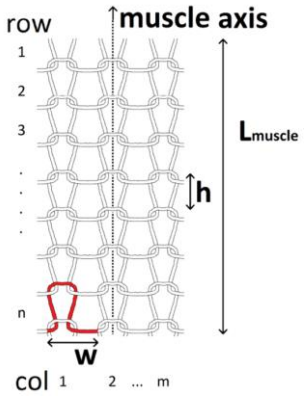

Figure B6: The structure of a knitted muscle outer sheath [36]

Ball has more recently researched this type of actuator [36], [37]. The knit material used here was Spectra (UHMWPE) braided fishing line due to its strength and low coefficient of friction. A polyethylene bag was used for the membrane so as to eliminate the elastic expansion that would otherwise be required. Interestingly the knit was not bonded in this muscle, thus allowing the stiches to get pulled in the circumferential direction (direction w in Figure B6) and shortening the stich in the longitudinal direction. This may increase contraction, but the friction will reduce the muscles lifetime. A model of the muscle was suggested but this showed poor agreement with the experimental results. Testing showed that contraction could be as high as 51% of the muscle length. The maximum force output was 100N at 14 kPa. The muscle pressures used were extremely low, 14-100 kPa. It is suggested that the knitted muscle more closely matches the force output as a function of length of mammalian muscle, though a normalised force scale is used.

Textile muscles are very similar to knitted muscles except a textile is used instead of a knitted material. Practically this means that fibres run the length of the muscle, from end fitting to end fitting, with perpendicular fibres holding them in place. The mechanism of contraction is the same as that of straight fibre muscles, the bulging of the muscles pushes out on the longitudinal fibres forcing the end fittings closer together.

Sirolli and researchers at the Politecnico di Torino developed prototypes of the textile pneumatic muscle [38]. The first used a warp and weft fabric called Superflex Mecpor EBW PU 343/2 and the other Gerstop LPE 0203 (which is

composed of two layers of polyester with a polyurethane inner layer). In both cases a tubular structure is formed by sewing a flat piece of fabric. Latex is used as a bladder in both cases. Pressure was limited to 1 bar due to the strength of the materials. The first prototype showed a maximum contraction of 10% with the knitted fabric only performing slightly better. Metal rings were used to improve contraction as with the straight fibre PAM and pleated PAM. Hysteresis is however much more apparent with the knitted fabric. The research group later pursued braided muscles to achieve greater contraction ratios [39].

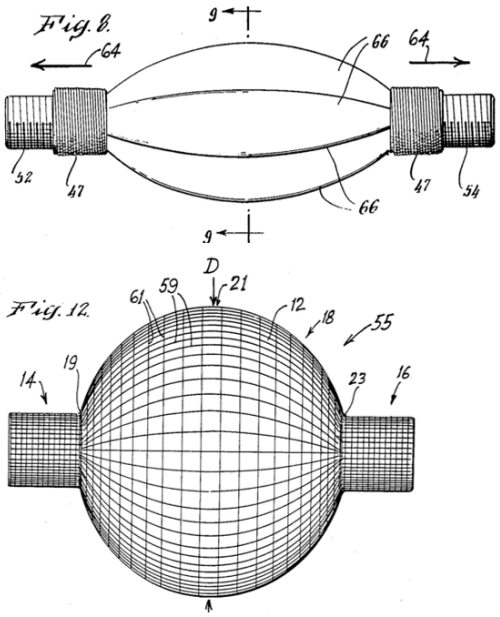

Paynter [27]

Sirolli [38]

Ball [37]

Figure B7 Examples of knitted and netted muscles

ROTATIONAL MUSCLES

While the muscles discussed up to this point have provided a linear pull, which could be used, through some additional mechanism, to provide a rotational force, this section describes artificial muscles which directly provide a rotational force. This concept is quite different to biological muscle operation, however the mechanism to achieve rotation is based on tension due to pressurised fluid and so can be compared to pneumatic artificial muscles. A number of these actuators are shown in Figure B8 and discussed below.

Kleinwachter and Geerk describe a torsion muscle in a 1972 patent [40]. This device consists toroid membrane positioned around the shaft to be rotated. Stiff fibres wrap around the shaft and are attached to the stationary outer edge of the membrane. When the membrane is inflated, the fibres are put under tension and apply a force which acts to cause rotation of the shaft. It is suggested that the elasticity of the membrane could provide the restoring force.

Berthaud patented a rather simple device to operate valves in 1970 [41]. It consists of a tube which runs from a stationary end plug to the valve to be turned (or some intermediate mechanism) The tube is normally twisted so that it forms a helical surface. Upon inflation of the tube, the helix tends to straighten, actuating the valve. A second unit can be used to close the valve. The preferred material is an elastomer such as nitrile rubber with a stiff fibre reinforcing. It is argued that the device greatly simplifies valve actuation when compared to traditional solutions as it can be designed to naturally stop at the valve end position rather than requiring feedback control, reduces cost and does not require reduction gearing (as in the case of electric motors) or torque limiters.

Paynter patented and manufactured a device known as the Twistor [34], [42] which is somewhat similar to the Berthaud actuator. A flexible, hollow, thin-walled elastic shell is reinforced with several inextensible flexible strands which run helically around the elastic shell. Inflating the elastic shell tensions the fibres, causing them to uncoil and exert a rotational force. Two of these arrangements can be used to actuate a joint in both directions, or a coiled spring can return the joint to its

original position once deflated. The device can be used at frequencies of up to 125 Hz and has an operating life in excess of 500,000 cycles. A second patent suggests the use of the proposed muscle structure to form the joint itself, as well as actuate it, thus removing the need for bearings etc [43]. Several studies by the inventor have examined the properties of the actuator [34], [44], [45]. This analysis suggests that , at constant pressure, the actuators volume and generated torque is linearly proportional to the twist angle (a zero twist angle being when the fibres run straight across the twistor, though only twist angles from 35°-80° are considered). In [46] a spherical joint is controlled with two twistor pairs, and used to position a laser light and actuate an artificial "eyeball". It is suggested that the joint position is directly proportional to the pressure difference between the twistors in the pair, though this seems to ignore the effect of the applied torque on the joint.

The Flexator was invented by Jim Hennequin and was originally used to actuate the "Spitting Image" puppets [47]. It has also been used to actuate a rehabilitation robot mounted on a wheel chair[48] and investigated for use on a horticultural robot [49]. The actuator is composed of a lay flat firehouse. This is looped back on itself and placed around a cylinder which is concentric with the joint to be actuated. A window in this cylinder allows a strap that runs over the fire hose to connect to the joint internally. When the fire hose is inflated, it pulls the strap, thus rotating the joint. A pair of these actuators can be used to rotate the joint in both directions and through a rotation of almost 360 degrees [49]. The torque available for a muscle of size 60 mm width by 90 mm length ranges from 1 to 15 Nm.

The curved pneumatic muscle actuator, proposed by Zhang et al, makes use of a standard Festo fluidic muscle but it operates in a substantially different way [50]. Instead of pulling in straight contraction the muscle wraps around the joint to be actuated and it is the combined force of the muscle contraction and straightening under pressure that actuates the joint. It weakens the coupling relationship between the output torque/force and displacement. New modelling techniques are used to model the behaviour of this actuator although these show poor agreement with experimental results. The actuator arrangement is implemented

on a wearable elbow exoskeleton and controlled with a hybrid fuzzy controller. While the prototype did work effectively it should be noted that the muscle datasheet states that the muscle should operate in pure tension, with no contact on its sides [51]. Using in a curved configuration will likely reduce the actuators lifetime, though it may be possible to overcome this with a more specialised muscle design.

The ribbon air muscle (RAM) is a simple device capable of delivering large rotations which operates in a similar manner to the Flexator and was developed by Majoe et al [52]. Constructed with flexible, non-elastic films such as polyethylene or nylon, the actuator consists of an inflatable compartment with ribbons extending from each side. This is wrapped around a cylinder at the actuated joint. Inflating the muscle pushes the outer surface away from the cylinder, drawing in the ribbons. This effect is used to actuate the joint with working pressures of up to 140kPa delivering an output force of 117N. Force output as a function of pressure and contraction is complicated by the change in contact properties of the muscle with the internal cylinder as the muscle inflates, thus the force

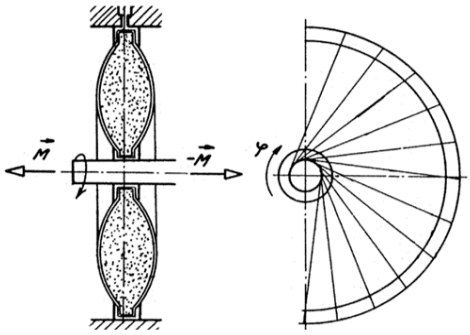

Kleinwachter [40]

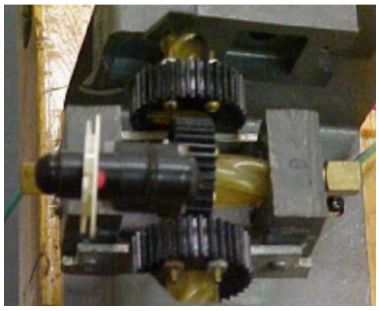

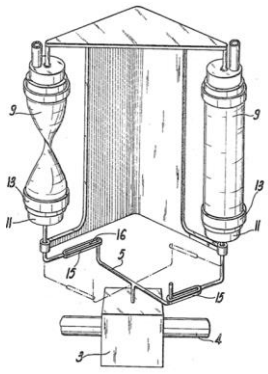

Berthaud [41]

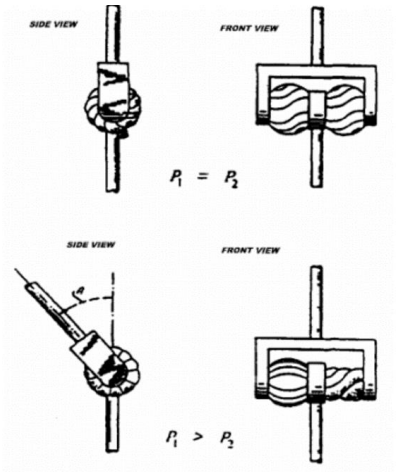

Paynter [44]

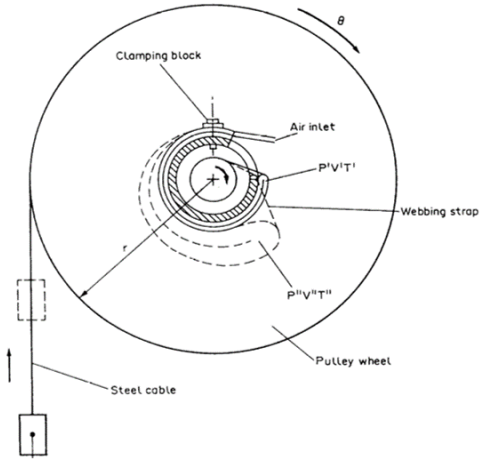

Prior (Flexator) [47]

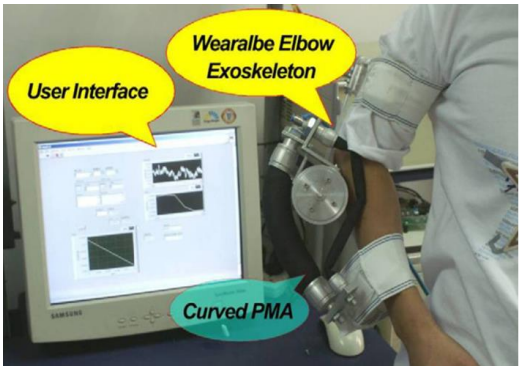

Zhang [50]

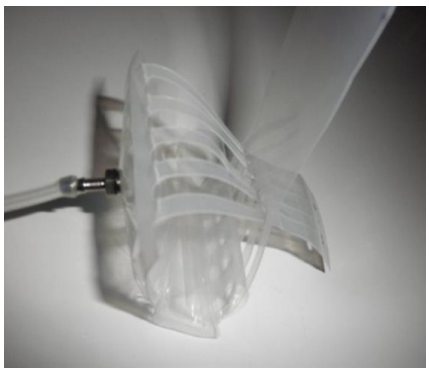

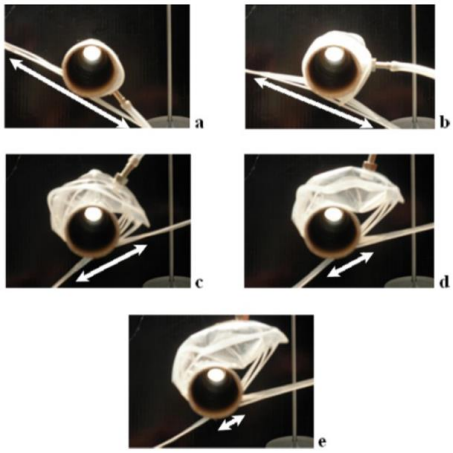

Majoe (RAM) [52]

Figure B8 A selection of rotational muscles

output is difficult to model. The RAM is used in a “Monkey” robot that can move at high speed (while suspended). The muscle was later modified to include the ability to heat a refrigerant inside, the boiling of which (at ~70°C) was used as the working fluid for the muscle. It has also been used on a wearable exoskeleton, designed to increase endurance [53].

VACUUM DRIVEN MUSCLES

Though far less popular, there have been some attempts to actuate muscle like actuators using a vacuum rather than pressurised gas or liquid. Two of these are described below and illustrated in Figure B9.

The under-pressure artificial muscle (UPAM) produces a contractile force when a vacuum is applied[54]. This is similar in design to many of the straight fibre muscles discussed previously. When the air is sucked out, it causes the muscle to collapse, pulling the end-fittings closer together. Contractions of 20% for a muscle of length 100mm and diameter 50mm is suggested, with force output of 20-140N [12]. The force is quite limited as at ambient atmospheric pressure, the maximum pressure difference is 100kPa.

The Vacuum Actuated Muscle (VAMP) is composed of a number of interconnected air chambers [55]. When air is removed from these they collapse under atmospheric pressure. Contractions of up to 40% are possible. One advantage of these actuators is that due to their operation under vacuum, small holes naturally tend to seal. They can perform upwards of a million cycles without degradation of performance. However, as with the UPAM, the force output is limited due to the relatively small differential pressure that is possible.

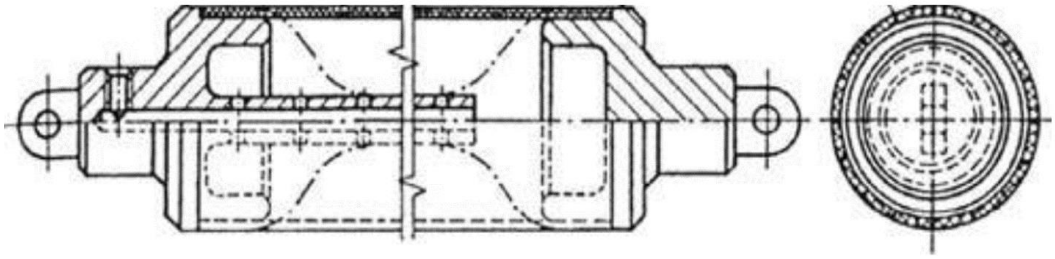

Palko (UPAM) [54]

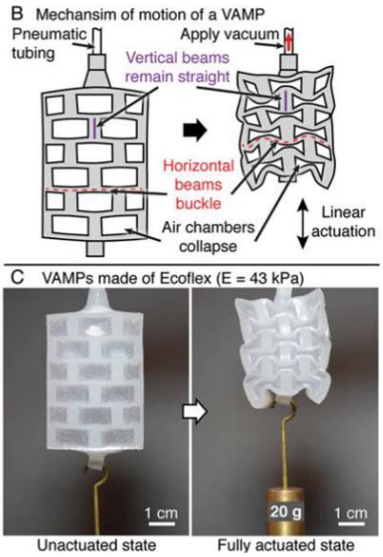

Yang (VAMP) [55]

Figure B9: Vacuum actuated muscles

REFERENCES

[1] G. Belforte, G. Eula, A. Ivanov, and A. L. Visan, "Bellows textile muscle," *J. Text. Inst.*, vol. 105, no. 3, pp. 356–364, 2014.

[2] F. A. & C. KG, "Bionic Handling Assistant," 2010.

[3] T. E. Pillsbury, Q. Guan, and N. M. Wereley, "Comparison of contractile and extensile pneumatic artificial muscles," *IEEE/ASME Int. Conf. Adv. Intell. Mechatronics, AIM*, vol. 2016-Septe, pp. 94–99, 2016.

[4] H. A. Baldwin, "Realizable Models of Muscle Function," in *Biomechanics: Proceeding of the First Rock Island Arsenal Biomechanics Symposium April 5--6, 1967*, D. Bootzin and H. C. Muffley, Eds. Boston, MA: Springer US, 1995, pp. 139–147.

[5] C. Ferraresi, W. Franco, and M. B. A., "Straight fibres pneumatic muscle: an

actuator with high traction force," in *The Sixth International Conference on Fluid Power*, 1999, pp. 787–798.

[6] T. Nakamura, N. Saga, and K. Yaegashi, "Development of a Pneumatic Artificial Muscle based on Biomechanical Characteristics," in *Industrial Technology, 2003 IEEE International Conference on*, 2003, vol. 2, pp. 729–734.

[7] N. S. N. Saga, T. S. T. Saikawa, and H. O. H. Okano, "Flexor mechanism of robot arm using pneumatic muscle actuators," *IEEE Int. Conf. Mechatronics Autom. 2005*, vol. 3, no. July, pp. 1261–1266, 2005.

[8] D. Kamo, M. Maehara, D. Tanaka, and T. Nakamura, "Development of artificial muscle manipulator with differential gear mechanism," *IECON 2011 - 37th Annu. Conf. IEEE Ind. Electron. Soc.*, pp. 98–103, 2011.

[9] N. Saga, T. Nakamura, and K. Yaegashii, "Mathematical model of pneumatic artificial muscle reinforced by straight fibers," *J. Intell. Mater. Syst. Struct.*, vol. 18, no. 2, pp. 175–180, 2007.

[10] A. Manuello Bertetto and M. Ruggiu, "Characterization and modeling of air muscles," *Mech. Res. Commun.*, vol. 31, no. 2, pp. 185–194, 2004.

[11] J. Wirekoh and Y.-L. Park, "Design of flat pneumatic artificial muscles," *Smart Mater. Struct.*, vol. 25, no. 11, pp. 1–14, 2017.

[12] F. Daerden and D. Lefeber, "Pneumatic artificial muscles: actuators for robotics and automation," *Eur. J. Mech. Environ. Eng.*, vol. 47, no. 1, pp. 11–21, 2002.

[13] F. Daerden, "Conception and Realization of Pleated Pneumatic Artificial Muscles and their Use as Compliant Actuation Elements," p. 176, 1999.

[14] F. Daerden and D. Lefeber, "The concept and design of pleated pneumatic artificial muscles.," *Int. J. Fluid Power*, vol. 2, no. 3, pp. 41–50, 2001.

[15] B. Verrelst, R. Van Ham, B. Vanderborght, D. Lefeber, F. Daerden, and M. Van Damme, "Second generation pleated pneumatic artificial muscle and its robotic applications," *Adv. Robot.*, vol. 20, no. 7, pp. 783–805, 2006.

[16] B. Verrelst, R. Van Ham, B. Vanderborght, F. Daerden, D. Lefeber, and J. Vermeulen, “The pneumatic biped ‘lucy’ actuated with pleated pneumatic artificial muscles,” *Auton. Robots*, vol. 18, no. 2, pp. 201–213, 2005.

[17] B. Vanderborght *et al.*, “LUCY, a Bipedal Walking Robot with Pneumatic Artificial Muscles,” *Mechatronics*, 2004.

[18] B. Verrelst, R. V. A. N. Ham, F. Daerden, and D. Lefeber, “Design of a Biped Actuated by Pleated Pneumatic Artificial Muscles,” *CLAWAR 2002 5th Int. Conf. Climbing Walk. Robot.*, 2002.

[19] M. Van Damme, F. Daerden, and D. Lefeber, “A pneumatic manipulator used in direct contact with an operator,” *Proc. - IEEE Int. Conf. Robot. Autom.*, vol. 2005, no. April, pp. 4494–4499, 2005.

[20] P. Beyl, M. Van Damme, R. Van Ham, B. Vanderborght, and D. Lefeber, “Design and Control of a Lower Limb Exoskeleton for Robot-assisted Gait Training,” *Appl. Bionics Biomech.*, vol. 6, no. 2, pp. 229–243, 2009.

[21] D. Villegas, M. Van Damme, B. Vanderborght, P. Beyl, and D. Lefeber, “Third–Generation Pleated Pneumatic Artificial Muscles for Robotic Applications: Development and Comparison with McKibben Muscle,” *Adv. Robot.*, vol. 26, no. 11–12, pp. 1205–1227, 2012.

[22] D. Villegas Casi, “Development of the production process of PPAM,” Universidad Pública de Navarra (España), 2009.

[23] D. A. Kingsley, “A cockroach robot with artificial muscles,” Case Western Reserve University, 2005.

[24] S. Terryn, J. Brancart, D. Lefeber, G. Van Assche, and B. Vanderborght, “A pneumatic artificial muscle manufactured out of self-healing polymers that can repair macroscopic damages,” *IEEE Robot. Autom. Lett.*, vol. 3766, no. JUNE, pp. 1–1, 2017.

[25] J. Yarlott and H. Mass, “Fluidic Actuator,” 3,645,173, 1972.

[26] Trish Energetics, “Ampflex - Model F-125.” Hravard Massachusetts, 1971.

[27] H. M. Paynter, “High Pressure Fluid-driven Tension Actuators and Method for Constructing Them,” 4751869, 1985.

[28] J. C. Gray, “Spray Coating Apparatus,” 3,844,483, 1979.

[29] M. Kukolj and G. Immega, “Axially Contractable Actuator,” 4939982, 1990.

[30] B. Hannaford and J. M. Winters, *Actuator properties and movement control: biological and technological models. In Multiple Muscle Systems*. Springer-Verlag, 1990.

[31] C. Zoo, “1986 - ROMAC Pneumatic Actuator - Guy Immega and Mirko Kukolj (American) - cyberneticzoo.com,” 2012. [Online]. Available: http://cyberneticzoo.com/bionics/1986-romac-pneumatic-actuator-guy-immega-and-mirko-kukolj-american/. [Accessed: 25-Jul-2017].

[32] K. Mirko, “AXIALLY CONTRACABLE ACTUATOR,” 1988.

[33] H. M. Paynter, “Hyperboloid of revolution fluid-driven tension actuators and methods of making,” 4 721 030, 1988.

[34] H. M. Paynter, “Low-Cost Pneumatic Arthrobots Powered by Tug-and-Twist Polymer Actuators,” *Proc. Japan-USA Symp. on Flexible Automation*, vol. 1. pp. 107–110, 1996.

[35] J. Lerro, “Dynacycle radial motor,” *Des. news*, vol. 28, 1973.

[36] E. John Ball, “Novel Methods in Meso-Scale And Nano-Scale Actuation,” Cornell University, 2016.

[37] E. J. Ball, M. A. Meller, J. B. Chipka, and E. Garcia, “Modeling and testing of a knitted-sleeve fluidic artificial muscle,” *Smart Mater. Struct.*, vol. 25, no. 11, pp. 1–14, 2016.

[38] S. Sirolli, G. Belforte, G. Eula, A. Ivanov, and T. Raparelli, “Textile Pneumatic Muscles,” vol. 4, no. 3, pp. 4–10, 2016.

[39] G. Belforte, G. Eula, A. Ivanov, and S. Sirolli, “Soft Pneumatic Actuators for Rehabilitation,” *Actuators*, vol. 3, no. 2, pp. 84–105, 2014.

[40] H. Kleinwachter and J. Geerk, “Device with a pressurizable variable capacity chamber for transforming a fluid pressure into a motion,” 1972.

[41] J. Berthaud, “Valve Operating Device,” 3490733, 1970.

[42] H. M. Paynter, “Fluid-driven torsional operators for turning rotary valves and the like.,” 1978.

[43] H. M. Paynter, “METHOD AND SYSTEM EMPLOYING DOUBLE-ACTING, FLUID-DRIVEN TWISTOR-PAIRS AS COMBINED JOINTS AND MOTORS IN ARTHROBOTS,” pp. 2–6, 1979.

[44] H. M. Paynter and M. Nagurka, “OPPOSED TUGGER-PAIR AND TWISTOR-PAIR PNEUMATIC POLYMERIC MECHATRONIC ACTUATORS,” no. c, pp. 1–5, 2000.

[45] H. M. Paynter, “THERMODYNAMIC TREATMENT of TUG- & -TWIST TECHNOLOGY Part 2 : Thermodynamic Twistor Design,” pp. 10–13, 1999.

[46] H. M. Paynter, L. S. Member, and J. M. Juarez, “Thermodynamic Analysis of a Mechatronic Pneumatically Driven Spherical Joint,” vol. 5, no. 2, pp. 153–157, 2000.

[47] S. D. Prior and A. S. White, “Measurements and simulation of a pneumatic muscle actuator for a rehabilitation robot,” *Simul. Pract. Theory*, vol. 3, no. 2, pp. 81–117, 1995.

[48] S. D. Prior, P. R. Warner, J. T. Parsons, and P. Oettinger, “Design and Development of an electric wheelchair mounted robotic arm for use by people with physical disabilities,” in *Robotics, Mechatronics and Manufacturing Systems*, Elsevier Science, 1993.

[49] N. D. Tillett, “FLEXIBLE PNEUMATIC ACTUATORS FOR HORTICULTURAL ROBOTS--A FEASIBILITY STUDY,” *Mechatronics*, vol. 3, no. 3, pp. 315–328, 1993.

[50] J. F. Zhang, C. J. Yang, Y. Chen, Y. Zhang, and Y. M. Dong, “Modeling and control of a curved pneumatic muscle actuator for wearable elbow exoskeleton,” *Mechatronics*, vol. 18, no. 8, pp. 448–457, 2008.

[51] Festo, “DMSP Fluidic Muscle DMSP / MAS,” 2016.

[52] D. Majoe, L. Widmer, and J. Gutknecht, “Pneumatic air muscle and pneumatic sources for light weight autonomous robots,” *Proc. - IEEE Int. Conf. Robot. Autom.*, pp. 3243–3250, 2011.

[53] D. Majoe and L. Widmer, “Power and endurance for comfortable wearable robotics,” *Proc. - IEEE Int. Conf. Robot. Autom.*, pp. 4811–4818, 2014.

[54] A. Palko and J. Smrcek, “The use of pneumatic artificial muscles in robot construction,” *Ind. Robot An Int. J.*, vol. 38, no. 1, pp. 11–19, 2011.

[55] D. Yang *et al.*, “Buckling Pneumatic Linear Actuators Inspired by Muscle,” *Adv. Mater. Technol.*, vol. 1, no. 3, p. 1600055, 2016.

APPENDIX C: THEORETICAL PAM MODELLING

This section examines the various factors which have been included in theoretical modelling of PAMs

BLADDER PROPERTIES

Both Schulte et al. and Chou and Hannaford attempted to make some allowance for the bladder properties of the muscle. Schulte included a term in the model representing the contribution made to the axial force of the muscle due to the elastic stretch of the bladder when the muscle is stretched past its natural length.

$$F_b = k_e \pi D(L - L_0); L - L_0 > 0 \quad \text{(C1)}$$

Where F_b is the axial tension force as a result of the bladder being stretched, k_e is an elastic constant and L_0 is the rest length of the muscle. In most cases k_e is also a function of L and D. Consideration is also given for a reduction in the force exerted on the braid as a result of the required pressure to expand the bladder radially. However, due to difficulty in evaluating k_e both these affects are omitted from the final model.

Chou and Hannaford merely account for the internal volume reduction in the muscle as a result of the bladder wall thickness with the expression for this becoming

$$V = \frac{1}{4}\pi(D - 2t_k)^2 L \quad \text{(C2)}$$

Where t_k is the thickness of the bladder.

Klute and Hannaford sought to account for the elastic energy storage in the muscle as a result of the bladder [1], [2]. The equation for PAM force was modified so it takes the form

$$F = P' \frac{dV}{dL} - V_b \frac{dW_{bladder}}{dL} \quad \text{(C3)}$$

Where V_b is the volume of bladder material and $dW_{bladder}$ is the change in strain energy density. A nonlinear material model developed by Mooney and Rivlin can be used to estimate W [3]

$$W_{bladder} = \sum_{i=0,j=0}^{\infty} C_{ij}(I_1 - 3)^i (I_2 - 3)^j \quad \text{(C4)}$$

Where C_{ij} are empirical constants and I_1 and I_2 are strain invariants of the actuator based on the strain of the bladder in three dimensions. Only two C_{ij} constants were used (C_{10}=118.4kPa and C_{01}=105.7kPa) for latex rubber. When this is used in equation (C3), the resulting model approximately halves the error in force for a muscle operating at 5 bar, although the expression becomes much more complex than the original model. Further enhancements of this model have been contributed by Delson et al., who used more precise terms for strain of the bladder [4], an adjustment which is particularly important for smaller diameter actuators [5]. Ball et al. expanded upon this to also include bladder prestrain, whereby the bladder is stretched in the muscle's relaxed state [6].

Braid Extension

A common assumption in the modelling of PAMs is that the fibres in the braid are inextensible. This assumption is not valid at high pressures however, as discussed by Davis et al. [7]. Here, the extension due to forces in the radial and longitudinal direction are considered. This leads to the following expression which can be substituted for b; in the model

$$b = \frac{Jb_{min} + \sqrt{(Jb_{min})^2 + 12L^2(J+1)}}{2(J+1)} + \frac{2P(b_{min}\sin\theta)^2}{ED_s n\pi^2} \quad \text{(C5)}$$

Where $J = \frac{4n^2\pi EA}{Pb_{min}L}$

D_s is the diameter of the fibres in the braid and E is the Young's modulus of the material in the fibres. The first part of the expression is as a result of the

longitudinal muscle tension while the second part accounts for the hoop stress. Figure C1 shows that when this approach is used, much better agreement with experimental data can be achieved than in previous models.

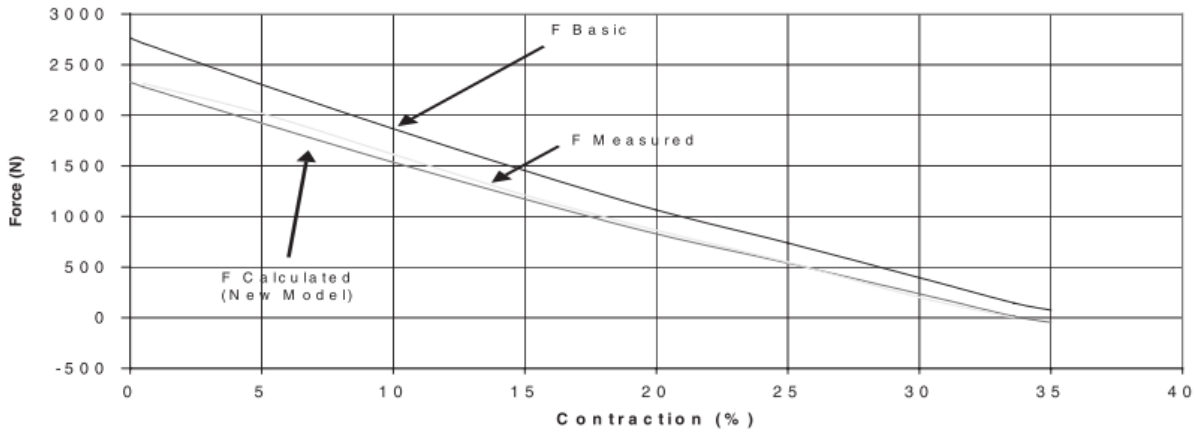

Figure C1: Comparison with experimental data of two models. The "new model" considers the stretch in the muscle fibres according to equation (C5). The muscle tested has length = 1.77m, b_{min} = 1.97m n =9, D_s=0.2mm.

Kothera examined the effect of energy storage in the braid due to the applied tension and subsequent stretch [5]. Assuming a cylindrical muscle, $V = AL$ where A is the current muscle cross sectional area the equation for muscle force becomes

$$F = -P'\frac{dV}{dL} = -P'A - P'L\frac{dA}{dL} \tag{C6}$$

Kothera states “the force $P'A$ [is] taken by the air” and so can be ignored when calculating the force in the braid, however the two terms here will operate against each other as $\frac{dA}{dL}$ will be negative, thus increasing the force on the braid. Therefore the forces calculated are somewhat smaller than they should be when they are calculated using equation (C7).

$$F_{braid} = -\frac{P'L}{Nsin\theta}\frac{dA}{dL} = \frac{P'b}{N}\frac{dA}{dL} \tag{C7}$$

With N being the number of fibres in the braid.

The strain energy density is given by

$$W_{braid} = \frac{1}{2}\sigma_{braid}\varepsilon_{braid} = \frac{1}{2}\frac{F_{braid}}{A_{braid}}\frac{F_{braid}}{EA_{braid}} \tag{C8}$$

With σ_{braid}, ε_{braid} and A_{braid} being the stress, strain and cross sectional area of the braid respectively. This gives the elastic force in the muscle as

$$F_{Br} = V_{braid} \frac{dW_{braid}}{dL} \tag{C9}$$

From Figure 2-36 using the Pythagorean theorem,

$$D = \frac{\sqrt{b^2 - L^2}}{n\pi} \tag{C10}$$

Using this in equation(C7) and inserting this in (C8) and differentiating, allows (C9) to be expressed as

$$F_{Br} = V_{braid} \frac{1}{EA_{braid}^2 N^2} \frac{4\pi^2 P'^2 b^2 L}{(2\pi n)^4} \tag{C11}$$

Or if the additional force from the pressure acting on axially in the muscle is accounted for (the $P'A$ term in equation (C6))

$$F_{Br} = V_{braid} \frac{P'^2 \pi^2 b^2}{EA_{braid}^2 N^2 (2\pi n)^4} \left(4L + 2\left(\frac{b^2}{L^2} + 1\right) - \frac{b^2}{L^3}\right) \tag{C12}$$

When F_{Br} from equation (C11) is applied to the muscle model, the accuracy is improved, especially at high pressures. The force error at 415 kPa for a muscle of length 100mm and diameter 13mm is reduced by 50%.

MUSCLE SHAPE DURING EXPANSION

Most authors make the simplifying assumption that the muscle always expands as a perfect cylinder across the entirety of its length. This is evidently untrue as the muscle is restrained to a fixed diameter at the end caps.

Tondu and Lopez introduced a parameter k ($k \geq 1$) which accounts for the reduction in the active part of the muscle as it increases in diameter as a consequence of the conical shape at both ends of the muscle. The strain in the active section of the muscle is amplified by the parameter k. They initially expressed the PAM force in the form:

$$F = \pi {r_0}^2 P(f(1 - \epsilon)^2 - g) \tag{C13}$$

With

$$\epsilon = \frac{(L_0 - L)}{L} \qquad f = \frac{3}{\tan^2 \theta_0} \qquad g = \frac{1}{\sin^2 \theta_0} \tag{C14}$$

Where ϵ is the contraction ratio and L_0 and θ_0 are the length and braid angle respectively of the muscle at rest. In this form the equation can be separated into a force which occurs when the muscle is not strained and a force reduction when the muscle contracts.

If the strain in the active part of the muscle is now amplified by k. The force output in (C13) becomes

$$F = \pi {r_0}^2 P(f(1 - k\epsilon)^2 - g) \tag{C15}$$

Here it is clear that the force output is not modified when the muscle is in its relaxed state (strain is 0) as there is no conical shape on the end fitting then. A constant value of k was initially considered (in the case of the muscles tested values between 1.25 and 1.35 were appropriate) but this was found to perform poorly at low pressures. k was therefore modified to be pressure dependant

$$k = a_k e^{-P\prime} + b_k \tag{C16}$$

Where a_k and b_k must be determined experimentally. The results of this are shown in Figure C2. Kang et al, used an identical approach, but with k being determined by

$$k = 1 + c_k e^{d_k P\prime} \tag{C17}$$

Where c_k and d_k are evaluated experimentally [8].

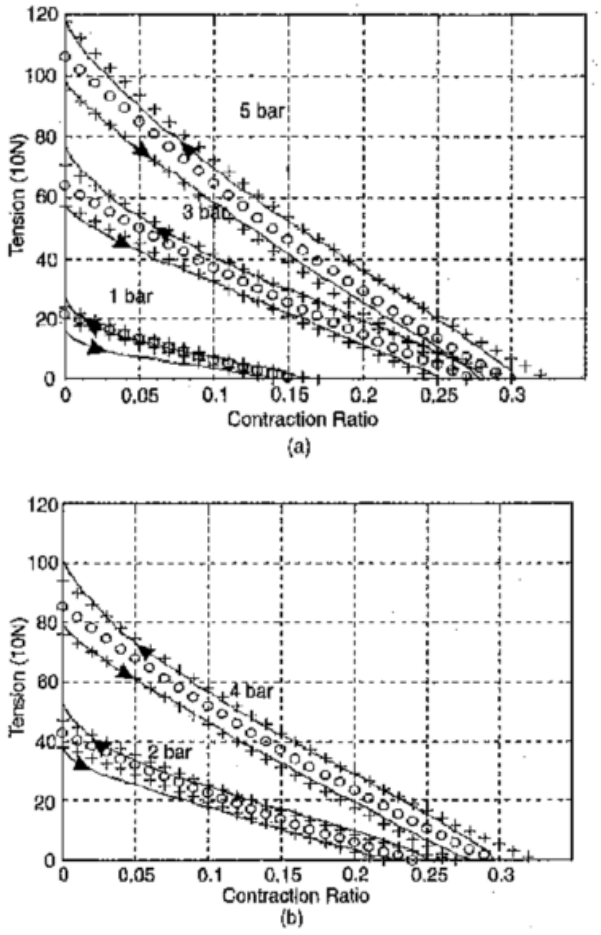

Figure C2: Testing results for Tondu and Lopez for an actuator operating at (a) 1,3,5 bar and (b) 2,4 bar [9]***. The solid lines are experimental results, circular marks are the model discussed in "Muscle Shape During Expansion***

Tsagarakis and Caldwell derived an identical expression for PAM force as Chou and Hannaford again using geometric considerations and the principle of virtual work [10]. However when the muscle operates in the range where the muscle diameter is less than that of the muscle end cap, which may occur when the muscle is close to its maximum stretched length, the equation is modified to account for a reduction in driving force. There is always a force acting in opposition to the muscle contraction as a result of the muscle pressure acting on the circular cross section of the muscle. In general the diameter of the muscle is the relevant dimension, but when the end cap diameter is greater than this, it is more accurate to use this diameter.

The output force of the muscle is also modified by the authors to account for the curved shape here. The shape of the muscle close to the end fitting is accounted for by splitting the muscle into a cylindrical section (the body) and the two identical cap sections:

$$F = F_{body} + 2\,F_{end} \tag{C18}$$

F_{end}, the force generated in the curved section close to one of the end fittings, is then evaluated by integrating the braid angle across this region of the muscle (the braid angle at the end cap cannot change as the braid is held in place).

$$F_{end} = \pi {D_{90}}^2 P \frac{\int_{\theta}^{\theta_{min}} \cos^2\theta \sin^2\theta d\theta}{\int_{\theta}^{\theta_{min}} sin\,\theta d\theta} \tag{C19}$$

Where θ_{min} is the minimum value of the braid angle, which occurs at the end caps.

The combination of these two approaches, as well as a simple empirical model for effective pressure reduction due to the bladder and a rudimentary friction model as mentioned previously, gives results which are 30-50% more accurate than the model by Chou and Hannaford.

Doumit derived a static model of a PAM in which the tension in the fibres is calculated based on both the radial and longitudinal stresses as a result of the applied pressure [11], [12]. Similar to Tsagarakis and Caldwell, the muscle is divided into two regions, the body and the two sections close to the end fittings. In this case the tension in the fibres are summed across these regions. The output force of the muscle is then found from this combined tension accounting for the angle at which the fibres meet the end fittings.

$$F = NT_f cos\beta \cos\theta_{min} \tag{C20}$$

Where N is the number of fibres, β is the angle the cone formed by the inflated muscle meets the end fitting and T_f is the total tension in the braid.

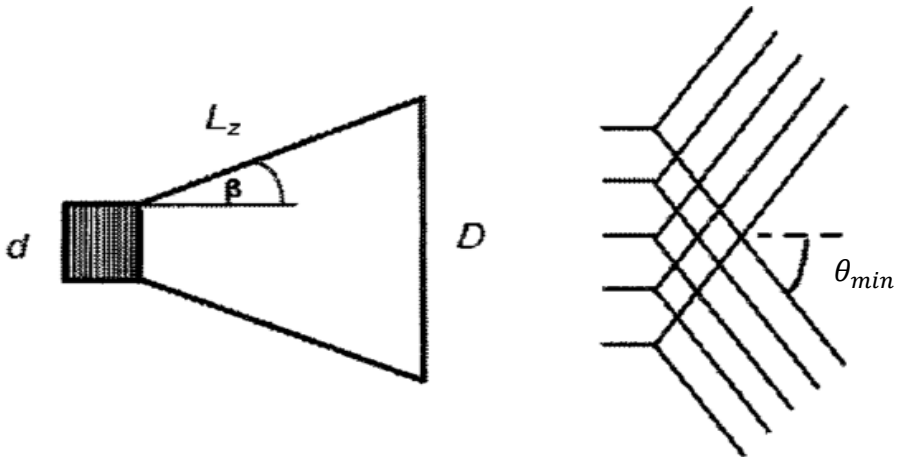

Figure C3. The assumed shape of the muscle close to the end fittings as assumed by Doumit [11], [12]

Kothera et al, observed that the shape the muscle adopts at the end fittings is approximately circular [5]. They proposed a correction factor to be applied to the muscle length to account for the additional contraction in line with this

$$L' = L - \delta \tag{C21}$$

$$\delta = (D - D_0) \tag{C22}$$

Where D_0 is the original muscle diameter and D is the adjusted one. This correction has no effect on the blocked force as $D = D_0$ but improves the accuracy of the model at high contractions.

Braid Friction

Friction in the muscle braid reduces the force output of the muscle and causes a damping effect as well as hysteresis. Owing to the wide variety of braid geometries and materials available it is difficult to model these robustly.

Chou and Hannaford attributed the hysteresis in the muscle to coulomb friction between the braid and shell, between the fibres which make up the braid and the shape change of the bladder [13]. The magnitude of the force hysteresis is independent of frequency. They suggest that due to difficulties in modelling this a constant value (for the muscle they tested 2.5N) be added to or subtracted from the modelled force when the muscle is lengthening or shortened. Tsagarakis and Caldwell adopted the same approach[10].

Tondu and Lopez argue the predominant source of friction is between fibres in the braid as the bladder is kept in rigid contact with the braid at all times and so there is no sliding here [9]. Furthermore, it is generally assumed that there is no sliding between fibres, but rather all friction is due to the relative rotation of the fibres due to the change in braid angle [9], [11], [14]. The total static friction force between the fibres (and therefore change in force output of the muscle) can be expressed as

$$\left|F_{static\ dry\ friction}\right| = \mu_s S_{contact} P' \tag{C23}$$

Where μ_s is the static coefficient of friction between the fibres and $S_{contact}$ is the contact area between all the fibres. Ignoring the cylindrical nature of the fibres and assuming they are flat, $S_{contact}$ can be approximated by the total surface area of the muscle when it is at its maximum length ($2\pi r_0 L_0$), assuming this is when the fibres are in their jammed position. As it contracts this surface area decreases as the angle between the fibres increase leading to the following expression for the total contact braid area of the muscle.

$$S_{contact} = 2\pi r_0 L_0 \frac{r_0}{r}\frac{L_0}{L} = 2\pi r_0 L_0 \frac{sin\theta_0}{(1-\epsilon)\sqrt{1-\cos^2\theta_0(1-\epsilon)^2}} \tag{C24}$$

Where r_0, L_0 and θ_0 are the muscle radius length and braid angle in the fully extended state. Applying this model a coefficient of friction was found from experimental data with a muscle. This value was far below known values for the material in question (rayon) and thus it is assumed that due to the cylindrical nature of the fibres $S_{contact}$ is only 1/13 of that in (C24). The results of using this model when compared to experimental data are shown in Figure C2.

Tondu and Lopez also include a dynamic friction model in their analysis as a means to quantify muscle damping. They found kinetic friction to be greater than that of static friction even at modest speeds. A general dynamic dry friction coefficient was considered

$$\mu = \mu_d + (\mu_s - \mu_d)e^{\frac{\dot{x}}{\dot{x}_s}} \quad \text{(C25)}$$

Where μ_d is the maximum kinetic dry friction, $\dot{x}$ is the contraction velocity and $\dot{x}_s$ is a velocity constant. The dynamic force output is finally

$$F_{dyn} = F - \mu\left(\frac{1}{S_{scale}}\right)S_{contact}P'sign(\dot{x}) \quad \text{(C26)}$$

Here F is that from equation (C15), which accounts for the increased strain in the active part of the muscle due to the curvature of the end fittings with the k parameter, and S_{scale} is a correction for $S_{contact}$ due to the shape of the fibres. The friction coefficients as well as S_{scale} and $\dot{x}_s$ must be determined experimentally. The resulting model offers good agreement with experimental data except for where muscle motion begins at low pressure.

Davis and Caldwell sought to reduce the dependence on experimental data when constructing the static friction model above [14]. They also formulated $S_{contact}$ so that the variation in braid strand length may also be accounted for (using equation (C5)).

$$S_{contact} = \frac{b^2 \sin^2\theta_0 \cos^2\theta_0}{nsin\theta cos\theta} \quad \text{(C27)}$$

As was the case with Tondu and Lopez, this assumes flat braids. In reality they are cylindrical (although many braids feature multiple fibres running beside each other). If the fibres were treated as being non-deformable, the contact area would be negligible (Figure C4 (a), however this is clearly not the case. With deformation the contact area is similar to Figure C4 (b), known as the Hertz contact area. For the case of braids which cross at an arbitrary angle, the calculation of the Hertz contact area is very complex and so this is simplified to the contact between two spheres, as shown in Figure C5

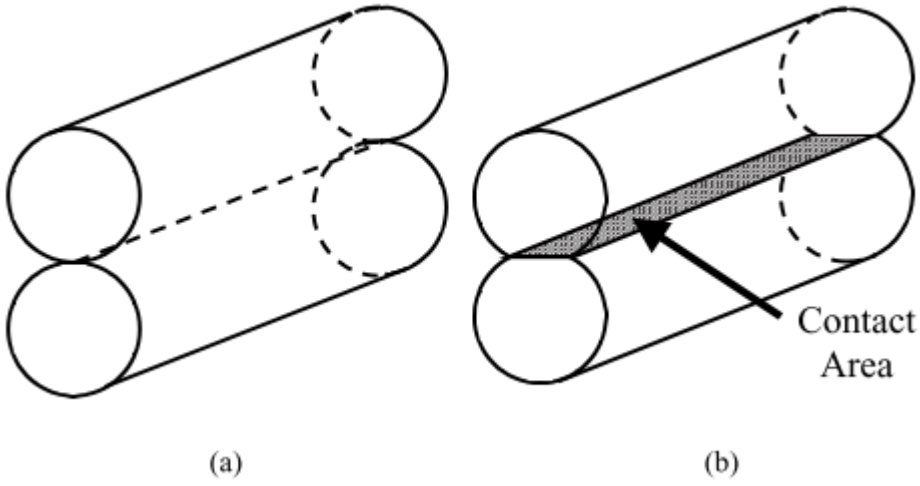

Figure C4: Hertz contact area between two parallel cylinders [14]

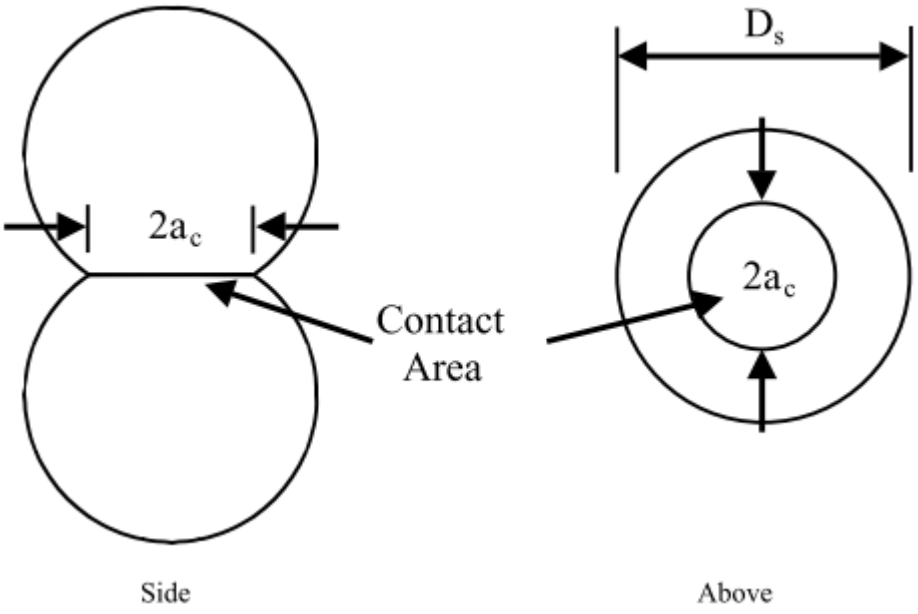

Figure C5:Contact area between braids treated as two spheres [14]**.**

It is argued that the scaling factor for contact area between flat and cylindrical fibres is then

$$S_{scale} = \frac{a_{c\,flat}}{a_{c\,sphere}} \tag{C28}$$

Where a_c is the diameter of the area which remains in contact between two fibres if one of the fibres preforms a full revolution. For flat fibres it is given by

$$a_{c\,flat} = \frac{D_s}{2} \tag{C29}$$

For two spheres it is found by [15]

$$a_{c\,sphere} = 0.721\sqrt[3]{F_{comp} K_d C_e}$$

$$C_e = \frac{2(1-\nu^2)}{E} \qquad F_{comp} = P' {D_s}^2 \qquad K_d = \frac{D_s}{2} \tag{C30}$$

Where F_{comp} is the force pushing two fibres in the braid together at a crossover point and ν is the Poisson's ratio of the braid material. The expression for K_d is only valid for 2 spheres of the same size. Using this formulation values for S_{scale} can be generated which are pressure dependant (due to increased force pushing the fibres together) and which agree with experimentally determined values to within 10%.

This model is clearly a simplification as the spherical contact area is an approximation of that of the braids. In particular there is no change in contact area with braid angle. Doumit aims to address this [11], [12].

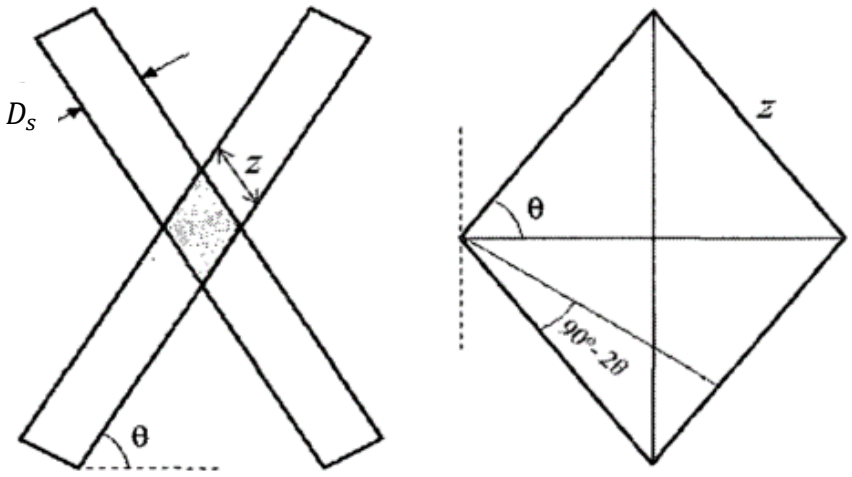

Figure C6: A braid crossover point as illustrated by Doumit *[11]*

Examining Figure C6, and assuming there are not multiple fibres running next to each other in the braid

$$z = \frac{D_s}{\cos(2\theta - 90)} \tag{C31}$$

The total number of crossover points is given by

$$q = 2n\left(\frac{N}{2}\right)^2 + \frac{N}{2} \tag{C32}$$

Where N is the number of fibres in the muscle.

The total contact area between all the fibres in the muscle is then

$$S_{contact} = D_s z q \tag{C33}$$

This assumes a flat braid. In order to estimate the actual contact area a formula from Roark et al is used to estimate w in Figure C7 [16].

$$w = 1.6\sqrt{pK_d C_e} \tag{C34}$$

$$p = \frac{F_{comp}}{z} \tag{C35}$$

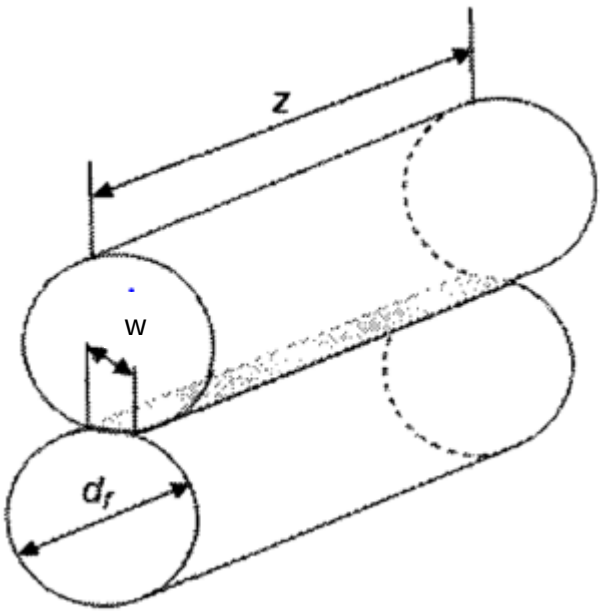

Figure C7 Braid contact between two fibres [11]

This means that the effective contact area is given by

$$A_{ff} = wzq \tag{C36}$$

Based on the muscle operating conditions a number of expressions can then be given for the total muscle braid frictional force (dynamic and static).

$$F_{fr} = \begin{cases} -P' A_{ff} \mu_d & \dot{L} < 0 \\ \sum F + P' A_{ff} \mu_d & \sum \dot{F} \leq 0, \dot{L} = 0 \\ P' A_{ff} \mu_s & \sum \dot{F} \leq 0, \dot{L} = 0 \\ P' A_{ff} \mu_d & \dot{L} > 0 \end{cases} \tag{C37}$$

Where μ_s and μ_d are the static and dynamic coefficients of friction respectively.

While the majority of these models assume that the braid is the only source of friction in the muscle, this is not necessarily the case. For example, later work by Doumit found that braids with a fewer number of fibres (and therefore fewer crossover points and associated braid friction) had greater hysteresis, suggesting more friction[17]. This result means that the interplay between bladder and fibres requires further study to fully understand this complex behaviour.

Braid Jamming

Braid jamming occurs at the extremes of operation of the muscle (full elongation or contraction) and it defines the limits of travel. It occurs when the braid angle reaches its minimum or maximum possible value. A number of authors have studied the maximum contraction of the muscle, with the maximum braid angle being found to be 54.7° [12], [18].

Taking equation 2.17 it is clear that when the following expression is true the force becomes 0, as would be the case when the braid is in its jamming position.

$$3L^2 - b^2 = 0 \tag{C38}$$

$$L = \frac{b}{\sqrt{3}} \tag{C39}$$

Then using equation 2.9

$$b\ cos\theta = \frac{b}{\sqrt{3}} \tag{C40}$$

After cancelling the bs this can be solved for θ=54.7°.

There has been less investigation for jamming at maximum extension with authors mainly relying on experimental techniques. Davis and Caldwell adopted a more analytical approach [14]. Considering Figure C8, it is evident that

$$Y = \frac{X}{cos\theta} = \frac{W_B}{2cos\theta} \tag{C41}$$

W_B is the width of the individual braid. In most cases the braid is composed of multiple fibres running next to each other and so W_B is the combined diameters of these.

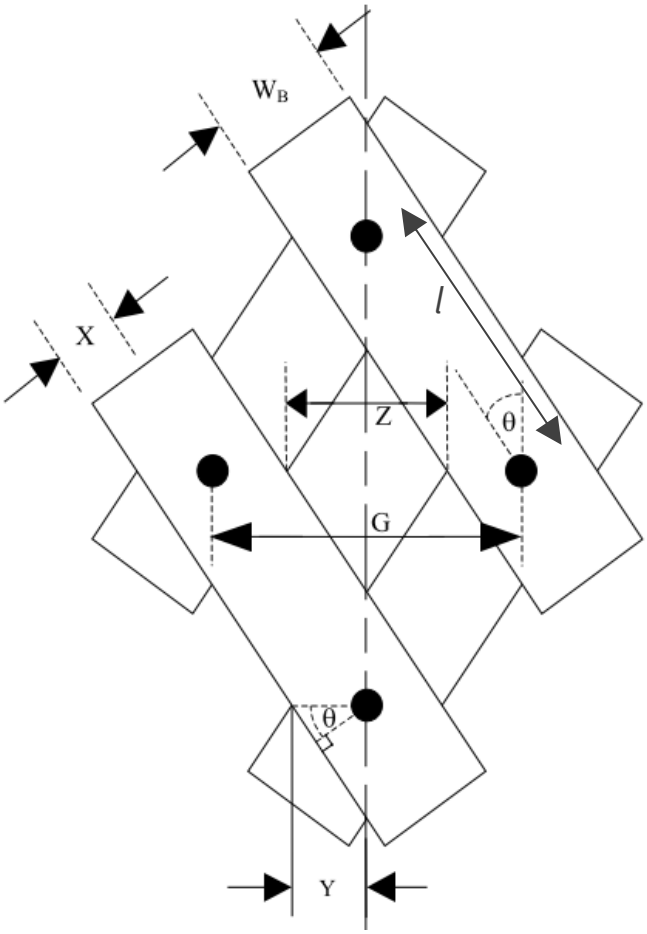

Figure C8: Braid angle analysis to identify the minimum braid angle (assumes single strands) [14]***.***

Considering the case where θ is 90°, the diameter of the muscle is given by

$$D_{90} = 2lN_c = \frac{b}{n\pi} \tag{C42}$$

Where l is the distance between two nodes along the braid (see Figure C8) and N_c is the number of crossover points around the circumference of the muscle at one point ($N_c = \frac{N}{2}$, if N is the number of fibres in the braid . Rearranging gives

$$l = \frac{\pi D_{90}}{2N_c} \tag{C43}$$

From Figure C8 the distance along the muscle circumference between two cross over points is given by

$$G = 2lsin\theta \tag{C44}$$

The minimum braid angle occurs when $G = 2Y$. Therefore, using equations (C41) and (C44) as well as the expression for l in (C43) and the trigonometric identity $sin(2u) = 2\sin(u)\cos(u)$, the minimum braid angle is

$$\theta_0 = \frac{\sin^{-1}\left(\frac{2W_B N_c}{\pi D_{90}}\right)}{2} \tag{C45}$$

This can be used with equation 2.11 to get the corresponding muscle length which is useful when specifying muscle length in many applications or in control to predict where a sudden increase in force due to extension will occur. The results were verified experimentally with good agreement with the model. This approach however does not take into account the effects of the bladder in the braid or restrictions in the minimum diameter of the muscle due to the end fittings.

REFERENCES

[1] G. K. Klute and B. Hannaford, “Fatigue characteristics of McKibben artificial muscle actuators,” *Int. Conf. Intell. Robot. Syst.*, vol. 3, no. October, pp. 1776–1781, 1998.

[2] G. K. Klute and B. Hannaford, “Accounting for Elastic Energy Storage in McKibben Artificial Muscle Actuators,” *J. Dyn. Syst. Meas. Control*, vol. 122, no. 2, p. 386, 2000.

[3] L. R. G. Treloar, *The physics of rubber elasticity*. London: Oxford University Press, 1958.

[4] N. Delson, T. Hanak, K. Loewke, and D. N. Miller, “Modeling and implementation of McKibben actuators for a hopping robot,” *2005 Int. Conf. Adv. Robot. ICAR ’05, Proc.*, vol. 2005, pp. 833–840, 2005.

[5] C. S. Kothera, M. Jangid, J. Sirohi, and N. M. Wereley, “Experimental Characterization and Static Modeling of McKibben Actuators,” *J. Mech. Des.*, vol. 131, no. 9, p. 091010, 2009.

[6] E. Ball and E. Garcia, “Effects of Bladder Geometry in Pneumatic Artificial Muscles,” *J. Med. Device.*, vol. 10, no. 4, p. 041001, 2016.

[7] S. Davis, N. Tsagarakis, J. Canderle, and D. G. Caldwell, “Enhanced modelling and performance in braided pneumatic muscle actuators,” *Int. J. Rob. Res.*, vol. 22, no. 3, pp. 213–227, 2003.

[8] B. S. Kang, C. S. Kothera, B. K. S. Woods, and N. M. Wereley, “Dynamic modeling of mckibben pneumatic artificial muscles for antagonistic actuation,” *Proc. - IEEE Int. Conf. Robot. Autom.*, pp. 182–187, 2009.

[9] B. Tondu and P. Lopez, “Modeling and control of McKibben artificial muscle robot actuators,” *IEEE Control Syst. Mag.*, vol. 20, no. 2, pp. 15–38, 2000.

[10] N. Tsagarakis and D. G. Caldwell, “Improved modelling and assessment of pneumatic muscle actuators,” *Proc. 2000 ICRA. Millenn. Conf. IEEE Int. Conf. Robot. Autom. Symp. Proc. (Cat. No.00CH37065)*, vol. 4, pp. 3641–3646, 2000.

[11] M. D. Doumit, “Characterization, modeling and design of the braided pneumatic muscle,” University of Ottawa, 2009.

[12] M. Doumit, A. Fahim, and M. Munro, “Analytical modeling and experimental validation of the braided pneumatic muscle,” *IEEE Trans. Robot.*, vol. 25, no. 6, pp. 1282–1291, 2009.

[13] C.-P. Chou and B. Hannaford, “Measurement and modelling of McKibben pneumatic artificial muscles,” *Robot. Autom. IEEE Trans.*, vol. 12, no. 1, pp. 90–102, 1996.

[14] S. Davis and D. G. Caldwell, “Braid Effects on Contractile Range and Friction Modeling in Pneumatic Muscle Actuators,” *Int. J. Rob. Res.*, vol. 25, no. 4, pp. 359–369, 2006.

[15] T. A. STOLARSKI and T. A. STOLARSKI, “3 – Elements of contact mechanics,” in *Tribology in Machine Design*, 1990, pp. 64–96.

[16] R. J. Roark, W. C. Young, and R. Plunkett, *Formulas for Stress and Strain*, vol. 43, no. 3. 1976.

[17] M. Doumit and J. Leclair, “Development and testing of stiffness model for pneumatic artificial muscle,” *Int. J. Mech. Sci.*, vol. 120, no. November 2016, pp. 30–41, 2017.

[18] H. F. Schulte, D. F. Adamski, and J. R. Pearson, “Characteristics of the Braided Fluid Actuator,” 1961.

APPENDIX D: CAD DRAWINGS OF SLEEVE AND TRADITIONAL PAMS

SLEEVE PAM

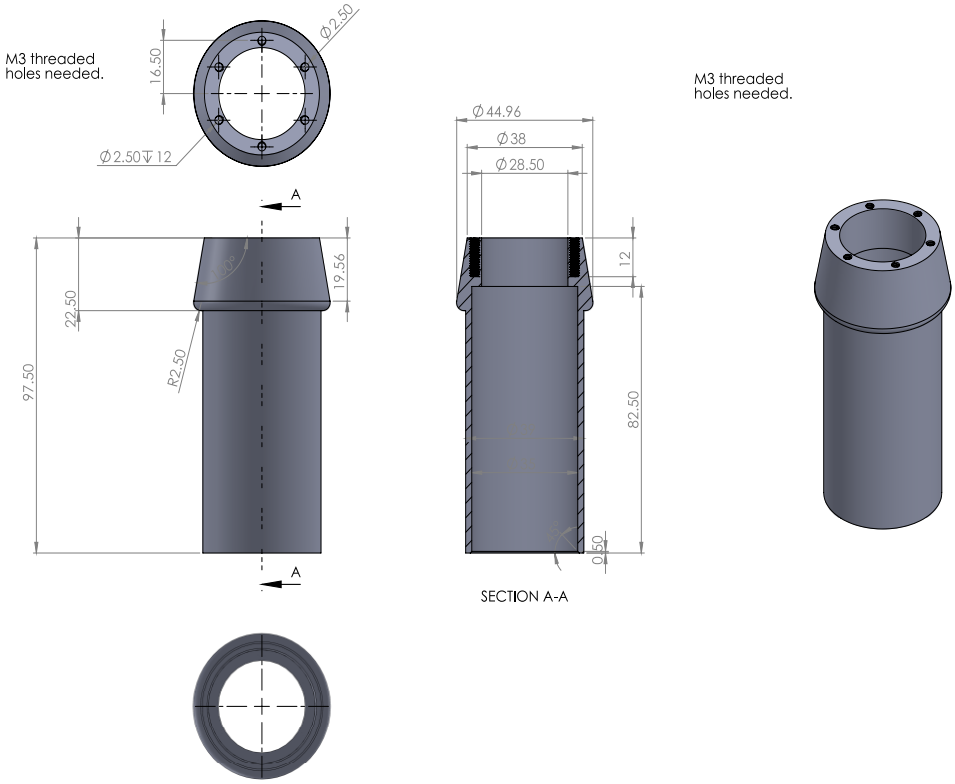

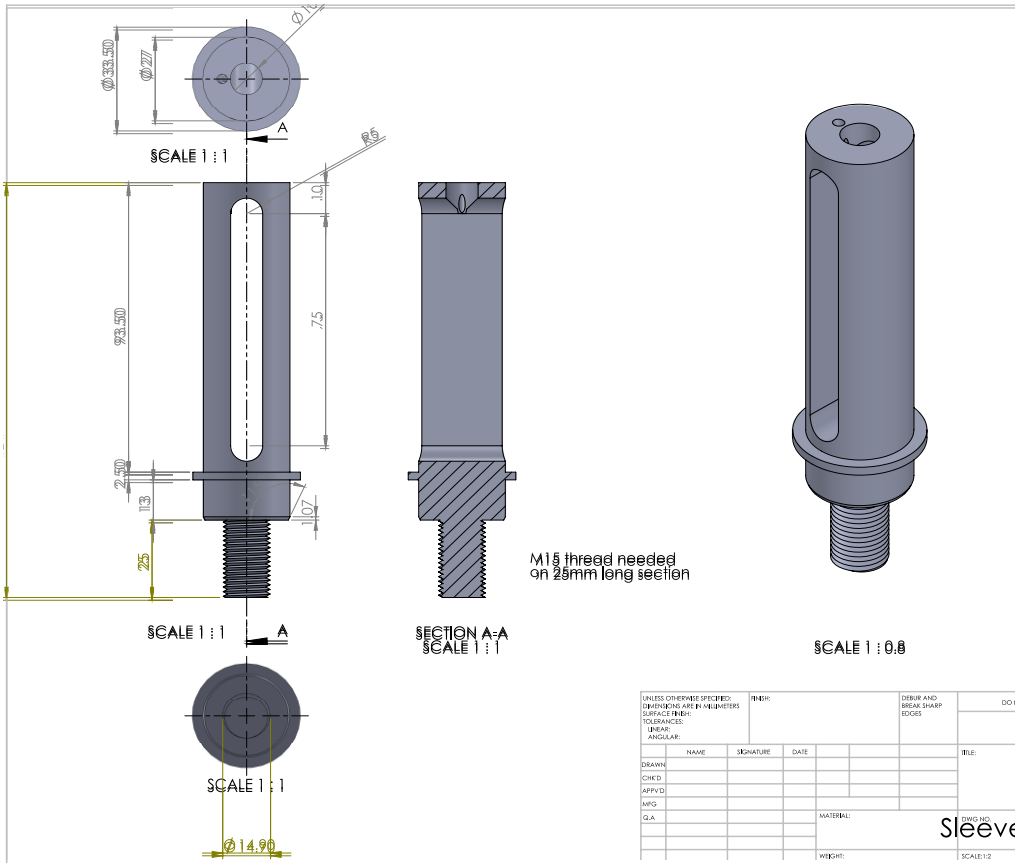
Ø33.500
Ø27
A
SCALE 1 : 1
R5
10
33.500
7.5
2.500
11.3
10.7
25
SCALE 1 : 1
A
M15 thread needed
on 25mm long section
SECTION A-A
SCALE 1 : 1
SCALE 1 : 0.8
SCALE 1 : 1
Ø14.90
UNLESS OTHERWISE SPECIFIED:
DIMENSIONS ARE IN MILLIMETERS
SURFACE FINISH:
TOLERANCES:
LINEAR:
ANGULAR:
FINISH:
DEBUR AND
BREAK SHARP
EDGES
NAME
SIGNATURE
DATE
DRAWN
CHK'D
APPV'D
MFG
Q.A
TITLE:
MATERIAL:
DWG NO.
Sleeve
WEIGHT:
SCALE:1:2

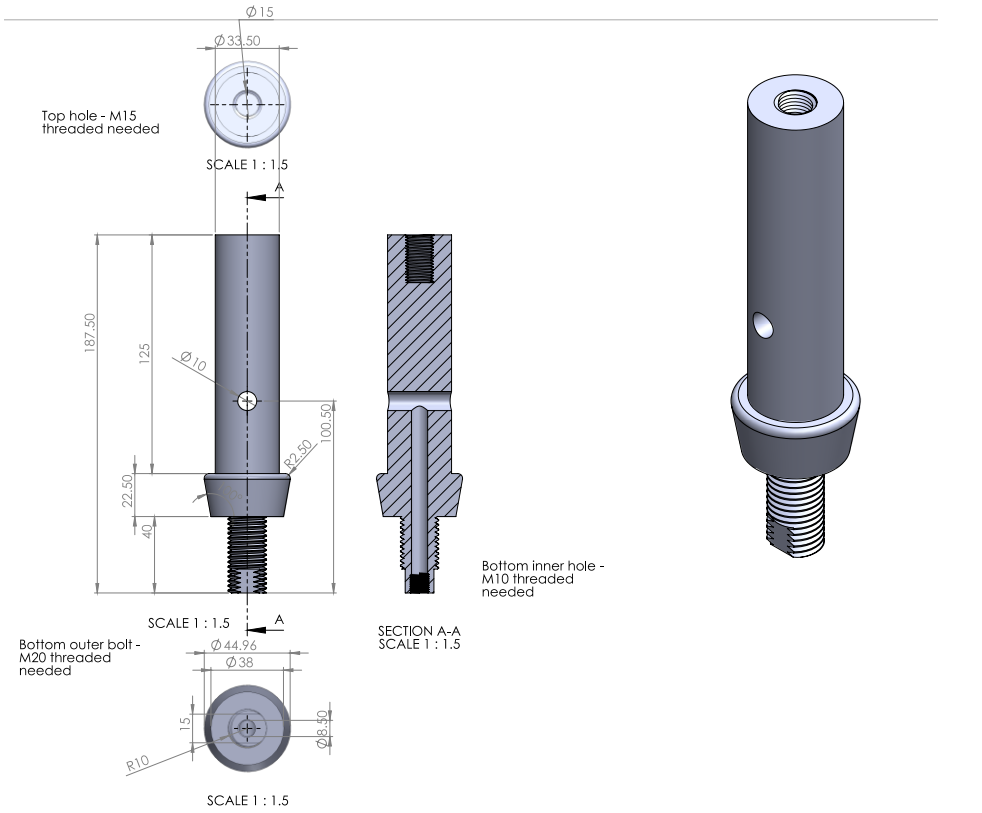
Ø15
Ø33.50
Top hole - M15
threaded needed
SCALE 1 : 1.5
A
187.50
125
Ø10
100.50
R2.50
22.50
40
SCALE 1 : 1.5
A
Bottom outer bolt -
M20 threaded
needed
Ø44.96
Ø38
15
Ø8.50
R10
SCALE 1 : 1.5
Bottom inner hole -
M10 threaded
needed
SECTION A-A
SCALE 1 : 1.5

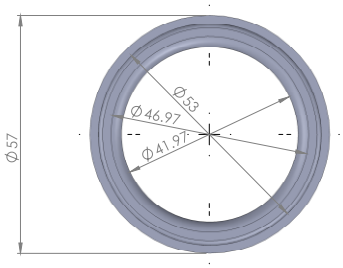

SCALE 1 : 0.75

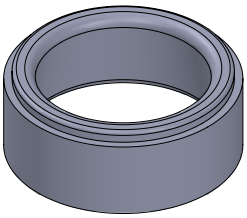

SCALE 1 : 0.75

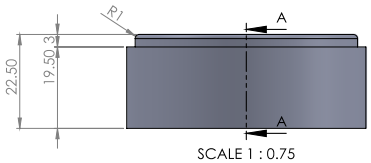

SCALE 1 : 0.75

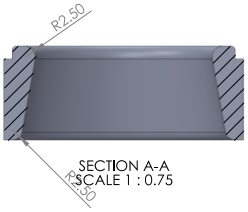

SECTION A-A
SCALE 1 : 0.75

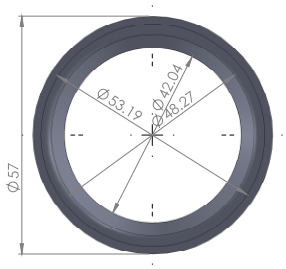

SCALE 1 : 0.75

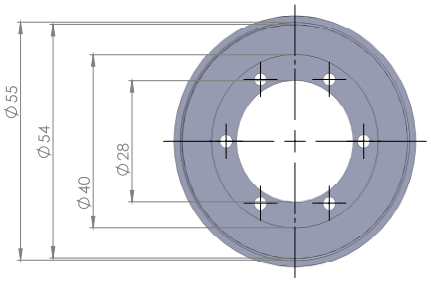

SCALE 1 : 0.8

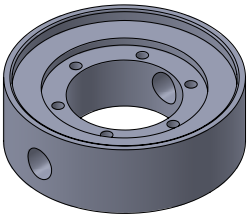

SCALE 1 : 0.8

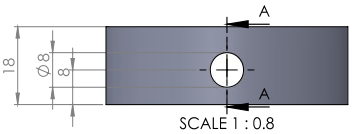

SCALE 1 : 0.8

SECTION A-A
SCALE 1 : 0.8

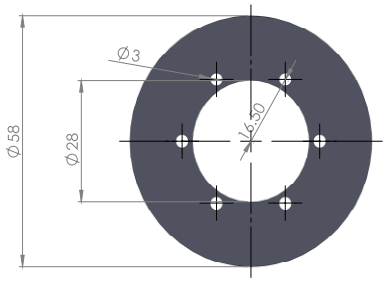

SCALE 1 : 0.8

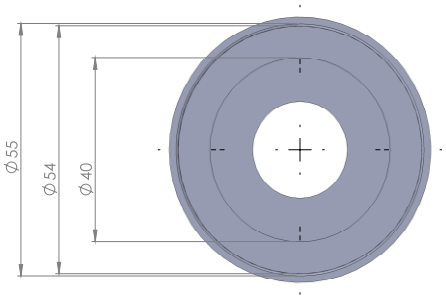

SCALE 1 : 0.75

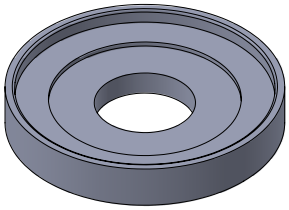

SCALE 1 : 0.7

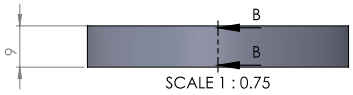

SCALE 1 : 0.75

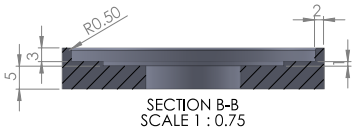

SECTION B-B
SCALE 1 : 0.75

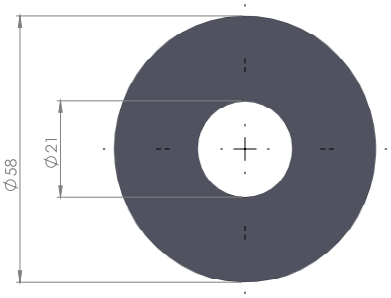

SCALE 1 : 0.75

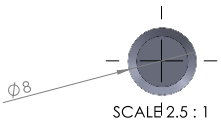

SCALE 2.5 : 1

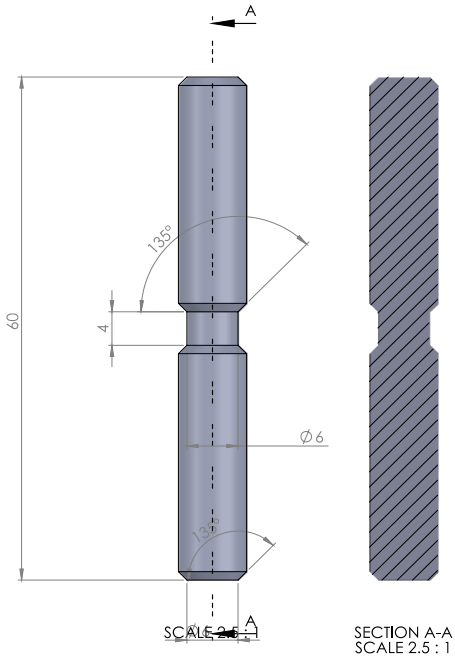

SECTION A-A
SCALE 2.5 : 1

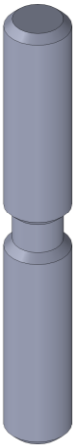

SCALE 2.5 : 1

TRADITIONAL PAM

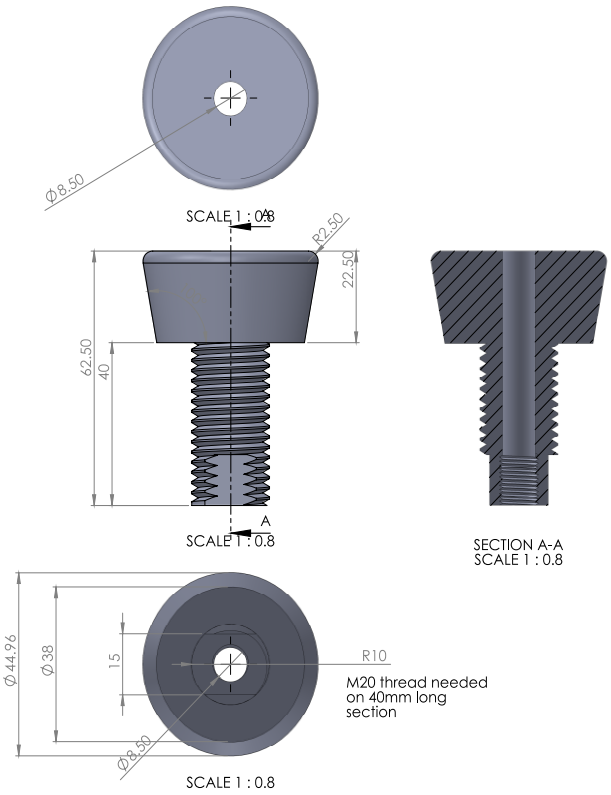

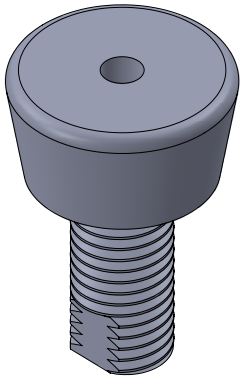

SCALE 1 : 0.6

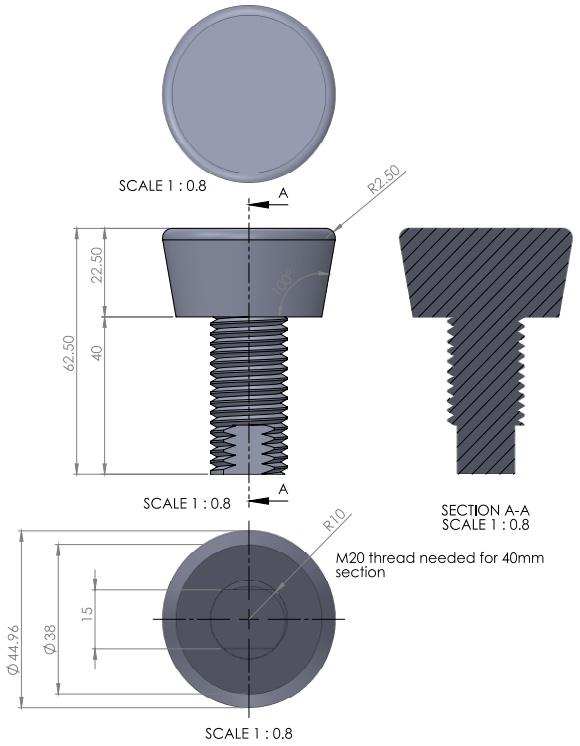

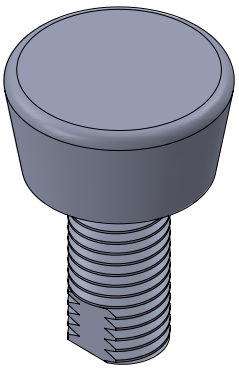

SCALE 1 : 0.6

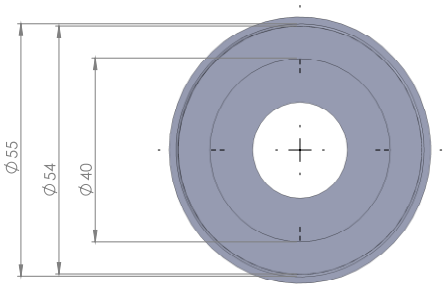

SCALE 1 : 0.75

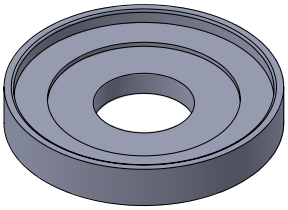

SCALE 1 : 0.7

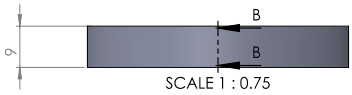

SCALE 1 : 0.75

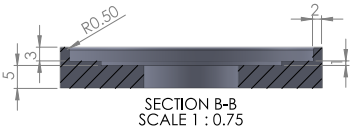

SECTION B-B
SCALE 1 : 0.75

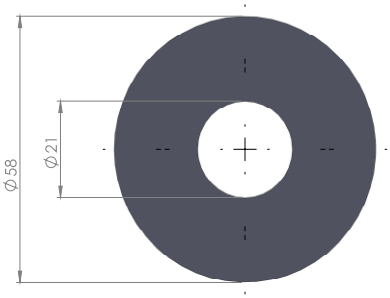

SCALE 1 : 0.75

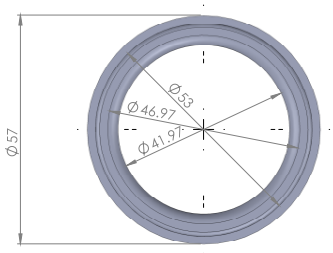

SCALE 1 : 0.75

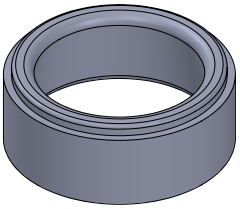

SCALE 1 : 0.75

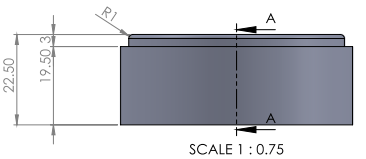

SCALE 1 : 0.75

SECTION A-A
SCALE 1 : 0.75

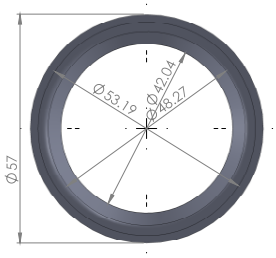

SCALE 1 : 0.75